Mechanistic Understanding as a Driving Force for Developments in Nickel-Catalyzed Coupling Methods

by

Martyn Taylor Haynes

A dissertation submitted in partial fulfillment
of the requirements for the degree of
Doctor of Philosophy
(Chemistry)
in the University of Michigan
2014

Doctoral Committee:

Professor John Montgomery, Chair
Professor Anne J. McNeil
Professor Phillip E. Savage
Professor John P. Wolfe

DEDICATION

This work is dedicated to Amanda Haynes. I know that the last decade of our lives is only a hint of what is to come. Without you, I would be a tenth the man I am today.

ACKNOWLEDGEMENTS

I would first like to thank my advisor John Montgomery for his guidance and support over the years. Working in the Lab has helped me become an independent thinker, and has provided ample opportunities to develop as a leader among my peers. I would also like to thank my committee: Anne McNeil, John Wolfe, and Phil Savage, for their direction in my research endeavors, as well as their flexibility in coordinating numerous meetings.

I would like to thank my colleagues in the Montgomery Lab, for all of the day-to-day help and direction. No matter how insane the idea, someone in the lab was always willing to listen. I would especially like to thank Evan and Zach for editing my thesis, helping me greatly in this final stretch.

From a young age I was interested in science and engineering, and I have my family to thank for their encouragement and support through the years. My parents taught me how to be compassionate for others, and pushed me to always do my best. Thank you for all that you have done for me!

Lastly, I would like to thank my spiritual family at Grace Ann Arbor. Graduate school has been a long and arduous process, but you have supported me every step of the

way. My community group has been a family for us here, and given us something to look forward to every week. Being involved with the church has also been amazing as a reminder of why I work and live as a part of this world.

TABLE OF CONTENTS

LIST OF TABLES

LIST OF SCHEMES

LIST OF FIGURES

LIST OF ABBREVIATIONS

nBu	n-butyl
tBu	tert-butyl
tBuOK	potassium tertbutoxide
^{o}C	degrees celcius
COD	cyclooctadiene
d.r.	diastereomeric ratio
dmfu	dimethylfumarate
Equiv.	equivalent
Et	ethyl
Et3SiH	triethylsilane
Et3SiD	triethylsilyl-deuteride
Pr3SiH	tripropylsilane
GC/MS	gas chromatography mass spectrometry
cHex	cyclohexyl
nHex	n-hexyl
hr.	hour(s)
min.	minute(s)
d	day(s)
IMes·HCl	1,3-bis(2,6-diisopropylphenyl)-imidazolium chloride
IPr·HCl	1,3-bis(2,4,6-trimethylphenyl)-imidazolium chloride
SIMes·HCl	1,3-bis(2,4,6-trimethylphenyl)-imidazolinium chloride
NHC	N-Heterocyclic Carbene
PCC	pyridinium chlorochromate
Ph	phenyl
i-pr	isopropyl
n-pr	n-propyl
r.t.	room temperature
ret. time	retention time
rs	regioselectivity
TBS	tertbutyldimethylsilane

THF	tetrahydrofuran
Tol.	toluene

ABSTRACT

Investigating the mechanism of nickel-catalyzed reductive couplings of aldehydes and alkynes has provided evidence of several potential metallacycle intermediates. Through a series of double-labeling experiments employing deutero-triethylsilane and tripropylsilane, the influence of multiple organometallic intermediates along the reactive pathway was investigated. The nature of both the catalyst structure and the reactant structure were found to directly effect the formation of complex metallacycles.

To further refine the mechanistic hypothesis for the reductive coupling of aldehydes and alkynes, a preliminary kinetics profile was compiled using a series of initial rate studies. From these investigations, a mechanism is proposed beginning with a stable bis-aldehyde nickel complex in equilibrium with the active mixed π-component species.

The application of an air-stable nickel-NHC catalyst system was explored in a number of coupling reactions. The catalyst system was found to be a versatile catalyst for a range of Kumada-Corriu coupling reactions, but found limited applicability to Buchwald-Hartwig couplings and the reductive coupling of aldehydes and alkynes. The synthesis of electron-rich catalyst systems, bearing a saturated NHC ligand, is also

reported, as well as the synthesis of a functionalized nickel catalyst from commercially available and bench-stable starting materials.

Chapter 1: Nickel Catalysis in Organic Synthesis

1.0.0 Nickel Catalysis in Organic Synthesis

Transition metal catalyzed transformations have been shown to be both robust and versatile in the synthesis of a variety of structural moieties. The incredible scope of cross-coupling reactions catalyzed by transition metal catalysis earned the Nobel Prize in 2010, awarded to the creation of the field and further developments by Heck, Suzuki, and Negishi.[1] Although many different transition metals have been explored for their reactivity and versatility in organometallic transformations, the work utilizing nickel, an inexpensive and versatile catalyst, will be further explored in this work.

An early investigation into the catalytic activity of nickel in organometallic transformations comes from the work of Wilke on ethene polymerization.[2] A nickel catalyst was used to dimerize ethene to 1-butene (Scheme 1.01). The report shows one of the first effective nickel-catalyzed processes reported and also exhibits selectivity for the synthesis of 1-butene. Further oligomers of ethylene were formed in minor amounts, control over which is still an area of development for modern methods. Further refinements of the process, such as the Shell higher olefin process (SHOP)[3], have allowed

for the development of related reaction providing higher carbon chains or control over the formation of linear or branched hydrocarbons.

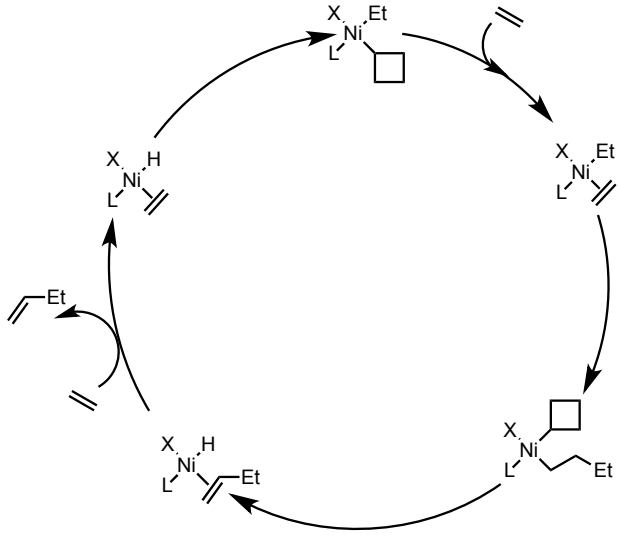

Scheme 1.01 – Mechanism of Wilke ethene dimerization

1.1.0 Ligand Classes for Nickel-Catalysis

Intricately linked to the development of catalytic systems and metal-mediated processes is the development and growth of ligand classes. Many ligands have been employed in tandem with nickel organometallic catalysis, with amino groups, phosphines, and recently *N*-heterocyclic carbenes[4] (NHC) finding the most application. The strong σ donation of these ligands allows for stabilization of the metal in solution as well as altering the electronics of the metal center dramatically, imparting reactivity and selectivity for a number of reactions.

1.2.0 *N*-Heterocyclic Carbenes as a Ligand Class

Initial reports into stabilized carbenes come from the work of Ofele[5] and Wanzlick.[6] The stable hypochlorite salt of the free carbene was found to be deprotonated

in solution, and subsequently binds to form a mercury salt in the form of a stable bis-carbene complex (Scheme 1.02). The strongly σ-donating character of the NHC allowed for the formation of the stable catalyst in solution; however, the free carbene itself was not isolable.

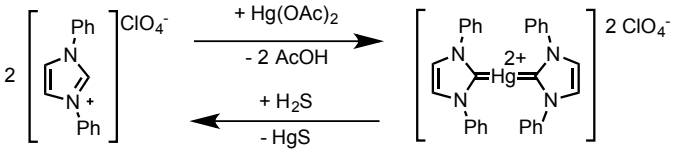

Scheme 1.02 – Initial report of a carbene stabilized by neighboring nitrogen

1.2.1 Arduengo Carbenes, Isolation and Characterization

The use of NHCs as ligands saw little development until the report of the stable IAd carbene by Arduengo[7] (Scheme 1.03). The bis-adamantyl substitution of the imidazolium created a steric environment hindering further reactivity, coupled with the stabilization of the carbene through the aromaticity of the imidazolium ring, allowed for the observation of the free carbene. Further study expanded the class of stable carbenes that could be isolated, and the ability of less sterically hindered carbenes to dimerize in solution. These dimeric carbene species could fragment under thermal conditions back to the corresponding free carbene.

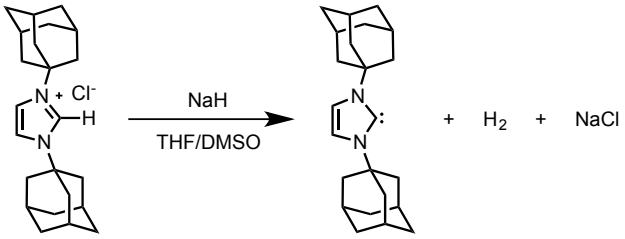

Scheme 1.03 – Isolation of stable carbene intermediates

1.2.2 Metal Complexes of Arduengo Carbenes

Manganese metal centers stabilized by NHC ligands were among the first reported metal-NHC systems.[8] The use of carbene ligands has also been shown to impart dramatically increased reactivity on different metal catalyst systems. One such example is the activation of technetium catalyst,[9] which was found to activate siloxane grease, a notoriously unreactive species. The strong binding of the NHC, coupled with the corresponding changes to catalyst stability and reactivity, have led to the widespread development of NHCs as a ligand class for transition metal catalysis.

1.3.0 Nickel Catalyzed Reductive Couplings in Organic Synthesis

1.3.1 Allylic Alcohols, Utility and Synthesis

The allylic alcohol functional moiety serves as a starting material for a number of versatile transformations that have seen wide application in synthesis. Molecular complexity can be rapidly generated from the use of allylic alcohols through a number of divergent mechanisms such as directed epoxidation,[10] nucleophilic displacement reactions, generation of π-allyl metal complexes, and Claisen rearrangements.[11] This utility in the synthesis of complex small molecules has generated interest into a robust and selective pathway for forming allylic alcohols. Two common approaches to the

synthesis of allylic alcohols are derived from either the 1,2 reduction of α,β-unsaturated ketones or from the coupling of aldehydes with nucleophilic vinyl surrogates (Figure 1.01).

Figure 1.01 – General Methods for the synthesis of Allylic Alcohols

One of the earliest reported synthetic routes to allylic alcohols is the Wharton olefin synthesis (Scheme 1.04).[12] Utilizing the same reagents as in the Wolff-Kishner reaction,[13] the decomposition of α,β-epoxy ketones provides reliable access to allylic alcohols. The main limitation of the method is the highly reactive nature of the epoxy ketone starting materials, which limits the applicability as well as the scope of the reaction.

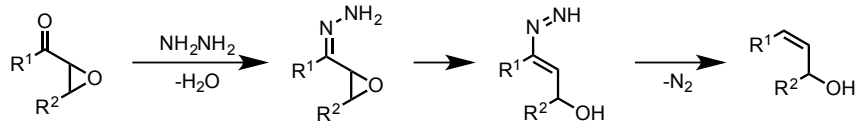

Scheme 1.04 – The Wharton olefin synthesis as an access to allylic alcohols

Beginning from terminal alkenes and formaldehyde, the Prins reaction provides access to allylic alcohols in addition to other hydroxylation products from simple starting materials (Scheme 1.05).[14] Careful manipulation of the reaction conditions allows for selectivity in the formation of specific products. Developments focused on controlling the Prins reaction have crafted a versatile method in the synthesis of different products that are fundamentally related to allylic alcohols. Variants of the Prins reaction employing organometallic transformations have been developed that further extend the

reaction methodology into different classes of starting materials including the use of aldehydes and more complex alkene components.[15]

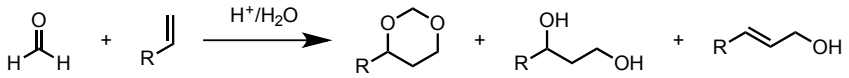

Scheme 1.05 – The Prins reaction in the synthesis of allylic alcohols and related hydroxylated products

Utilizing pericyclic rearrangements has provided another route to allylic alcohols from simple starting materials and common functional groups. The Guillemonat variation of the Riley oxidation uses a selenium reagent to oxidize the allylic position of a hydrocarbon chain.[16] The resulting allylic selenium-oxide undergoes a rearrangement, which upon hydrolysis provides the unprotected allylic alcohol (Scheme 1.06). This allylic oxidation method has been employed in a number of small molecule syntheses, including work by Corey[17] and Furstner.[18] In a related process, the activation of allylic sulfoxides in the Mislow Evans reaction allows for the synthesis of allylic alcohols,[19] however the synthesis of allylic sulfoxides can also prove to be non-trivial.

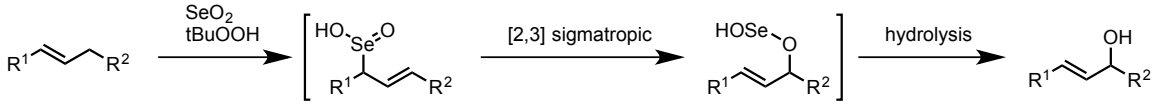

Scheme 1.06 – Guillemonat variation of the Riley oxidation

Numerous reductive methods have been developed for the synthesis of allylic alcohols. The Luche reduction is selective for the 1,2 reduction of α,β-unsaturated ketones providing the corresponding allylic alcohols.[20] The reduction of aldehydes by different nucleophilic species also serves as a route to the allylic alcohol structural moiety. The Baylis-Hillman reaction couples an aldehyde with a terminal alkene to

generate the corresponding allylic alcohol under mild reaction conditions.[21] The generation and use of a wide variety of vinyl metal species can also serve to reduce aldehydes to generate allylic alcohols. Methods have been developed for the selective reduction of terminal alkynes, which generate vinyl boron[22] or zirconium[23] species. These intermediates can undergo transmetallation with dialkyl zinc to generate an active vinyl zinc reagent, which can be used in reducing an aldehyde (Figure 1.02). These methods can also be carried out in the presence of a chiral promoter, providing access to an array of enantiomerically enriched allylic alcohols.

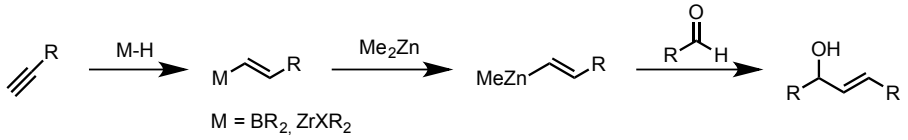

Figure 1.02 – Reduction of alkynes to generate vinyl-zinc species for the reduction of aldehydes

Transition-metal-mediated reactions are also prevalent and highly selective in the synthesis of allylic alcohols through multicomponent coupling reactions. The use of titanium,[24] rhodium,[25,26] and ruthenium[27] catalysts in the reductive coupling of aldehydes and alkynes provides convenient access to the allylic alcohol functional group (Figure 1.03). While robust methods have been developed, each metal catalyst comes with a limiting set of conditions. The most versatile methods employing titanium in the reductive coupling process require stoichiometric quantities of the metal complex. Methods have been developed that are catalytic in titanium, however these systems show a more restricted substrate scope.[28] Similarly, rhodium and ruthenium catalysts are limited in the cost and rarity of the metal used in catalysis.

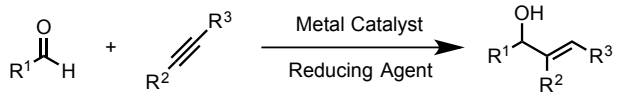

Figure 1.03 – Metal catalyzed reductive coupling methods

The most versatile and widely employed method for the synthesis of allylic alcohols is the Nozaki-Hiyama-Kishi reaction.[29] Utilizing vinyl iodides with nickel and chromium, the stereospecific formation of allylic alcohols can be enacted (Scheme 1.07).[30] This reaction exhibits an extensive substrate scope, tolerating a variety of aldehydes and vinyl iodides. However, the need for stereodefined vinyl iodides can limit the applicability in synthesis. Recent developments have allowed for the use of allylic halides,[31] however the synthesis of these molecules and their storage can also be non-trivial.

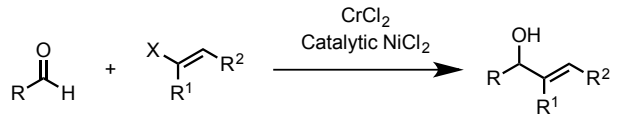

Scheme 1.07 – The Nozaki-Hiyama-Kishi reaction

Developments in the Montgomery laboratory have aimed to improve reductive coupling methods to provide a robust synthetic method in the formation of allylic alcohols. The use of a nickel catalyst benefits from being a readily available and inexpensive metal catalyst, and the simple substrates employed provide a versatile method in the synthesis of various allylic alcohols.

1.3.2 Development of Nickel-Catalyzed, Three Component Reductive Coupling

Early work in the Montgomery laboratory served to develop the reductive coupling of enones and alkynes.[32] Initial work elucidated an intramolecular coupling

reaction where product selectivity is largely controlled based upon the ligand used in conjunction with a nickel catalyst (Scheme 1.08). Without the addition of a phosphine ligand, the nickel catalyst was found to perform the alkylative coupling after transmetallation with diethyl zinc to provide the functionalized tetrasubstituted olefin. However, when triphenylphosphine was added to the reaction, the nickel was found to undergo β-hydride elimination to generate the reductive coupling product.

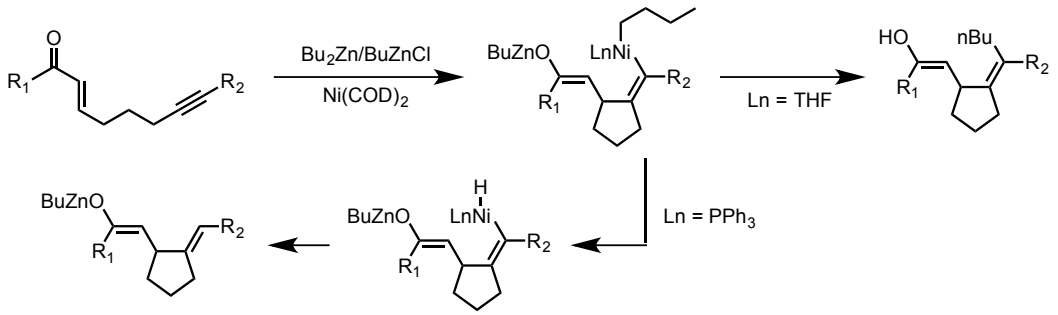

Scheme 1.08 – Changes in product synthesis based upon presence of ligand

The use of nickel catalysis in the reductive coupling of π-systems continued with the development of a reductive coupling of aldehydes and alkynes to provide access to allylic alcohols.[33] Expanding on the coupling of enones and alkynes, both the alkylative and reductive formation of allylic alcohol products can be accessed in good conversion for a variety of substrate systems (Scheme 1.09).

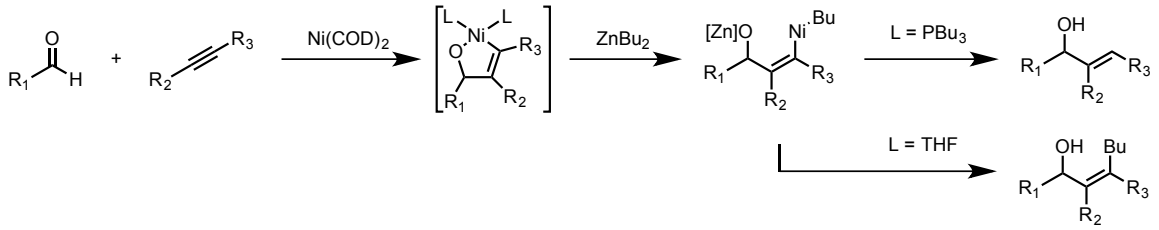

Scheme 1.09 – Early reductive coupling of aldehydes and alkynes, reduced by alkyl-zinc

A number of natural products contain the allylic alcohol structural motif, expanding the utility of reductive coupling in the synthesis of many small molecules. One such series of compounds is the allopumiliotoxin family, where a late stage reductive coupling serves to close a key ring-juncture (Scheme 1.10).[34] The coupling of an aldehyde and alkyne was later applied to the synthesis of a number of structures in the allopumiliotoxin family beyond the initial report on allopumiliotoxin 267A.[35]

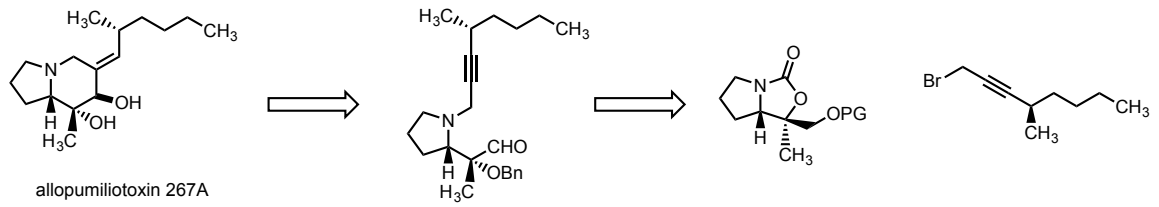

Scheme 1.10 – Allopumiliotoxin 267A retrosynthetic scheme

Substrate sensitivity in the synthesis of the allopumiliotoxin series required the use of a milder reducing agent than diethyl zinc. Using silanes as a reducing agent proved to be mild enough for the synthesis, and provides a conveniently protected allylic alcohol (Scheme 1.11). Easily deprotected under a variety of conditions, the use of silanes provides an attractive method for reductive coupling.

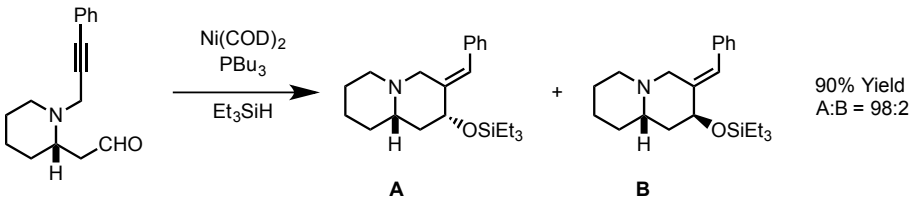

Scheme 1.11 – Silane used as reducing agent in the synthesis of Allopumiliotoxin

In addition to use as a protecting group, silicon-carbon bonds are attractive precursors to a variety of cross-coupling reactions. The use of a dialkylsilane in a reductive coupling allows for access to highly functionalized silacycles as well as access to deoxygenated products.[36] The formation of deoxygenated products was enacted through a decomposition of siloxane intermediates isolated in the reductive coupling of aldehydes and alkynes using dialkylsilanes (Scheme 1.12). However, initial difficulties in the synthesis of the silacycle products, coupled with advances in the use of NHC ligands within the Montgomery laboratory, led to the optimization of a method to synthesize a variety of silacycles (Scheme 1.13).

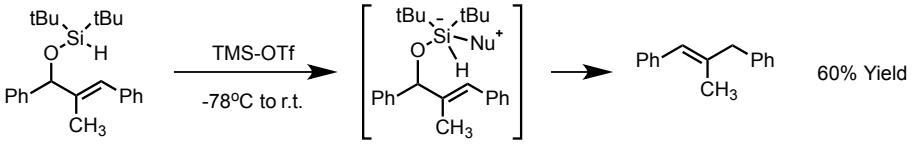

Scheme 1.12 – Siloxanes leading to the production of deoxygenated products

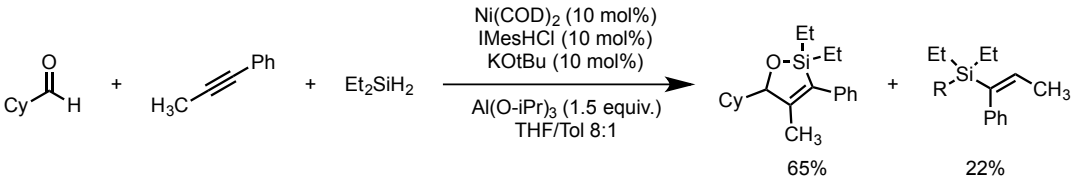

Scheme 1.13 – Use of dialkylsilanes in the synthesis of silacycles

As a ligand class gaining traction in organometallic transformations, the use of NHC ligands with nickel in the reductive coupling of aldehydes and alkynes proved to be a robust catalyst system (Scheme 1.14).[37] In addition to high turnovers and a wide substrate scope, the use of NHC ligands exhibited divergent mechanistic behavior, giving drastically different results in a series of double-labeling experiments. At the time, these discrepancies led to the hypothesis that the mechanistic pathways of the phosphine and NHC ligated systems were fundamentally different. The relationship of the proposed mechanistic pathways will be further explored in Chapter 2.

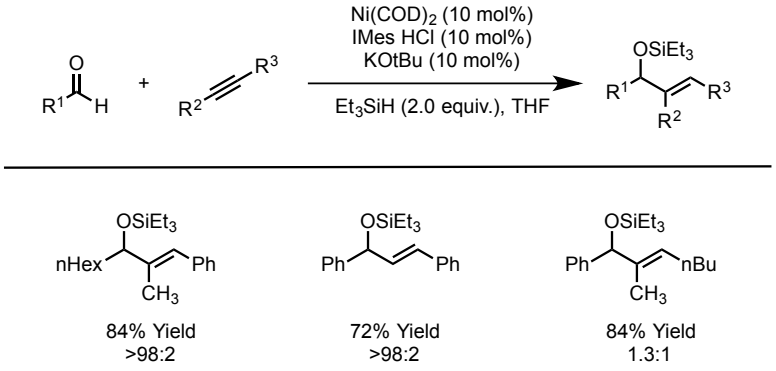

Scheme 1.14 – Initial application of Ni-NHC catalysis to reductive coupling

The continued development of NHCs as ligands in the reductive coupling led to a steric-controlled coupling reaction that proved to be exceptionally regioselective (Figure 1.04).[38] The use of a ligand that places a large steric group proximate to the nickel center was found to form the previously observed minor product. This trend was found to be

extremely general, even allowing for the selective synthesis of a single regioisomer, over-riding the innate bias of the substrates. Computational studies were performed to provide further insight into the role of steric encumberance on product selectivity in the NHC-Ni catalyzed system.[39]

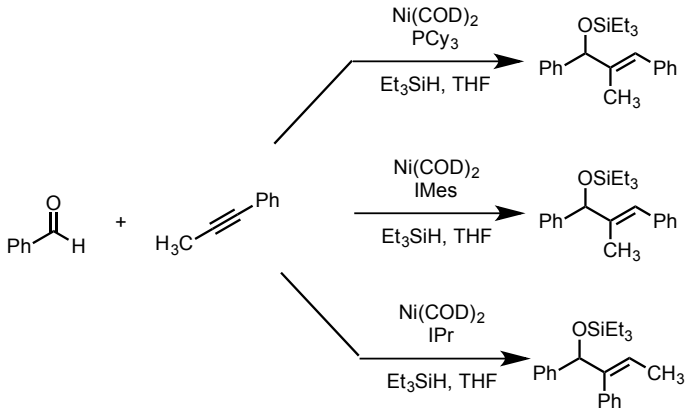

Figure 1.04 – Selectivity difference in the use of phosphine and NHC ligands in reductive coupling

The selectivity is predicted to arise from the steric bulk of the NHC ligand interacting with the aldehyde and alkyne bound to the nickel center (Figure 1.05). As the bulk is increased, the selectivity shifts towards the internally substituted products. These regioisomers would be difficult to synthesize using phosphine catalysts, but due to the nature of the bond between the nickel center and the NHC, good regioselectivities can be observed.

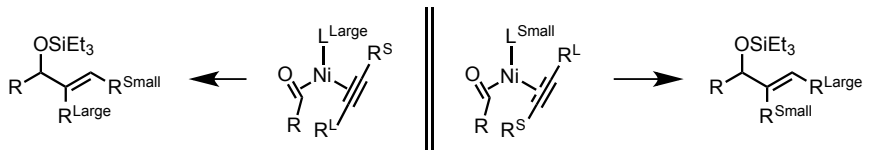

Figure 1.05 – Model for selectivity using NHC ligands for reductive coupling

1.3.7 Reductive Coupling in Divergent Total Syntheses

After the development of the nickel-NHC reductive coupling method, the synthesis of structurally related natural products was carried out, differing from a late-stage cyclization of an ynal substrate. Natural product YC-17 is a known partner in PikC oxidations, which has been extensively studied and modified. By diverting into the exocyclic alkene homologue of YC-17, specific structural considerations can be probed in the oxidation catalyzed by PikC. The use of a very large NHC, DP-IPr, allowed for the selective synthesis of this homologue as well as the application of a smaller NHC to synthesize the natural product (Scheme 1.15).[40]

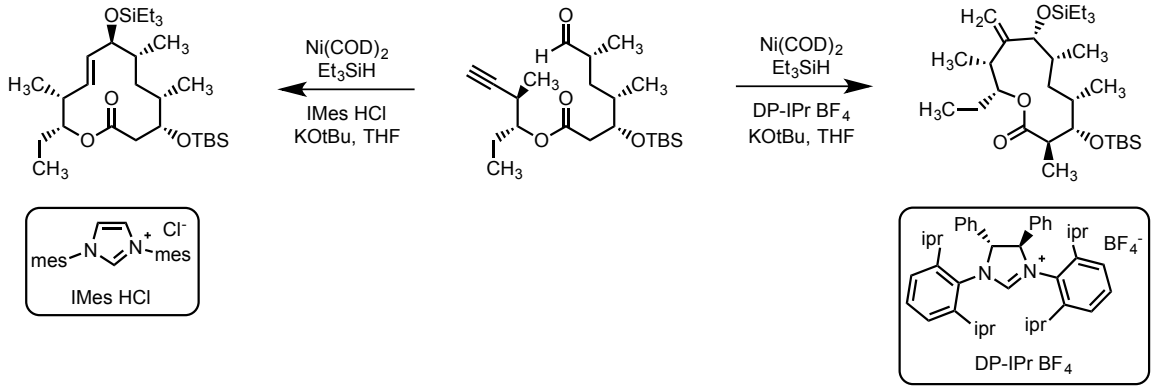

Scheme 1.15 – Synthesis of macrocycle YC-17 and the exocyclic alkene homologue

1.4.0 Nickel Cross-Coupling Reactions

In addition to reductive couplings, the use of nickel in a variety of well-known transition metal-catalyzed processes has been developed. Many methods developed using palladium catalysis have been found to transfer well to the use of nickel catalysts, with unique challenges and applications arising as a part of changing the identity of the metal center. Despite these challenges, the versatility and control imparted by developments in the use of NHC ligands have transformed nickel into a viable catalyst for numerous coupling reactions.

1.4.1 Nickel-NHC Catalysis in Kumada Coupling

An efficient method for the synthesis of carbon-carbon bonds utilizing nickel catalysis is the Kumada-Corriu coupling, first pioneered by Herrmann using a nickel-NHC catalyst (Scheme 1.16).[41] In the seminal report, Herrmann reports on the effective coupling of numerous aryl chlorides with various aryl Grignard reagents to yield biaryl products. Later development expanded the methodology to include the use of aryl

fluorides as coupling partner.[42] A preformed nickel-NHC catalyst also provided analogous results compared with *in situ* generation of the catalyst.

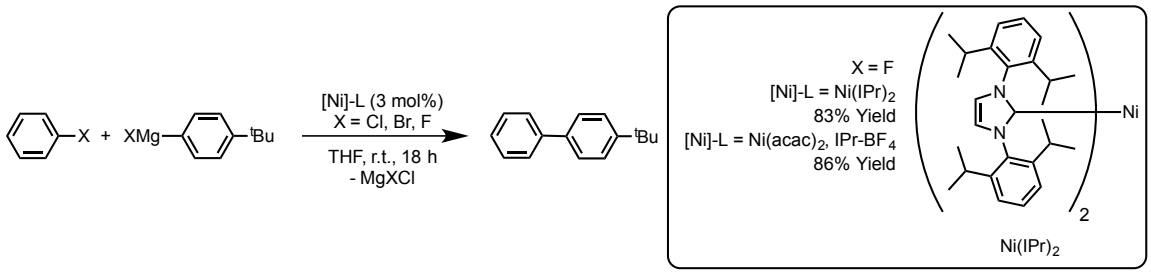

Scheme 1.16 – Kumada coupling catalyzed by a nickel-NHC complex

The scope of nickel-catalyzed Kumada couplings was further expanded to include heteroaryl halides in the work of Fürstner.[43] The substrate scope was expanded by the use of a new class of isolable nickel-NHC complexes bearing different ligand frameworks (Figure 1.06). These variations in ligand composition proved to increase the scope of nickel-catalyzed Kumada couplings.

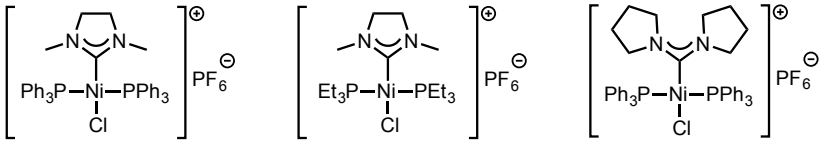

Figure 1.06 –NHC-Ni complexes used for various Kumada couplings

Aryl sulfamates are another class of electrophiles utilized in various cross-coupling reactions, expanding the scope of substrate classes productive in the formation of biaryl compounds (Scheme 1.17).[44]

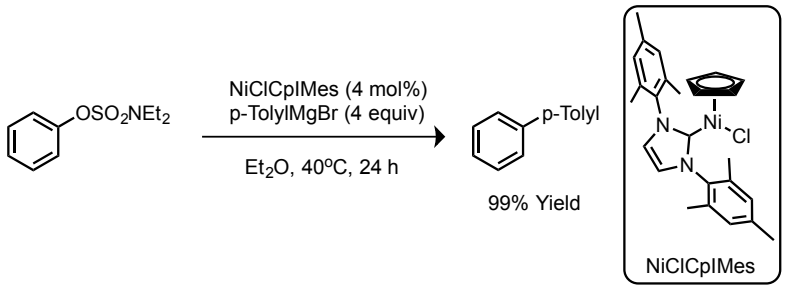

Scheme 1.17 – Use of sulfamates in Kumada couplings

New catalyst structures continued to drive the development of nickel-catalyzed Kumada couplings (Figure 1.07). An interesting catalyst bearing both an NHC as well as a triphenylphosphine ligand was developed for use in Kumada couplings.[45] The enhanced reactivity observed was credited to the lability of the phosphine ligand in solution, while serving to stabilize the catalyst outside of the catalytic cycle. Other catalysts developed by Inamoto[46] and Chen[47,48,49] allowed for a catalyst loading as low as 0.5%.

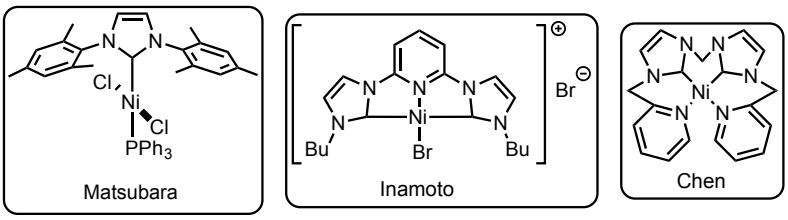

Figure 1.07 – Catalysts developed to lower loading required

Mechanistic understanding of the Kumada coupling was expanded by the isolation of a nickel(I) intermediate by Matsubara (Scheme 1.18),[50] and further investigated by Louie.[51] A number of experiments support the mechanistic hypothesis involving the generation of a nickel(I) species in the reaction between nickel(0)-NHC complexes with aryl-halides. Further studies show that this proposed species can serve to

catalyze a number of carbon-carbon bond-forming reactions, suggesting it to be a viable intermediate in a number of Kumada couplings.

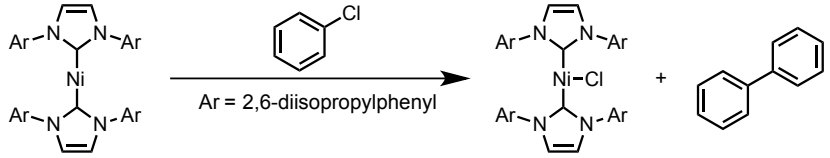

Scheme 1.18 – Nickel(I)-NHC complexes; potential intermediates in Kumada couplings

1.4.2 Nickel-NHC Catalysis in Buchwald-Hartwig Coupling

The first report of using nickel catalysis in the formation of carbon-nitrogen bonds came from the work of Fort.[52] Following the initial report, an expansion of scope and reactivity was described, which explored the viability of a number of NHC ligands employed in the reaction.[53] This study showed the effective coupling of numerous secondary and aryl amines with aryl chlorides (Scheme 1.19). An intramolecular variant was also explored in the synthesis of various heterocycles.[54] Spectroscopic studies were carried out by Schneider, which elucidated the resting state of the nickel catalyst in the proposed reactions as having two NHC units bound to the nickel center.[55]

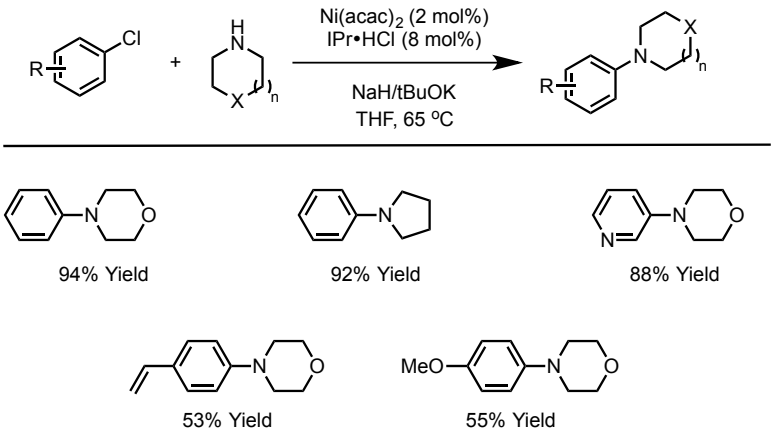

Scheme 1.19 – Nickel-catalyzed haloarene amination

The scope of *N*-arylation reactions was greatly expanded through the exploration of different coupling partners (Figure 1.08). Utilizing carbamates[56] as the electrophilic coupling partner allowed for the cleavage of a carbon-oxygen bond in the process of forming the carbon nitrogen bond. In addition to carbamates, a wide range of sulfamates,[57,58] tosylates,[59] and phosphates have also been reported as effective coupling partners.

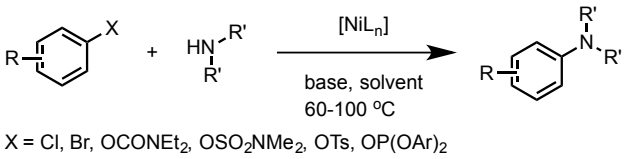

Figure 1.08 – Other electrophilic components used in C-N bond formations

1.5.0 Nickel-NHC Systems as a Catalyst for Related Coupling Reactions

The synthesis of thioethers has been developed using various nickel-NHC complexes. The first report by Ying[60] highlighted the ability of a nickel catalyst to couple thiophenol with a variety of aryl bromides and iodides, producing high yields of diaryl thioethers. The use of a recyclable nickel-NHC catalyst was also used in the

formation of carbon-sulfur bonds, but was still restricted to the synthesis of diaryl thioethers.[61] Well-defined allyl nickel complexes were shown to be efficient for both the formation of carbon-sulfur and carbon-nitrogen bonds.[62] However, *in situ* catalyst generation allowed for the synthesis of a wide range of aryl thioethers, including the use of benzyl and aliphatic thiols (Scheme 1.20).[63]

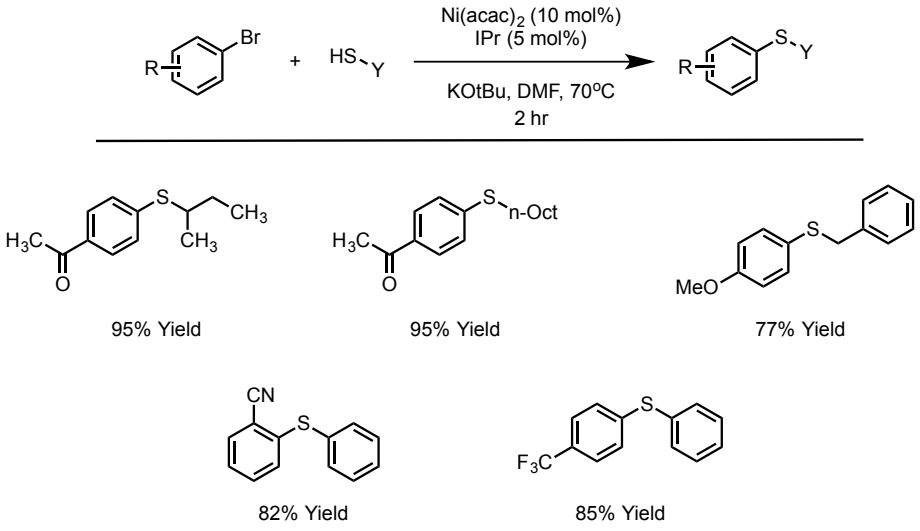

Scheme 1.20 – Nickel catalyzed carbon-sulfur bond formation

The oxidation of alcohols to the corresponding aldehyde or ketone has also been established. In a related process to the dehalogenation of arenes, secondary alcohols can be oxidized to the corresponding ketone using an aryl chloride as the oxidant.[64,65] Notably, a bench-stable nickel(0) catalyst could be used in the reaction, although reaction times increased (Scheme 1.21). Use of primary alcohols was reported by Itami and co-workers in a one pot sequence in which a primary alcohol could be oxidized and then consumed by 1,2-addition of an organoboronate ester, resulting in either the ketone from primary alcohols or tertiary alcohols starting from secondary alcohols.[66] This sequence can be used iteratively to generate tertiary alcohols from primary alcohols.

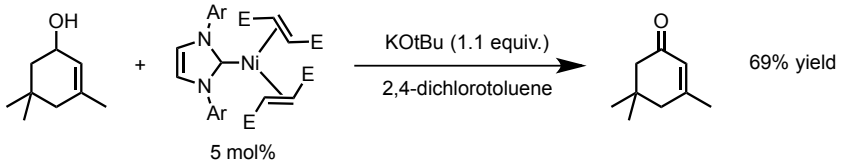

Scheme 1.21 – Oxidation of alcohols catalyzed by nickel

In parallel with the reductive coupling of aldehydes and alkynes, nickel catalysis has been shown to be effective in the hydrosilylation of alkynes[67] as well as allenes,[68] allowing for the highly selective formation of allyl and vinyl silanes. The use of a nickel catalyst has allowed for the highly selective hydrosilylation of ketones,[69] using a carbohydrate based silane, which allows for the synthesis of functionalized carbohydrates (Scheme 1.22). This process is tolerant of orthogonal functional groups, which can be manipulated using different metal catalyst systems for further functionalization.

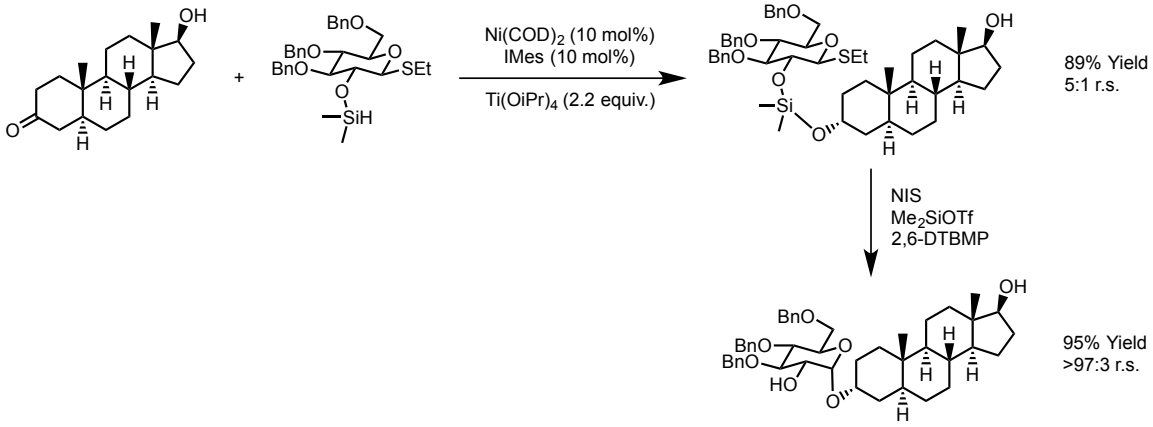

Scheme 1.22 – Ketone hydrosilylation for the regioselective synthesis of functionalized carbohydrates

Nickel has been shown to be effective in an array of cycloaddition reactions. The use of CO_2[70,71] or an aldehyde[72,73] in a [2+2+2] cycloaddition has been established as an effective route in the synthesis of highly substituted polycycles (Figure 1.09). Related

methods have been developed for the synthesis of heterocycles, arising from the analogous cyclization involving isocyanate,[74,75,] cyano,[76] or cyanamide[77] functionalities.

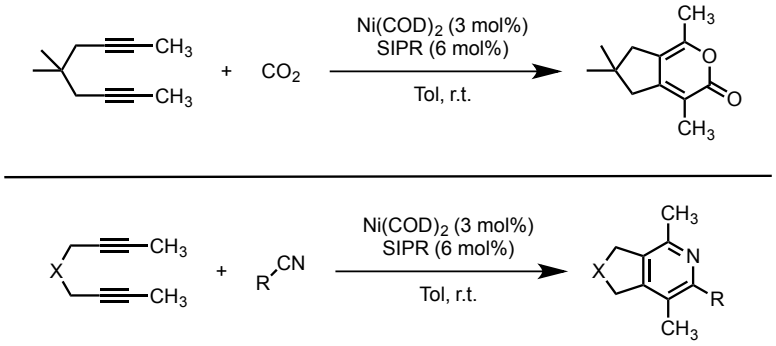

Figure 1.09 – Nickel catalyzed [2+2+2] cycloaddition

1.6.0 Directions for the Development and Application of Nickel Catalysis

Applications of nickel catalysis to a wide variety of reductive couplings have created a powerful method capable of synthesizing different structural variations from simple starting materials. Through the process of development, a number of interesting mechanistic details have been reported, but a comprehensive understanding of the factors related to reductive coupling has not been proposed. The mechanistic investigation of reductive couplings would provide insight into the details pertinent to the transformation, and subsequently allow for the further development and application as a synthetic tool. An investigation into the various substrate and catalyst factors that influence the mechanism for reductive coupling will be presented in Chapter 2.

Along with developments in reductive coupling, the use of NHC ligands in nickel-catalyzed processes has been greatly developed and expanded. The use of highly functionalized and tailored ligands has allowed for excellent selectivity and reactivity in a number of complex transformations. However, a number of these transformations

require the generation of the active catalyst *in situ*, leaving a myriad of potential activation steps in the formation of the catalyst unknown. Further developments into the synthesis and application of functionalized discrete nickel catalysts will allow for the creation of a more general method for nickel-catalyzed transformations, these efforts will be presented in Chapter 3.

Chapter 2: An Experimental and Theoretical Mechanistic Evaluation of Silane-Mediated, Nickel-Catalyzed Aldehyde-Alkyne Reductive Couplings

2.0.0 Reductive Coupling Mechanistic Developments

2.0.1 Double-Labeling Experiments Used to Understand Organometallic Reaction Mechanisms

The use of double-labeling experiments is a common practice to probe mechanisms where fragmentation may occur; it can provide insight into the molecularity of intermediates as well as distinguish dissociation events in metal-catalyzed reactions. At the core of a double-labeling, or "crossover", experiment is the use of similar materials that are each labeled to follow the respective components throughout the course of a reaction (Figure 2.01). By analyzing the product ratios, information about the mechanism can be deduced.

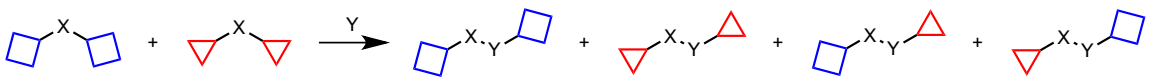

Figure 2.01 – Double-labeling Experiment

The use of double-labeling experiments can provide deeper mechanistic understanding for organometallic transformations, where dissociation and transmetallation steps can complicate proposed mechanisms of reaction. One investigation utilizing double-labeling experiments is the investigation into the reductive elimination of a platinum catalyst in the generation of methane (Scheme 2.01).[78] To determine the ability of the platinum catalyst to exchange hydrides, a double labeling study was performed. It was found that almost no crossover products were observed, providing support for a reaction mechanism proceeding through a unimolecular pathway without opportunity for exchange between metal centers.

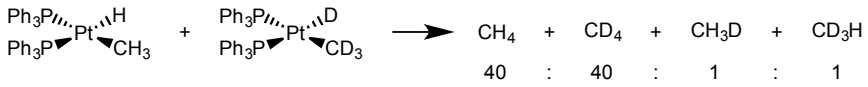

Scheme 2.01 – Double-labeling Organometallic Experiment

In addition to organometallic transformations, double-labeling experiments can provide insight into the possible fragmentation of reactants in the reactive pathway. To understand reductions of organic peroxides to the corresponding alcohols, a double-labeling study was constructed to follow the silyl protecting group through the course of the reaction (Scheme 2.02).[79] No significant formation of crossover products was observed, indicating that fragmentation and dissociation of the peroxide was not a reasonable mechanism. As with all evidence regarding reaction mechanisms, crossover

experiments are capable of providing insight into potential mechanistic pathways and excluding proposed mechanisms but cannot provide prove a single pathway to be correct.

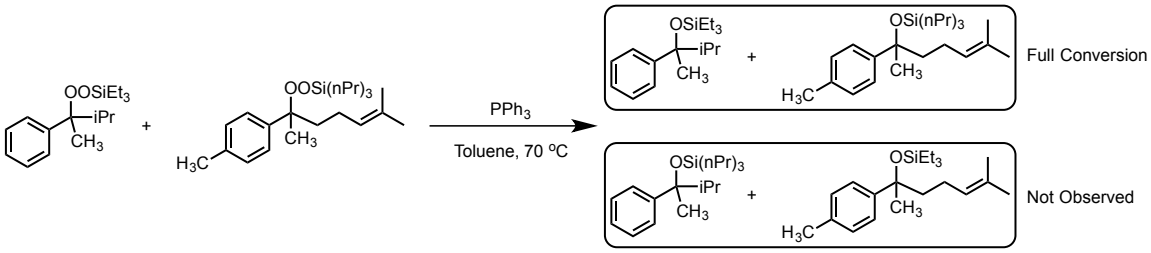

Scheme 2.02 – Substrate-based Double-Labeling Experiment

2.0.2 Mechanistic Disparity in the Results of Double-Labeling Experiments for Nickel-Catalyzed Reductive Coupling

During the initial investigation into the use of NHC's as potential ligands for nickel-catalyzed reductive couplings, an interesting disparity was observed in the results of a series of double-labeling experiments between phosphine-ligated systems and NHC-ligated systems. In the presence of triethylsilyl-deuteride and tripropylsilane, a reductive coupling mediated by a phosphine-nickel complex gave a near statistical mixture of all four possible products, however the use of an NHC-nickel catalyst system provided no noticeable presence of the crossover products (Table 2.01).

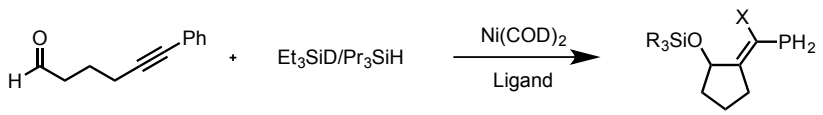

Ligand	R = Et, X =H	R = Et, X =D	R = Pr, X =H	R = Pr, X =D
IMes	<2	55	41	<2
PBu_3	25	34	23	18

Table 2.01 – Double-labeling results comparing phosphine and NHC catalyst systems

With mechanistic evaluation being difficult, a working hypothesis was developed that, while the products are identical for most reductive coupling, the reactive pathways for the NHC and phosphine system must be fundamentally different. Four potential pathways were described that could account for the observed results from the double – labeling experiments and be consistent with data gathered for similar systems. The key difference proposed between pathways lies in the interaction of the nickel catalyst and the silane reducing agent.

For pathways that could provide significant amounts of crossover products, the active catalyst would either be a nickel(0) complex or a formal nickel(II) complex resulting from a formal insertion into the silicon-hydride bond of the silane (Figure 2.02). In pathway A, the nickel(0) would undergo an oxidative cyclization yielding a metallacycle which would subsequently undergo a σ-bond metathesis with the silane, liberating the silyl-protected allylic alcohol and regenerating the catalyst. Proposed pathway B would begin with an insertion into the silicon-hydride bond, followed by insertion into the alkyne, analogous to previously reported hydrosilylations catalyzed by nickel. This insertion product would then coordinate and subsequently insert into the carbonyl of an aldehyde in solution, liberating a nickel(0) catalyst which would re-enter the catalytic cycle upon insertion into the silicon-hydride bond of the silane. Both

mechanisms show the incorporation of the silane and the corresponding hydride or deuteride into a single molecule of product.

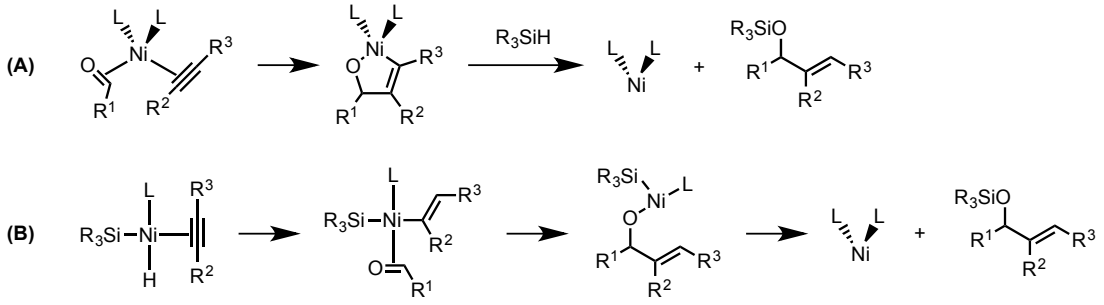

Figure 2.02 – Proposed pathways resulting in no crossover product formation

Analogous to the previously proposed pathways, pathways that would generate crossover products were proposed (Figure 2.03). These pathways begin from potential nickel(I) species that can be envisioned to form in solution under the reaction conditions. In the first pathway, either a neutral nickel(I) species or a cationic nickel(I) would undergo an insertion into an alkyne. This vinyl nickel complex would then subsequently react with a unit of aldehyde generating the common alkoxy-nickel intermediate. An alternative proposed pathway also begins with a nickel(I) catalyst bound to a both an aldehyde and alkyne unit, before undergoing an oxidative cyclization in a proposed nickel(I) to nickel(III) cycle. This metallacycle would reductively eliminate the hydrogen atom to the vinyl position to arrive at the common nickel species. This alkoxy-nickel complex could react with a new unit of either silane to regenerate the corresponding silyl-protected allylic alcohol and the nickel-hydride catalyst. The proposed mechanism pathways show the separation of a silyl group and the corresponding hydride or deuteride, leading to incorporation of each fragment into different molecules of product.

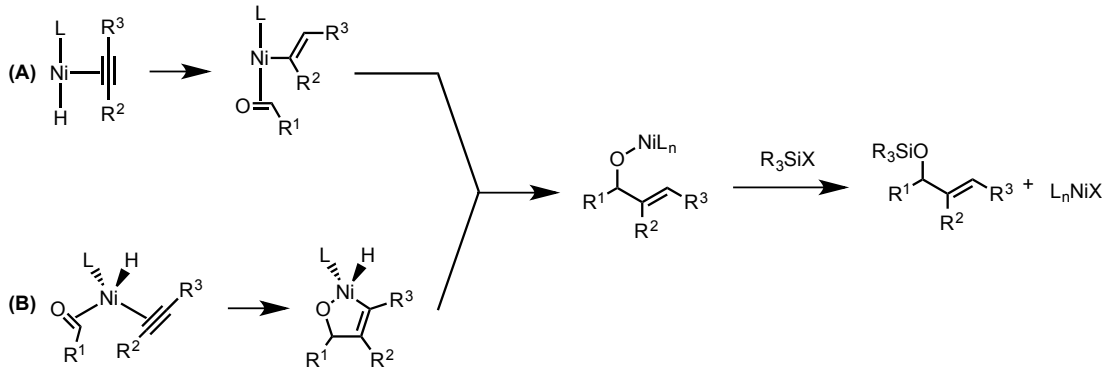

Figure 2.03 – Proposed pathways resulting in the formation of crossover products

2.0.3 Synthesis of Dimeric Metallacycle

In 2008, Ogoshi and coworkers isolated a dimeric metallacycle intermediate under conditions analogous to those used in the reductive coupling of aldehydes and alkynes (Scheme 2.03).[80] Derived from the cyclization of benzaldehyde and 2-butyne in the absence of a reducing agent, the resulting metallacycle can dimerize to a stable metallacycle.

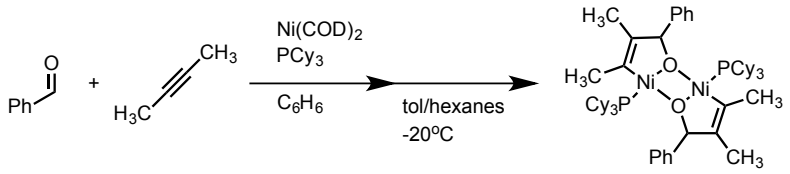

Scheme 2.03 – Synthesis of Dimeric Metallacycle

The dimeric metallacycle was shown to undergo reduction using dialkyl zinc as the reducing agent (Scheme 2.04). However, in contrast to known methodology, the reduction requires forcing conditions including a large excess of aldehyde and additional phosphine ligand. When the dimeric metallacycle was treated with dimethylzinc directly, no reduction was observed. The need for additional phosphine and aldehyde was not

explained, but presumably serves to coordinate to the complex in solution and dissociate larger aggregate structures of the metallacycle to undergo further reactivity.

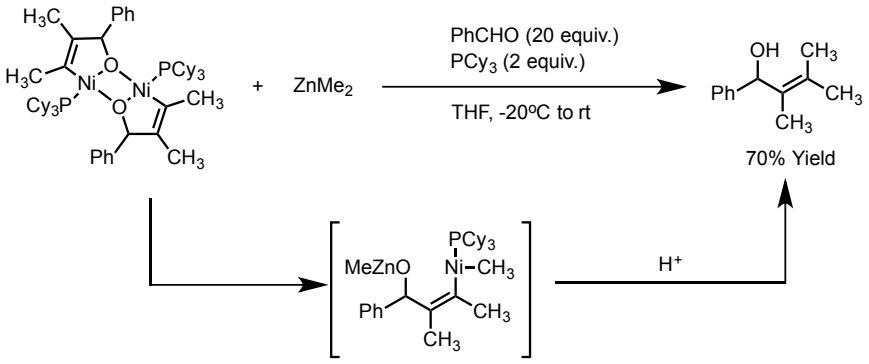

Scheme 2.04 – Reactivity of Dimeric Metallacycle with dimethyl-zinc

In addition to reduction by alkylzinc reagents, the dimeric metallacycle was found to undergo carbonylation under an atmosphere of carbon monoxide, as well as a thermal degradation pathway providing α,β-unsaturated carbonyl complexes (Scheme 2.05).

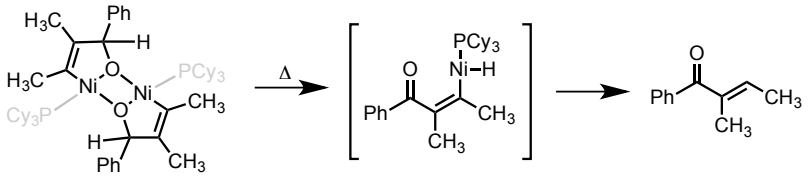

Scheme 2.05 – Thermal degradation of dimeric nickel metallacycle

A synthetic approach for the use of the thermal degradation pathway was proposed and investigated by Dr. Ryan Baxter in the Montgomery research group in a series of hydroacylation reactions (Scheme 2.06). It was found that outside of a few specific examples, the formation of desired products required the use of a microwave reactor. These intense reaction conditions are not tolerant of more delicate functionality, limiting the applicability of the method to organic synthesis.

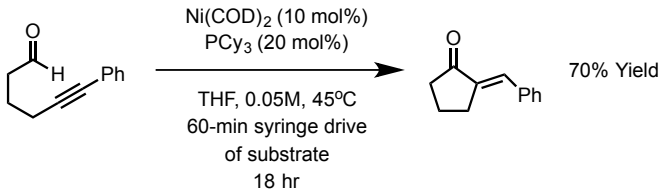

Scheme 2.06 – Hydroacylation development from the Montgomery Laboratory

2.0.4 Kinetic Profile of Intramolecular Reductive Coupling

Mechanistic studies into the reductive cyclization of ynal substrates were reported in 2012.[81] Using a ReactIR to follow the reaction progress, it was found that there was a first order dependence on both the ynal substrate as well as the catalyst employed (Figure 2.04). The reaction was found to also have a zero-order dependence on silane concentration. This led to the proposal of a mechanism where the oxidative cyclization of ynal was the rate-limiting step, followed by coordination and σ-bond metathesis with the silane.

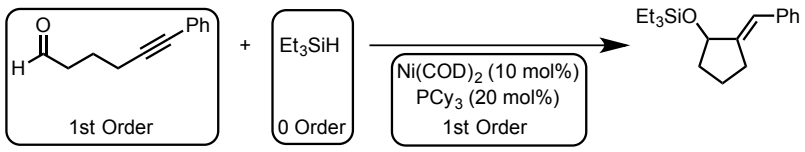

Figure 2.04 – Kinetic profile for intramolecular reductive coupling

Alternative mechanisms were proposed consistent with the kinetic profile constructed for the reagents in the reductive coupling that involved the silane in different capacities. To address these potential pathways, a series of silane consumption experiments were performed (Scheme 2.07). It was found that the silane was unaffected by the presence of the nickel catalyst in solution, ruling out the initial insertion of the nickel catalyst into the silicon-hydride bond of the silane, resulting in a formal nickel(II)

intermediate as the resting state. Further experiments showed that hydrosilylation of either the aldehyde, alkyne, or ynal substrates were not operating in the reaction conditions. All of the consumption experiments provide evidence for a mechanism supporting a rate-limiting oxidative cyclization for ynal substrates employing a nickel-phosphine catalyst system.

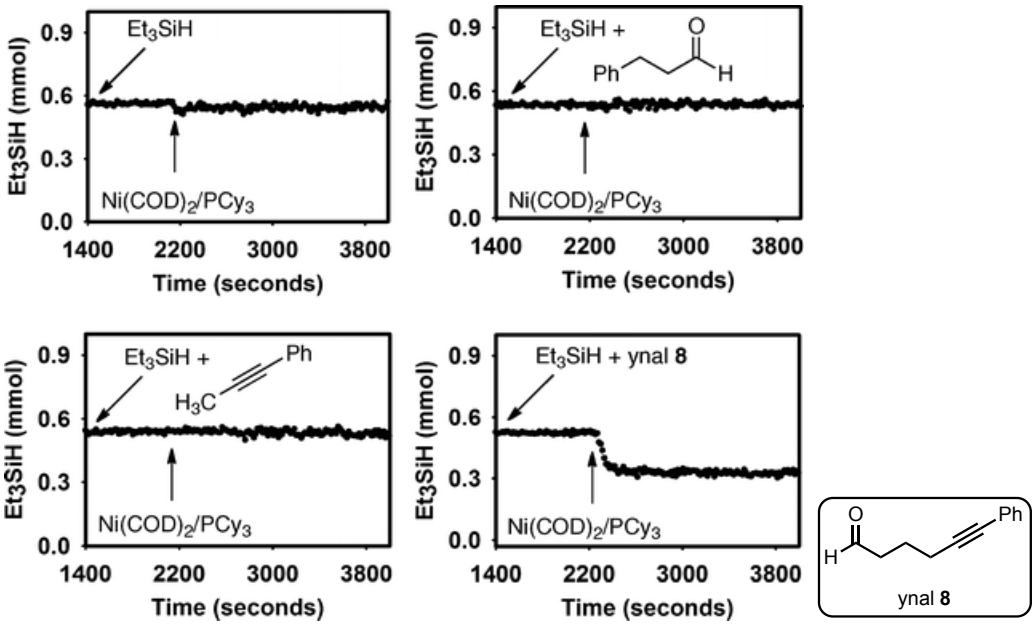

Scheme 2.07 – Silane consumption experiments

2.1.0 Unified Mechanistic Proposal

2.1.1 Proposed Catalytic Cycle for Nickel-Catalyzed Reductive Coupling of Aldehydes and Alkynes

Combining the evidence put forth by kinetic analysis with the isolation and characterization of the dimeric metallacycle species by Ogoshi, a unified mechanistic picture can be constructed that provides insight into the reductive coupling of aldehydes and alkynes (Figure 2.05). The mechanism is proposed to undergo an oxidative

cyclization to generate a monomeric nickel metallacycle, which exists in equilibrium with the dimeric metallacycle. From either metallacycle, association with silane and subsequent σ-bond metathesis will generate the observed silyl protected allylic alcohols, and liberate the catalyst to re-enter the catalytic cycle.

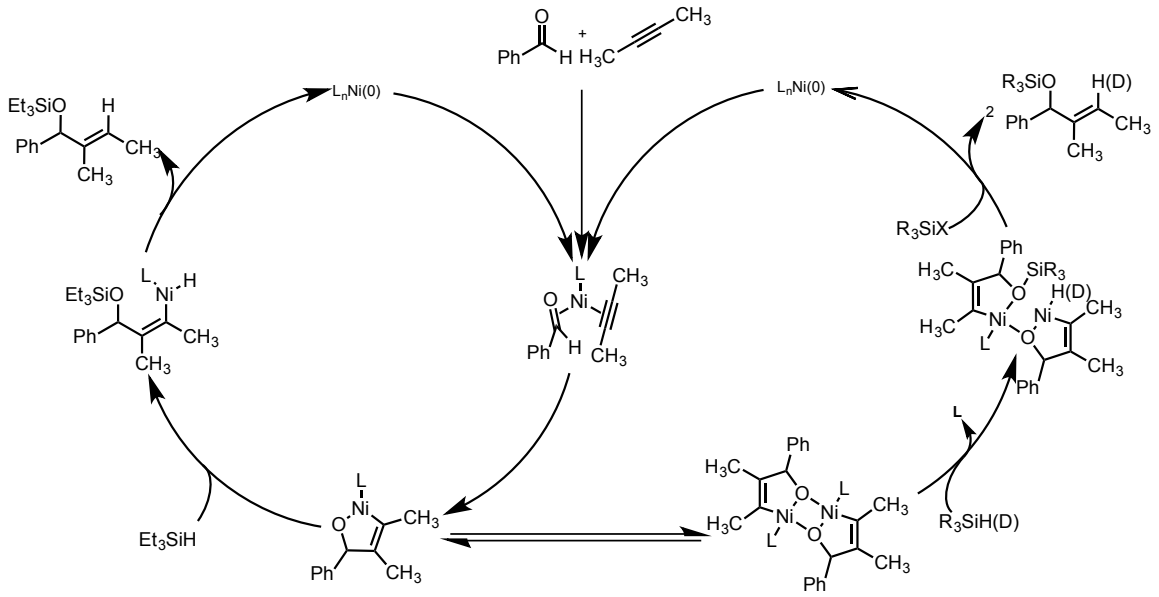

Figure 2.05 – Unified Mechanism, unifying kinetics profile with dimeric metallacycle

2.1.2 Double-Labeling Study as a means to Understand Post-Rate Limiting Factors

Recent mechanistic developments into the reductive coupling of aldehydes and alkynes allow for a single mechanistic proposal for both the phosphine-ligated pathway and the NHC-ligated pathway. Where the initial report proposed fundamentally different pathways to explain changes in product distribution, the existence of the dimeric metallacycle provides an explanation for the disparity. The mechanistic picture consists of two fundamental pathways, where the monomeric metallacycle pathway will incorporate both the silyl group and the corresponding hydride or deuteride into a single

molecule of product resulting in no formation of crossover products, or an alternative pathway where the dimeric metallacycle will allow for the separation of the silyl component and the corresponding hydride or deuteride into different molecules of product (Figure 2.06). With this operating mechanism, the steric bulk and strong binding affinity of NHC ligands would prevent dimerization of the metallacycle, forcing the reaction to only occur via the monomeric metallacycle pathway. In contrast, the smaller and more labile phosphine ligated systems can dimerize depending on a number of substrate factors. However, directly analyzing the effects of potential metallacycle dimerization is made difficult because these intermediates are proposed to occur after the rate-limiting step of the reaction.

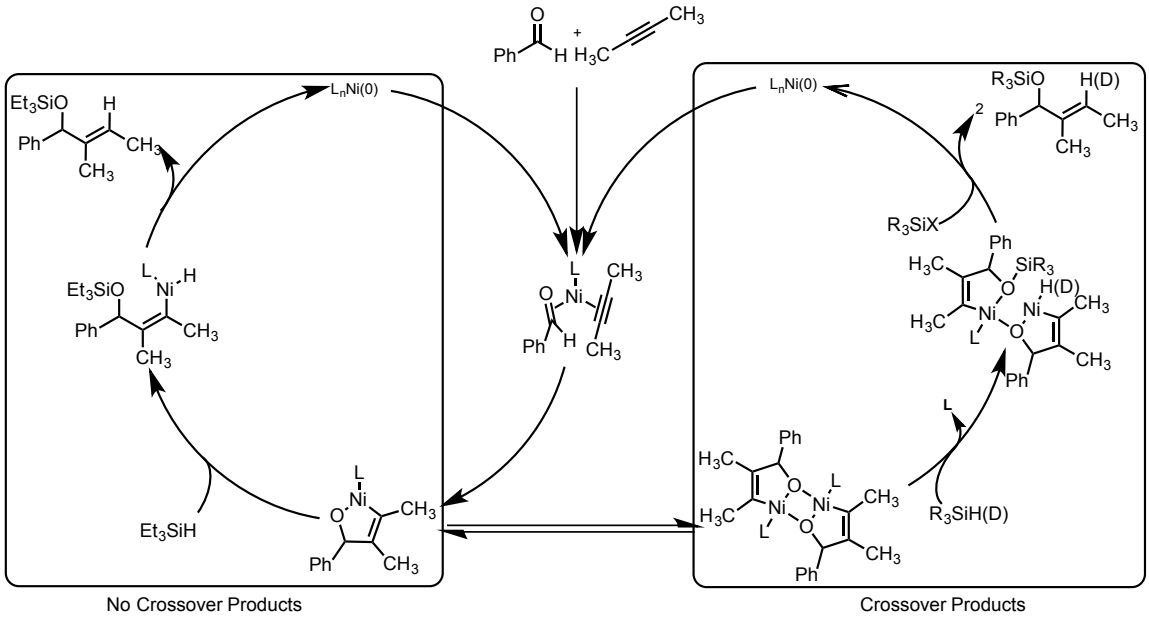

Figure 2.06 – Divergent routes leading to crossover products or non-crossover products

Double-labeling experiments can be used to understand the implications of dimerization of the metallacycle in solution, despite occurring after the rate-limiting step. There are two principle steps that will be probed in their influence over the formation of

the dimeric metallacycle: the oxidative cyclization step to form the monomer, and the equilibrium between the monomeric and dimeric metallacycles (Figure 2.07). Measuring the total crossover of each reaction serves as an indication of the degree of dimeric metallacycle formation.

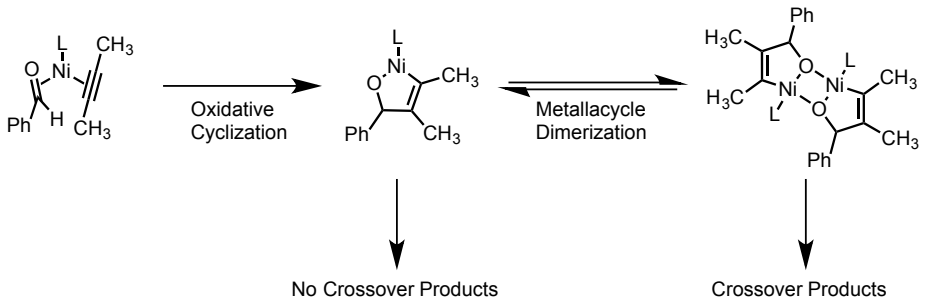

Figure 2.07 – Altering proposed steps effects on the generation of crossover products

2.1.3 Utility of Mass Spectrometry Methods over Traditional Methods in Analysis of Double-Labeling Study

The analysis of the crossover products was conducted using mass spectrometry methods, as previously reported in the studies on the reductive coupling of aldehydes and alkynes. To gain meaningful data in a double-labeling experiment, the differences between the reagents (in this case, silanes) needs to be minimized; each silane must have similar steric and electronic parameters that would allow them to react in near equal proportions and at similar rates with the substrates. This similarity hinders the use of NMR analysis, where the resulting products would all be similar enough that any diagnostic resonances may be overlapping, making analysis difficult. However, the use of mass spectrometry allows for the composition of products to be derived based upon ion ratios of pre-synthesized authentic samples of each potential product.

2.2.0 System changes effecting the energetics of the reactive pathway

Altering the formation of the metallacycle through changes to two fundamental steps will allow further understanding of factors related to the dimerization event in the mechanism for the reductive coupling of aldehydes and alkynes. First, the effects of changing specific factors related to the oxidative cyclization will be discussed. By disfavoring the formation of the monomeric metallacycle in solution through a variety of alterations, the influence of the dimeric metallacycle on the productive reaction pathway will be investigated (Figure 2.08).

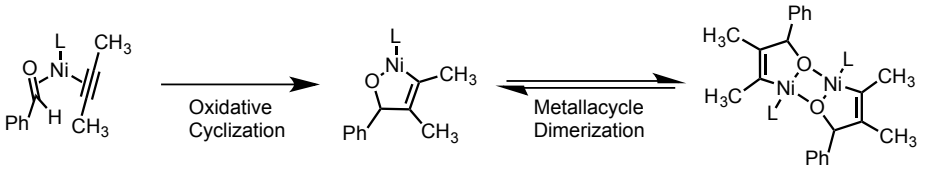

Figure 2.08 – Altering the effective concentration of the metallacycle by altering factors related to the rate limiting step

2.2.1 Substituent effects on the oxidative cyclization of aldehydes and alkynes

Alterations to the nature of the aldehyde and alkyne will have a dramatic effect on the energetics of the oxidative cyclization. Through disfavoring the formation of the monomeric metallacycle, the observable effects (crossover product formation) of the dimeric mechanistic pathway will be minimized. Changes in the intramolecular cyclization through expansion of the ring size being formed, as well as the impact of molecularity on the reductive coupling of aldehydes and alkynes are indicative of the control the substrate constitution has over the formation of crossover products (Figure 2.09).

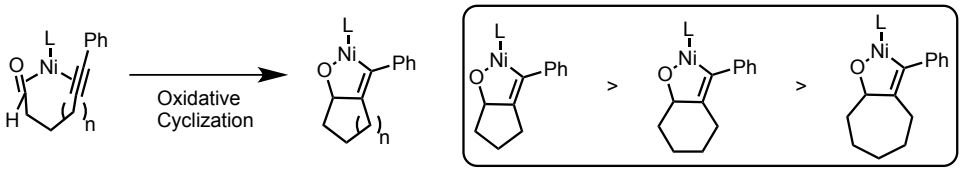

Figure 2.09 – Effect of ring size on energy of oxidative cyclization

The energy required to cyclize larger ring systems will directly alter the energy required for oxidative cyclization. The use of longer alkyl chain ynal substrates will result in lower amounts of observed crossover products due to a disfavored oxidative cyclization step. For systems of relatively similar energies, the formation of five and six membered rings, the amount of crossover products formed is very similar. However, the formation of the more highly strained seven membered ring shows a significant decrease in the amount of crossover products formed (Table 2.02).

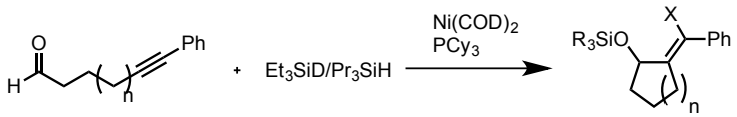

Entry	n	R = Et X = H	R = Et X = D	R = Pr X = H	R = Pr X = D	% Total Crossover
1	1	6	55	35	4	10
2	2	5	52	39	4	9
3	3	<1	57	41	<1	<2

Table 2.02 – Alteration of ring size on double-labeling experiments

In comparison to their intramolecular counterparts, the absence of chelation in an intermolecular reductive coupling will also manifest itself in the degree of crossover products formed. Inherently, the bimolecular nature of an intermolecular reductive coupling will manifest in a higher entropic cost of reaction. It was observed that intermolecular reductive couplings exhibited far less of the crossover products than the

corresponding intramolecular systems, with regards to the steric influence of the alkyne substitution (Table 2.03).

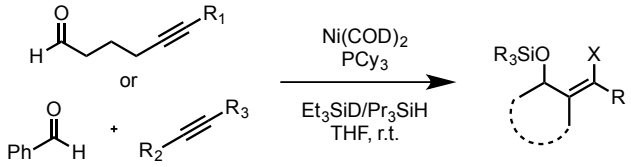

Entry	R1	R2	R3	R = Et X = H	R = Et X = D	R = Pr X = H	R = Pr X = D	% Total Crossover
1	Ph			6	55	35	4	10
2		Me	Ph	<1	59	39	<1	<2
3	Me			19	35	27	19	38
4		Me	Me	9	46	37	6	15

Table 2.03 – Molecularity changes to oxidative cyclization

2.2.2 Double-Labeling changes arising from changes in catalyst loading

Previous kinetic analysis of reductive couplings found the catalyst concentration to have a first-order effect on the rate of the reaction. It was hypothesized that by increasing the concentration of the catalyst, an increase in the concentration of the metallacycles would be observed. However, there was found to be little effect on the observance of crossover products based on changes in catalyst concentration (Table 2.04).

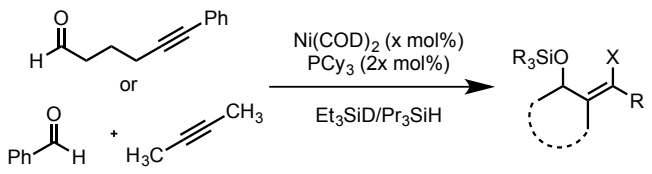

Entry	Substrate	X mol% $Ni(COD)_2$	R = Et X = H	R = Et X = D	R = Pr X = H	R = Pr X = D	% Total Crossover
1	ynal	10	6	55	35	4	10
2	ynal	20	7	54	34	5	12
3	Aldehyde/Alkyne	5	7	51	36	6	13
4	Aldehyde/Alkyne	10	9	46	35	8	17
5	Aldehyde/Alkyne	20	9	46	37	6	15

Table 2.04 – Catalyst concentration effects on double-labeling experiments

2.3.0 System alteration effects on stability of dimeric metallacyle

Changing conditions of the reaction can also serve to directly affect the ability or stability of the metallacycle in the dimerization event (Figure 2.10). Measuring the degree of crossover while changing the system will provide an indication of the relative importance of different factors related to the dimerization equilibrium.

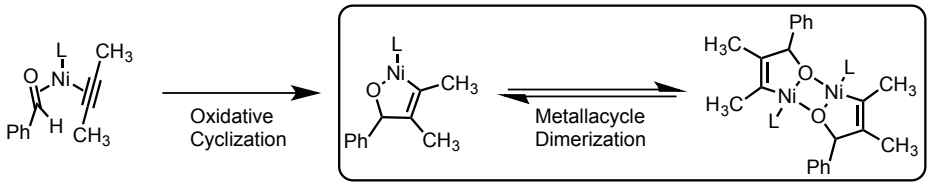

Figure 2.10 – Measuring crossover changes through altering equilibrium of metallacycles

2.3.1 Substrate/Ligand Interactions

Through alterations to the steric environment of the alkyne substituent or the phosphine ligand, the energy for dimerization of the metallacycle should be directly changed (Figure 2.11). Through the dimerization event, the substituent of the alkyne and

the phosphine ligand are moved into much closer proximity, thus an increase in size for either should disfavor the formation of the dimeric metallacycle.

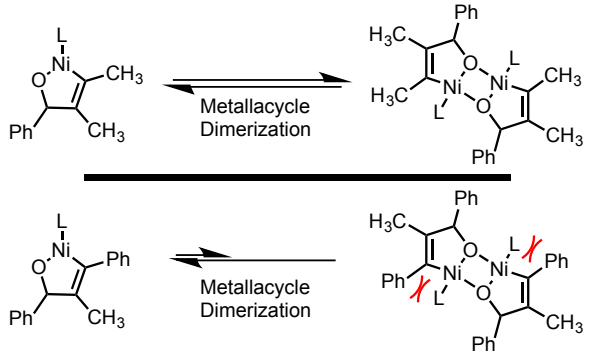

Figure 2.11 – Impact of alterations to substrate or ligand structure on the dimerization of metallacycle

Increasing the steric bulk of the alkyne substituent shows a marked decrease in the amount of crossover products formed in both intramolecular and intermolecular reductive couplings (Table 2.05). As the alkyne substitution for the series of ynals increases in size, ranging from a terminal alkyne to a bulky bis-substituted aryl, a severe decrease in the amount of crossover products formed is observed. Similarly in a series of intermolecular examples, the steric bulk of the alkyne substituent was directly related to the ratio of products formed.

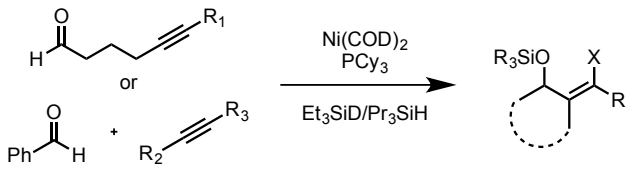

Entry	R1	R2	R3	R = Et X = H	R = Et X = D	R = Pr X = H	R = Pr X = D	% Total Crossover
1	H			22	30	32	16	38
2	Me			19	35	27	19	38
3	Ph			6	55	35	4	10
4	Ar			4	61	32	3	7
5		Me	Me	9	46	37	6	15
6		Et	Et	5	56	47	2	7
7		Me	Ph	<1	59	39	<1	<2

Ar = 3,5 ditertbutyl phenyl

Table 2.05 – Alkyne substitution effects on intramolecular double-labeling experiments

Increasing the bulk of the phosphine ligand also demonstrated an effect on the formation of crossover products in the double-labeling experiments (Table 2.06). Compared to the initial reports of crossover data, the increase in bulk from n-butyl to cyclohexyl phosphine showed a corresponding decrease in the formation of crossover products.

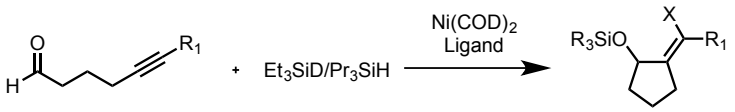

Entry	L	R1	R = Et X = H	R = Et X = D	R = Pr X = H	R = Pr X = D	% Total Crossover
1	PBu_3	Ph	22	37	27	14	36
2	PCy_3	Ph	6	55	35	4	10
3	PBu_3	Ar	26	34	24	16	38
4	PCy_3	Ar	4	61	32	3	7

Ar = 3,5 ditertbutyl phenyl

Table 2.06 – Ligand substitution effects on double-labeling experiments

2.3.2 Silane Concentration Effects on Double-Labeling Experiments

Following the investigation into the effects of catalyst concentration, the effects of silane concentration were investigated. It was hypothesized that an increase in the concentration of silane in solution would lead to a rapid consumption of the metallacycle before the dimerization could occur. However, it was observed that an increase in silane concentration was found to increase the amount of crossover products being formed for a few substrate systems (Table 2.07). One explanation for this trend is a comparison in the relative rates of silane σ-bond metathesis and dimerization of the metallacycle. Depending on the substrate employed, the dimerization event is fast compared to reaction with the silane. Therefore an increase in silane concentration would serve to increase the rate of dimer consumption, limiting the equilibrium back to the monomeric metallacycle.

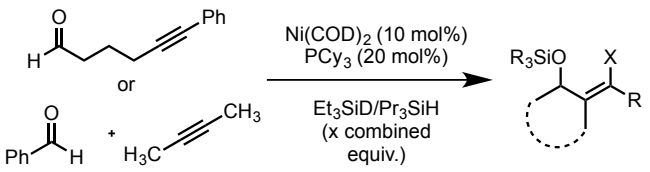

Entry	Substrate	X equiv. Silane	R = Et X = H	R = Et X = D	R = Pr X = H	R = Pr X = D	% Total Crossover
1	ynal	2	6	55	35	4	10
2	ynal	4	14	52	26	9	23
3	ynal	6	17	53	20	10	27
4	ynal	8	21	54	16	9	30
5	Aldehyde/Alkyne	2	9	46	35	8	17
6	Aldehyde/Alkyne	4	10	54	28	8	18
7	Aldehyde/Alkyne	8	19	50	21	10	29

Table 2.07 – Silane concentration effects on double-labeling experiments

2.3.3 Temperature Effects on Double-Labeling Experiments

The dimerization of the metallacycle does have a natural enthalpic stabilization, but entropic factors are also significant in the free energy changes in the system. The relationship of the free energy changes in an equilibrium can be directly correlated to the distribution of products. Through derivation of the Arrhenius equation, the role of temperature on an equilibrium can also be further explored. Lowering the temperature of reaction is directly correlated with a shift in the equilibrium towards the more stable product, in this example the dimeric metallacycle. Shifting the equilibrium towards the dimeric metallacycle should provide for an increase in the observance of crossover products.

As the temperature was lowered, the amount of crossover products increased significantly in all substrate systems. For both intramolecular (Table 2.08) and intermolecular (Table 2.09) systems, the equilibrium was shifted in favor of the dimeric metallacycle. Even in cases providing little crossover at room temperature, such as the

cyclization of the ynal providing a 7-membered ring, showed significant formation of crossover products at lowered temperatures.

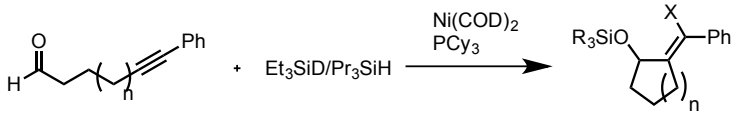

Entry	n	Temp (°C)	R = Et X = H	R = Et X = D	R = Pr X = H	R = Pr X = D	% Total Crossover
1	1	-25	26	36	24	24	50
2	1	0	7	58	40	5	12
3	1	25	6	55	35	4	10
4	1	45	4	55	37	4	8
5	2	-25	22	34	23	221	43
6	2	25	5	52	39	4	9
7	3	-25	10	52	33	5	15
8	3	25	<1	57	41	<1	<2

Table 2.08 – Temperature effects on double-labeling experiments, intramolecular reductive coupling

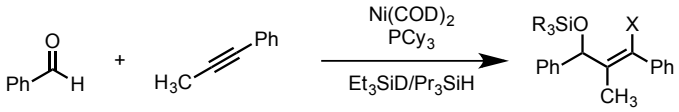

Entry	Temp (°C)	R = Et X = H	R = Et X = D	R = Pr X = H	R = Pr X = D	% Total Crossover
1	-25	6	46	42	6	12
2	25	<1	59	39	<1	<2

Table 2.09 – Temperature effects on double-labeling experiments, intermolecular reductive coupling

2.4.0 Computational Evaluation of Dimeric Metallacycle

In tandem with the experimental evidence supporting the unified mechanistic hypothesis, collaboration with the Houk Laboratory at UCLA provided theoretical insights into the details of the reductive coupling mechanism. The computed reactive

pathway for both the consumption of the monomeric and dimeric metallacycles shows that the predicted oxidative cyclization appears to be the rate limiting step for both pathways, and highlights the extreme stability of the dimeric metallacycle (Scheme 2.08).

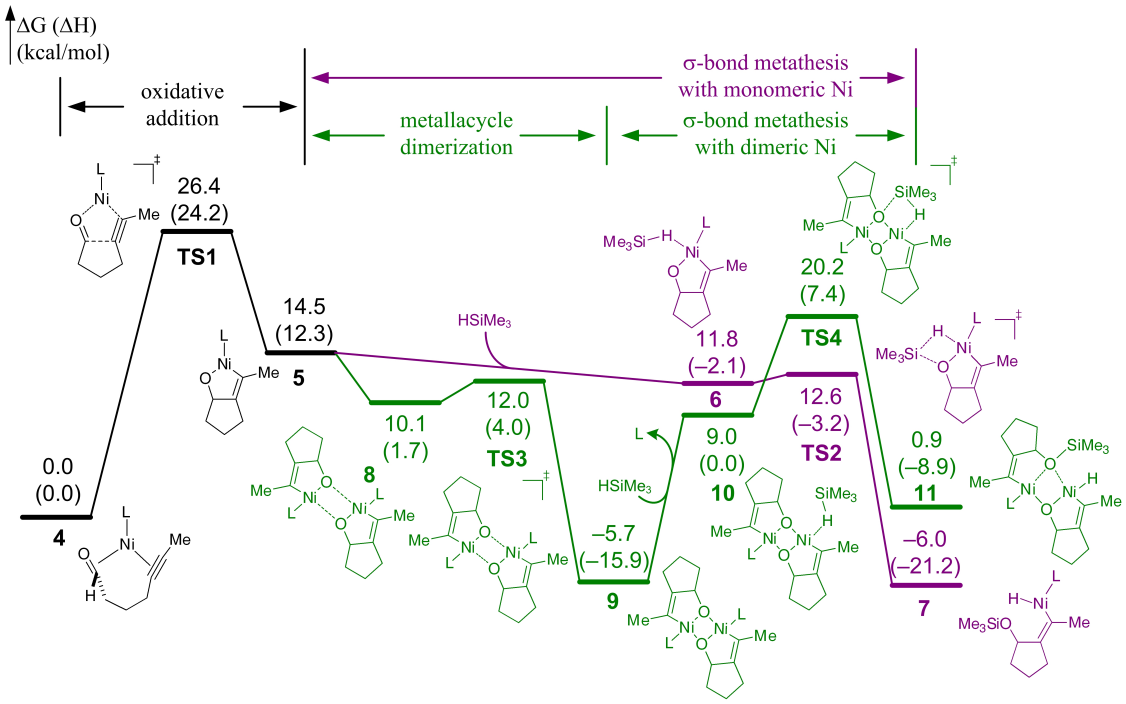

Scheme 2.08 – Potential energy surface of Monomeric and Dimeric metallacycle pathways

Computations of the reactive pathway also elucidate a few key complexes and transition states that dramatically improve our understanding of the reductive coupling mechanism.[82] First, the extreme stability of the dimeric metallacycle, and the subsequent high-energy steps to the σ-bond metathesis, explain the difficulty that Ogoshi presented in the reduction of the isolated dimeric complex. Another interesting feature is the existence of a stable ground state for a Van der Waal complex of two monomeric metallacycles. This complex serves as an intermediate state in the equilibration between the metallacycles. Lastly, the existence of several near-barrierless transition states

elucidates the difficulty in understanding the system experimentally after the rate-limiting step.

Computations also support the hypothesis regarding the role of the steric interactions between the alkyne substituent and phosphine ligand on the formation of the dimeric metallacycle. It was found that as the bulk of the phosphine ligand was increased, there was a dramatic increase in the energy required for dimerization, consistent with the observed experimental data (Table 2.10). The modeling of systems bearing an extremely small NHC ligand also highlights the difficulty in reaction of the dimer with silane, consistant with the minimal formation of crossover products with the use of any NHC ligand. With a similar trend, the steric encumbrance of the alkyne substituent also exhibits a direct effect on the energy for dimerization and subsequent reactivity with silane (Table 2.11).

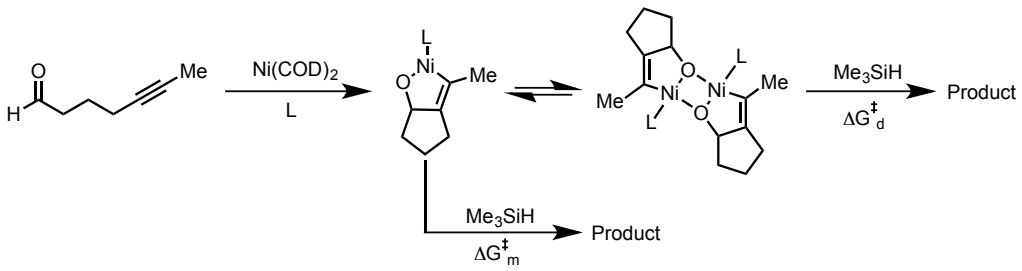

Entry	Ligand	monomer	dimer	$\Delta G^{\ddagger}_{m}$ ($\Delta H^{\ddagger}_{m}$)	$\Delta G^{\ddagger}_{d}$ ($\Delta H^{\ddagger}_{d}$)	$\Delta\Delta G^{\ddagger}$ ($\Delta\Delta H^{\ddagger}$)
1	PMe_3	20.3 (28.2)	0.0 (0.0)	20.3 (28.2)	25.9 (23.3)	5.7 (-4.9)
2	$P(i\text{-}Pr)_3$	15.2 (24.0)	0.0 (0.0)	15.2 (24.0)	24.2 (24.0)	9.0 (0.0)
3	IPh	23.7 (32.1)	0.0 (0.0)	23.7 (32.1)	44.9 (45.3)	21.2 (13.2)

Table 2.10 – Ligand substituent effects on the energetics of dimerization

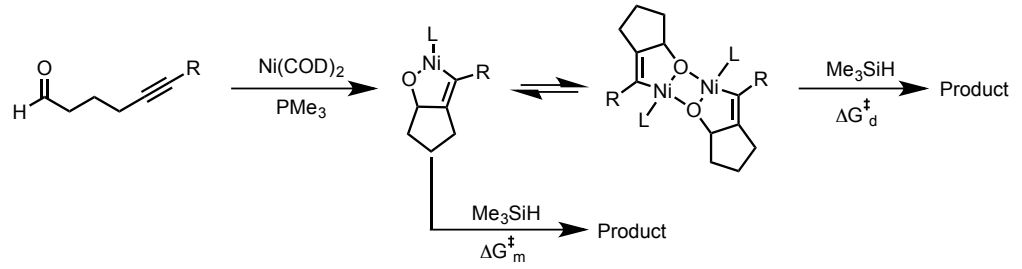

Entry	R	monomer	dimer	$\Delta G^{\ddagger}_{m}$ ($\Delta H^{\ddagger}_{m}$)	$\Delta G^{\ddagger}_{d}$ ($\Delta H^{\ddagger}_{d}$)	$\Delta\Delta G^{\ddagger}$ ($\Delta\Delta H^{\ddagger}$)
1	Me	20.3 (28.2)	0.0 (0.0)	20.3 (28.2)	25.9 (23.3)	5.7 (-4.9)
2	Ph	22.3 (30.0)	0.0 (0.0)	22.3 (30.0)	31.9 (29.3)	9.5 (-0.7)

Table 2.11 – Alkyne substituent effects on the energetics of dimerization

2.5.0 Kinetics Profile of N-Heterocyclic Carbene Ligated Reductive Coupling

During the investigation into the kinetic profile for the intramolecular reductive coupling, a brief study explored the mechanism for NHC-Ni catalyzed reductive couplings. The reaction progress was monitored using ReactIR technology (Figure 2.12). The rate of reaction is measured in the disappearance of the starting aldehyde carbonyl

stretch, which is easily plotted due to the intensity of the absorbance. Initial investigations into the NHC-Ni system for reductive coupling proved to have a more complex kinetic profile than simple order analysis can explain.

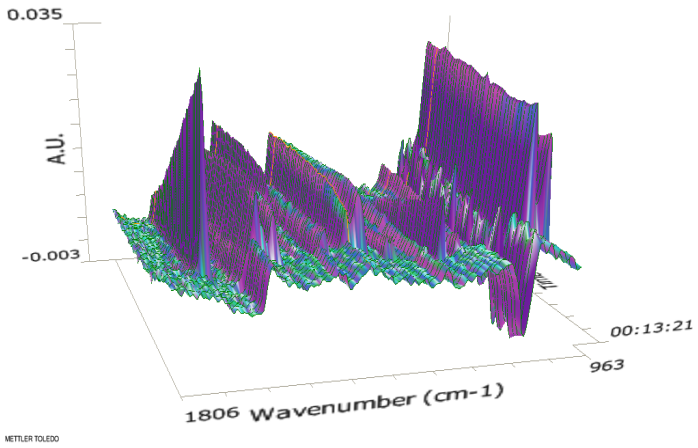

Figure 2.12 – Representative ReactIR Reaction Analysis

2.5.1 Initial Rate Analysis

Selecting a system for a thorough investigation required optimization of several substrate-based parameters. For the ligand employed, it was found that the use of IPr-HCl with $Ni(COD)_2$ provided clear and consistent reaction profiles using the ReactIR, with enough data in the initial conversion to derive an initial rate. Internal alkynes were used to negate issues of regioselectivity in the rate of product formation. Initial studies employed 3-hexyne as in the internal alkyne, but manipulations of the system accelerated the rate of the reaction to the point where a consistent initial rate could not be obtained. Therefore, the use of 4-octyne was investigated and found to have a reasonable reaction rate in the study. The final system chosen for the initial investigation into the NHC-Ni

catalyzed reductive coupling was the use of IPr, benzaldehyde, and 4-octyne (Figure 2.13).

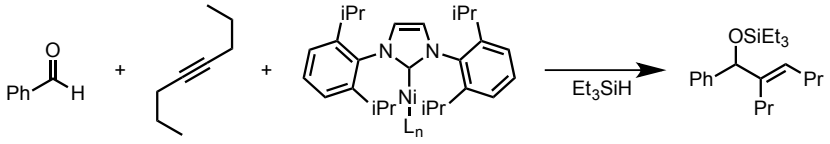

Figure 2.13 – System for investigating the kinetic profile of nickel-NHC catalyzed reductive coupling

Investigating the rate of reaction as a function of each component provided interesting insights into the intricacies of the nickel-NHC catalyst system. Analogous to the reductive cyclization of ynal substrates catalyzed by a nickel-phosphine system, the reductive coupling using a nickel-NHC system showed a positive order dependence on catalyst concentration (Scheme 2.09).

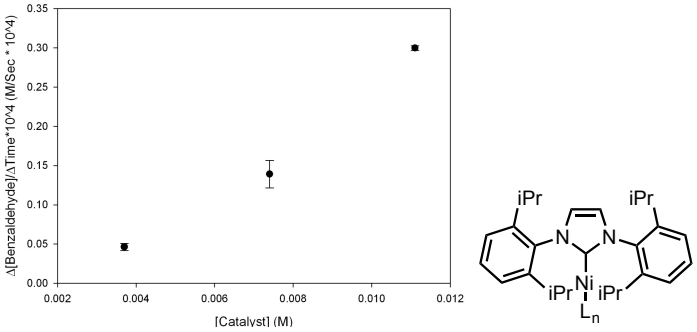

Scheme 2.09 – Rate dependence on concentration of Catalyst

The intermolecular nature of the reductive coupling created a very different system than was observed in the intramolecular reductive cyclization. The reaction dependence on alkyne concentration closely resembles saturation kinetics (Scheme 2.10). Saturation kinetics describes a first-order dependence, where at low concentrations there is a positive dependence on reaction rate, which diminishes to zero-order dependence at

high concentrations. The observed dependence on concentration is commonly observed in systems that involve equilibrium between active species, such as many enzymatic transformations.

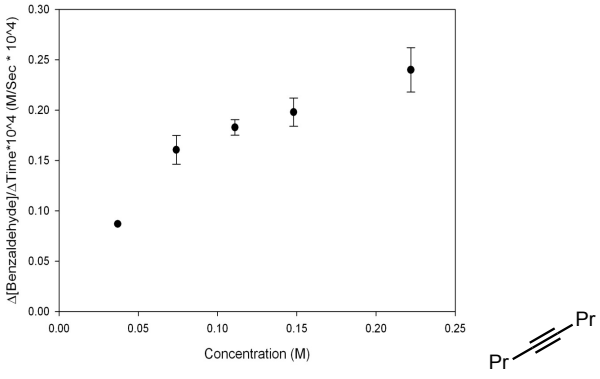

Scheme 2.10 – Rate dependence on concentration of alkyne

The study of aldehyde concentration dependence showed an inverse relationship to the rate of reaction (Scheme 2.11). The concentration dependence is consistent with a dissociation event in the productive reaction pathway. Above four equivalents of aldehyde, the reaction stops entirely.

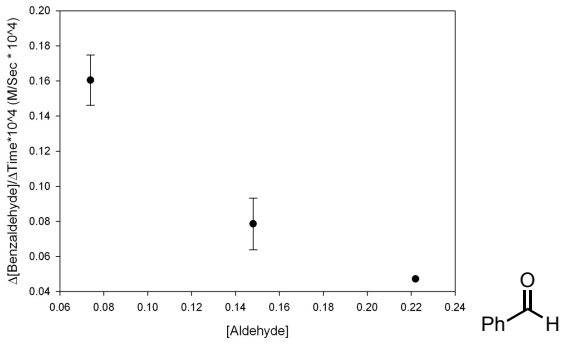

Scheme 2.11 – Rate dependence on concentration of aldehyde

To account for the observed order dependence in the reductive coupling, an alternative ground state for the catalyst was proposed. The bis-aldehyde complex has precedent as a low-energy state for a nickel catalyst used in a variation of the Tishchenko

reaction.[83] The system analysis provided by the rate dependence on aldehyde and alkyne concentration supports a bis-aldehyde complex as a ground state, with equilibrium between the various π components in solution (Figure 2.14).

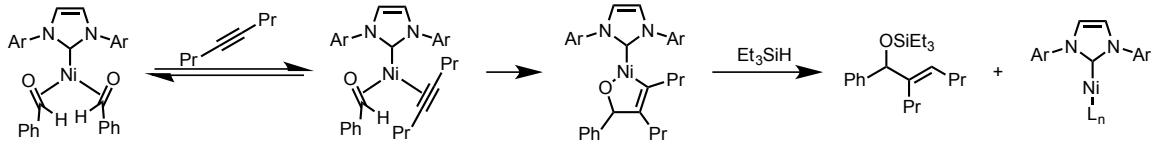

Figure 2.14 – Proposed mechanism to account for kinetics profile

2.5.2 Derivation of Rate Law Governing the Intermolecular Reductive Coupling of Aldehydes and Alkynes

Using a simplified equilibrium mechanism, a rate law can be derived consistent with the mechanistic data gathered (Scheme 2.12). To describe the equilibrium as only being between the bis-aldehyde complex and the mixed aggregate complex is a simplification to ease analysis, but in turn incorporates any other potential nickel complexes into a general equilibrium that may occur between the two pathways. Employing the simplified mechanistic proposal, a rate law can be derived that elucidates the nature of the complex reaction kinetics.

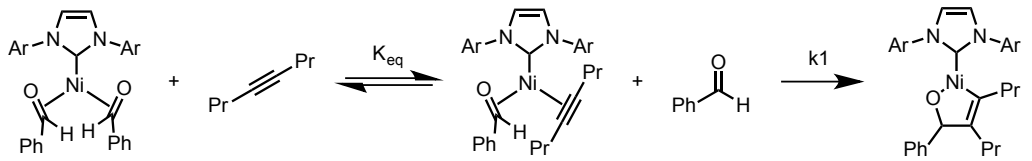

$$Rate = \frac{Keq * k1 * [Octyne][Catalyst]}{[Benzaldehyde] + Keq * [Octyne]}$$

Scheme 2.12 – Rate law derivation for simplified equilibrium proposed mechanism

2.5.3 Reciprocal Plot Analysis and Implications on Reactivity

Taking the reciprocal of the rate law equation provides a linear function (Scheme 2.13). When the kinetics results are fitted to this equation, a trend line can be used to understand the constants involved. From this reciprocal equation, the value for the equilibrium constant can also be derived. The equilibrium constant describing the equilibrium between the bis-aldehyde complex and the mixed aggregate varies between ligands employed, explaining the disparity in the visual analysis of the reaction progress between the IMes and the IPr catalyst systems.

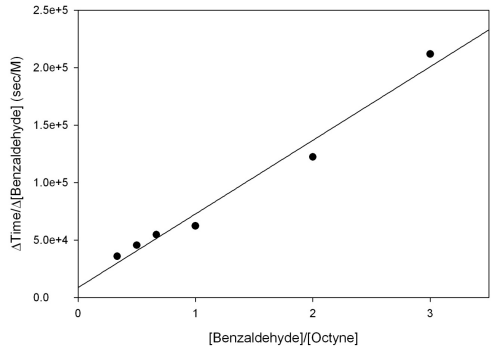

$$\frac{1}{Rate} = \frac{1}{Keq * k1 * [Catalyst]} * \frac{[Benzaldehyde]}{[Octyne]} + \frac{1}{k1 * [Catalyst]}$$

Scheme 2.13 – Derivation and plotting of reciprocal equation

Based upon the equilibrium constant derived from the reciprocal equation, the relative ratios of nickel complexes in solution can be expressed. Using the IPr-Ni catalyst system, it appears that 93% of the nickel in solution is resting in the bis-aldehyde complex.

2.6.0 Chapter 2 Summary

Through systematic variation of a number of parameters relate to nickel-catalyzed reductive couplings, the mechanistic inquiry into the phosphine-ligated pathway was investigated through a series of double-labeling experiments. The existence and equilibrium of a dimeric metallacycle was probed and found to be readily altered based upon substrate and reaction conditions. The use of larger ligands and larger substrates led to a marked decrease in the influence of the dimeric metallacycle reactive pathway, proposed to be a result of extreme steric interactions that arise as a result of the dimerization process. Also, the most compelling evidence for the existence of the metallacycle for all substrates is the effect of temperature on the results of the double-labeling experiments. As the reaction temperature was lowered, there was a dramatic

increase in the formation of the crossover products even in systems that exhibited no crossover at room temperature. These factors have elucidated the mechanistic influence of the dimeric metallacycle in the reactive pathway, and as a result have provided a wealth of insight into reaction optimization regarding mechanistic steps that occur after the rate-limiting step.

In tandem with developments in our understanding of the nickel-phosphine systems, an initial kinetics study on the use of N-heterocyclic carbenes led to the proposal of an equilibration responsible for the sequestration of the active catalyst. With bis-aldehyde complexes appearing to be a stable ground state for nickel-NHC complexes in reductive coupling, our ability to optimize and control the reaction is advanced. Final thoughts and directions for future development arising from both the kinetics analysis as well as the understanding of the dimeric metallacycle will be expanded upon in Chapter 4.

Chapter 3: Isolation and Application of Air-Stable Discrete NHC-Ni Complexes Stabilized by Fumarate Ligands

3.0.0 N-Heterocyclic Carbene Nickel complexes refined for Organic Synthesis

The use of NHCs as ligands has been a growing trend in recent years, finding utility in a wide variety of transformations as well as effective partners with a number of different metal catalysts. These advances have continued to spawn further refinements of catalytic systems tailored for the highly selective formation of specific bonds.

3.0.1 Discrete nickel(0)-NHC catalysts

A number of nickel(0)-NHC catalysts have been synthesized that are stabilized through various π systems (Figure 3.01). The first reported discrete nickel(0)-NHC catalyst was stabilized by two cyclooctene molecules.[84] In the absence of other stabilizing ligands or solvents, Sadighi[85] isolated a bimetallic system, where each nickel center is stabilized by the aromatic system of the NHC ligand. Catalysts developed by Belderrain & Nicasio,[86] as well as work by Cavell[87] display stable and isolable nickel(0) catalysts bearing a single NHC unit. Additionally, the isolation of a nickel catalyst

stabilized by the crown tetra-NHC by Spicer, Tuttle, and Murphy[88] is another highly functionalized and active catalyst for organometallic transformations (Figure 3.01).

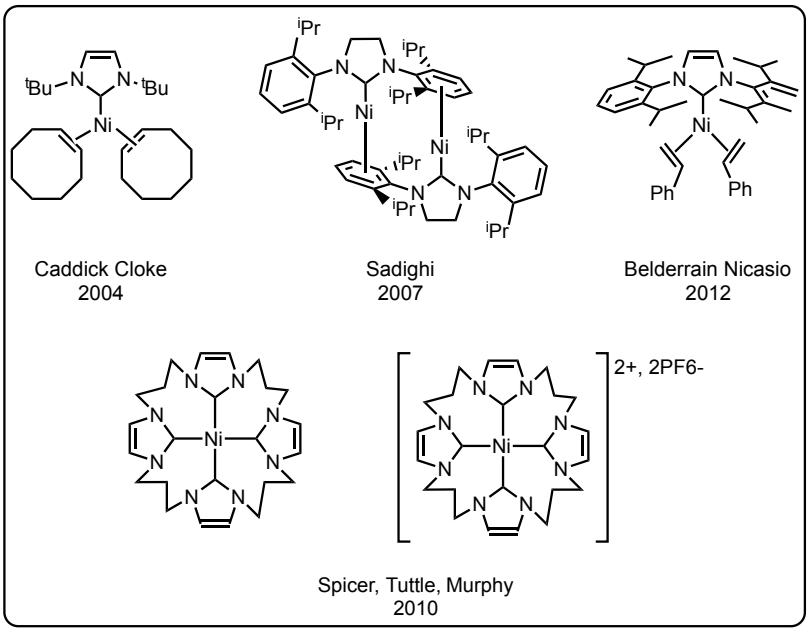

Figure 3.01 – Nickel(0)-NHC catalyst systems

3.0.2 Differences in reactivity for the in situ preparation of nickel-NHC catalysts and the application of discrete pre-formed catalysts

A number of methods exist to generate a metal-NHC bond *in situ* (Figure 3.02). The simplest method of using a nucleophilic NHC in solution with a metal[89] often yields the desired complex. However, these unstabilized carbenes often suffer from air and moisture sensitivity that complicate their use in catalysis. Salts of various NHCs are often more stable, and require the use of a base to generate the active carbene in solution.[90] While being more robust than the unstabilized variant, the use of NHC salts requires the use of a base, which can be incompatible with specific reaction conditions. In these cases, methanol,[91] perfluoro,[92] and nitrile[93] adducts of NHCs exist that can

undergo thermolytic cleavage to yield the active carbene in situ. Unique carbenes containing different substitutions at the imidazolium carbon can yield metal-NHC complexes through a direct oxidative addition process. These carbenes exist as chloro, aliphatic, and aromatic adducts.[94] Finally, if steric or electronic parameters limit the use of previous methods, several pre-functionalized metal-NHC complexes [95,96,97] can deliver a NHC unit to nickel in solution.

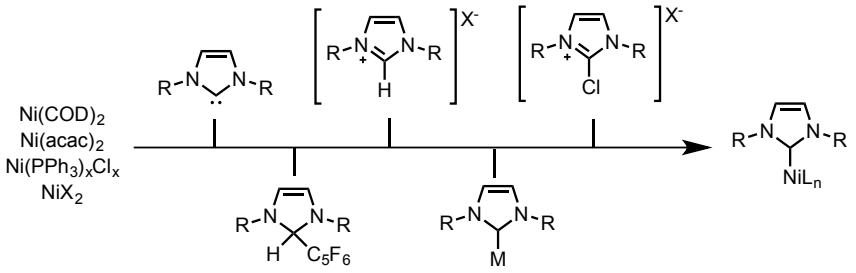

Figure 3.02 – Methods to generate Nickel-NHC complexes in solution

The ability to generate active catalysts in situ is a convenient method for the screening of conditions for different reactions, however the use of discrete nickel catalysts have been shown to increase the reactivity of coupling reactions in comparison to the *in situ* catalyst generation. In addition to higher turnover numbers for the metal catalyst, developments in pre-formed discrete catalysts have also greatly expanded the scope of reagents tolerated in productive couplings. The synthesis and application of discretely formed NHC-Ni catalyst systems has seen great development in the past decade.

3.0.3 Isolation of NHC-Ni Catalysts Stabilized by Fumarate Ligands

Work by Cavell[98] has recently shown the synthesis and isolation of a number of NHC-metal complexes stabilized by fumarate ligands. The use of common palladium

precatalyst, Pd_2dba_3, proved problematic when the NHC interacted with the dba ligand. The use of palladium diazobutadiene circumvented this unfavorable side reaction, and a variety of palladium species could be isolated (Scheme 3.01).

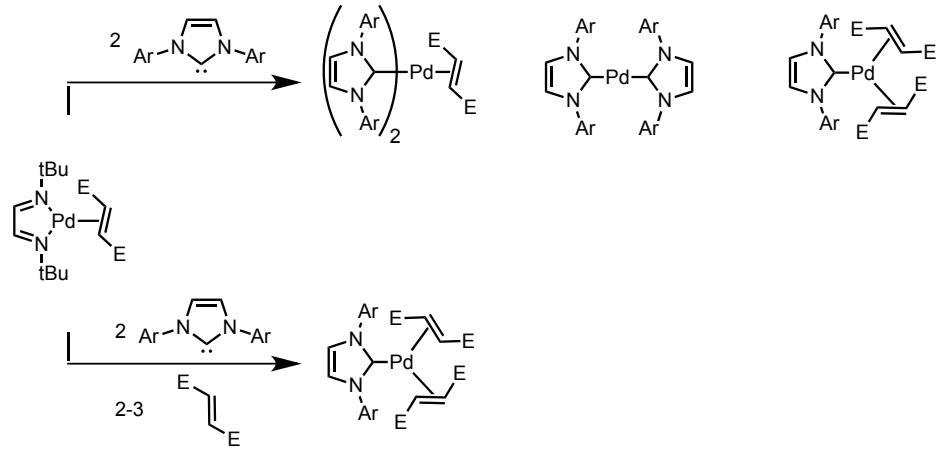

Scheme 3.01 – Synthesis of Pd fumarate catalyst by Cavell

With the synthesis of palladium based complexes established, the isolation of nickel-NHC complexes followed. Based upon manipulation of the stoichiometry of the reaction, a number of different complex structures can be isolated. The simple monomeric nickel species can be readily isolated from nickel cyclooctadiene (Scheme 3.02), the resulting complex was found to be remarkably air-stable for a nickel(0) complex.

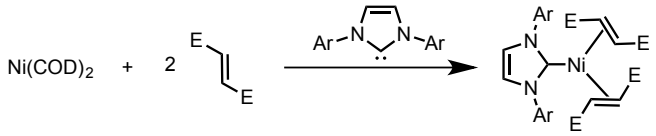

Scheme 3.02 – Synthesis of (IMes)Ni(dmfu)$_2$

Increasing the equivalence of NHC in solution allowed for the isolation of a nickel center bearing two NHC ligands and a single fumarate ligand (Scheme 3.03). A number of nickel complexes bearing two NHCs have been reported, ranging back to

initial reports by Arduengo. However, the presence of the fumarate distorts the geometry of the complex significantly which may dramatically alter its reactivity in solution.

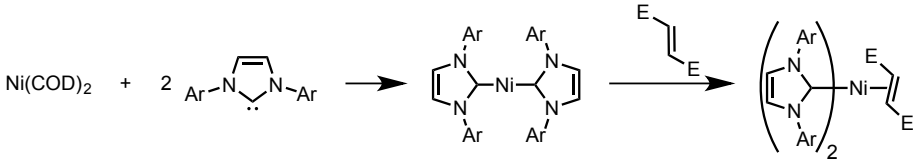

Scheme 3.03 – Synthesis of $(IMes)_2Ni(dmfu)$

Isolation of a dimeric catalyst, bearing fumarate as bridging ligands between metal centers, proved to be more difficult than the corresponding monomeric species (Scheme 3.04). The stability of $(IMes)Ni(dmfu)_2$ was found to interfere with the formation of the desired dimeric complex. In solution, NMR analysis showed the equilibrium between the dimeric complex and $(IMes)Ni(dmfu)_2$ to lie in favor of the monomeric complex. Through recrystallization, the desired bridging complex was isolated in moderate yields.

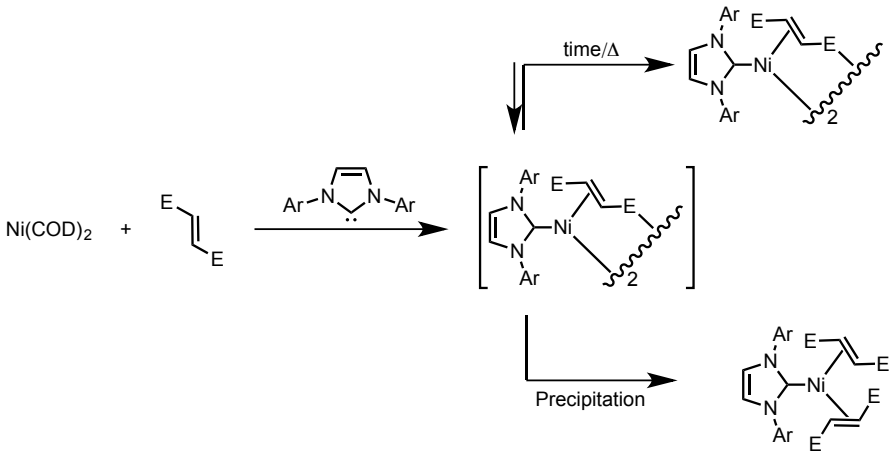

Scheme 3.04 – Synthesis of $[(IMes)Ni(dmfu)]_2$

The initial reports by Cavell only elucidated complexes bearing IMes NHC ligands, however a report by the Navarro research group has shown the synthesis and

isolation of a structurally analogous IPr nickel catalyst.[99,100] The IPr catalyst was found to be an active catalyst for the oxidation of secondary alcohols, analogous to the in situ prepared nickel-NHC catalyst (Scheme 3.05).

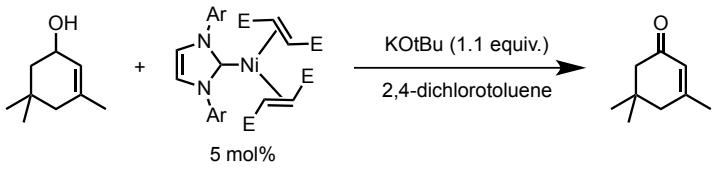

Scheme 3.05 – IPrNi(dmfu)$_2$ in Nickel-catalyze oxidation of secondary alcohols

3.1.0 Synthesis Employing Nickel Cyclooctadiene as a Nickel Source

The isolation of fumarate complexes derived from IMes and IPr NHC salts can be performed on a large scale, with the only requirement of a glovebox being for the storage and handling of nickel cyclooctadiene. Performed under nitrogen gas, with manipulations being handled with basic Schlenk techniques can provide an easy route to both of these complexes, which are both thermally and air stable (Scheme 3.06).

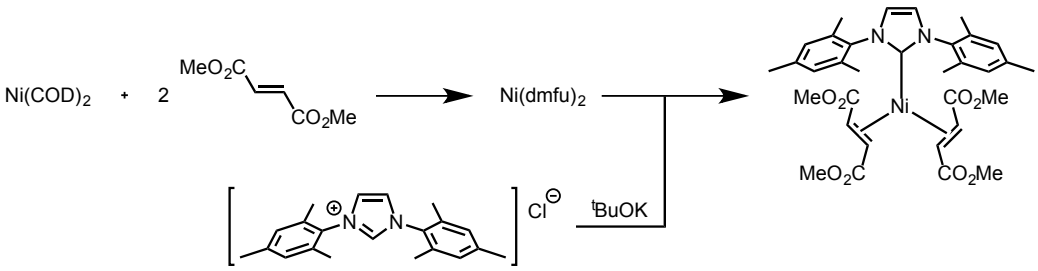

Scheme 3.06 – Synthesis of IMes discrete catalyst, (IMes)Ni(dmfu)$_2$

Attempts to synthesize more structurally complex or electron rich NHC-Ni complexes were met with decomposition products, with no evidence for significant binding of the fumarate ligand to the metal center. With Cavell's work elucidating a number of different catalyst states, and the propensity for nickel complexes to adopt a 2:1

ratio of fumarate to nickel, the equivalents of fumarate was increased. When the discrete catalyst (IMes)Ni(dmfu)$_2$ was treated with two additional equivalents of fumarate, there was no decomposition away from the initial nickel complex by NMR (Scheme 3.07).

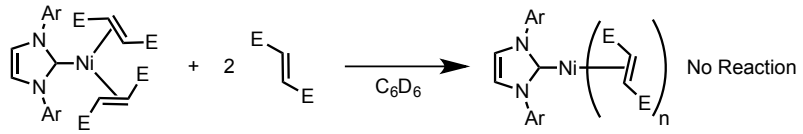

Scheme 3.07 – Stability of (IMes)Ni(dmfu)$_2$ to additional dmfu

Where previous attempts to synthesize (NHC)Ni(dmfu)$_2$ variants containing saturated NHCs were unsuccessful, increasing the equivalents of fumarate in solution allowed for the isolation and characterization of (SIMes)Ni(dmfu)$_2$ (Scheme 3.08). This nickel complex is the first saturated NHC variant of the fumarate catalyst system characterized.

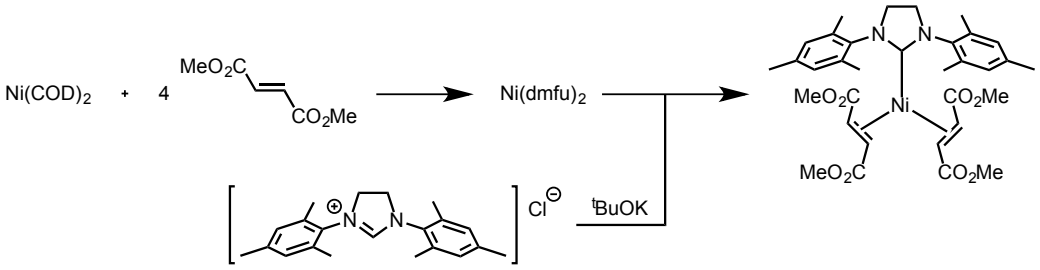

Scheme 3.08 – Synthesis of saturated NHC catalyst, (SIMes)Ni(dmfu)$_2$

3.1.2 Synthesis Employing Nickel Acetylacetonate as a Nickel Source

The ease of use and synthesis for the fumarate catalysts is a strong benefit to their use in catalysis, but the need for a glovebox for the storage and handling of Ni(COD)$_2$ limits the generality of the method. In addition to the air-sensitivity of Ni(COD)$_2$, it is also flammable and much more expensive than a number of other nickel sources. The

ability to access the nickel-fumarate complexes starting from bench-stable reagents would significantly advance the utility of the method.

Reports for the reduction of $Ni(acac)_2$ have shown that in the presence of a large excess of sodium hydride,[101] the isolation of NHC_2Ni complexes can be performed (Scheme 3.09). A significant limitation is the large excess of sodium hydride required, due to the stability of the nickel starting catalyst as well as the solubility of sodium hydride in organic solvents. Also, heating and significant reaction times limit the use of the method.

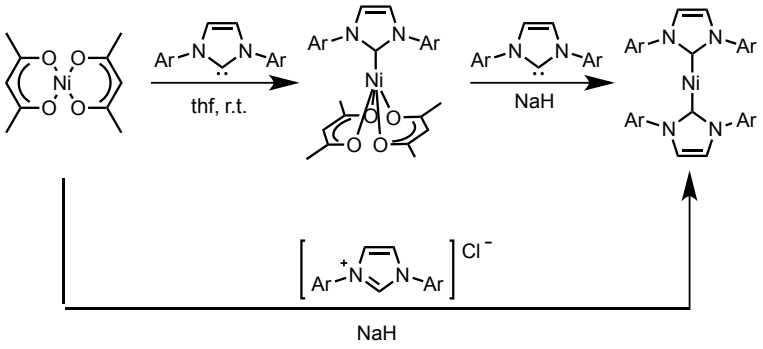

Scheme 3.09 – Reduction of $Ni(acac)_2$ using sodium hydride

A general method for the synthesis of ligated analogues to nickel cyclooctadiene has been reported starting from bench-stable $NiCl_2$.[102] The use of allyl magnesium bromide undergoes subsequent transmetallations, where the bis-allyl nickel complex can reductively eliminate 1,5-hexadiene, which remains bound to the nickel center (Figure 3.03). The resulting functionalized nickel center is similar to cyclooctadiene with an appended 1,5-hexadienyl ligand. While a versatile and attractive route for the synthesis of complex ligand scaffolds, the intermediate nickel species is air-sensitive and must be handled using a glovebox.

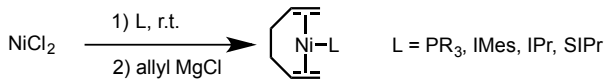

Figure 3.03 – Reduction of $NiCl_2$ using allyl Grignard

Recent developments in the Montgomery laboratory have been underway in the use of bench-stable $Ni(acac)_2$ in the reductive coupling of aldehydes and alkynes.[103] In order to catalyze the reaction, the $Ni(acac)_2$ precatalyst must first be reduced in situ to afford a nickel(0) catalyst. The developed method employs the use of a silane and weak base to reduce the nickel complex (Scheme 3.10). Early studies show the formation of a number of different silylated products, including mono and bis-silylated acetylacetonate as well as silylated tert-butoxide.

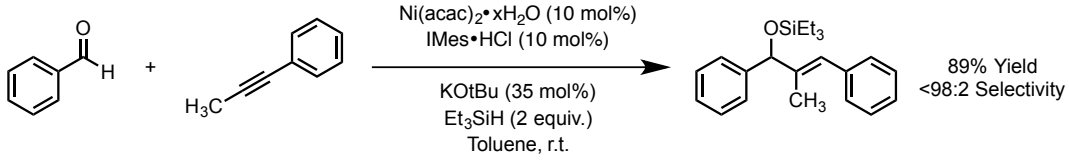

Scheme 3.10 – in situ reduction of $Ni(acac)_2$ using silane and alkoxide base

Coupling the methodology developed for isolation of the fumarate complexes with the reduction of $Ni(acac)_2$ in situ, a route to the formation of $(NHC)Ni(dmfu)_2$ can be envisioned. Upon treatment with an excess of base, silane, and fumarate in the presence of an NHC, the productive formation of the desired $(IMes)Ni(dmfu)_2$ can be observed (Scheme 3.11). This method provides a route to the fumarate complexes that negates the need for a glovebox entirely.

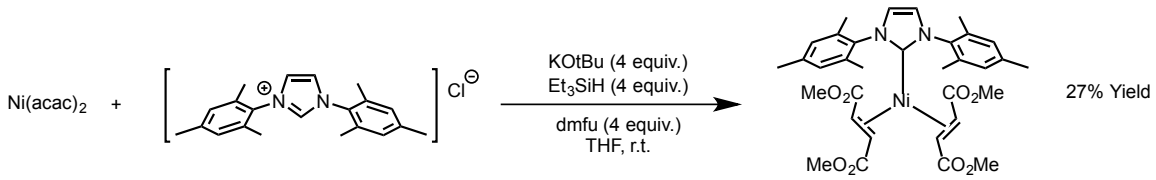

Scheme 3.11 – Synthesis of (IMes)Ni(dmfu)$_2$ originating from air-stable Ni(acac)$_2$

3.2.0 Use of Air-Stable Nickel Catalysts for Kumada Cross-Coupling[104]

The use of nickel catalysts in the formation of carbon-carbon bonds via Kumada couplings is well precedented (Section 1.3.1), however many advances come through the development and tailoring of the ligand system which increase the complexity and cost of the transformation. The use of (NHC)Ni(dmfu)$_2$ complexes can serve as a general catalyst for Kumada coupling, while being easily synthesized, stored, and handled. One feature that makes the fumarate complexes desirable as Kumada coupling catalyst systems is that the catalyst activation utilizes reagents required for the coupling reaction. The reduction of the fumarate ligands by Grignard addition can be envisioned, yielding a highly active nickel catalyst available to perform the coupling (Figure 3.04).

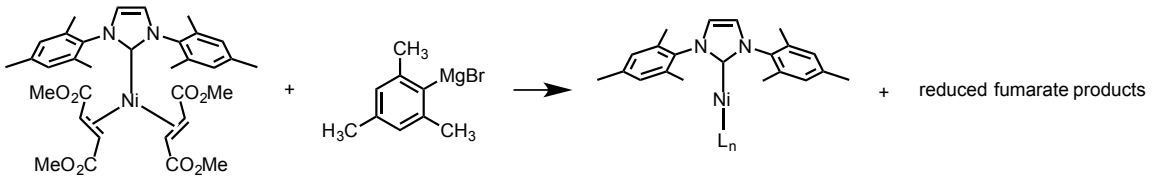

Figure 3.04 – Proposed activation of dmfu catalysts by Grignard reagents

3.2.1 Substrate Scope for Kumada Cross-Coupling

The coupling of aryl halides with aryl Grignard reagents was found to be extremely general and versatile with the use of (NHC)Ni(dmfu)$_2$ as catalysts (Scheme 3.12). Variations in the structure and electronics of the aryl halide component were

found to be insignificant in the coupling reaction, even in the case of extremely sterically demanding couplings such as the coupling of 3,5 di-t-butylphenylbromide with mesityl magnesium bromide.

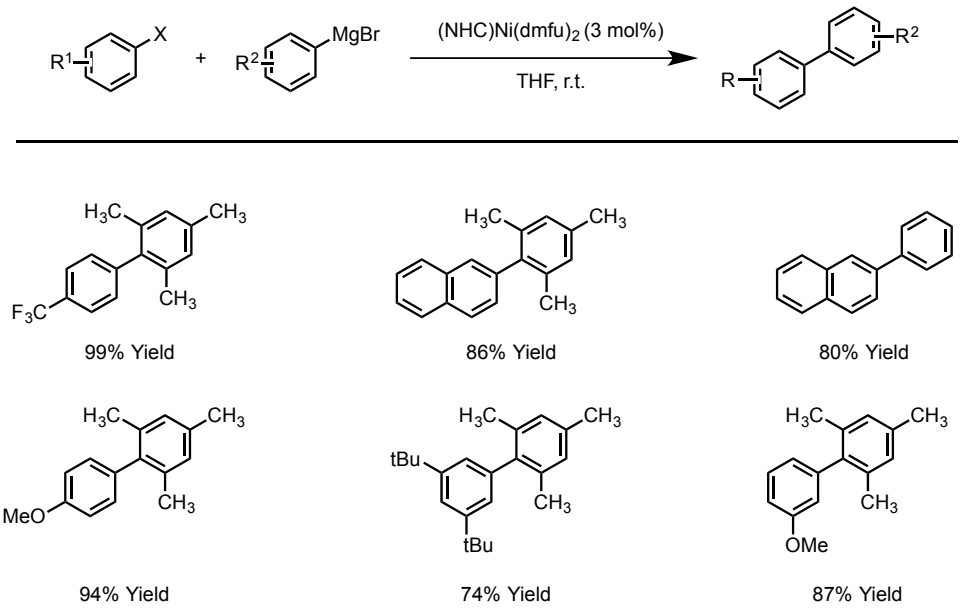

Scheme 3.12 – Substrate Scope of Nickel-Catalyzed Kumada Couplings

3.2.2 Ease of Use Improvements Over Related Methods

The use of an air stable catalyst, as well as the ability to bypass the careful measurement of numerous reagents to generate an active catalyst in situ, allows for extremely low catalyst loading in Kumada coupling. Previous reports by Chen show the lowest catalyst loading for effective Kumada coupling to be 1 mol%, however the use of the fumarate complexes allows for loadings as low as 0.25 mol% without significant decreases in conversion (Table 3.01). In addition, for all reactions the catalyst was stored and handled outside of the glovebox, with reactions run under an inert atmosphere.

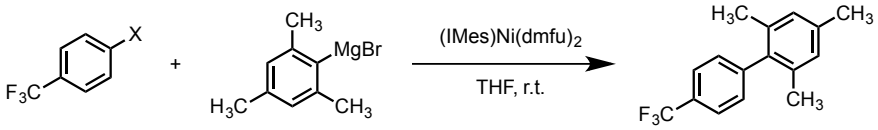

Entry	Catalyst Loading (mol%)	Yield
1	3	98%
2	1	97%
3	0.25	92%
4	0.01	95%

Table 3.01 – Catalyst Loading Reduction for Kumada Coupling

3.3.0 Use of Air-Stable Nickel Catalysts for Buchwald-Hartwig Cross-Coupling

3.3.1 Substrate Scope and Limitations

While being a highly effective catalyst for Kumada coupling, the fumarate series of catalysts does not show the same broad applicability for the Buchwald-Hartwig cross coupling. The optimal substrates for the formation of carbon-nitrogen bonds are electron-poor aryl chlorides coupled to secondary amines (Table 3.02). Using these substrates, the reactions require forcing conditions to provide reasonable yields, with the optimal reaction conditions being in a sealed tube with refluxing toluene. The substrate scope was found to be limited to the use of electron poor aryl chlorides, with aryl bromides not showing conversion to the desired products (Scheme 3.13). Primary amines were tolerated in the reaction, however minor formation of the tertiary amine was observed. The stability of the fumarate ligands may be serving to inhibit the productive reaction pathway, where as the Kumada couplings were initially activated by addition of the Grignard reagent to the fumarate to liberate the nickel catalyst.

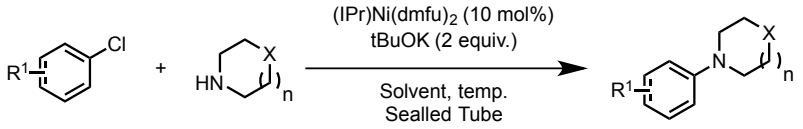

Entry	R^1	Amine	Solvent	Temperature	Yield
1	4-methyl	morpholine	THF	65 °C	N.R.
2	4-methyl	morpholine	Toluene	65 °C	32%
3	4-methyl	morpholine	Toluene	110 °C	53%
4	3-methoxy	morpholine	Toluene	110 °C	87%
5	3-methoxy	pyrrolidine	Toluene	110 °C	74%
6	3-methoxy	Pyrrolidine (4 equiv.)	Toluene	110 °C	93%

Table 3.02 – Optimization of Buchwald-Hartwig coupling

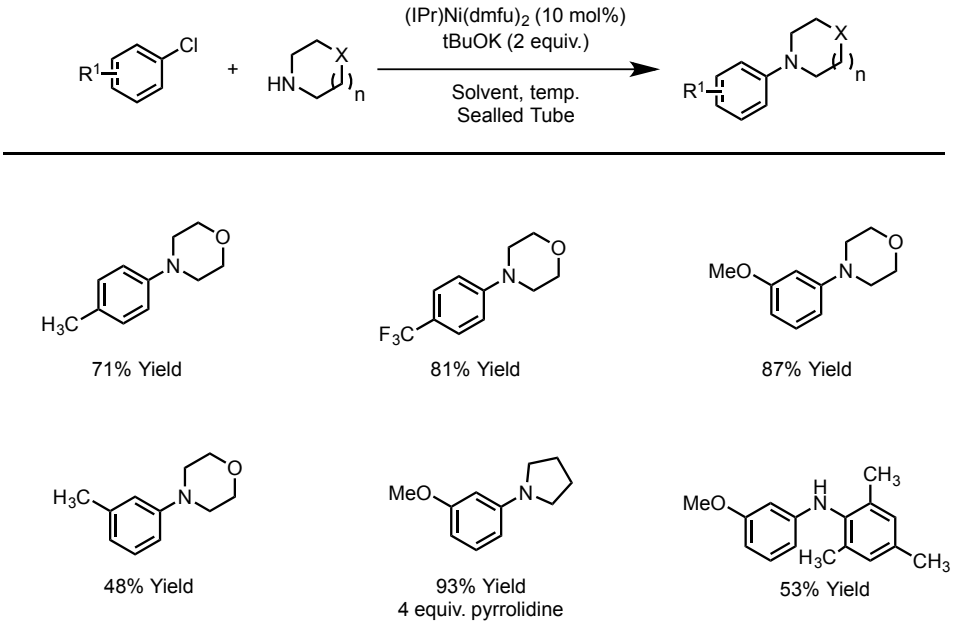

Scheme 3.13 – Substrate scope for the nickel-catalyzed Buchwald-Hartwig Coupling

3.4.0 Use of Nickel-Fumarate Catalysts for Reductive Coupling of Aldehydes and Alkynes

The wealth of study focused on the nickel-catalyzed reductive coupling of aldehydes and alkynes has created a general method for the synthesis of allylic alcohols,

however all currently developed methods rely upon the use of nickel cyclooctadiene. The development and use of an air stable nickel catalyst would allow for a bench-stable system, enhancing the applicability and ease of use as a method.

Utilizing unsymmetrical alkynes provides a route to the synthesis of multiple regioisomers in the reductive coupling of aldehydes and alkynes; therefore initial optimization of the system was done with symmetric alkyne substrates. The use of the fumarate catalysts in the reductive coupling show regioselectivities similar to published results using an *in situ* generated nickel catalyst (Scheme 3.14). The use of terminal alkynes was not tolerated in the reaction, showing minimal conversion but only a single regioisomer by GC/MS.

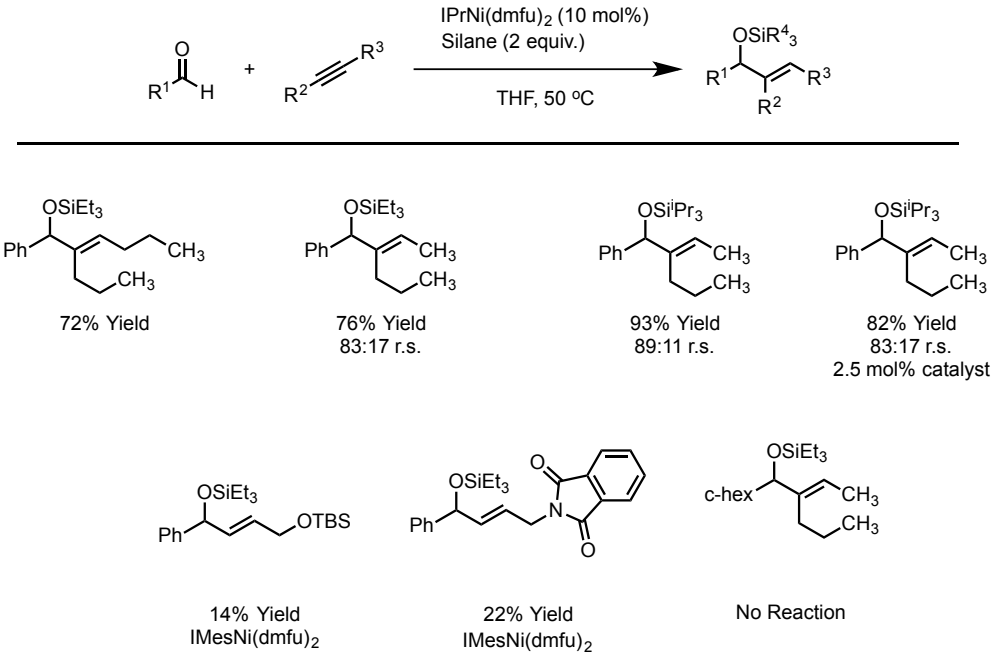

Scheme 3.14 – Substrate Scope and Selectivities for reductive coupling of aldehydes and alkynes

From the initial investigation into reductive couplings, the main limitations for the use of discrete fumarate catalysts are the need for elevated temperatures and the lack of

reactivity of aliphatic systems. Where the *in situ* protocol for reductive coupling can be carried out at room temperature, the discrete catalyst reactions required heating to 50 ^{o}C to observe any product formation. This decrease in reactivity is a sacrifice for the stability of the discrete catalyst, where the elevated temperature is needed to displace the fumarate ligands on the nickel center before the oxidative cyclization can occur. In a related limitation, aliphatic aldehydes do not bind strongly enough to nickel to effectively displace the fumarate. As the synthesis and scope of nickel catalyst is continually expanded, these issues of activation of the nickel catalyst will be addressed.

3.5.0 Summary

Investigation into the utility and applications of discrete nickel complexes has led to the expansion of synthetic methods to access discrete complexes as well as the application to coupling reactions of various types. Notably, the development in the synthesis of air-stable, functionalized nickel-NHC complexes starting from entirely air-stable materials is significant in the applicability of the fumarate stabilized series of nickel catalysts. Where many reaction that are reliant upon the use of nickel(0) precatalysts require the use of a glovebox and manipulations under an inert atmosphere, the ability to generate and use these versatile fumarate complexes using fundamental laboratory skills can expand the desirability of nickel catalysis for the field. Initial investigation into the ability to catalyze different cross coupling and reductive coupling reactions has elucidated challenges to the use of the stabilized catalysts, which will be addressed further in Chapter 4.

Chapter 4: Concluding Remarks and Future Directions

4.0.0 Research Directions Arising from Mechanistic Investigation Studies

4.0.1 Detailed Kinetics Analysis for the Reductive Coupling of Aldehydes and Alkynes

The construction of a basic kinetic profile for the reductive coupling of aldehydes and alkynes employing a nickel-NHC catalyst system was elucidated in Chapter 2 (Figure 4.01), but does not serve as a general understanding for the complete mechanism. The complexities of the system create a myriad of potential sources for investigation and optimization.

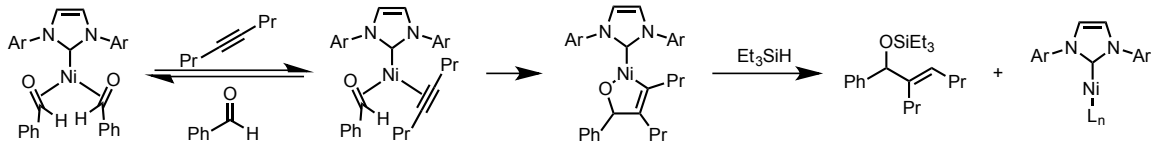

Figure 4.01 – Mechanism proposed based upon Kinetics Study

The equilibrium between potential catalyst structures has many interesting facets for exploration. The nature of NHCs employed in catalysis can vary greatly in steric and electronic parameters, which will directly affect the energetics of the proposed

equilibrium. An investigation into different NHC ligands can lead to a better understanding of the equilibrium at play, and whether sterics or electronics serve as a stronger governing factor in the reductive coupling (Figure 4.02). Previous studies have shown that changing the NHC from the aromatic IPr ligand to the saturated SIPr ligand can increase reactivity and selectivity. Investigation into the rate of the reaction can allow for a better understanding of the importance of the bis-aldehyde complex in solution.

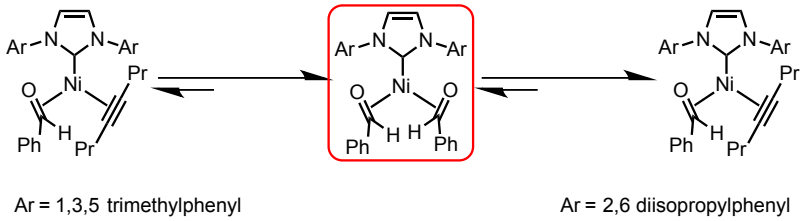

Figure 4.02 – Potential ligand effects on nickel complex equilibrium

Recent developments in the Montgomery laboratory have elucidated a change in the regioselectivity based upon silane concentration and constitution.[105] As a reactive component, this is unsurprising, however all gathered mechanistic data supports a zero-order dependence upon silane concentration. This change to regioselectivity is pronounced in several benchmark reactions, and serves to complicate our understanding of the mechanism. It was proposed that for specific substrate combinations, the oxidative cyclization step of the mechanism could be reversible allowing for a rate-limiting σ-bond metathesis with the silane. This change would account for the role of silane in altering the regiodetermining step of the reaction.

To further investigate this proposal, initial-rate studies were carried out using GC/MS analysis for the coupling of benzaldehyde and phenyl propyne. Where all ReactIR studies were performed with symmetric alkynes to negate the impact of forming

different products, the use of an asymmetric alkyne complicates the use of in situ IR monitoring. However, the use of GC/MS allows for the direct measure of the formation of each product instead of the decomposition of starting materials. This led to an interesting discovery by Evan Jackson of the Montgomery Laboratory in the specific case of benzaldehyde and phenyl propyne, where there may be differing rate dependency for each regioisomer. The mechanistic picture is complicated further by this, where only the formation of the minor metallacycle may be reversible (Figure 4.03). This expansive mechanistic hypothesis accounts for the observed rate dependence in the specialized system employing phenyl propyne as well as providing an explanation for the zero-order dependence on silane observed with the majority of substrate systems.

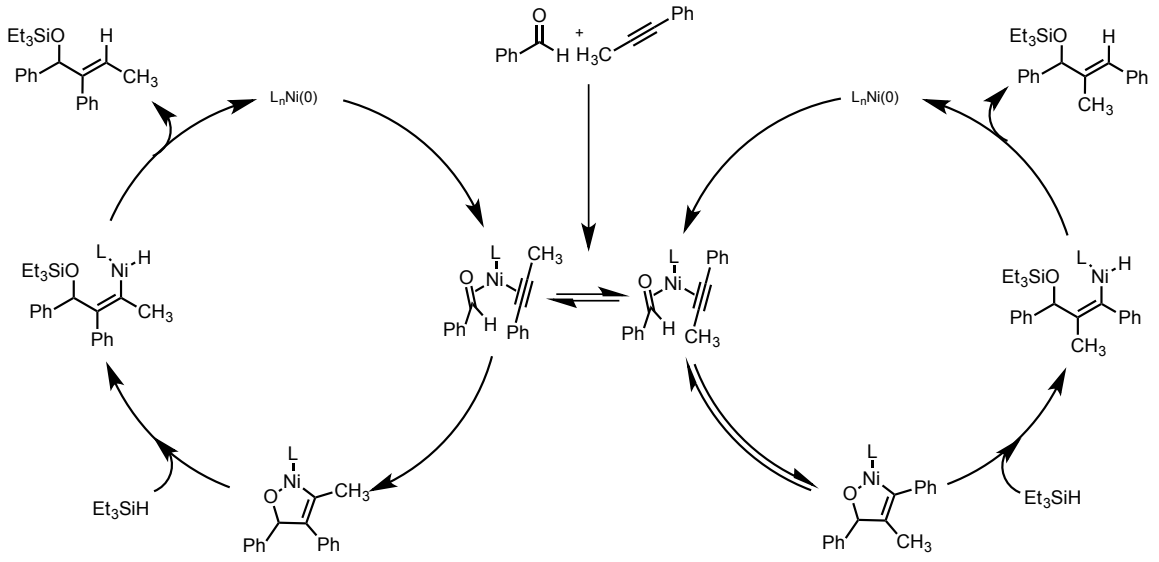

Figure 4.03 – Mechanism proposal, exploring role of silane in determining regioisomers formed

Continuing the investigation of the mechanism of reductive coupling will elucidate the factors important to a potentially reversible oxidative cyclization. Systematic alterations of the catalyst structure and more importantly evaluation of

different alkynes will allow for the screening and understanding of how the π components alter the energetics and formation of key intermediates in the reductive coupling mechanism.

4.0.2 Advances in Hydroacylation using a nickel catalyst

Partial investigation into the hydroacylation of ynals was carried out previously in the Montgomery laboratory, where only the formation of 5-membered rings was found to be effective in the transformation.[106] However, a key double-labeling experiment was carried out during this investigation, providing evidence of a bimolecular fragmentation yielding the hydroacylation products. Coupled with the thermal degradation of the dimeric metallacycle shown by Ogoshi, a reasonable proposal shows the dimeric metallacycle being a key intermediate in the formation of α,β-unsaturated ketone products.

The newly developed understanding of factors related to the formation and stability of the dimeric metallacycles can be applied to the system to advance the limited scope and applicability of the previously investigated nickel-catalyzed hydroacylation. The use of ligands without a strong steric presence was shown to increase the influence of the dimeric metallacycle, as well as an understanding of factors related to the substrate constitution. With an understanding of factors related to the dimerization of the metallacycle, changing the reaction to favor its formation should allow access to a broader variety of hydroacylation products.

4.1.0 Discrete Catalyst Studies

4.1.1 Catalyst isolation to Investigate Factors related to reductive coupling

DFT studies have elucidated the nature of nickel-NHC complexes, however highly functionalized NHC systems have not been fully characterized and studied in catalysis. Ligands at both extremes of regiocontrol for the reductive coupling of aldehydes and alkynes, such as DP-IPr variants for the large ligand class and the IPr-BAC variants for the small ligand class, are not well understood. Small NHC ligands are known to form complexes bearing multiple NHC ligands per metal center in solution, which makes the application as a catalytic system complicated. In parallel, the large ligands exhibit such a strong steric encumbrance that reactivity can be dramatically altered, with the actual formation of the catalyst in solution being questionable. The synthesis of discrete nickel catalysts bearing these extremes of NHC ligand classes would allow for better understanding and applications of these systems to catalysis (Figure 4.04).

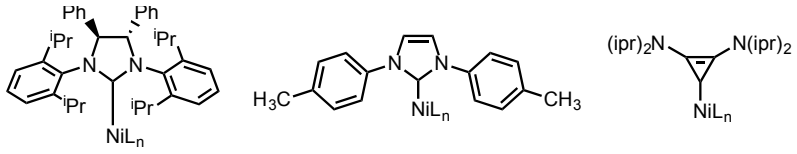

Figure 4.04 – New NHC-Ni complexes that would benefit catalysis

4.1.2 Catalyst Variation for Synthetic Utility

The synthesis and isolation of new catalyst structures can directly impact the development and advancement of nickel-catalysis. While dimethylfumarate serves as an excellent ligand for nickel, the dissociation to open coordination sites on the metal center

is difficult. The exploration of different fumarate analogues may lead to the development of a nickel system that be easily activated for catalysis in solution (Figure 4.08). Further exploration of potential stabilizing ligands can be tailored to specific NHC systems to fit the needs of the catalyst, such as the use of small chelating fumarate ligands with extremely large NHC ligands to create stable complexes to be employed in catalysis, or the use of larger fumarates in the formation of nickel complexes bearing extremely small NHCs such as the various NHCs analogous to IPr-BAC (Figure 4.05).

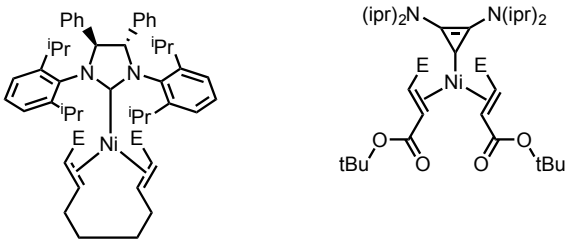

Figure 4.05 – Variations in stabilizing ligands to access catalysts bearing unique NHC structures

4.2.0 Mechanistic Understanding as a Driving Force for Reaction Development

As synthetic methods continue to expand, the ability to synthesize increasing complex molecules from simpler starting materials in fewer steps is increasingly the focus of organic synthesis. However, the power and utility of these transformations lies in the process itself. Through understanding the intricate details of reaction mechanisms, synthetic techniques will be continually refined to expand the applications to a number of different substrate systems.

Chapter 5: Supporting Information

5.1 General Experimental Information

Unless otherwise noted, all reactions were conducted in flame-dried or oven dried (120 °C) glassware with magnetic stirring under an atmosphere of dry nitrogen. THF and CH_2Cl_2 were purified under nitrogen using a solvent purification system (Innovative Technology, inc., Model # SPS-400-3 and PS-400-3). Aldehydes were distilled prior to use. Silanes were passed through alumina. Ynal substrates were oxidized using pyridinium-chlorochromate and purified by column chromatography prior to use. $Ni(COD)_2$ (Strem Chemicals, Inc.) and tricyclohexyl phosphine (Aldrich) were stored and weighed in an inert atmosphere glovebox.

Analytical thin layer chromatography (TLC) was performed on Kieselgel 60 F254 (250 μm silica gel) glass plates and compounds were visualized with UV light and potassium permanganate stain. Flash column chromatography was performed using Kieselgel 60 (230-400 mesh) silica gel. Eluent mixtures are reported as v:v percentages of the minor constituent in the major constituent. All compounds purified by column chromatography were sufficiently pure for use in further experiments unless otherwise indicated.

^{1}H NMR spectra were measured at 400 MHz on a Varian MR400 instrument. The proton signal of the residual, nondeuterated solvent (δ 7.24 for $CHCl_3$) was used as an internal reference for ^{1}H NMR spectra. ^{13}C NMR spectra were completely heterodecoupled and measured at 175 MHz. Residual chloroform (δ 77.0) was used as an internal reference. High-resolution mass spectra were recorded on a VG 70-250-s spectrometer manufactured by Micromass Corp. (Manchester UK) at the University of Michigan Mass Spectrometry Laboratory. Regioisomeric ratios were determined on crude reaction mixtures using NMR or GC/MS. GC analyses were carried out on an HP 6890 Series GC system with an HP-5MS column. In situ FTIR data were acquired on a Mettler-Toledo React-IR^{TM} 45m module fitted with a 9.5mm diamond-tipped probe.

5.2.0 Chapter 2 Experimental Data

5.2.1 General Procedures for Chapter 2

General Procedure A - Authentic Sample Preparation

A solid mixture of 10 mol% $Ni(COD)_2$ and 20 mol% PCy_3 were dissolved in 0.1 M THF under a Nitrogen atmosphere and allowed to stir for 10 min. Aldehyde (1.0 equiv), alkyne (1.0 equiv), and silane (2.0 equiv) were added in a 0.5 M THF solution to the reaction flask and allowed to stir until starting materials were consumed. The reaction mixture was filtered through silica gel eluting with 50% EtOAc/hexanes. The solvent was removed *in vacuo*, and the crude residue was purified via flash chromatography on silica gel to afford the desired product.

General Procedure B - Crossover Experimental

A solid mixture of 10 mol% $Ni(COD)_2$ and 20 mol% PCy_3 were dissolved in 0.1 M THF under a Nitrogen atmosphere and allowed to stir for 10 min. Aldehyde (1.0 equiv), alkyne (1.0 equiv), triethylsilyl-deuteride (1.0 equiv) and tri-n-propylsilane (1.0 equiv) were added in a 0.5 M THF solution to the reaction flask. Aliquots were removed for GCMS analysis.

5.2.1 Authentic Sample Characterization

(E)-triethyl((2-methyl-1-phenylbut-2-en-1-yl)oxy)silane:

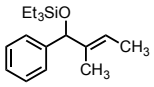

Following general procedure A, $Ni(COD)_2$ (15 mg, 0.055 mmol), PCy_3 (30 mg, 0.110 mmol), benzaldehyde (50 mg, 0.47 mmol), 2-butyne (26 mg, 0.48 mmol), and triethylsilane (175 mg, 1.51 mmol) gave a crude residue which was purified *via* flash chromatography (5:95 EtOAc:Hexanes) to afford the product as a clear oil (68 mg, 52% Yield). **^{1}H NMR (400 MHz, CDCl3):** δ 7.35 (d, J = 5.2 Hz, 2H), 7.27 (t, J = 7.2 Hz, 2H), 7.19 (t, J = 6.8 Hz, 1H), 5.61 (q, J = 6.4 Hz, 1H), 5.08 (s, 1H), 1.61 (d, J = 6.8 Hz, 3H), 1.40 (s, 3H), 0.91 (t, J = 8 Hz, 9H), 0.58 (q, J = 8 Hz, 6H). **^{13}C NMR (175 MHz, CDCl3):** δ 143.8, 138.6, 127.7, 126.5, 125.9, 120.3, 79.7, 13.1, 10.5, 6.8, 5.0, 4.8. **IR**: ν 701, 739, 854, 1007, 1238, 1454, 1676, 2173 cm^{-1}. **MS (EI) (*m*/*z*):** [M]+ calc'd for $C_{17}H_{28}OSi$ 276.1909, found 276.1912. **GC/MS (ret. time):** 11.069 min. **GC/MS (m/z:intensity):** 276:864448, 277:213120

(E)-triethyl(3-deutero(2-methyl-1-phenylbut-2-en-1-yl)oxy)silane:

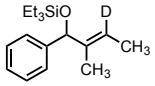

Following general procedure A, $Ni(COD)_2$ (15 mg, 0.055 mmol), PCy_3 (30 mg, .110 mmol), benzaldehyde (50 mg, 0.47 mmol), 2-butyne (26 mg, 0.48 mmol), and triethylsilyl-deuteride (125 mg, 1.1 mmol) gave a crude residue which was purified *via* flash chromatography (5:95 EtOAc:Hexanes) to afford the product as a clear oil (79 mg, 61% Yield). **^{1}H NMR (400 MHz, CDCl3):** δ 7.34 (d, J = 8Hz, 2H), 7.28 (t, J = 8.4 Hz, 2H), 7.20 (t, J = 7.2 HzHz, 1H), 5.09 (s, 1H), 1.62 (s, 3H), 1.41 (s, 3H), 0.92 (t, J = 8 Hz, 9H), 0.59 (q, J = 8 Hz, 6H). **^{13}C NMR (175 MHz, CDCl3):** δ 143.8, 138.5, 127.7, 126.5, 125.9, 120.1, 120.0, 119.9, 79.6, 12.939, 10.9, 6.8, 4.9, 4.8. **IR:** ν 704, 739, 854, 1004, 1238, 1454, 1676, 2173 cm^{-1}. **MS (EI) (*m*/*z*):** [M]+ calc'd for $C_{17}H_{27}OD$ 277.1972, found 277.1965. **GC/MS (ret. time):** 11.069 min. **GC/MS (m/z:intensity):** 276:261312, 277:496896

(E)-((2-methyl-1-phenylbut-2-en-1-yl)oxy)tripropylsilane:

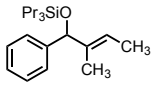

Following general procedure A, $Ni(COD)_2$ (15 mg, 0.055 mmol), PCy_3 (30 mg, 0.110 mmol), benzaldehyde (50 mg, 0.47 mmol), 2-butyne (26 mg, 0.48 mmol), and tripropylsilane (200 mg, 1.51 mmol) gave a crude residue which was purified *via* flash chromatography (5:95 EtOAc:Hexanes) to afford the product as a clear oil (117 mg, 78% Yield). **^{1}H NMR (400 MHz, CDCl3):** δ 7.32 (d, J = 7.6 Hz, 2H), 7.28 (t, J = 7.2 Hz, 2H), 7.19 (t, J = 7.2 Hz), 5.61 (q, J = 6.8 Hz, 1H), 5.07 (s, 1H), 1.61 (d, J = 6.8 Hz, 3H),

1.39 (s, 3H), 1.34 (m, 6H), 0.92 (t, J = 7.2 Hz, 9H), 0.57 (m, 6H). **^{13}C NMR (175 MHz, CDCl3):** δ 143.8, 138.6, 127.7, 126.5, 125.9, 120.3, 79.7, 18.4, 16.9, 16.8, 16.79, 13.1, 10.9. **IR:** ν 701, 740, 856, 1054, 1206, 1450 cm^{-1}. **MS (EI) (*m*/*z*):** [M]+ calc'd for $C_{20}H_{34}OSi$ 318.2379, found 318.2380. **GC/MS (ret. time):** 12.813 min. **GC/MS (m/z:intensity):** 317: 743232, 318:2545664, 319:725120

(E)-triethyl((2-ethyl-1-phenylpent-2-en-1-yl)oxy)silane:

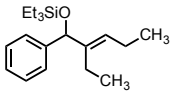

Following general procedure A, $Ni(COD)_2$ (15 mg, 0.055 mmol), PCy_3 (30 mg, 0.110 mmol), benzaldehyde (50 mg, 0.47 mmol), 3-hexyne (40 mg, 0.48 mmol), and triethylsilane (125 mg, 1.08 mmol) gave a crude residue which was purified *via* flash chromatography (5:95 EtOAc:Hexanes) to afford the product as a clear oil (98 mg, 68% Yield). **^{1}H NMR (400 MHz, CDCl3):** δ 7.32 (d, J = 7.6 Hz, 2H), 7.21 (t, J = 7.2 Hz, 2H), 7.18 (t, J = 7.6 Hz, 1H), 5.50 (t, J = 7.2 Hz,1H), 5.08 (s, 1H), 2.51 (m, 2H), 1.87 (m, 2H), 1.32 (m, 6H), 1.00 (t, J = 7.6 Hz, 3H), 0.90 (t, J = 7.2 Hz,9H), 0.71 (t, J = 7.6 Hz, 3H), 0.56 (m, 6H). **^{13}C NMR (175 MHz, CDCl3):** δ 144.1, 142.7, 128.1, 127.7, 126.5, 126.3, 78.9, 20.8, 19.7, 18.4, 17.0, 16.9, 16.8, 14.4, 14.3. **IR:** ν 712, 850, 1068, 1120, 1379, 1450, 1728 cm^{-1}. **MS (EI) (*m*/*z*):** [M]+ calc'd for $C_{19}H_{32}OSi$ 304.2222, found 304.2225. **GC/MS (ret. time):** 12.328 min. **GC/MS (m/z:intensity):** 275:156736, 276:38224, 304:69672, 305:18328

(E)-triethyl(3-deutero(2-ethyl-1-phenylpent-2-en-1-yl)oxy)silane:

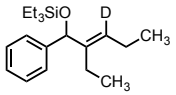

Following general procedure A, $Ni(COD)_2$ (15 mg, 0.055 mmol), PCy_3 (30 mg, 0.110 mmol), benzaldehyde (50 mg, 0.47 mmol), 3-hexyne (40 mg, 0.48 mmol), and triethylsilyl-deuteride (125 mg, 1.08 mmol) gave a crude residue which was purified *via* flash chromatography (5:95 EtOAc:Hexanes) to afford the product as a clear oil (95 mg, 66% Yield). **^{1}H NMR (400 MHz, CDCl3):** δ 7.33 (d, J = 8 Hz, 2H), 7.26 (t, J = 7.2 Hz, 2H), 7.18 (t, J = 7.2 Hz, 1H), 5.08 (s, 1H), 2.01 (m, 2H), 1.87 (m, 2H), 0.99 (t, J = 7.6 Hz, 3H), 0.90 (t, J = 8 Hz, 9H), 0.72 (t, J = 7.6 Hz, 3H), 0.57 (q, J = 8 Hz, 6H). **^{13}C NMR (175 MHz, CDCl3):** δ 114.1, 142.6, 127.7, 126.6, 126.3, 78.8, 20.7, 19.7, 14.4, 14.3, 6.9, 4.9. **IR:** ν 709, 850, 1065, 1120, 1379, 1450, 1728 cm^{-1}. **MS (EI) (*m*/*z*):** [M]+ calc'd for $C_{19}H_{31}ODSi$ 305.2285, found 305.2282. **GC/MS (ret. time):** 12.328 min. **GC/MS (m/z:intensity):** 275:17848, 276:1400320, 304:337984, 305:645440

(E)-((2-ethyl-1-phenylpent-2-en-1-yl)oxy)tripropylsilane:

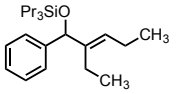

Following general procedure A, $Ni(COD)_2$ (15 mg, 0.055 mmol), PCy_3 (30 mg, 0.110 mmol), benzaldehyde (50 mg, 0.47 mmol), 3-hexyne (40 mg, 0.48 mmol), and tripropylsilane (200 mg, 1.08 mmol) gave a crude residue which was purified *via* flash chromatography (5:95 EtOAc:Hexanes) to afford the product as a clear oil (116 mg, 71% Yield). **^{1}H NMR (400 MHz, CDCl3):** δ 7.33 (d, J = 8 Hz, 2H), 7.26 (t, J = 7.2 Hz, 2H), 7.18 (t, J = 6.8 Hz, 1H), 5.50 (t, J = 7.2 Hz, 1H), 5.01 (s, 1H), 2.05 (m, 2H), 1.88 (m, 2H),

0.99 (t, J = 7.6 Hz, 3H), 0.91 (t, J = 7.6 Hz, 9H), 0.72 (t, J = 7.6 Hz, 3H), 0.57 (q, J = 8 Hz, 6H). **^{13}C NMR (175 MHz, CDCl3):** δ 144.1, 142.7, 128.2, 127.7, 126.5, 126.4, 78.9, 20.7, 19.7, 14.3, 6.9, 4.8. **IR:** ν 704, 838, 1007, 1065, 1241, 1450, 1690 cm^{-1}. **MS (EI) (*m*/*z*):** [M]+ calc'd for $C_{22}H_{38}OSi$ 346.2692, found 346.2683. **GC/MS (ret. time):** 13.880 min. **GC/MS (m/z:intensity):** 345:160512, 346:411776, 347:122944

triethyl((2-methylenecyclopentyl)oxy)silane:

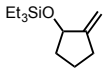

Following general procedure A, $Ni(COD)_2$ (15 mg, 0.054 mmol), PCy_3 (30 mg, 0.11 mmol), hex-5-ynal (50 mg, 0.53 mmol), and triethylsilane (125 mg, 1.08 mmol) gave a crude residue which was purified *via* flash chromatography (5:95 EtOAc:Hexanes) to afford the product as a clear oil (75 mg, 67% Yield). **^{1}H NMR (400 MHz, CDCl3):** δ 5.14 (s, 1H), 5.02 (s, 1H), 4.47 (m, 1H), 2.47 (m, 1H), 2.37 (m, 1H), 1.99 (m, 1H), 1.85 (m, 1H), 1.62 (m, 2H), 1.06 (t, J = 8 Hz, 9H), 0.73 (q, J = 8 Hz, 6H). **^{13}C NMR (175 MHz, CDCl3):** δ 154.0, 106.4, 75.1, 35.6, 29.4, 20.8, 6.8, 4.8. **IR:** ν 650, 731, 1002, 1070, 1709 cm^{-1}. **MS (EI) (*m*/*z*):** [M]+ calc'd for $C_{12}H_{24}OSi$ 212.1596, found 212.1600. **GC/MS (ret. time):** 6.569 min. **GC/MS (m/z:intensity):** 183:2074624, 184:363648, 185:105072, 212:109424, 213:19656

triethyl(2-deutero(2-methylenecyclopentyl)oxy)silane:

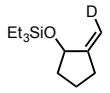

Following general procedure A, $Ni(COD)_2$ (15 mg, 0.054 mmol), PCy_3 (30 mg, 0.11 mmol), hex-5-ynal (50 mg, 0.53 mmol), and triethylsilyl-deuteride (100 mg, 0.85 mmol) gave a crude residue which was purified *via* flash chromatography (5:95 EtOAc:Hexanes) to afford the product as a clear oil (83 mg, 74% Yield). **^{1}H NMR (400 MHz, CDCl3):** δ 4.91 (s, 1H), 4.37 (m, 1H), 2.37 (m, 1H), 2.29 (m, 1H), 1.89 (m, 1H), 1.75 (m, 1H), 1.51 (m, 2H), 0.96 (t, J = 8 Hz, 9H), 0.62 (q, J = 8 Hz, 6H). **^{13}C NMR (175 MHz, CDCl3):** δ 154.0, 106.3, 106.2, 106.1, 75.0, 35.6, 29.4, 20.8, 6.8, 5.0, 4.8. **IR:** ν 651, 729, 1002, 1070, 1709 cm^{-1}. **MS (EI) (*m*/*z*):** [M]+ calc'd for $C_{12}H_{23}ODSi$ 213.1659, found 213.1662. **GC/MS (ret. time):** 6.569 min. **GC/MS (m/z:intensity):** 183:63504, 184:1916928, 185:338624, 212:15448, 213:118994

((2-methylenecyclopentyl)oxy)tripropylsilane:

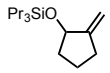

Following general procedure A, $Ni(COD)_2$ (15 mg, 0.054 mmol), PCy_3 (30 mg, 0.11 mmol), hex-5-ynal (50 mg, 0.53 mmol), and tripropylsilane (170 mg, 1.08 mmol) gave a crude residue which was purified *via* flash chromatography (5:95 EtOAc:Hexanes) to afford the product as a clear oil (94 mg, 71% Yield). **^{1}H NMR (400 MHz, CDCl3):** δ 5.01 (s, 1H), 4.91 (s, 1H), 4.35 (m, 1H), 2.36 (m, 1H), 2.29 (m, 1H), 1.87 (m, 1H), 1.75 (m, 1H), 1.51 (m, 2H), 1.37 (m, 6H), 0.94 (t, J = 7.6 Hz, 9H), 0.60 (m, 6H). **^{13}C NMR (175 MHz, CDCl3):** δ 154.1, 106.4, 75.1, 35.6, 29.4, 20.8, 18.5, 17.1, 16.9. **IR:** ν 685,

732, 1004, 1070, 1241, 1714 cm^{-1}. **MS (EI) (*m*/*z*):** [M]+ calc'd for $C_{15}H_{30}OSi$ 254.2066, found 254.2071. **GC/MS (ret. time):** 9.055 min. **GC/MS (m/z:intensity):** 211:34960, 212:6783, 253:348, 254:4698, 255:1459

(E)-triethyl((2-ethylidenecyclopentyl)oxy)silane:

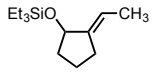

Following general procedure A, $Ni(COD)_2$ (10 mg, 0.04 mmol), PCy_3 (20 mg, 0.08 mmol), hept-5-ynal (0.045 mg, 0.41 mmol), and triethylsilane (100 mg, 0.70 mmol) gave a crude residue which was purified *via* flash chromatography (5:95 EtOAc:Hexanes) to afford the product as a clear oil (55 mg, 60% Yield). **^{1}H NMR (400 MHz, CDCl3):** δ 5.47 (m, 1H), 4.34 (m, 1H), 2.27 (m, 1H), 2.18 (m, 1H), 1.83 (m, 2H), 1.59 (d, J = 6.8 Hz, 3H), 1.49 (m, 2H), 0.95 (t, J = 8 Hz, 9H), 0.61 (q, J = 8 Hz, 6H). **^{13}C NMR (175 MHz, CDCl3):** δ 145.0, 116.9, 75.4, 36.1, 26.4, 21.1, 14.5, 6.8, 5.4, 5.1, 4.8. **MS (EI) (*m*/*z*):** [M]+ calc'd for $C_{13}H_{26}OSi$ 226.1753, found 226.1756. **GC/MS (ret. time):** 7.735 min. **GC/MS (m/z:intensity):** 226:349312, 227:71264, 228:19488

(E)-triethyl(1-deutero(2-ethylidenecyclopentyl)oxy)silane:

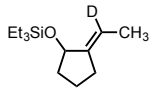

Following general procedure A, $Ni(COD)_2$ (10 mg, 0.04 mmol), PCy_3 (20 mg, 0.08 mmol), hept-5-ynal (0.045 mg, 0.41 mmol), and triethylsilyl-deuteride (100 mg, 0.85 mmol) gave a crude residue which was purified *via* flash chromatography (5:95 EtOAc:Hexanes) to afford the product as a clear oil (58 mg, 63% Yield). **^{1}H NMR (400**

MHz, CDCl3): δ 4.34 (m, 1H), 2.30 (m, 1H), 2.17 (m, 1H), 1.8 (m, 2H), 1.58 (s, 3H), 1.49 (m, 2H), 0.95 (t, J = 7.6 Hz, 9H), 0.60 (q, J = 7.6 Hz, 6H). **^{13}C NMR (175 MHz, CDCl3):** δ 144.9, 116.7, 116.6, 116.4, 75.4, 36.1, 26.4, 26.3, 21.1, 14.4, 6.8, 4.9, 4.7, 1.0. **MS (EI) (*m*/*z*):** [M]+ calc'd for $C_{13}H_{25}OSiD$ 227.1816, found 227.1816. **GC/MS (ret. time):** 7.735 min. **GC/MS (m/z:intensity):** 226:40448, 227:669120, 228:139456, 229:36512

(E)-((2-ethylidenecyclopentyl)oxy)tripropylsilane:

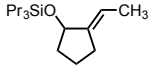

Following general procedure A, $Ni(COD)_2$ (10 mg, 0.04 mmol), PCy_3 (20 mg, 0.08 mmol), hept-5-ynal (0.045 mg, 0.41 mmol), and tripropylsilane (100 mg, 0.70 mmol) gave a crude residue which was purified *via* flash chromatography (5:95 EtOAc:Hexanes) to afford the product as a clear oil (62 mg, 56% Yield). **^{1}H NMR (400 MHz, CDCl3):** δ 5.45 (m, 1H), 4.33 (m, 1H), 2.28 (m, 1H), 2.17 (m, 1H), 1.8 (m, 2H), 1.59 (m,, 3H), 1.49 (m, 2H), 1.37 (m, 6H), 0.95 (t, J = 7.6 Hz, 9H), 0.59 (m, 6H). **^{13}C NMR (175 MHz, CDCl3):** δ 145.0, 116.8, 75.4, 36.1, 26.3, 21.1, 18.5, 16.9, 16.8, 14.5. **MS (EI) (*m*/*z*):** [M]+ calc'd for $C_{16}H_{32}OSi$ 268.2222, found 268.2214. **GC/MS (ret. time):** 10.024 min. **GC/MS (m/z:intensity):** 267: 17400, 268: 1068032, 269:249280, 270:63112, 271:8843

(E)-((2-(3,5-di-tert-butylbenzylidene)cyclopentyl)oxy)triethylsilane:

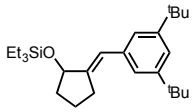

Following general procedure A, $Ni(COD)_2$ (7.5 mg, 0.027 mmol), PCy_3 (15 mg, 0.055 mmol), 6-(3,5-di-tert-butylphenyl)hex-5-ynal (50 mg, 0.18 mmol), and triethylsilane (45 mg, 0.39 mmol) gave a crude residue which was purified *via* flash chromatography (5:95 EtOAc:Hexanes) to afford the product as a clear oil (53 mg, 74% Yield). **^{1}H NMR (400 MHz, CDCl3):** δ 7.28 (s, 1H), 7.21 (s, 2H), 6.52 (s, 1H), 4.58 (t, J] 6.8 Hz, 1H), 2.65 (m, 2H), 1.90 (m, 2H), 1.58 (m, 2H), 1.35 (s, 18H), 1.04 (t, J = 8 Hz, 9H), 0.71 (q, J = 8 Hz, 6H). **^{13}C NMR (175 MHz, CDCl3):** δ 150.3, 146.1, 137.3, 123.2, 122.8, 120.3, 34.9, 34.8, 31.6, 31.4, 28.5, 21.6, 6.9, 5.0. **IR:** ν 734, 838, 1008, 1119, 1370, 1610 cm^{-1}. **MS (EI) (*m*/*z*):** [M]+ calc'd for $C_{26}H_{44}OSi$ 400.3161, found 400.3161. **GC/MS (ret. time):** 17.991 min. **GC/MS (m/z:intensity):** 371:24864, 372:9715, 400:157696, 401:53408.

(E)-(2-deutero(2-(3,5-di-tert-butylbenzylidene)cyclopentyl)oxy)triethylsilane:

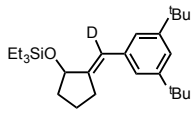

Following general procedure A, $Ni(COD)_2$ (7.5 mg, 0.027 mmol), PCy_3 (15 mg, 0.055 mmol), 6-(3,5-di-tert-butylphenyl)hex-5-ynal (50 mg, 0.18 mmol), and triethylsilyl-deuteride (50 mg, 0.45 mmol) gave a crude residue which was purified *via* flash chromatography (5:95 EtOAc:Hexanes) to afford the product as a clear oil (51 mg, 72% Yield). **^{1}H NMR (400 MHz, CDCl3):** δ 7.27 (s, 1H), 7.20 (s, 2H), 4.57 (t, J = 6Hz, 1H), 2.64 (m, 2H), 1.93 (m, 2H), 1.59 (m, 2H), 1.34 (s, 18H), 1.03 (t, J = 8 Hz, 9H), 0.71 (q, J

= 8 Hz, 6H). **^{13}C NMR (175 MHz, CDCl3):** δ 150.3, 145.9, 137.2, 122.9, 122.8, 122.7, 120.3, 34.9, 34.8, 31.5, 28.5, 21.6, 6.9, 5.0. **IR:** ν 733, 838, 1008, 1119, 1375, 1606, 1717 cm^{-1}. **MS (EI) (*m*/*z*):** [M]+ calc'd for $C_{26}H_{43}OSiD$ 401.3224, found 401.3228. **GC/MS (ret. time):** 17.991 min. **GC/MS (m/z:intensity):** 371:3344, 372:60400, 400:40832, 401:434880.

(E)-((2-(3,5-di-tert-butylbenzylidene)cyclopentyl)oxy)tripropylsilane:

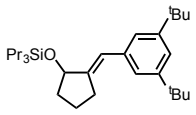

Following general procedure A, $Ni(COD)_2$ (7.5 mg, 0.027 mmol), PCy_3 (15 mg, 0.055 mmol), 6-(3,5-di-tert-butylphenyl)hex-5-ynal (50 mg, 0.18 mmol), and tripropylsilane (60 mg, 0.45 mmol) gave a crude residue which was purified *via* flash chromatography (5:95 EtOAc:Hexanes) to afford the product as a clear oil (52 mg, 68% Yield). **^{1}H NMR (400 MHz, CDCl3):** δ 7.28 (s, 1H), 7.20 (s, 2H), 6.50 (s, 1H), 4.56 (t, J = 7.2 Hz, 1H), 2.6 (m, 2H), 1.90 (m, 2H), 1.55 (m, 2H), 1.43 (m, 2H), 1.35 (s, 18H), 1.01 (t, J = 8 Hz, 9H), 0.70 (m, 6H). **^{13}C NMR (175 MHz, CDCl3):** δ 150.2, 146.0, 137.3, 123.2, 122.7, 120.3, 34.9, 34.7, 31.3, 28.5, 21.6, 18.5, 17.0. **IR:** ν 730, 835, 1010, 1607 cm^{-1}. **MS (EI) (*m*/*z*):** [M]+ calc'd for $C_{29}H_{50}OSi$ 442.3631, found 442.3625. **GC/MS (ret. time):** 19.131 min. **GC/MS (m/z:intensity):** 441:27848, 442:185216, 443:65896

6-(3,5-di-tert-butylphenyl)hex-5-yn-1-ol:

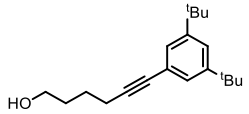

Trans-dichloro-bis(triphenylphosphine)-palladium (300 mg, 0.43 mmol), copper-iodide (150 mg, 0.79 mmol), and 1-bromo-3,5-di-tert-butylbenzene (1 g, 3.8 mmol) were added to a dry round bottomed flask. Tri-ethyl-amine (10 mL) was added, the resulting mixture was allowed to equilibrate to 45°C over 10 min. 5-hexyn-1-ol (500 mg, 5.1 mmol) was added and allowed to stir over 72 hr at 45°C. Reaction was concentrated *in vacuo* and chromatographed on a large silica column, affording a white powder (972 mg, 3.4 mmol, 89% yield). **^{1}H NMR (400 MHz, CDCl3):** δ 7.32 (t, J = 2 Hz, 1H), 7.23 (d, J = 2 Hz, 2H), 3.70 (q, J = 5.6 Hz, 2H), 2.45 (t, J = 6.8 Hz, 2H), 1.69 (m, 4H), 1.29 (s, 18H). **^{13}C NMR (175 MHz, CDCl3):** δ 148.1, 123.2, 120.2, 119.5, 85.8, 79.3, 60.0, 32.2, 29.4, 28.7, 25.5, 16.6.

(E)-((2-benzylidenecyclohexyl)oxy)triethylsilane:

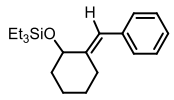

Following general procedure A, $Ni(COD)_2$ (8.6 mg, 0.03 mmol), PCy_3 (16.8 mg, 0.06 mmol), 7-phenylhept-6-ynal (86 mg, 0.46 mmol), and triethylsilane (105 mg, 0.9 mmol) gave a crude residue which was purified *via* flash chromatography (5:95 EtOAc:Hexanes) to afford the product as a clear oil (86 mg, 62% Yield). **^{1}H NMR (400 MHz, CDCl3):** δ 7.23 (t, J = 8 Hz, 2H), 7.18 (m, 3H), 6.52 (s, 1H), 4.15 (dd, J = 4 Hz, 8 Hz, 1H), 2.73, m, 1H), 1.99 (m, 1H), 1.87 (m, 2H), 1.57 (m, 2H), 1.47 (m, 2H), 0.98 (t, J = 8 Hz, 9H), 0.63 (q, J = 8 Hz, 6H). **^{13}C NMR (175 MHz, CDCl3):** δ 144.5, 138.2,

128.9, 127.9, 125.9, 120.2, 73.9, 37.8, 27.5, 27.3, 23.7, 6.9, 4.9. **IR:** ν 697, 850, 915, 1117, 1497 cm^{-1}. **MS (EI) (*m*/*z*):** [M]+ calc'd for $C_{19}H_{30}OSi$ 302.2066, found 302.2065. **GC/MS (ret. time):** 14.679 min. **GC/MS (m/z:intensity):** 301:31000, 302:614592, 303:160960, 304:42584.

(E)-((3-deutero-2-benzylidenecyclohexyl)oxy)triethylsilane:

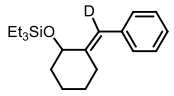

Following general procedure A, $Ni(COD)_2$ (8.6 mg, 0.03 mmol), PCy_3 (16.8 mg, 0.06 mmol), 7-phenylhept-6-ynal (86 mg, 0.46 mmol), and triethylsilyl-deuteride (105 mg, 0.9 mmol) gave a crude residue which was purified *via* flash chromatography (5:95 EtOAc:Hexanes) to afford the product as a clear oil (98 mg, 71% Yield). **^{1}H NMR (400 MHz, CDCl3):** δ 7.26 (t, J = 8 Hz, 2H), 7.21 (m, 3H), 4.16 (dd, J = 8.4 Hz, 3.6 Hz, 1H), 2.76 (m, 1H), 2.01 (ddd, J = 13.8 Hz, 10 Hz, 4.4 Hz, 1H), 1.89 (m, 2H), 1.55 (m, 2H), 1.44 (m, 2H), 0.99 (t, J = 8 Hz, 9H), 0.65 (q, J = 8 Hz, 6H). **^{13}C NMR (175 MHz, CDCl3):** δ 144.4, 138.2, 128.9, 128.0, 125.9, 74.0, 37.9, 27.5, 27.3, 23.7, 6.9, 4.9. **IR:** ν 696, 772, 853, 915, 1117, 1445, 1497 cm^{-1}. **MS (EI) (*m*/*z*):** [M]+ calc'd for $C_{19}H_{29}OSiD$ 303.2129, found 303.2128. **GC/MS (ret. time):** 14.679 min. **GC/MS (m/z:intensity):** 302:29160, 303:524864, 304:135744, 305:33912.

(E)-((2-benzylidenecyclohexyl)oxy)tripropylsilane:

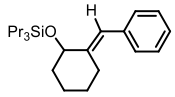

Following general procedure A, $Ni(COD)_2$ (8.6 mg, 0.03 mmol), PCy_3 (16.8 mg, 0.06 mmol), 7-phenylhept-6-ynal (86 mg, 0.46 mmol), and tripropylsilane (131 mg, 0.9 mmol) gave a crude residue which was purified *via* flash chromatography (5:95 EtOAc:Hexanes) to afford the product as a clear oil (130 mg, 72% Yield). **^{1}H NMR (400 MHz, CDCl3):** δ 7.30 (t, J = 6.8 Hz, 2H), 7.18 (m, 3H), 6.50 (s, 1H), 4.19 (J = 8.4 Hz, 3.6 Hz, 1H), 2.71 (m, 1H), 2.00 (m, 1H), 1.85 (m, 2H), 1.55 (m, 2H), 1.40 (m, 6H), 0.95 (t, J = 10.4 Hz, 9H), 0.62 (m, 6H). **^{13}C NMR (100 MHz, CDCl3):** δ 144.6, 138.3, 128.9, 128.0, 125.9, 120.2, 74.0, 37.8, 27.5, 27.3, 23.6, 18.5, 16.94, 16.90. **IR:** ν 702, 836, 1120, 1205, 1377, 1451 cm^{-1}. **MS (EI) (*m*/*z*):** [M]+ calc'd for $C_{22}H_{36}OSi$ 344.2535, found 344.2541. **GC/MS (ret. time):** 16.224 min. **GC/MS (m/z:intensity):** 343:8308, 344:510016, 345:147968, 346:40224.

(E)-((2-benzylidenecycloheptyl)oxy)triethylsilane:

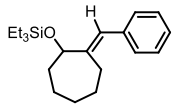

Following general procedure A, $Ni(COD)_2$ (9 mg, 0.03 mmol), PCy_3 (17 mg, 0.06 mmol), 8-phenyl-oct-7-ynal (60 mg, 0.3 mmol), and triethylsilane (69 mg, 0.6 mmol) gave a crude residue which was purified *via* flash chromatography (5:95 EtOAc:Hexanes) to afford the product as a clear oil (78 mg, 82% Yield). **^{1}H NMR (400 MHz, CDCl3):** δ 7.31 (t, J = 8 Hz, 2H), 7.25 (d, J = 7.2 Hz, 2H), 7.19 (t, J = 8 Hz, 1H), 6.51 (s, 1H), 4.32 (dd, J = 4.8 Hz, 6.4 Hz, 1H), 2.52 (m, 1H), 2.35 (m, 1H), 1.89 (m, 1H), 1.76 (m, 1H),

1.68 (m, 2H), 1.54 (m, 3H), 1.40 (m, 1H), 0.96 (t, J = 8 Hz, 9H), 0.61 (q, J = 8 Hz, 6H). **^{13}C NMR (175 MHz, CDCl3):** δ 146.0, 138.2, 128.6, 128.1, 126.1, 125.2, 38.8, 28.3, 27.1, 26.7, 23.9, 6.9, 4.9. **MS (EI) (*m*/*z*):** [M]+ calc'd for $C_{20}H_{32}OSi$ 316.2222, found 316.2236. **GC/MS (rt):** 15.641 min. **GC/MS (m/z:intensity):** 315:55256, 316:317120, 317:85376, 318:21136.

(E)-((3-deutero-2-benzylidenecycloheptyl)oxy)triethylsilane:

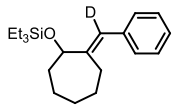

Following general procedure A, $Ni(COD)_2$ (9 mg, 0.03 mmol), PCy_3 (17 mg, 0.06 mmol), 8-phenyl-oct-7-ynal (60 mg, 0.3 mmol), and triethylsilyl-deuteride (69 mg, 0.6 mmol) gave a crude residue which was purified *via* flash chromatography (5:95 EtOAc:Hexanes) to afford the product as a clear oil (75 mg, 77% Yield). **^{1}H NMR (400 MHz, CDCl3):** δ 7.32 (t, J = 8 Hz, 2H), 7.27 (d, J = 6.4 Hz, 2H), 7.20 (m, 1H), 4.34 (dd, J = 7.2, 4.4 Hz, 1H), 2.54 (m, 1H), 2.37 (m, 1H), 1.91 (m, 1H), 1.78 (m, 1H), 1.69 (m, 1H), 1.55 (m, 1H), 1.41 (m, 1H), 0.98 (t, J = 8 Hz, 9H), 0.63 (q, J = 8 Hz, 6H). **^{13}C NMR (175 MHz, CDCl3):** δ 145.9, 138.1, 128.7, 128.1, 126.1, 76.7, 38.9, 28.3, 27.1, 26.7, 23.9, 6.9, 4.9. **MS (EI) (*m*/*z*):** [M]+ calc'd for $C_{20}H_{31}OSiD$ 317.2285, found 317.2288. **GC/MS (ret. time):** 15.641 min. **GC/MS (m/z:intensity):** 315: 3368, 316: 54904, 317:303616, 318: 80744.

(E)-((2-benzylidenecycloheptyl)oxy)tripropylsilane:

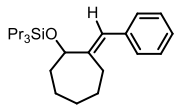

Following general procedure A, $Ni(COD)_2$ (9 mg, 0.03 mmol), PCy_3 (17 mg, 0.06 mmol), 8-phenyl-oct-7-ynal (60 mg, 0.3 mmol), and tripropylsilane (88 mg, 0.6 mmol) gave a crude residue which was purified *via* flash chromatography (5:95 EtOAc:Hexanes) to afford the product as a clear oil (100 mg, 93% Yield). **^{1}H NMR (400 MHz, CDCl3):** δ 7.31 (t, J = 8 Hz), 7.25 (m, 2H), 7.21 (m, 1H), 6.50 (s, 1H), 4.32 (dd, J = 4.8, 7.2 Hz), 2.50 (m, 1H), 2.35 (m, 1H), 1.65 (m, 6H), 1.40 (m, 6H), 0.96 (t, J = 7.2 Hz, 9H), 0.61 (m, 6H). **^{13}C NMR (175 MHz, CDCl3):** δ 146.1, 138.3, 128.6, 128.1, 126.1, 125.3, 76.7, 38.8, 28.3, 27.1, 26.7, 23.8, 18.5, 17.0. **MS (EI) (*m*/*z*):** [M]+ calc'd for $C_{23}H_{38}OSi$ 358.2692, found 358.2678. **GC/MS (ret. time):** 17.077 min. **GC/MS (m/z:intensity):** 357:22000, 358:213696, 359:64912, 360:16408.

5.2.2 Equation and Explanation for Calculation of Double-Labeling Data

Determination of isotopic distribution in products of catalytic crossover experiments - Representative Example:

Crossover of (E)-triethyl((2-ethyl-1-phenylpent-2-en-1-yl)oxy)silane

Pure samples of products derived from Et_3SiH (MW 304), Et_3SiD (MW 305), and Pr_3SiH (MW 346) were independently prepared, and GCMS analysis was performed. Based on similarity of the molecular ion regions of the Et_3SiH and Pr_3SiH-derived products, the molecular ion region of the Pr_3SiD-derived product was assumed resemble the ion region for Pr_3SiH shifted by one mass unit. Relative peak heights in the molecular ion region of the spectra of each pure compound were normalized, with a value of 1 assigned to the base peak.

In the crude product of an experiment that employed 1 equiv. each of Et_3SiD and Pr_3SiH, the ratio of Et_3Si products to Pr_3Si products was determined by GC. From the crude GCMS, the relative intensity of the 289 and 290 peaks were normalized, with a value of 1 assigned to the base peak. Ion peaks with the greatest intensity provide the most consistent data for analysis. The ratio of the Et_3Si-(H) product to Et_3Si-(D) product was determined as follows:

$$\frac{Intensity\ of\ 276\ peak\ in\ Crossover\ Experiment}{Intensity\ of\ 277\ peak\ in\ Crossover\ Experiment}$$

$$= \frac{[X](relative\ intensity\ of\ 276\ peak\ in\ Et3SiH\ Sample) + [Y](relative\ intensity\ of\ 276\ peak\ in\ Et3SiD\ Sample)}{[X](relative\ intensity\ of\ 277\ peak\ in\ Et3SiH\ Sample) + [Y](relative\ intensity\ of\ 276\ peak\ in\ Et3SiD\ Sample)}$$

$$[X] = \frac{1}{100} * Relative\ \%\ of\ Et3SiH\ Product$$

$$[Y] = \frac{1}{100} * Relative\ \%\ of\ Et3SiD\ Product = 1 - [X]$$

In the above equation, after substitution of [1 - X] for [Y], the equation can be solved for X. The resulting equation was used to create an excel spreadsheet included as an additional resource.

The ratio of the Pr_3Si-(H) product to Pr_3Si-(D) product was determined in a similar fashion. Merging the GC ratios of Et_3Si products to Pr_3Si products with the data calculated from the above equation, an overall ratio of the four possible products may be obtained.

5.2.3 Double-Labeling Experiments

Table 2.0.2 Entry 1

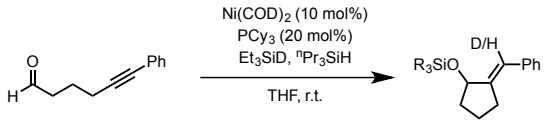

Retention Time 14.473 min.		Retention Time 16.041 min.	
Et3Si Products		Pr3Si Products	
Ion	Intensity	Ion	Intensity
288	23832	329	2447
299	144768	330	79624
300	35328	331	31232

Et Product Isotope Ratio (H:D)	9:91	Pr Product Isotope Ratio (H:D)	89:11
Et:Pr Product Ratio	61:39		

Complete Product Ratio

Et3Si-H Product	Et3Si-D Product	Pr3Si-H Product	Pr3Si-D Product
6	55	35	4

Table 2.0.2 Entry 2

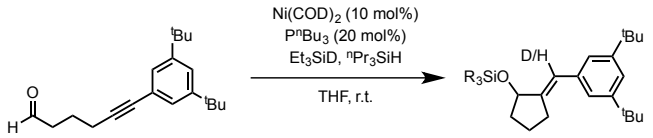

Retention Time 17.991 min.		Retention Time 19.131 min.	
Et3Si Products		Pr3Si Products	
Ion	Intensity	Ion	Intensity
400	91344	441	3256
401	129016	442	83904
402	42968	443	79136

Et Product Isotope Ratio (H:D)	44:55	Pr Product Isotope Ratio (H:D)	59:41
Et:Pr Product Ratio	60:40		

Complete Product Ratio			
Et3Si-H Product	Et3Si-D Product	Pr3Si-H Product	Pr3Si-D Product
26	34	24	16

Table 2.0.2 Entry 3

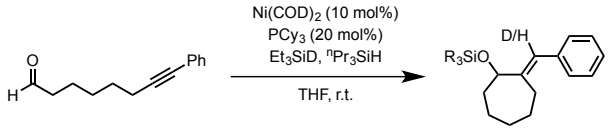

Retention Time 15.641 min.		Retention Time 17.071 min.	
Et3Si Products		Pr3Si Products	
Ion	Intensity	Ion	Intensity
316	40184	357	10955
317	219072	358	103344
318	60840	359	31056

Et Product Isotope Ratio (H:D)	1:99	Pr Product Isotope Ratio (H:D)	99:1
Et:Pr Product Ratio	58:42		

Complete Product Ratio			
Et3Si-H Product	Et3Si-D Product	Pr3Si-H Product	Pr3Si-D Product
<1	57	41	<1

Table 2.0.3 Entry 1

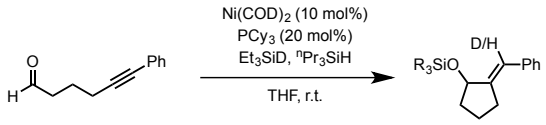

See Table 2.0.2 Entry 1

Table 2.0.3 Entry 2

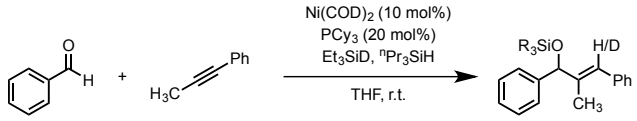

Matches previous published results

Table 2.0.3 Entry 3

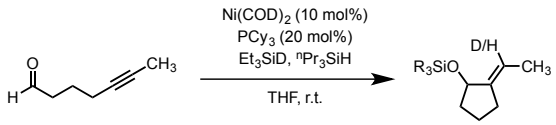

Retention Time 6.596 min.		Retention Time 9.055 min.	
Et3Si Products		Pr3Si Products	
Ion	Intensity	Ion	Intensity
226	107912	267	1559
227	211200	268	108856
228	42504	269	97912

Et Product Isotope Ratio (H:D)	35:65	Pr Product Isotope Ratio (H:D)	59:41
Et:Pr Product Ratio	54:46		

Complete Product Ratio			
Et3Si-H Product	Et3Si-D Product	Pr3Si-H Product	Pr3Si-D Product
19	35	27	19

Table 2.0.3 Entry 4

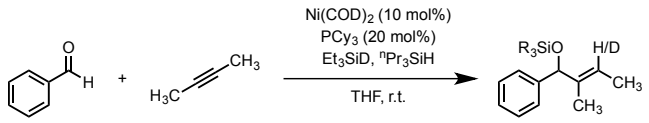

Retention Time 11.069 min.		Retention Time 12.813 min.	
Et3Si Products		Pr3Si Products	
Ion	Intensity	Ion	Intensity
276	1987072	318	2596352
277	2976256	319	1115136

Et Product Isotope Ratio (H:D)	15:85	Pr Product Isotope Ratio (H:D)	86:14
Et:Pr Product Ratio	57:43		

Complete Product Ratio			
Et3Si-H Product	Et3Si-D Product	Pr3Si-H Product	Pr3Si-D Product
9	46	37	6

Table 2.0.4 Entry 1

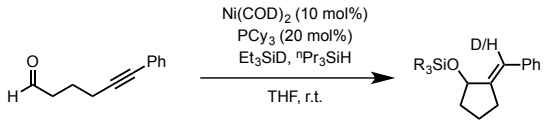

See Table 2.0.2 Entry 2

Table 2.0.4 Entry 2

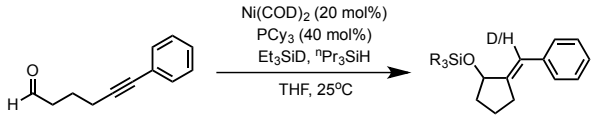

Retention Time 14.747 min.		Retention Time 16.041 min.	
Et3Si Products		Pr3Si Products	
Ion	Intensity	Ion	Intensity
288	34288	330	121608
289	170112	331	51696

Et Product Isotope Ratio (H:D)	12:88	Pr Product Isotope Ratio (H:D)	87:13
Et:Pr Product Ratio	61:39		

Complete Product Ratio			
Et3Si-H Product	Et3Si-D Product	Pr3Si-H Product	Pr3Si-D Product
7	54	34	5

Table 2.0.4 Entry 3

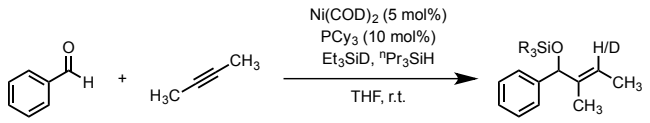

Retention Time 11.069 min.		Retention Time 12.815 min.	
Et3Si Products		Pr3Si Products	
Ion	Intensity	Ion	Intensity
276	1954918	318	2576725
277	3041280	319	1127477

Et Product Isotope Ratio (H:D)	12:88	Pr Product Isotope Ratio (H:D)	85:15
Et:Pr Product Ratio	58:42		

Complete Product Ratio			
Et3Si-H Product	Et3Si-D Product	Pr3Si-H Product	Pr3Si-D Product
7	51	36	6

Table 2.0.4 Entry 4

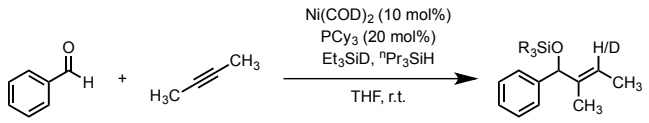

Retention Time 11.069 min.		Retention Time 12.813 min.	
Et3Si Products		Pr3Si Products	
Ion	Intensity	Ion	Intensity
276	1987072	318	2596352
277	2976256	319	1115136

Et Product Isotope Ratio (H:D)	15:85	Pr Product Isotope Ratio (H:D)	86:14
Et:Pr Product Ratio	57:43		

Complete Product Ratio			
Et3Si-H Product	Et3Si-D Product	Pr3Si-H Product	Pr3Si-D Product
9	46	37	6

Table 2.0.4 Entry 5

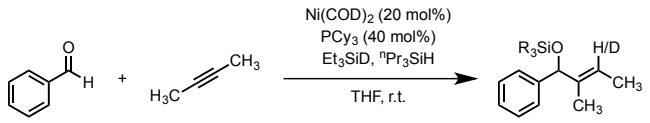

Retention Time 11.069 min.		Retention Time 12.815 min.	
Et3Si Products		Pr3Si Products	
Ion	Intensity	Ion	Intensity
276	2016256		
277	2985984	318	2604032
		319	1103360

Et Product Isotope Ratio (H:D)	15:85	Pr Product Isotope Ratio (H:D)	86:14
Et:Pr Product Ratio	57:43		

Complete Product Ratio			
Et3Si-H Product	Et3Si-D Product	Pr3Si-H Product	Pr3Si-D Product
9	46	37	6

Table 2.0.5 Entry 1

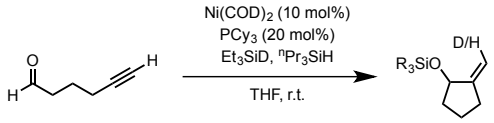

Retention Time 6.569 min.		Retention Time 9.055 min.	
Et3Si Products		Pr3Si Products	
Ion	Intensity	Ion	Intensity
183	80880	211	89096
184	71848	212	63104
185	13541	213	14273

Et Product Isotope Ratio (H:D)	42:58	Pr Product Isotope Ratio (H:D)	66:34
Et:Pr Product Ratio	52:48		

Complete Product Ratio			
Et3Si-H Product	Et3Si-D Product	Pr3Si-H Product	Pr3Si-D Product
22	30	32	16

Table 2.0.5 Entry 2

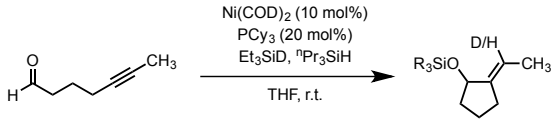

Retention Time 6.596 min.		Retention Time 9.055 min.	
Et3Si Products		Pr3Si Products	
Ion	Intensity	Ion	Intensity
226	107912	267	1559
227	211200	268	108856
228	42504	269	97912

Et Product Isotope Ratio (H:D)	35:65	Pr Product Isotope Ratio (H:D)	59:41
Et:Pr Product Ratio	54:46		

Complete Product Ratio			
Et3Si-H Product	Et3Si-D Product	Pr3Si-H Product	Pr3Si-D Product
19	35	27	19

Table 2.0.5 Entry 3

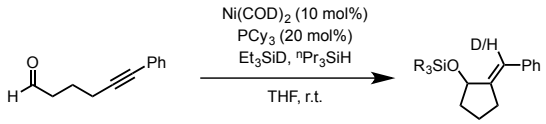

See Table 2.0.2 Entry 1

Table 2.0.5 Entry 4

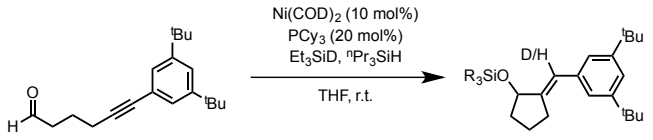

Retention Time 17.991 min.		Retention Time 19.131 min.	
Et3Si Products		Pr3Si Products	
Ion	Intensity	Ion	Intensity
400	38368	441	2376
401	216256	442	68752
402	71112	443	33304

Et Product Isotope Ratio (H:D)	9:91	Pr Product Isotope Ratio (H:D)	88:12
Et:Pr Product Ratio	65:35		

Complete Product Ratio			
Et3Si-H Product	Et3Si-D Product	Pr3Si-H Product	Pr3Si-D Product
4	61	32	3

Table 2.0.5 Entry 5

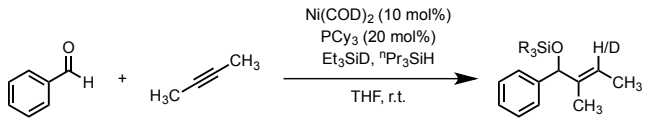

Retention Time 11.069 min.		Retention Time 12.813 min.	
Et3Si Products		Pr3Si Products	
Ion	Intensity	Ion	Intensity
276	1987072	318	2596352
277	2976256	319	1115136

Et Product Isotope Ratio (H:D)	15:85	Pr Product Isotope Ratio (H:D)	86:14
Et:Pr Product Ratio	57:43		

Complete Product Ratio			
Et3Si-H Product	Et3Si-D Product	Pr3Si-H Product	Pr3Si-D Product
9	46	37	6

Table 2.0.5 Entry 6

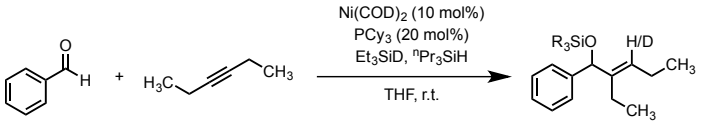

Retention Time 12.329 min.		Retention Time 13.088 min.	
Et3Si Products		Pr3Si Products	
Ion	Intensity	Ion	Intensity
275	2473	345	15974
276	105948	346	40624
277	24408	347	13161

Et Product Isotope Ratio (H:D)	8:92	Pr Product Isotope Ratio (H:D)	97:3
Et:Pr Product Ratio	61:49		

Complete Product Ratio			
Et3Si-H Product	Et3Si-D Product	Pr3Si-H Product	Pr3Si-D Product
5	56	47	2

Table 2.0.5 Entry 7

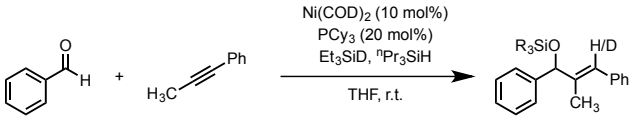

Matches previous published results

Table 2.0.6 Entry 1

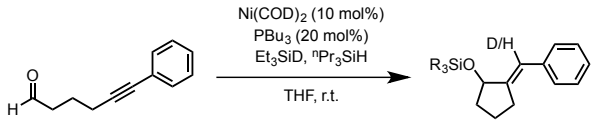

Matches previous published results

Table 2.0.6 Entry 2

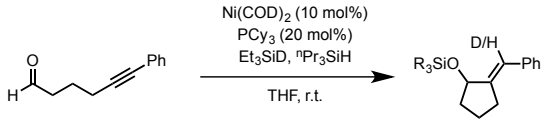

See Table 2.0.2 Entry 1

Table 2.0.6 Entry 3

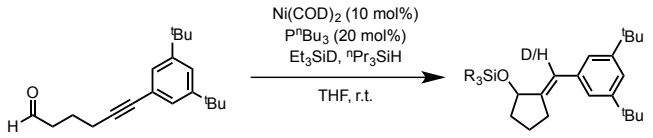

Retention Time 17.991 min.		Retention Time 19.131 min.	
Et3Si Products		Pr3Si Products	
Ion	Intensity	Ion	Intensity
400	91344	441	3256
401	129016	442	83904
402	42968	443	79136

Et Product Isotope Ratio (H:D)	44:55	Pr Product Isotope Ratio (H:D)	59:41
Et:Pr Product Ratio	60:40		

Complete Product Ratio			
Et3Si-H Product	Et3Si-D Product	Pr3Si-H Product	Pr3Si-D Product
26	34	24	16

Table 2.0.6 Entry 4

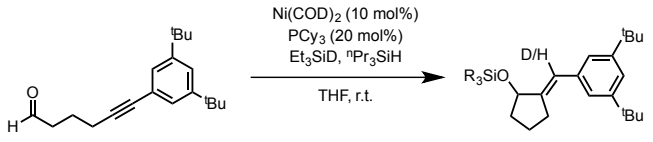

Retention Time 17.991 min.		Retention Time 19.131 min.	
Et3Si Products		Pr3Si Products	
Ion	Intensity	Ion	Intensity
400	38368	441	2376
401	216256	442	68752
402	71112	443	33304

Et Product Isotope Ratio (H:D)	9:91	Pr Product Isotope Ratio (H:D)	88:12
Et:Pr Product Ratio	65:35		

Complete Product Ratio			
Et3Si-H Product	Et3Si-D Product	Pr3Si-H Product	Pr3Si-D Product
4	61	32	3

Table 2.0.7 Entry 1

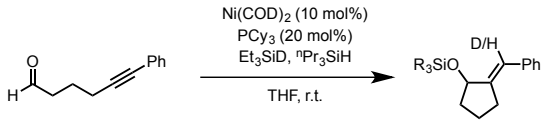

See Table 2.0.2 Entry 1

Table 2.0.7 Entry 2

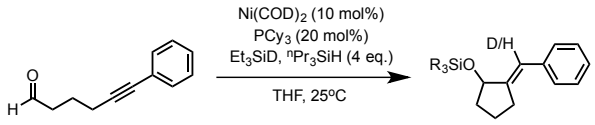

Retention Time 14.747 min.		Retention Time 16.041 min.	
Et3Si Products		Pr3Si Products	
Ion	Intensity	Ion	Intensity
288	157952	330	285824
289	481216	331	171200
290	126136	332	45896

Et Product Isotope Ratio (H:D)	22:78	Pr Product Isotope Ratio (H:D)	75:25
Et:Pr Product Ratio	66:34		

Complete Product Ratio			
Et3Si-H Product	Et3Si-D Product	Pr3Si-H Product	Pr3Si-D Product
14	52	26	9

Table 2.0.7 Entry 3

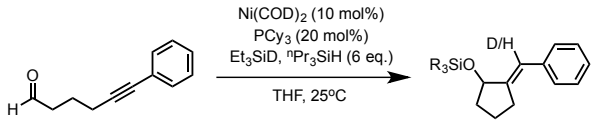

Retention Time 14.747 min.		Retention Time 16.041 min.	
Et3Si Products		Pr3Si Products	
Ion	Intensity	Ion	Intensity
288	173960	330	213696
289	455808	331	158208
290	117984	332	43416

Et Product Isotope Ratio (H:D)	25:75	Pr Product Isotope Ratio (H:D)	67:33
Et:Pr Product Ratio	70:30		

Complete Product Ratio			
Et3Si-H Product	Et3Si-D Product	Pr3Si-H Product	Pr3Si-D Product
17	53	20	10

Table 2.0.7 Entry 4

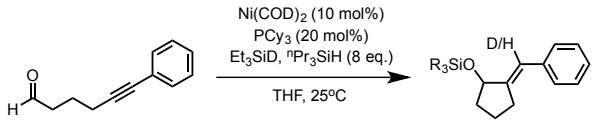

Retention Time 14.747 min.		Retention Time 16.041	
Et3Si Products		Pr3Si Products	
Ion	Intensity	Ion	Intensity
288	287040	330	352832
289	671488	331	282688
290	167808	332	78456

Et Product Isotope Ratio (H:D)	28:82	Pr Product Isotope Ratio (H:D)	64:36
Et:Pr Product Ratio	75:15		

Complete Product Ratio			
Et3Si-H Product	Et3Si-D Product	Pr3Si-H Product	Pr3Si-D Product
21	54	16	9

Table 2.0.7 Entry 5

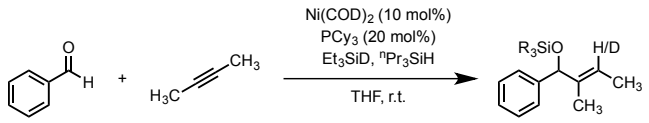

Retention Time 11.069 min.		Retention Time 12.813 min.	
Et3Si Products		Pr3Si Products	
Ion	Intensity	Ion	Intensity
276	1987072	318	2596352
277	2976256	319	1115136

Et Product Isotope Ratio (H:D)	15:85	Pr Product Isotope Ratio (H:D)	86:14
Et:Pr Product Ratio	57:43		

Complete Product Ratio			
Et3Si-H Product	Et3Si-D Product	Pr3Si-H Product	Pr3Si-D Product
9	46	37	6

Table 2.0.7 Entry 6

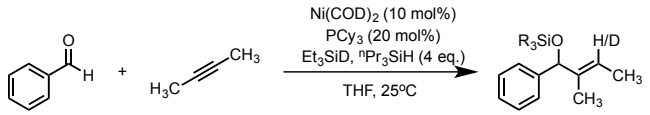

Retention Time 6.569 min.		Retention Time 9.055 min.	
Et3Si Products		Pr3Si Products	
Ion	Intensity	Ion	Intensity
275	7646	317	14183
276	45496	318	53824
277	66928	319	28088

Et Product Isotope Ratio (H:D)	16:84	Pr Product Isotope Ratio (H:D)	78:22
Et:Pr Product Ratio	64:36		

Complete Product Ratio			
Et3Si-H Product	Et3Si-D Product	Pr3Si-H Product	Pr3Si-D Product
10	54	28	8

Table 2.0.7 Entry 7

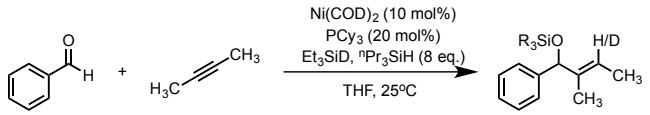

Retention Time 6.569 min.		Retention Time 9.055 min.	
Et3Si Products		Pr3Si Products	
Ion	Intensity	Ion	Intensity
275	98480	317	124800
276	438848	318	469312
277	530816	319	312448

Et Product Isotope Ratio (H:D)	28:72	Pr Product Isotope Ratio (H:D)	68:32
Et:Pr Product Ratio	69:31		

Complete Product Ratio			
Et3Si-H Product	Et3Si-D Product	Pr3Si-H Product	Pr3Si-D Product
19	50	21	10

Table 2.0.8 Entry 1

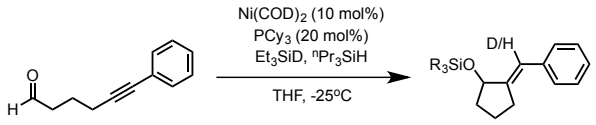

Retention Time 14.473 min.		Retention Time 16.041 min.	
Et3Si Products		Pr3Si Products	
Ion	Intensity	Ion	Intensity
288	14965	330	7599
289	21984	331	9032
290	5243	332	2812

Et Product Isotope Ratio (H:D)	42:58	Pr Product Isotope Ratio (H:D)	50:50
Et:Pr Product Ratio	63:47		

Complete Product Ratio			
Et3Si-H Product	Et3Si-D Product	Pr3Si-H Product	Pr3Si-D Product
26	36	24	24

Table 2.0.8 Entry 2

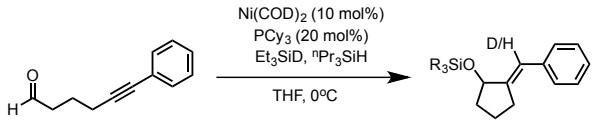

Retention Time 14.473 min.		Retention Time 16.041 min.	
Et3Si Products		Pr3Si Products	
Ion	Intensity	Ion	Intensity
288	28240	330	110424
289	157376	331	42776
290	39368	332	11269

Et Product Isotope Ratio (H:D)	10:90	Pr Product Isotope Ratio (H:D)	89:11
Et:Pr Product Ratio	65:35		

Complete Product Ratio			
Et3Si-H Product	Et3Si-D Product	Pr3Si-H Product	Pr3Si-D Product
7	58	40	5

Table 2.0.8 Entry 3

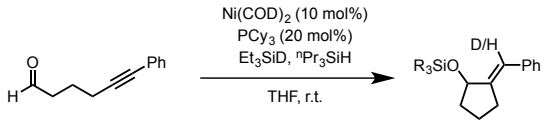

See Table 2.0.2 Entry 1

Table 2.0.8 Entry 4

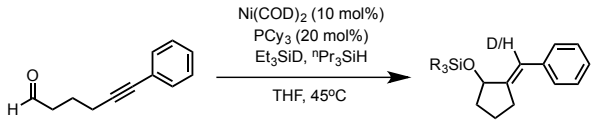

Retention Time 14.485 min.		Retention Time 16.058 min.	
Et3Si Products		Pr3Si Products	
Ion	Intensity	Ion	Intensity
288	10042	330	44184
289	76912	331	16512
290	19048	332	3854

Et Product Isotope Ratio (H:D)	6:94	Pr Product Isotope Ratio (H:D)	91:9
Et:Pr Product Ratio	59:41		

Complete Product Ratio			
Et3Si-H Product	Et3Si-D Product	Pr3Si-H Product	Pr3Si-D Product
4	55	37	4

Table 2.0.8 Entry 5

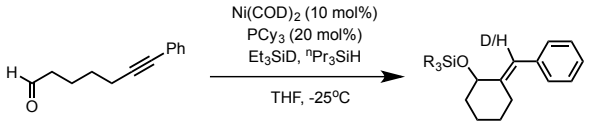

Retention Time 14.657 min.		Retention Time 16.196 min.	
Et3Si Products		Pr3Si Products	
Ion	Intensity	Ion	Intensity
302	59360	344	39320
303	100168	345	46992
304	26376	346	13934

Et Product Isotope Ratio (H:D)	39:61	Pr Product Isotope Ratio (H:D)	48:52
Et:Pr Product Ratio	56:44		

Complete Product Ratio			
Et3Si-H Product	Et3Si-D Product	Pr3Si-H Product	Pr3Si-D Product
22	34	23	21

Table 2.0.8 Entry 6

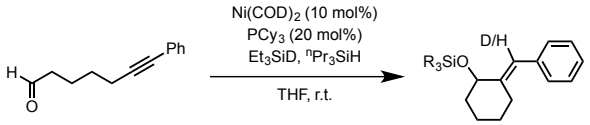

Retention Time 14.674 min.		Retention Time 16.219 min.	
Et3Si Products		Pr3Si Products	
Ion	Intensity	Ion	Intensity
302	32736	343	3024
303	240832	344	161280
304	63736	345	60448

Et Product Isotope Ratio (H:D)	8:92	Pr Product Isotope Ratio (H:D)	92:8
Et:Pr Product Ratio	57:43		

Complete Product Ratio			
Et3Si-H Product	Et3Si-D Product	Pr3Si-H Product	Pr3Si-D Product
5	52	39	4

Table 2.0.8 Entry 7

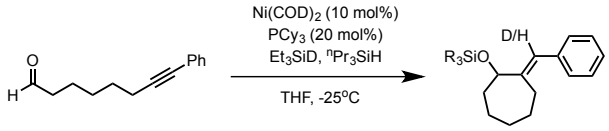

Retention Time 15.629 min.		Retention Time 17.066 min.	
Et3Si Products		Pr3Si Products	
Ion	Intensity	Ion	Intensity
316	8777	357	1259
317	24856	358	8444
318	6696	359	3642

Et Product Isotope Ratio (H:D)	19:81	Pr Product Isotope Ratio (H:D)	88:12
Et:Pr Product Ratio	62:38		

Complete Product Ratio			
Et3Si-H Product	Et3Si-D Product	Pr3Si-H Product	Pr3Si-D Product
10	52	33	5

Table 2.0.8 Entry 8

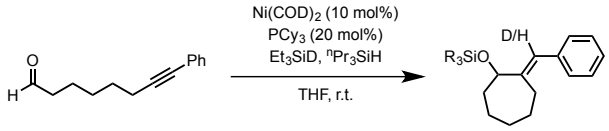

Retention Time 15.641 min.		Retention Time 17.071 min.	
Et3Si Products		Pr3Si Products	
Ion	Intensity	Ion	Intensity
316	40184	357	10955
317	219072	358	103344
318	60840	359	31056

Et Product Isotope Ratio (H:D)	1:99	Pr Product Isotope Ratio (H:D)	99:1
Et:Pr Product Ratio	58:42		

Complete Product Ratio			
Et3Si-H Product	Et3Si-D Product	Pr3Si-H Product	Pr3Si-D Product
<1	57	41	<1

Table 2.0.9 Entry 1

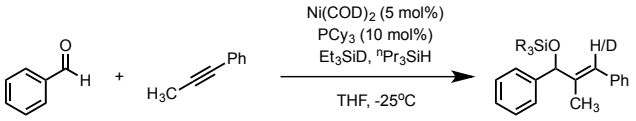

Retention Time 16.699 min.		Retention Time	
Et3Si Products		Pr3Si Products	
Ion	Intensity	Ion	Intensity
338	115056	379	48624
339	276928	380	145536
340	82560	381	48160

Et Product Isotope Ratio (H:D)	12:88	Pr Product Isotope Ratio (H:D)	87:13
Et:Pr Product Ratio	59:41		

Complete Product Ratio			
Et3Si-H Product	Et3Si-D Product	Pr3Si-H Product	Pr3Si-D Product
6	46	42	6

Table 2.0.9 Entry 2

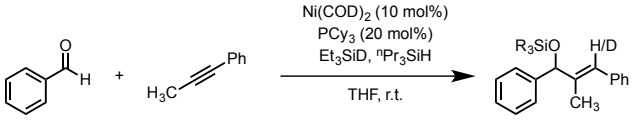

Matches previous published results

5.2.4 Kinetics Data Collection and Analysis

In situ reaction monitoring via React-IR™ was used to observe the rate of reaction for the intermolecular reductive coupling of aldehydes and alkynes using a nickel-NHC catalyst. While GC/MS can be used for monitoring reactions, the use of in

situ protocols has several pertinent benefits. First, the use of IR allows for rapid collection of data, where the use of GC/MS is limited by physical and practical restrictions for consistent and rapid collection. Secondly, in situ reaction monitoring allows for the preservation of the integrity of the system where the catalyst is air-sensitive. Lastly, the ability to remove the solvent from the IR spectra allows for easy manipulation of the system without altering the ability to collect data pertinent to the rate of reaction.

The rate of reaction was measured by observing the disappearance of the carbonyl stretching frequency of benzaldehyde over the course of the reaction. This stretch has a strong absorbance, and falls in an area of the spectrum that is not impacted by the other reagents in solution or any artifacts from the reaction. The products of the reaction do not exhibit any characteristic stretching frequency in a clear area of the spectrum.

Due to the relationship between absorbance and concentration, a simple calibration curve can be constructed to solve for the correlation constant (Figure 5.01). From Beer's Law, the correlation constant and refractive index are constant for the system and allows for rapid data analysis. Reaction rates are measured as change in concentration per unit time, therefore a reliable conversion factor is needed.

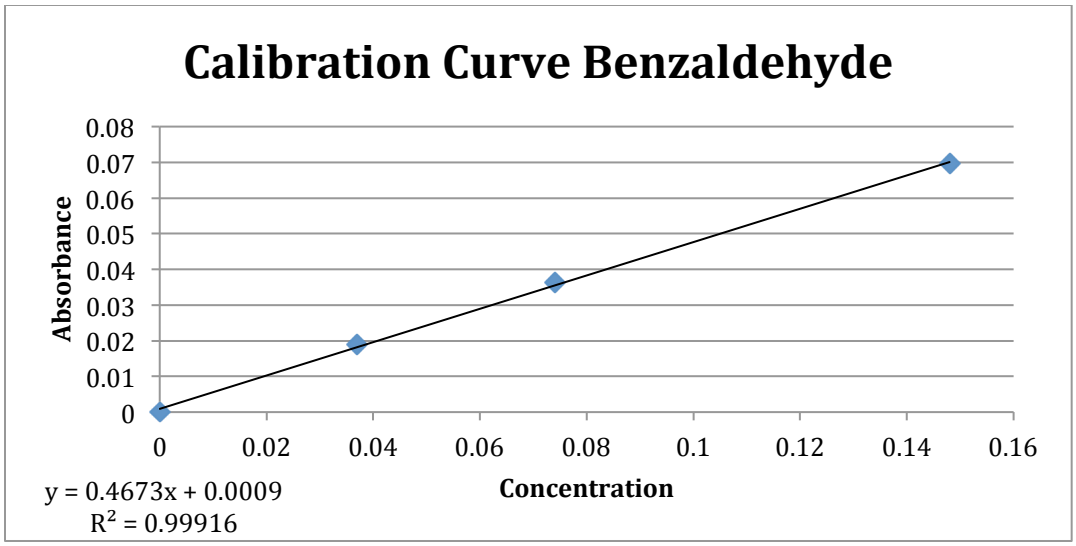

Figure 5.01 – Calibration curve to derive correlation constant for benzaldehyde carbonyl stretching frequency

To gather information about the relationship between the concentration of reactants and the rate of reaction, initial rate studies were performed. The first 10%-20% of the reaction was used to derive the initial rate of reaction (Figure 5.02), which can then be compared to analogous systems with the alteration of a single variable. The use of Microsoft Excel allowed for the direct conversion of absorbance to concentration, the construction of reaction plots, and the derivation of initial rates (Table 5.01).

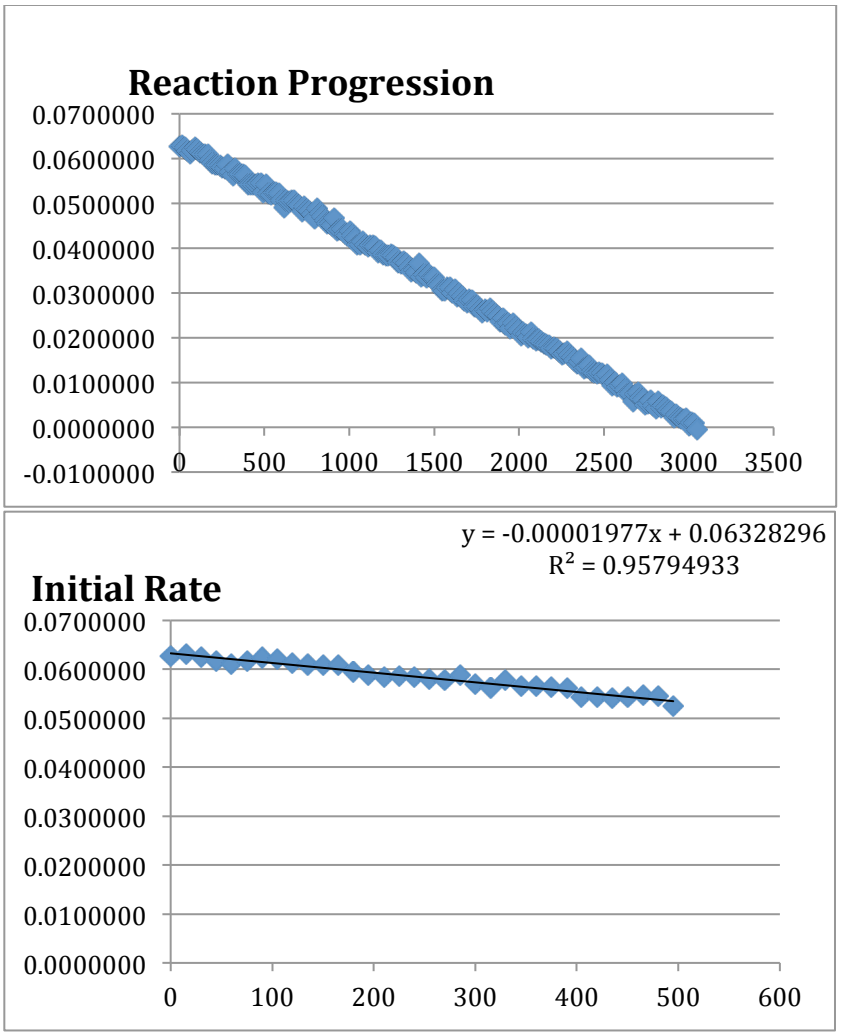

Figure 5.02 – Initial rate extraction from disappearance of carbonyl stretch of benzaldehyde

Time	Absorbance	Relative Time	Concentration
0:12:21	0.027133721	0	0.0576966
0:12:36	0.026861134	15	0.0580662
0:12:51	0.026510487	30	0.0574828
0:13:06	0.02621152	45	0.0567324
0:13:21	0.026543533	60	0.0560927
0:13:36	0.026806303	75	0.0568032
0:13:52	0.026656548	90	0.0573655
0:14:06	0.026304458	105	0.0570450
0:14:22	0.026135284	120	0.0562915
0:14:36	0.02608152	135	0.0559295
0:14:52	0.026086244	150	0.0558145

Table 5.01 – Sample Excel organization to process raw rate data

5.2.4.1 Initial Rate dependence on concentration of nickel catalyst

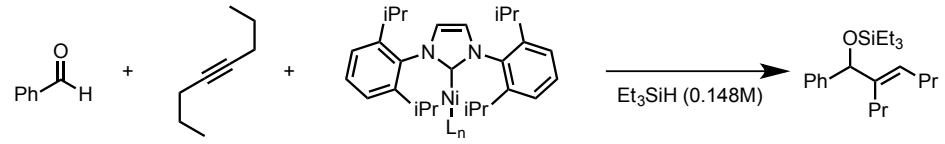

[Catalyst]	Δ[PhCHO]/Δt	Average Δ[PhCHO]/Δt	Standard Deviation
0.0037 M	0.0000042		
0.0037 M	0.0000051		
0.0037 M	0.0000046	0.0000046	0.00000045
0.0074 M	0.0000143		
0.0074 M	0.0000162		
0.0074 M	0.0000132		
0.0074 M	0.0000120	0.0000139	0.0000018
0.0111 M	0.0000302		
0.0111 M	0.0000301		
0.0111 M	0.0000297	0.00002998	0.00000030

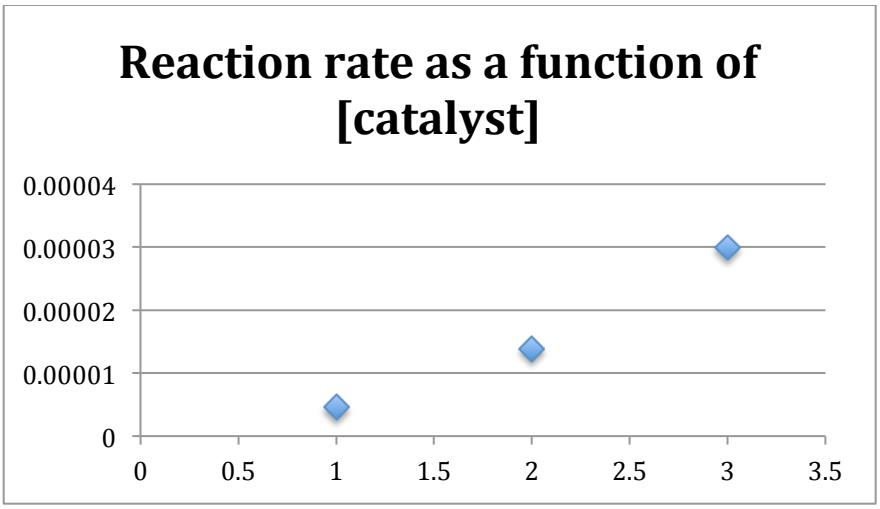

5.2.4.2 Initial Rate dependence on concentration of benzaldehyde

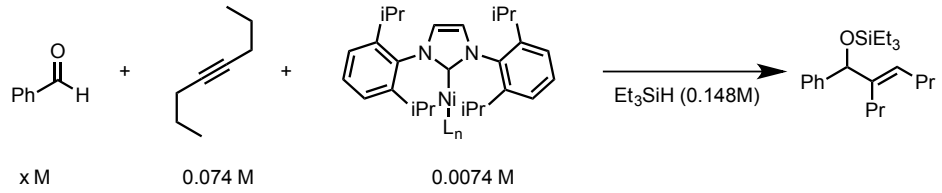

[PhCHO]	Δ[PhCHO]/Δt	Average Δ[PhCHO]/Δt	Standard Deviation
0.074 M	0.0000143		
0.074 M	0.0000162		
0.074 M	0.0000132		
0.074 M	0.0000120	0.0000139	0.0000018
0.148 M	0.0000077		
0.148 M	0.0000057	0.0000067	0.0000014
0.222 M	0.0000047	0.0000047	0

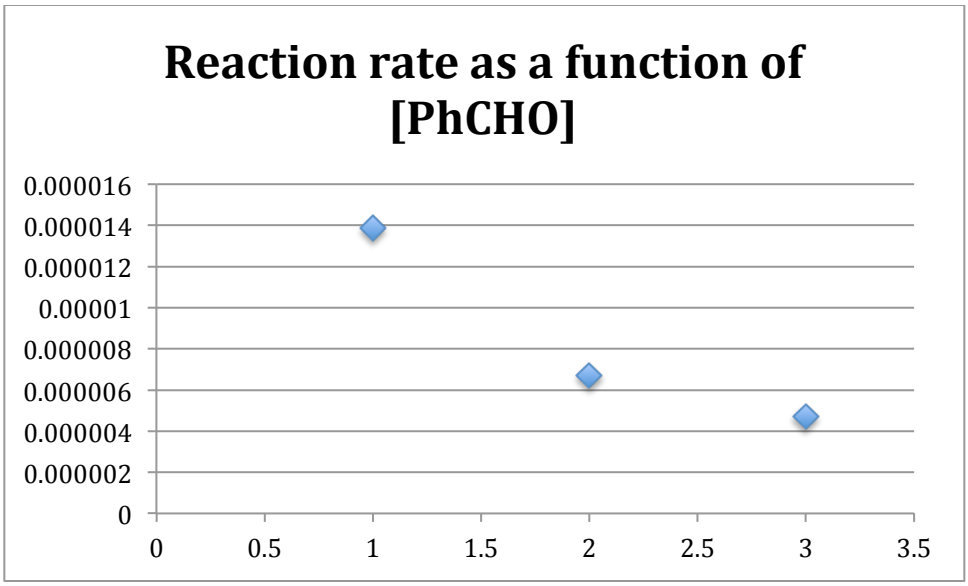

5.2.4.3 Initial Rate dependence on concentration of 4-octyne

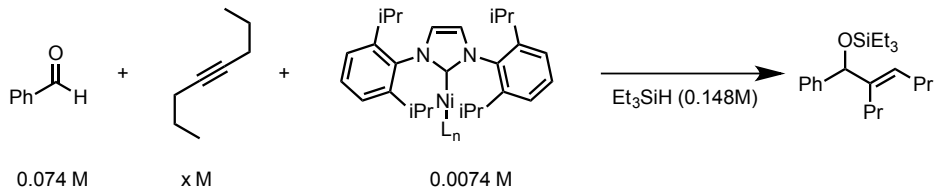

[octyne]	Δ[PhCHO]/Δt	Average Δ[PhCHO]/Δt	Standard Deviation
0.074 M	0.0000143		
0.074 M	0.0000162		
0.074 M	0.0000132		
0.074 M	0.0000120	0.0000139	0.0000018
0.111 M	0.0000172		
0.111 M	0.0000183	0.0000177	0.0000005
0.148 M	0.0000169		
0.148 M	0.0000215	0.0000192	0.0000027
0.222 M	0.0000229		
0.222 M	0.0000255	0.00002419	0000018

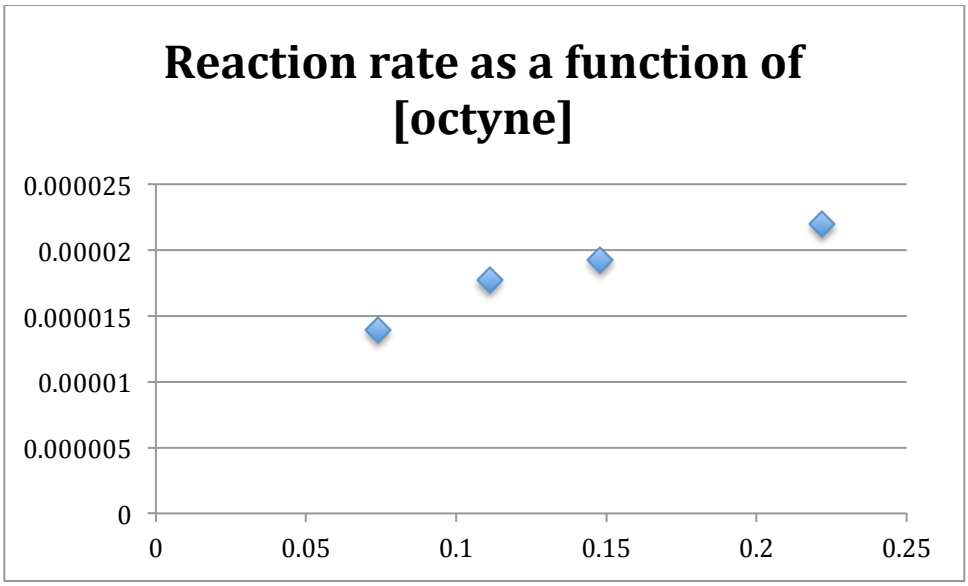

5.2.4.4 Reciprocal Plot

[PhCHO]/[octyne]	1/rate
0.333333333	35836
0.5	45527
1	62304
2	129493
3	211864.4068

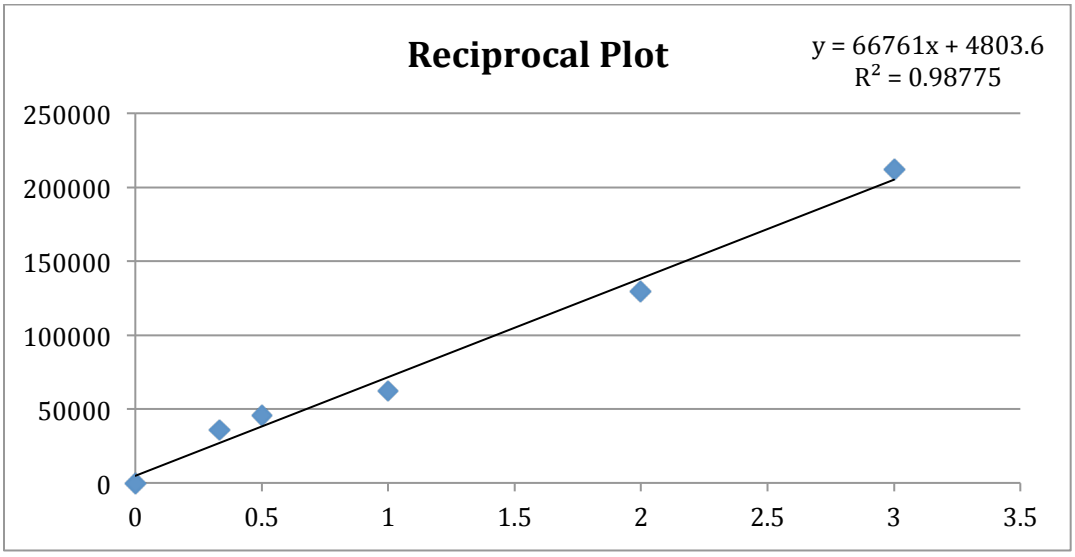

5.3.0 Chapter 3 Experimental Data

5.3.1 General Procedures for Chapter 3

Kumada Coupling General Procedure:

To an oven-dried vial, cooled in a desiccator, was added a stir bar and (NHC)Ni(dmfu)$_2$ and then sealed with a septum. The vial was then evacuated, and subsequently back-filled with nitrogen three times. To this, a solution of aryl halide in THF (reaction volume) was added. Grignard reagent was then added via syringe. At completion, the reaction was chromatographed on a silica column, eluting with 100% Hexanes to afford the biaryl product.

Buchwald-Hartwig General Procedure:

A solid mixture of (NHC)Ni(dmfu)$_2$ and t-BuOK was added to a heavy wall flask, which was sealed with a septum and evacuated then backfilled with nitrogen three times. Toluene was added via syringe, and the solution was allowed to stir for 5 minutes. A solution of aryl-halide and amine in toluene (0.5M) was then added to catalyst solution. Vessel was sealed, and placed in an oil bath for 16 hr. Reaction removed from oil bath and allowed to cool to room temperature, where it was then filtered through a short silica column eluting with 50:50 Hexanes:Ethyl Acetate. Filtrate was concentrated in vacuo, and chromatographed on silica column to afford the product.

Reductive Coupling General Procedure:

To an oven-dried vial, cooled in a desiccator, was added a stir bar and (NHC)Ni(dmfu)$_2$ and then sealed with a septum. The vial was then evacuated, and subsequently back-filled with nitrogen three times. Reaction placed in oil bath, and allowed to equilibrate for 5 minutes. A solution of aldehyde, alkyne, and silane in solvent (0.5 M) was then added to catalyst solution. Reaction allowed to stir for 16 hr. Reaction concentrated in vacuo, and chromatographed on a silica column to afford the silyl protected allylic alcohol.

5.3.2 Catalyst Synthesis Experimentals

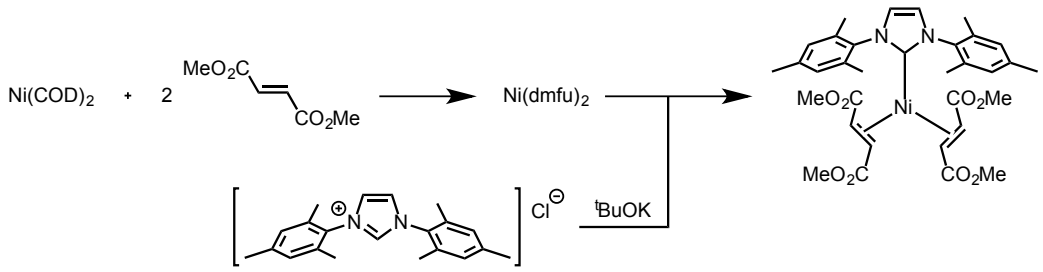

(IMes)Ni(dmfu)$_2$:

In a glove box, 1,3-bis(2,4,6-trimethylphenyl)-imidazolium chloride [IMes·HCl] (711 mg, 2.09 mmol) was stirred with potassium tert-butoxide (212 mg, 1,8 mmol) in THF (15 ml) for 2 hours. In a separate flask, a solution of dimethyl fumarate (576 mg, 4.00 mmol) in THF (15 mL) was added slowly to a solution of bis(1,5-cyclooctadiene)nickel(0) [Ni(cod)$_2$] (550 mg, 2.0 mmol) in THF (20 mL). The resulting orange-red solution was stirred for 5 minutes after which the solution of the preformed carbene was added, leading to a rapid darkening of the mixture. The mixture was stirred for 1 hour at room temperature and filtered through a celite pad. The solvent was removed from the filtrate and the remaining solid was washed with hexanes, filtered and dried *in vacuo* to afford

the complex (886 mg, 1.36 mmol, 68%) as a red solid. Spectral data matches reported values.[98]

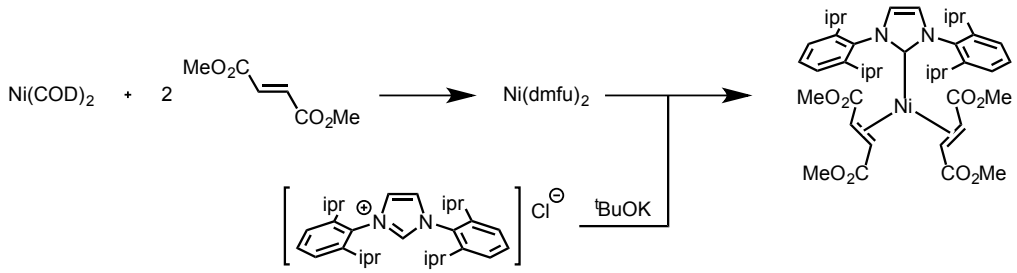

(IPr)Ni(dmfu)$_2$:

In a glove box, 1,3-bis(2,6-diisopropylphenyl)-imidazolium chloride [IPr·HCl] (893 mg, 2.1 mmol) was stirred with potassium tert-butoxide (212 mg, 1.9 mmol) in THF (15 ml) for 2 hours. In a separate flask, a solution of dimethyl fumarate (576 mg, 4.00 mmol) in THF (15 mL) was added slowly to a solution of bis(1,5-cyclooctadiene)nickel(0) [Ni(cod)$_2$] (550 mg, 2.0 mmol) in THF (20 mL). The resulting orange-red solution was stirred for 5 minutes after which the solution of the preformed carbene was added, leading to a rapid darkening of the mixture. The mixture was stirred for 1 hour at room temperature and filtered through a celite pad. The solvent was removed from the filtrate and the remaining solid was washed with hexanes, filtered and dried *in vacuo* to afford the complex (1.105 g, 1.5 mmol, 75%) as a red solid. Spectral data matches reported values.[98]

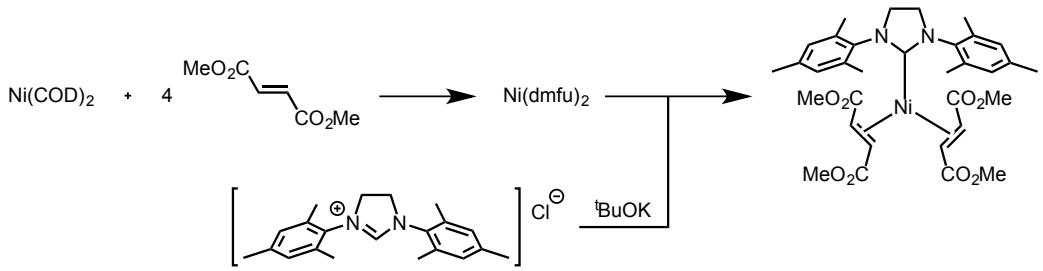

(SIMes)Ni(dmfu)$_2$:

In a glove box, 1,3-bis(2,4,6-trimethylphenyl)-imidazolinium chloride [SIMes·HCl] (356 mg, 1.04 mmol) was stirred with potassium tert-butoxide (106 mg, 0.91 mmol) in THF (10 ml) for 2 hours. In a separate flask, a solution of dimethyl fumarate (432 mg, 3.00 mmol) in THF (10 mL) was added slowly to a solution of bis(1,5-cyclooctadiene)nickel(0) [Ni(cod)$_2$] (275 mg, 1.00 mmol) in THF (10 mL). The resulting orange-red solution was stirred for 5 minutes after which the solution of the preformed carbene was added, leading to a rapid darkening of the mixture. The mixture was stirred for 1 hour at room temperature and filtered through a celite pad. The solvent was removed from the filtrate and the remaining solid was washed with hexanes, filtered and dried *in vacuo* to afford the complex (481 mg, 0.73 mmol, 73%) as a red solid.

^{1}H NMR (500 MHz, C_6D_6): δ 7.13 (s, 2H), 6.89 (s, 2H), 6.84 (s, 2H), 4.51 (d, J = 11 Hz, 2H), 3.91 (d, J = 11 Hz, 2H), 3.24 (s, 6H), 3.22 (s, 6H), 3.17 (s, 4H), 2.63 (s, 6H), 2.12 (s, 6H), 1.99 (s, 6H).

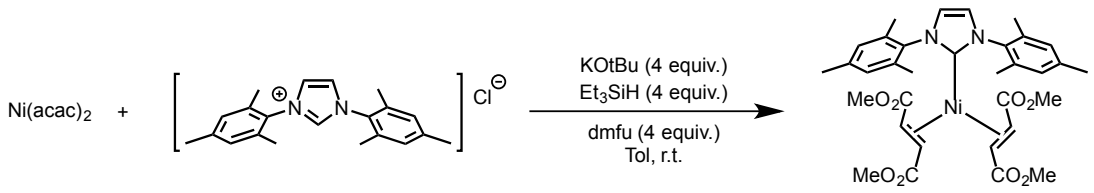

To an oven dried flask cooled in a desiccator was added nickel(acetylacetonate) (128 g, 0.50 mmol), 1,3-bis(2,4,6-trimethylphenyl)-imidazolium chloride [IMes·HCl] (170 mg, 0.5 mmol), potassium tertbutoxide (175 mg, 1.50 mmol), and dimethylfumarate (288 mg, 2.00 mmol). The flask was sealed with a septum, evacuated, and backfilled with nitrogen three times. Triethylsilane (232 mg, 2.00 mmol) in toluene (20 mL) was then added to

the solid mixture, and allowed to stir for 2 hours. The solution was then filtered through a celite pad, and concentrated *in vacuo*. The concentrate was then dissolved in a minimum of toluene and precipitated with hexanes. The mixture was then filtered, and the filtrate was washed with additional hexanes to afford the complex (89 mg, 0.135 mmol, 27%) as a red solid. Spectral data matches reported values.

5.3.3 Kumada Cross-Coupling Experimentals

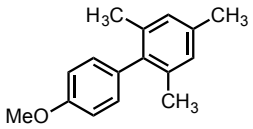

4'-methoxy-2,4,6-trimethyl-1,1'-biphenyl:

Following Kumada Coupling General Procedure: 4-bromoanisole (62 mg, 0.33 mmol), mesityl magnesium bromide (0.700 mL, 0.71 M, 0.5 mmol), and (IMes)Ni(dmfu)2 (7 mg, 0.01 mmol) in THF (1 mL) provided the biaryl product (73 mg, 0.32 mmol, 97%). NMR matches previously published results.(107)

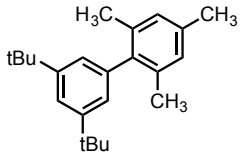

3',5'-di-*tert*-butyl-2,4,6-trimethyl-1,1'-biphenyl:

Following Kumada Coupling General Procedure: 3,5-ditertbutylphenylbromide (89 mg, 0.33 mmol), mesityl magnesium bromide (0.500 mL, 0.5 mmol), and (IMes)Ni(dmfu)$_2$ (7 mg, 0.01 mmol) in THF (1 mL) provided the biaryl product (75 mg, 0.24 mmol, 74%).

^{1}H NMR (500 MHz, $CDCl_3$): δ 7.37 (t, J = 2 Hz, 1H), 7.02 (d, J = 2 Hz, 2H), 6.99 (s, 2H), 2.37 (s, 3H), 2.06 (s, 6H), 1.36 (s, 18H). **MS (EI) (*m*/*z*):** [M]+ calc'd for $C_{23}H_{32}$ 308.2504, found 308.2515.

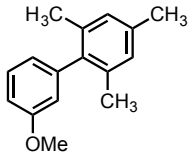

3'-methoxy-2,4,6-trimethyl-1,1'-biphenyl:

Following Kumada Coupling General Procedure: 3-chloroanisole (47 mg, 0.33 mmol), mesityl magnesium bromide (0.7 mL, 0.71 M, 0.5 mmol), and (IPr)Ni(dmfu)$_2$ (7 mg, 0.01 mmol) in THF (1 mL) provided the biaryl product (64 mg, 0.28 mmol, 86%). NMR matches previously reported results.[108] **^{1}H NMR (400 MHz, $CDCl_3$):** δ 7.34 (t, J = 10 Hz, 1H), 6.95 (s, 2H), 6.88 (s, 2H), 6.90 (dd, J = 8 Hz 1Hz, 1H), 6.88 (dd, J = 8 Hz, 1 Hz, 1H), 6.82 (s, 2H), 6.75 (dt, J = 9.5 Hz 1Hz, 1H), 6.71 (m, 1H), 3.82 (s, 3H), 2.34 (s, 3H), 2.04 (s, 6H).

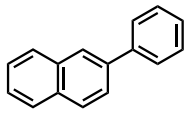

2-phenylnaphthalene:

Following Kumada Coupling General Procedure: 2-bromonapthalene (69 mg, 0.33 mmol), phenyl magnesium bromide (0.320 mL, 1.156 M, 0.37 mmol), and (IMes)Ni(dmfu)$_2$ (7 mg, 0.01 mmol) in THF (1 mL) provided the biaryl product (54 mg, 26 mmol, 80%). NMR spectra matches previously reported results.[109] **^{1}H NMR (500 MHz, $CDCl_3$):** δ 8.09 (s, 1H), 7.93 (m, 3H), 7.78 (m, 3H), 7.53 (m, 4H), 7.42 (m, 1H).

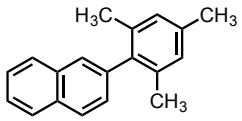

2-mesitylnaphthalene:

Following Kumada Coupling General Procedure: 2-bromonapthalene (69 mg, 0.33 mmol), mesityl magnesium bromide (0.37 mL, 1 M, 0.37 mmol), and (IMes)Ni(dmfu)$_2$ (7 mg, 0.01 mmol) in THF (1 mL) provided the biaryl product (69 mg, 0.28 mmol, 86%). NMR spectra matches previously reported results.[109] **^{1}H NMR (500 MHz, CDCl$_3$):** δ 7.93 (m, 2H), 7.88 (m, 1H), 7.66 (s, 1H), 7.54 (m, 2H), 7.33 (dd, J = 8.5 Hz, 1.5 Hz, 1H), 7.03 (2H), 2.41 (s, 3H), 2.08 (s, 6H).

Table 3.01 Entry 1

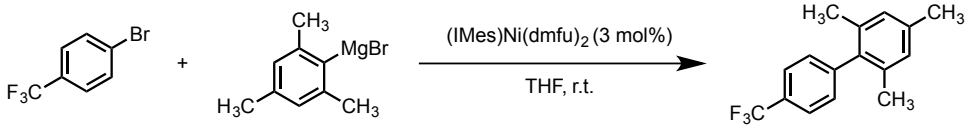

Following Kumada Coupling General Procedure: 4-bromophenyl trifluoride (74 mg, 0.33 mmol), mesityl magnesium bromide (0.7 mL, 0.71 M, 0.5 mmol), and (IMes)Ni(dmfu)$_2$ (7 mg, 0.01 mmol) in THF (1 mL) provided the biaryl product (89 mg, 0.32 mmol, 97%). NMR spectra matches previously reported results.[110] **^{1}H NMR (500 MHz, CDCl$_3$):** δ 7.83 (d, J = 8 Hz, 2H), 7.41 (d, J = 8 Hz, 2H), 7.12 (s, 2H), 2.50 (s, 3H), 2.15 (s, 6H).

Table 3.01 Entry 2

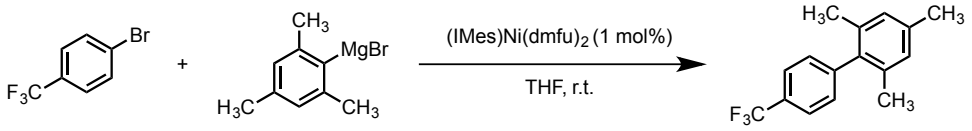

Following Kumada Coupling General Procedure: 4-bromophenyl trifluoride (222 mg, 0.99 mmol), mesityl magnesium bromide (2.1 mL, 0.71 M, 1.50 mmol), and (IMes)Ni(dmfu)$_2$ (7 mg, 0.01 mmol) in THF (1.5 mL) provided the biaryl product (256 mg, 0.97 mmol, 98%) as a white solid.

Table 3.01 Entry 3

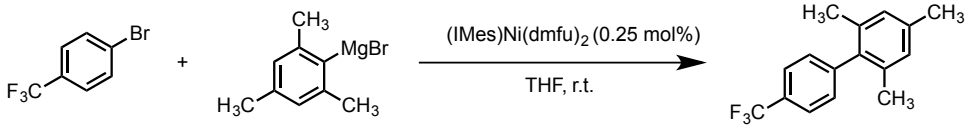

Following Kumada Coupling General Procedure: 4-bromophenyl trifluoride (444 mg, 1.98 mmol), mesityl magnesium bromide (4.2 mL, 0.71 M, 3 mmol), and (IMes)Ni(dmfu)$_2$ (4.2 mg, 0.005 mmol) in THF (3 mL) provided the biaryl product (477 mg, 1.81 mmol, 92%) as a white solid.

5.3.4 Buchwald-Hartwig Cross-Coupling Experimentals

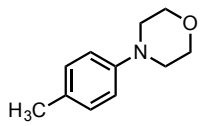

4-(*p*-tolyl)morpholine:

Following the Buchwald-Hartwig General Procedure: 4-chlorotoluene (69 mg, 0.55 mmol), morpholine (184 mg, 2.11 mmol), tBuOK (145 mg, 1.22 mmol), and (IPr)Ni(dmfu)$_2$ (18 mg, 0.025 mmol) in toluene (5 mL) provided the product (68 mg, 0.39

mmol, 71%). NMR matches previously published results.[53] **^{1}H NMR (500 MHz, $CDCl_3$):** δ 7.11 (m, 2H), 6.86 (m, 2H), 3.88 (m, 4H), 3.13 (m, 4H), 2.30 (s, 3H).

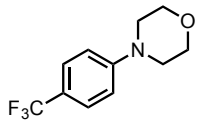

4-(4-(trifluoromethyl)phenyl)morpholine:

Following the Buchwald-Hartwig General Procedure: 4-chlorophenyltrifluoride (87 mg, 0.48 mmol), morpholine (55 mg, 0.63 mmol), tBuOK (145 mg, 1.25 mmol), and $(IPr)Ni(dmfu)_2$ (18 mg, 0.025 mmol) in toluene (5 mL) provided the product (69 mg, 0.39 mmol, 81%).**^{1}H NMR (500 MHz, $CDCl_3$):** δ 7.51 (d, J = 8.5 Hz, 2H), 6.93 (d, J = 8.5 Hz, 2H), 3.07 (t, J = 5 Hz, 2H), 3.25 (t, J = 5 Hz, 2H).

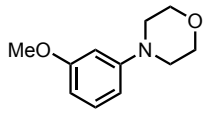

4-(3-methoxyphenyl)morpholine:

Following the Buchwald-Hartwig General Procedure: 3-chloroanisole (69 mg, 0.48 mmol), morpholine (55 mg, 0.63 mmol), tBuOK (145 mg, 1.25 mmol), and $(IPr)Ni(dmfu)_2$ (18 mg, 0.025 mmol) in toluene (5 mL) provided the product (82 mg, 0.42 mmol, 87%). NMR matches previously published results.[53] **^{1}H NMR (500 MHz, $CDCl_3$):** δ 7.16 (t, J = 16 Hz, 1H), 6.52 (m, 1H), 6.44 (m, 2H), 3.83 (t, J = 5 Hz, 4H), 3.78 (s, 3H), 3.13 (t, J = 5 Hz, 4H).

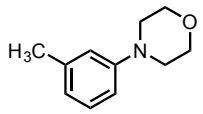

4-(*m*-tolyl)morpholine:

Following the Buchwald-Hartwig General Procedure: 3-chlorotoluene (61 mg, 0.48 mmol), morpholine (55 mg, 0.63 mmol), tBuOK (145 mg, 1.25 mmol), and $(IPr)Ni(dmfu)_2$ (18 mg, 0.025 mmol) in toluene (5 mL) provided the product (41 mg, 0.23 mmol, 48%). NMR matches previously published results.[53] **^{1}H NMR (500 MHz, $CDCl_3$):** δ 7.19 (t, J = 7.5 Hz, 1H), 6.76 (m, 1H), 6.75 (m, 1H), 6.73 (m, 1H), 3.87 (t, J = 5 Hz, 4H), 3.17 (t, J = 5 Hz, 4H), 2.35 (s, 3H).

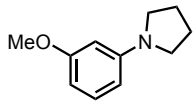

1-(3-methoxyphenyl)pyrrolidine:

Following the Buchwald-Hartwig General Procedure: 3-chloroanisole (69 mg, 0.48 mmol), pyrollidine (138 mg, 1.94 mmol), tBuOK (145 mg, 1.25 mmol), and $(IPr)Ni(dmfu)_2$ (18 mg, 0.025 mmol) in toluene (5 mL) provided the product (80 mg, 0.45 mmol, 93%). NMR matches previously published results.[53] **^{1}H NMR (500 MHz, $CDCl_3$):** δ 7.16 (t, J = 8.5 Hz, 1H), 6.27 (dd, J = 8 Hz 2 Hz, 1H), 6.23 (dd, J = 8 Hz 2 Hz, 1H), 6.14 (t, J = 2.5 Hz), 3.79 (s, 3H), 3.27 (m, 4H), 1.98 (m, 4H).

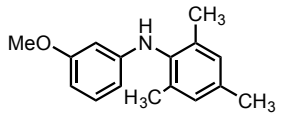

***N*-(3-methoxyphenyl)-2,4,6-trimethylaniline:**

Following the Buchwald-Hartwig General Procedure: 3-chloroanisole (69 mg, 0.48 mmol), 1,3,5-trimethylaniline (260 mg, 1.92 mmol), tBuOK (145 mg, 1.25 mmol), and (IPr)Ni(dmfu)$_2$ (18 mg, 0.025 mmol) in toluene (x mL) provided the product (61 mg, 0.25 mmol, 53%).

5.3.5 Reductive Coupling Experimentals

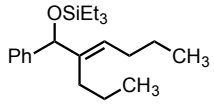

(*E*)-triethyl((1-phenyl-2-propylhex-2-en-1-yl)oxy)silane:

Following the Reductive Coupling General Procedure, benzaldehyde (53 mg, 0.5 mmol), 4-octyne (55 mg, 0.5 mmol), triethylsilane (116 mg, 1.0 mmol), and (IPr)Ni(dmfu)$_2$ (37 mg, 0.05 mmol) in THF (5 mL) at 50^{o}C afforded silyl allylic alcohol (114 mg, 0.343 mmol, 72%) as a clear and colorless oil.

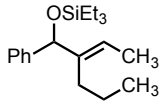

(*E*)-triethyl((2-ethylidene-1-phenylpentyl)oxy)silane:

Following the Reductive Coupling General Procedure, benzaldehyde (53 mg, 0.5 mmol), 2-hexyne (41 mg, 0.5 mmol), triethylsilane (116 mg, 1.0 mmol), and (IPr)Ni(dmfu)$_2$ (37 mg, 0.05 mmol) in THF (5 mL) at 50^{o}C afforded silyl allylic alcohol (116 mg, 0.382 mmol, 76%) as a clear and colorless oil.

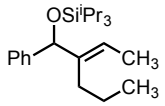

(*E*)-((2-ethylidene-1-phenylpentyl)oxy)triisopropylsilane:

Following the Reductive Coupling General Procedure, benzaldehyde (27 mg, 0.25 mmol), 2-hexyne (21 mg, 0.25 mmol), triisopropylsilane (80 mg, 0.5 mmol), and (IPr)Ni(dmfu)$_2$ (19 mg, 0.05 mmol) in THF (2.5 mL) at 50^{o}C afforded silyl allylic alcohol (80 mg, 0.23 mmol, 93%) as a clear and colorless oil.

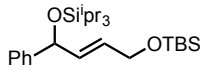

(*E*)-10,10-diethyl-2,2,3,3-tetramethyl-8-phenyl-4,9-dioxa-3,10-disiladodec-6-ene:

Following the Reductive Coupling General Procedure, benzaldehyde (54 mg, 0.5 mmol), tertbutyldimethylsilyl-propargyl alcohol (104 mg, 0.61 mmol), triisopropylsilane (158 mg, 1.0 mmol), and (IMes)Ni(dmfu)$_2$ (34 mg, 0.05 mmol) in THF (5 mL) at 50^{o}C afforded silyl allylic alcohol (17 mg, 0.06 mmol, 12%) as a clear and colorless oil.

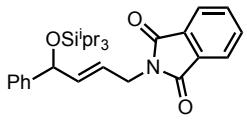

(*E*)-2-(4-phenyl-4-((triethylsilyl)oxy)but-2-en-1-yl)isoindoline-1,3-dione:

Following the Reductive Coupling General Procedure, benzaldehyde (27 mg, 0.25 mmol), propargyl pthalamide (57 mg, 0.31 mmol), triisopropylsilane (79 mg, 0.5 mmol), and (IPr)Ni(dmfu)$_2$ (17 mg, 0.025 mmol) in THF (x mL) at 50^{o}C afforded silyl allylic alcohol (24 mg, 0.053 mmol, 21%).

5.4.0 NMR Spectra

5.4.1 Chapter 2 NMR Spectra

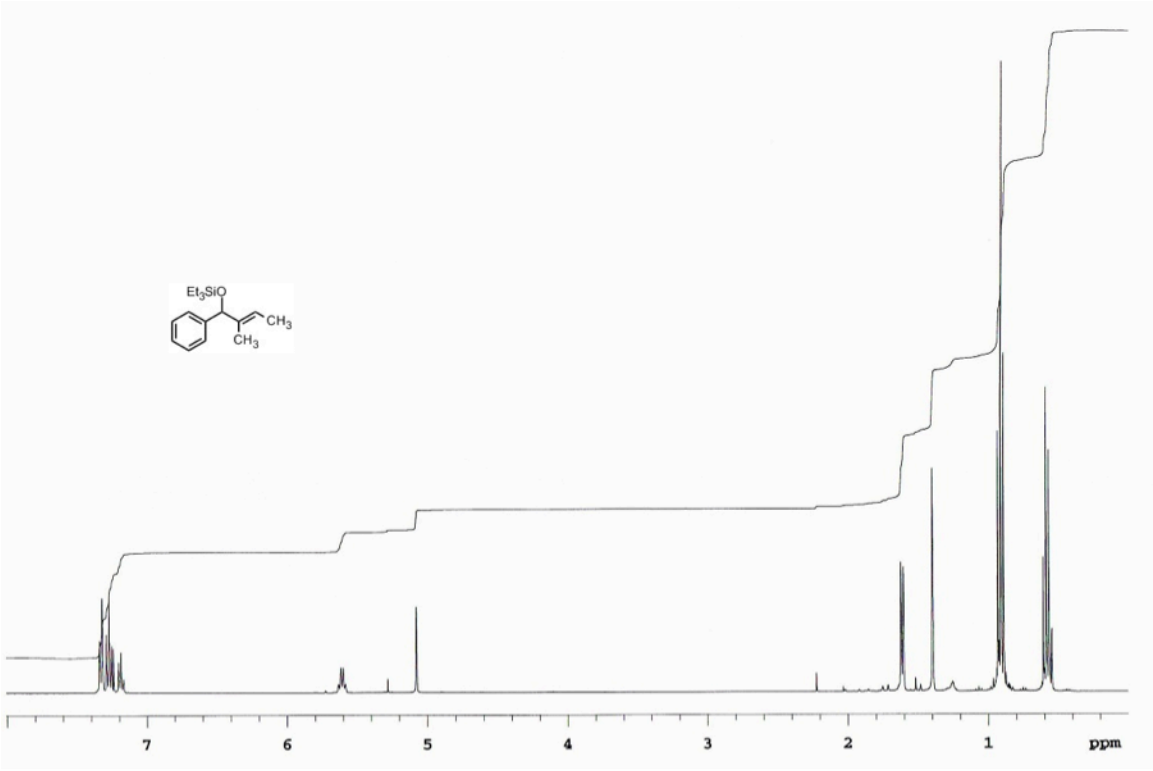

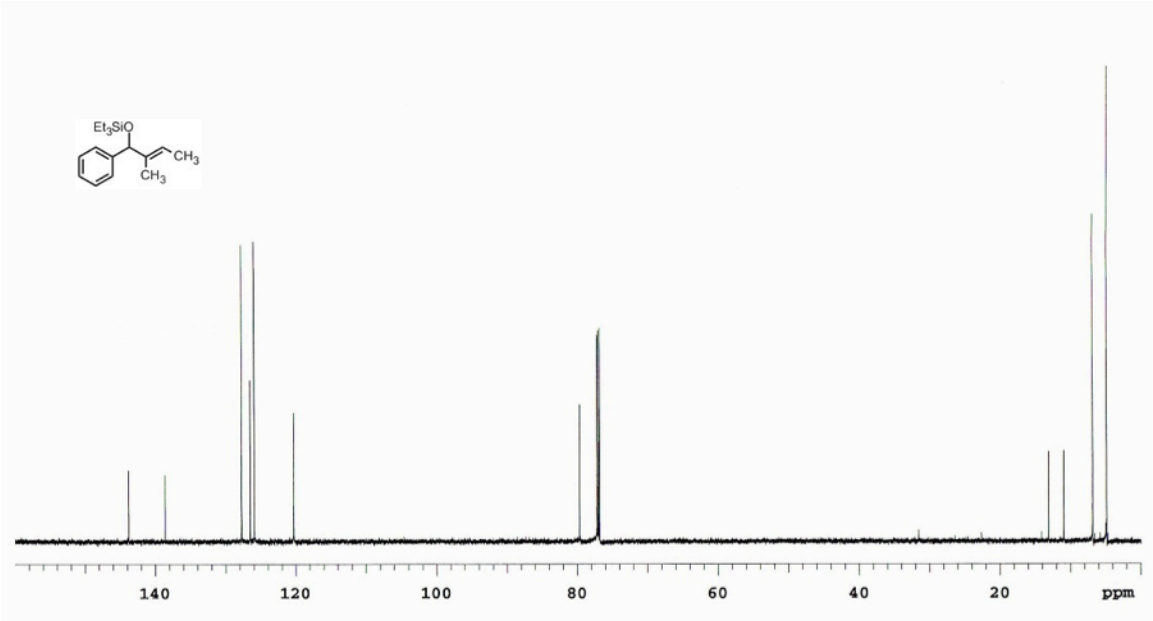

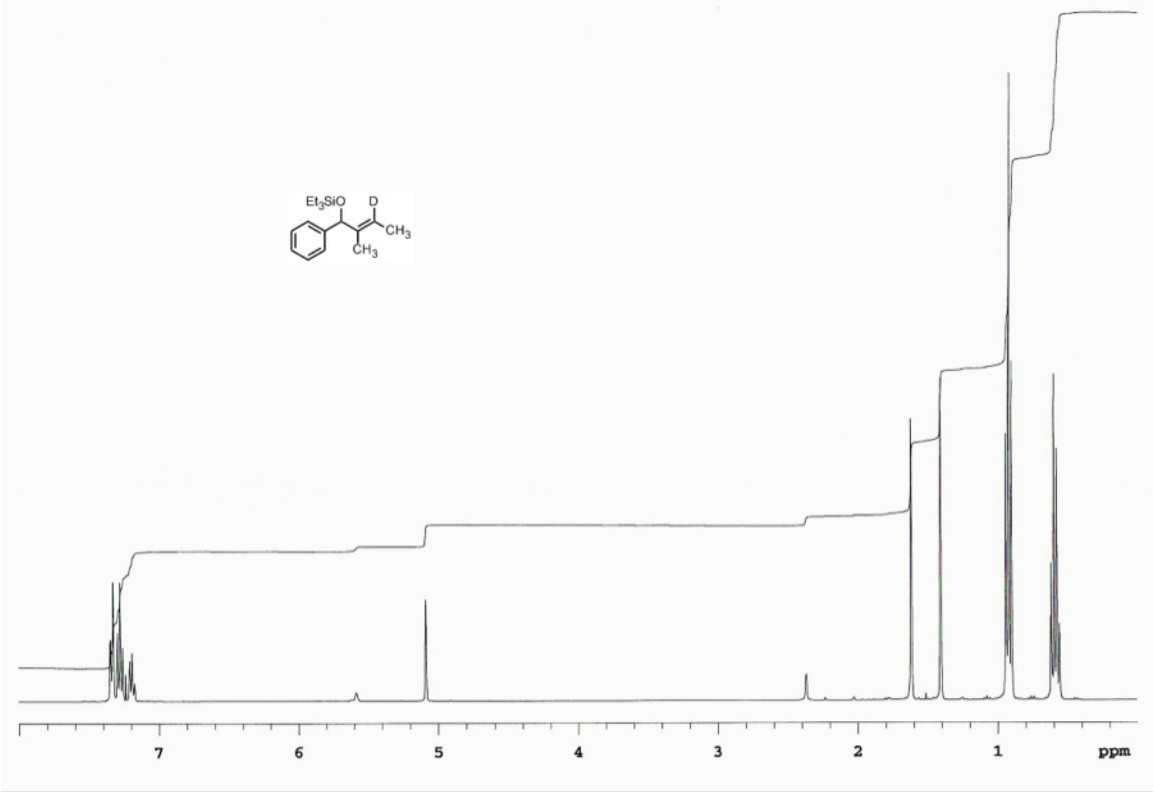
Et3SiO
D
CH3
CH3
7
6
5
4
3
2
1
ppm

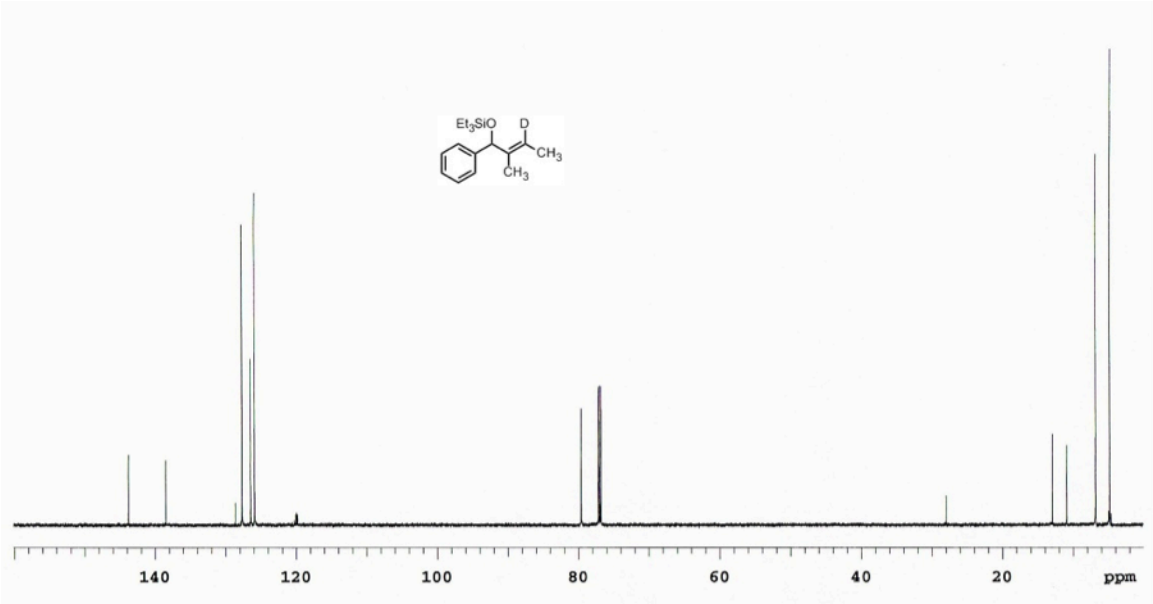
Et3SiO
D
CH3
CH3
140
120
100
80
60
40
20
ppm

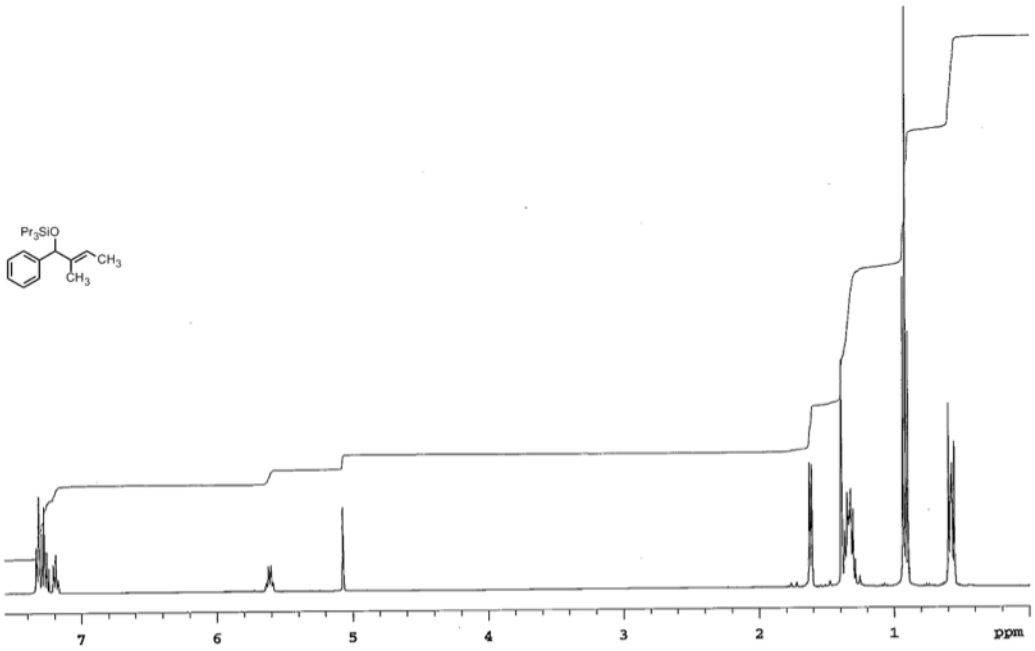
Pr3SiO
CH3
CH3
7
6
5
4
3
2
1
ppm

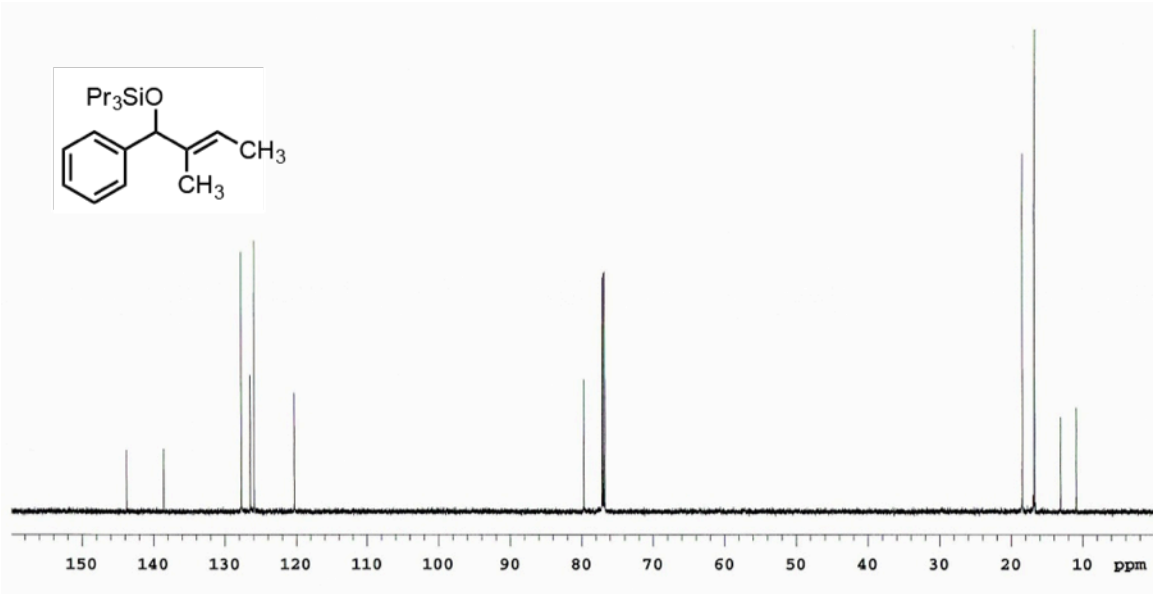
Pr3SiO
CH3
CH3
150
140
130
120
110
100
90
80
70
60
50
40
30
20
10
ppm

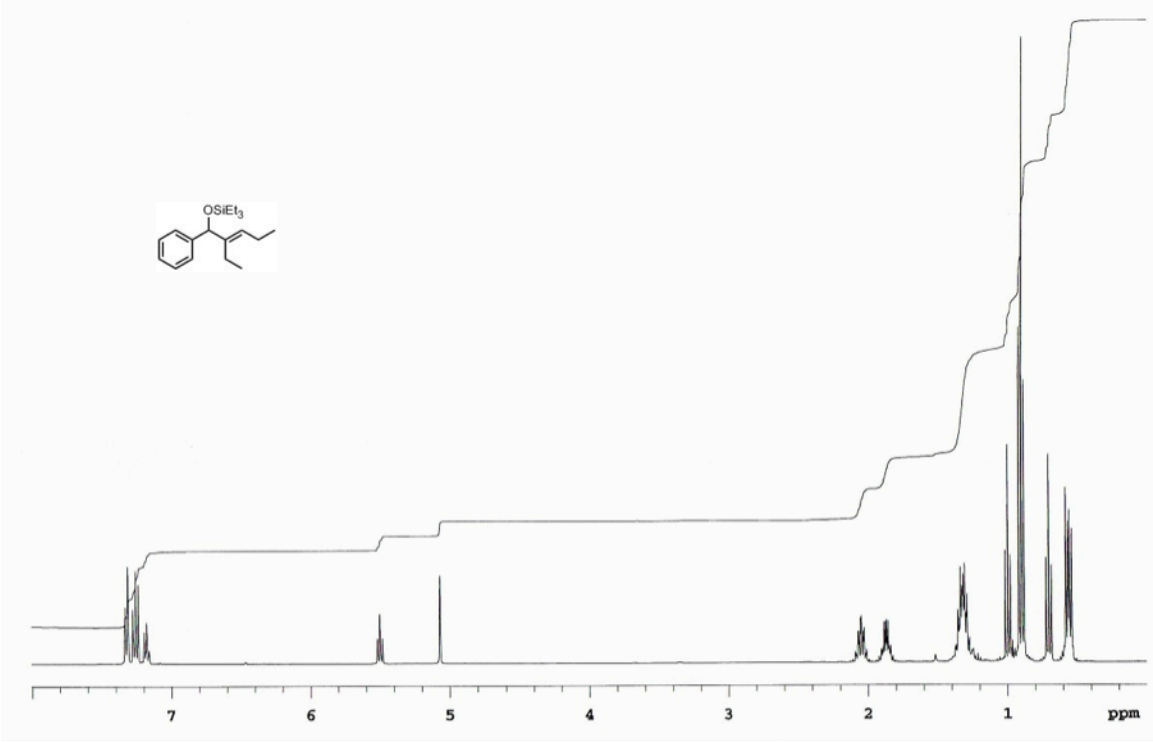
OSiEt3
7
6
5
4
3
2
1
ppm

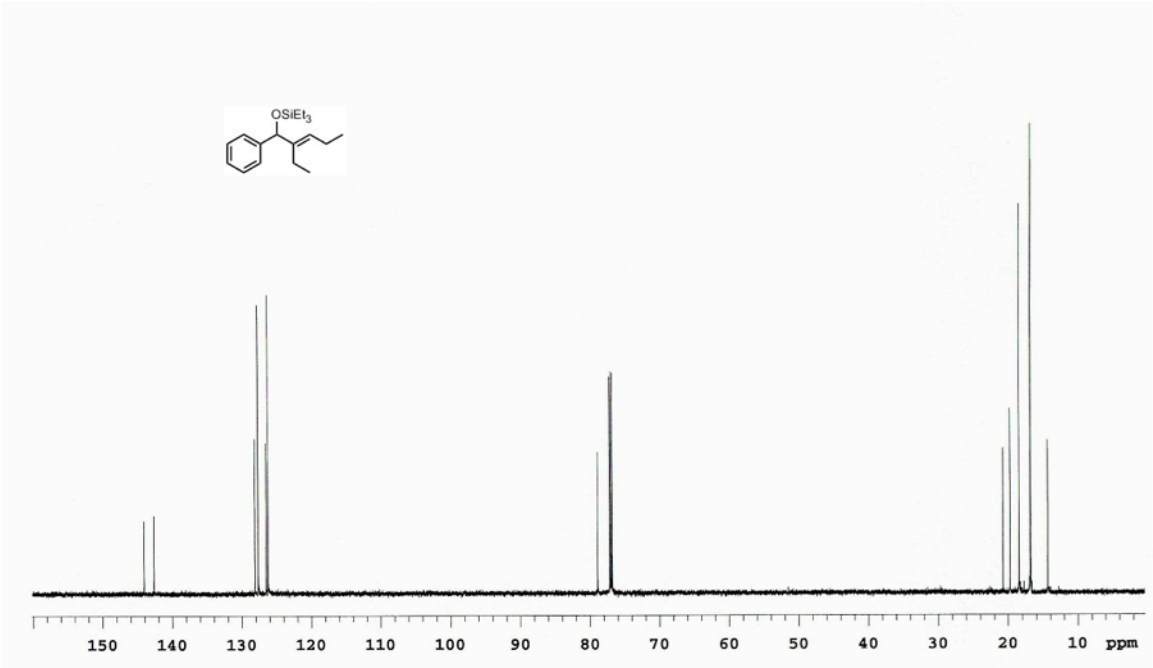
OSiEt3
150
140
130
120
110
100
90
80
70
60
50
40
30
20
10
ppm

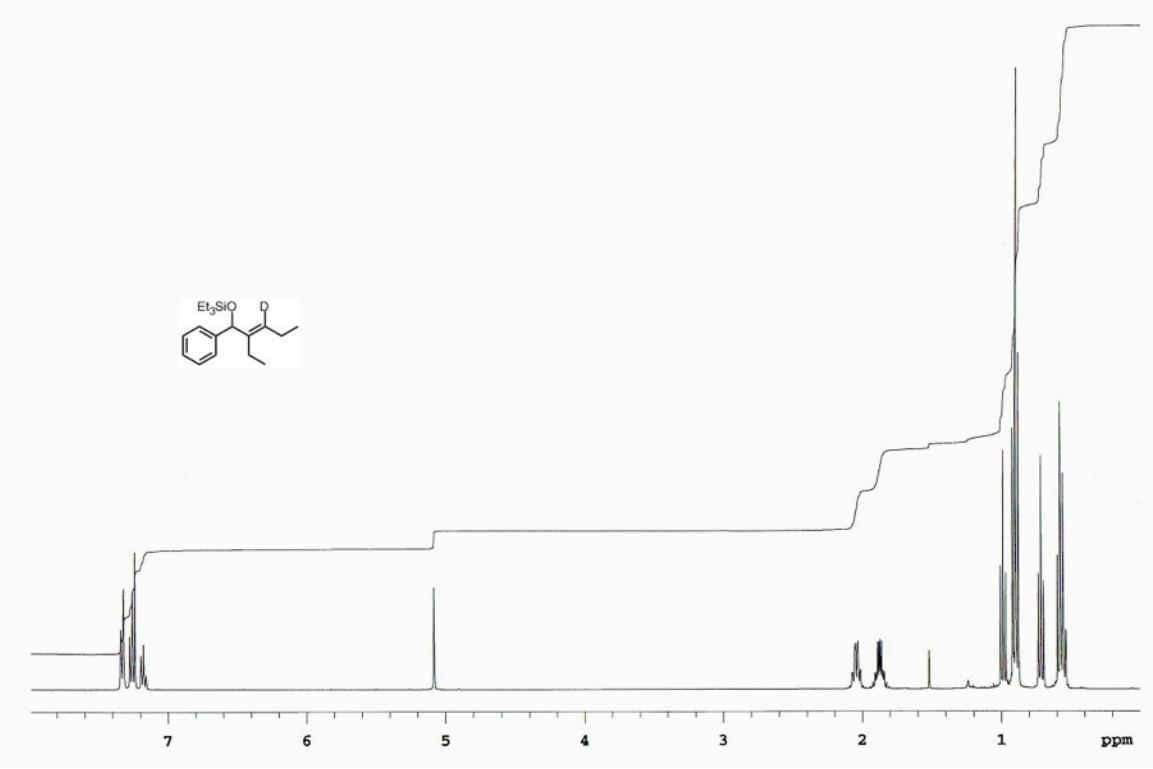
Et3SiO
D
7
6
5
4
3
2
1
ppm

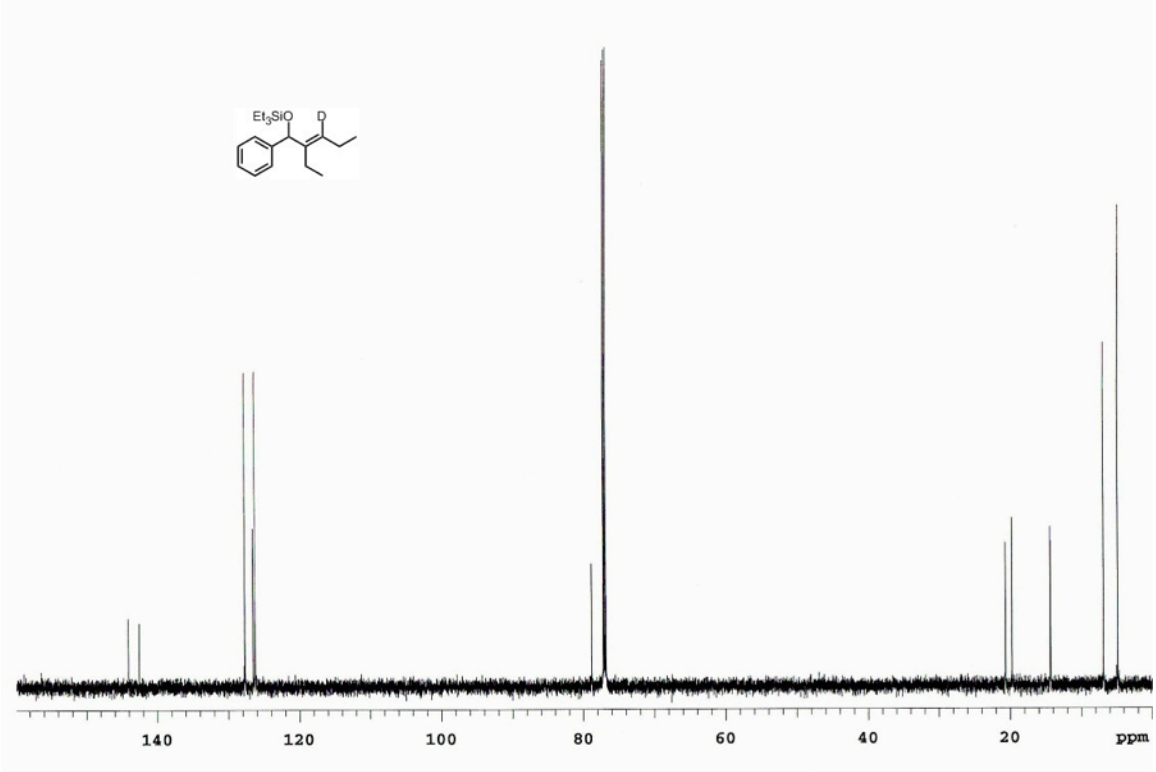
Et3SiO
D
140
120
100
80
60
40
20
ppm

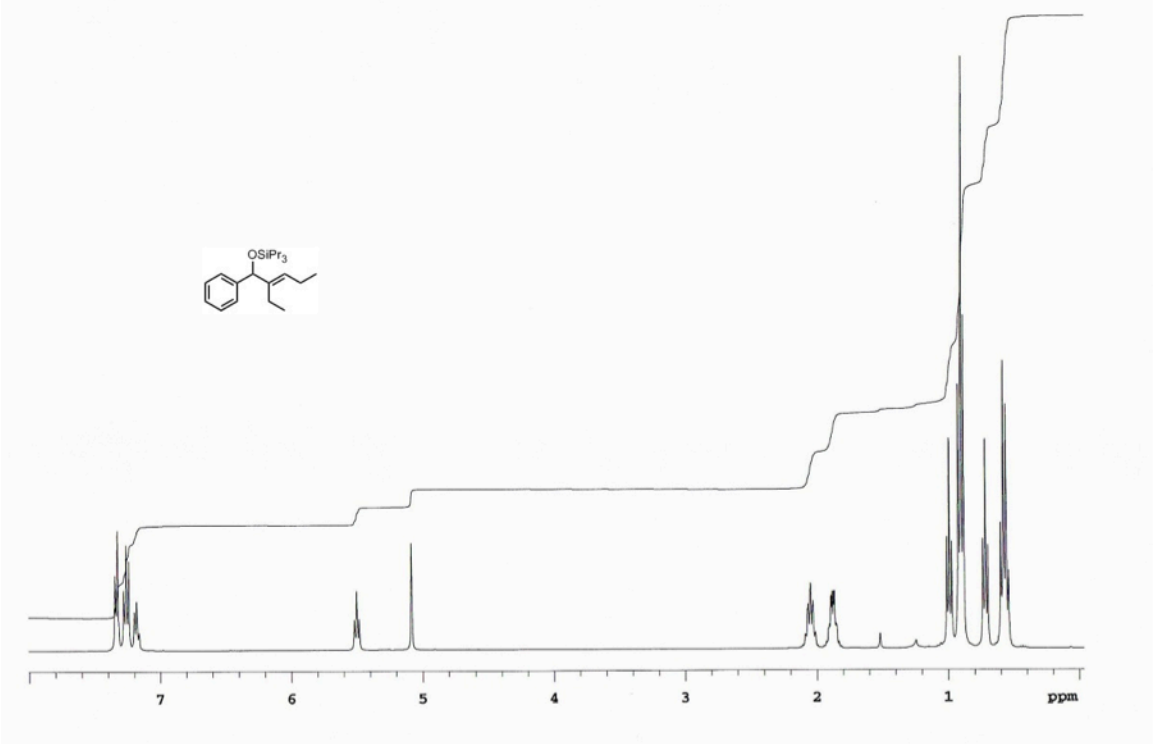
OSiPr3
7
6
5
4
3
2
1
ppm

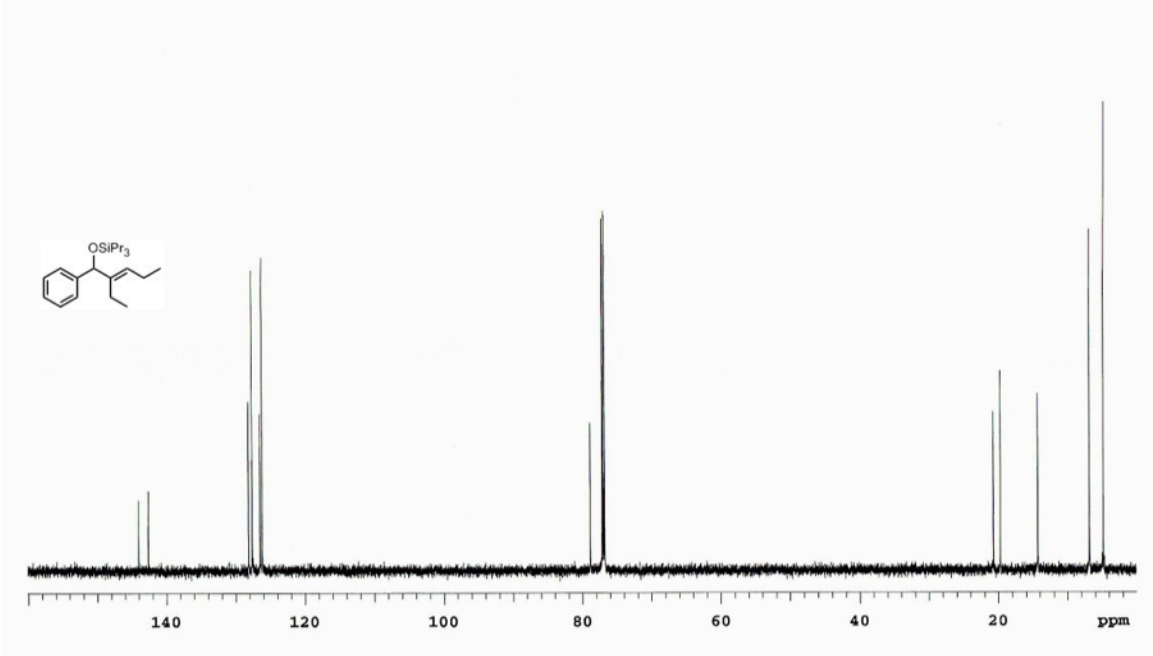
OSiPr3
140
120
100
80
60
40
20
ppm

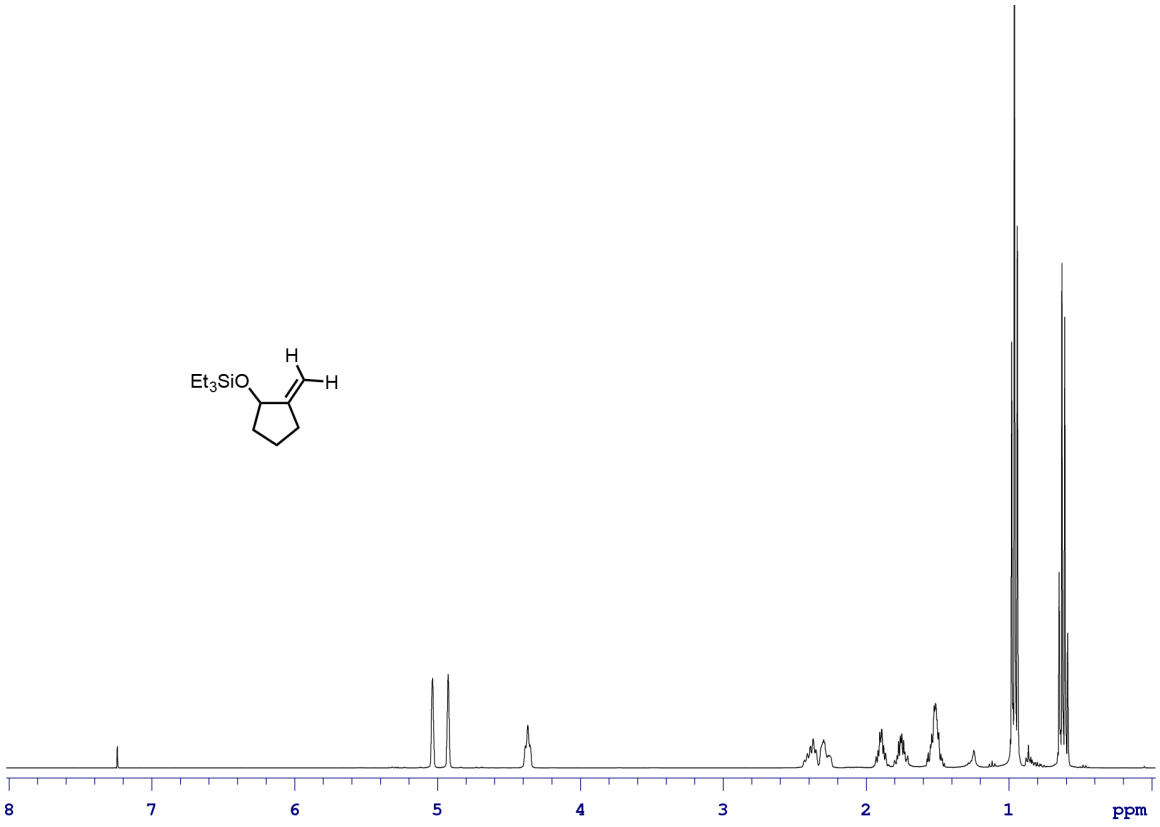
H
Et3SiO
H
8
7
6
5
4
3
2
1
ppm

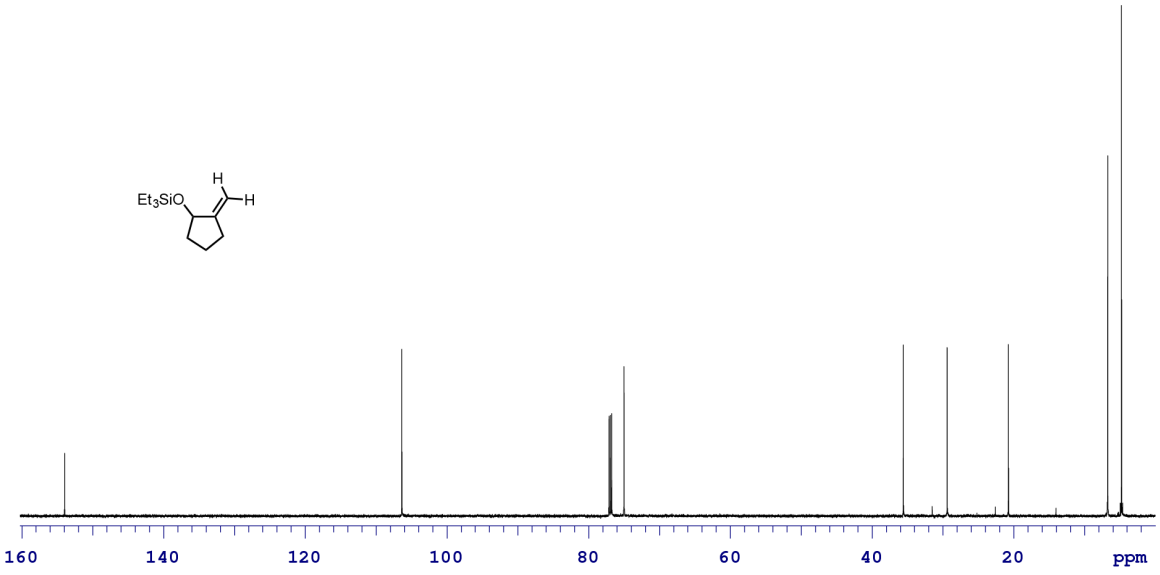
H
Et3SiO
H
160
140
120
100
80
60
40
20
ppm

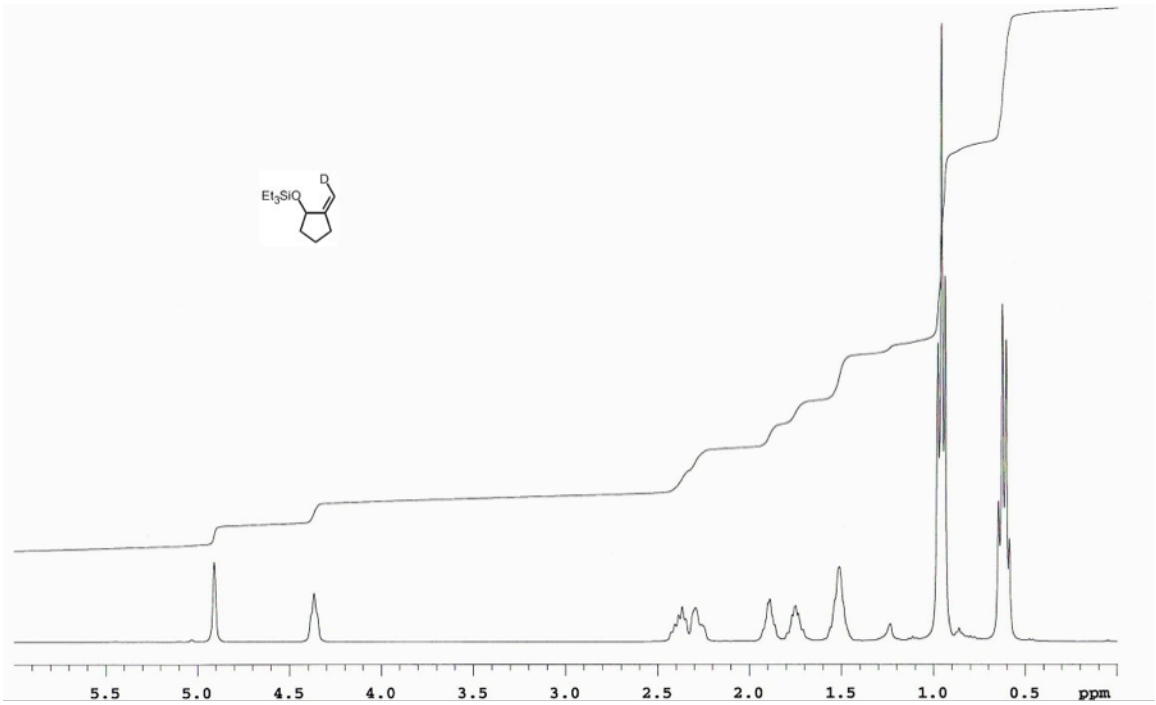
Et3SiO
D
5.5
5.0
4.5
4.0
3.5
3.0
2.5
2.0
1.5
1.0
0.5
ppm

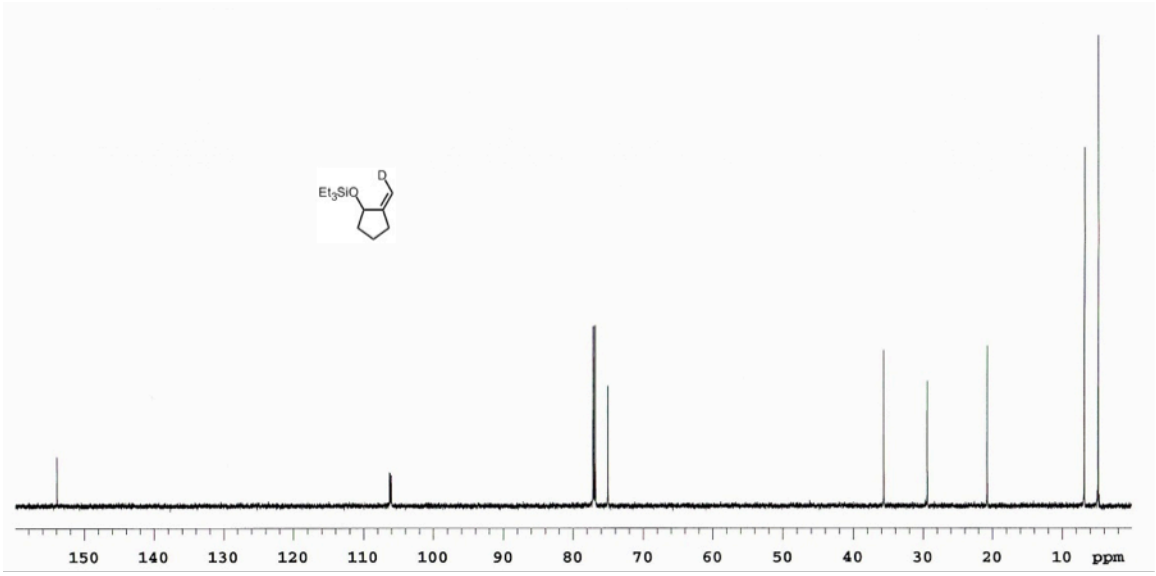
Et3SiO
D
150
140
130
120
110
100
90
80
70
60
50
40
30
20
10
ppm

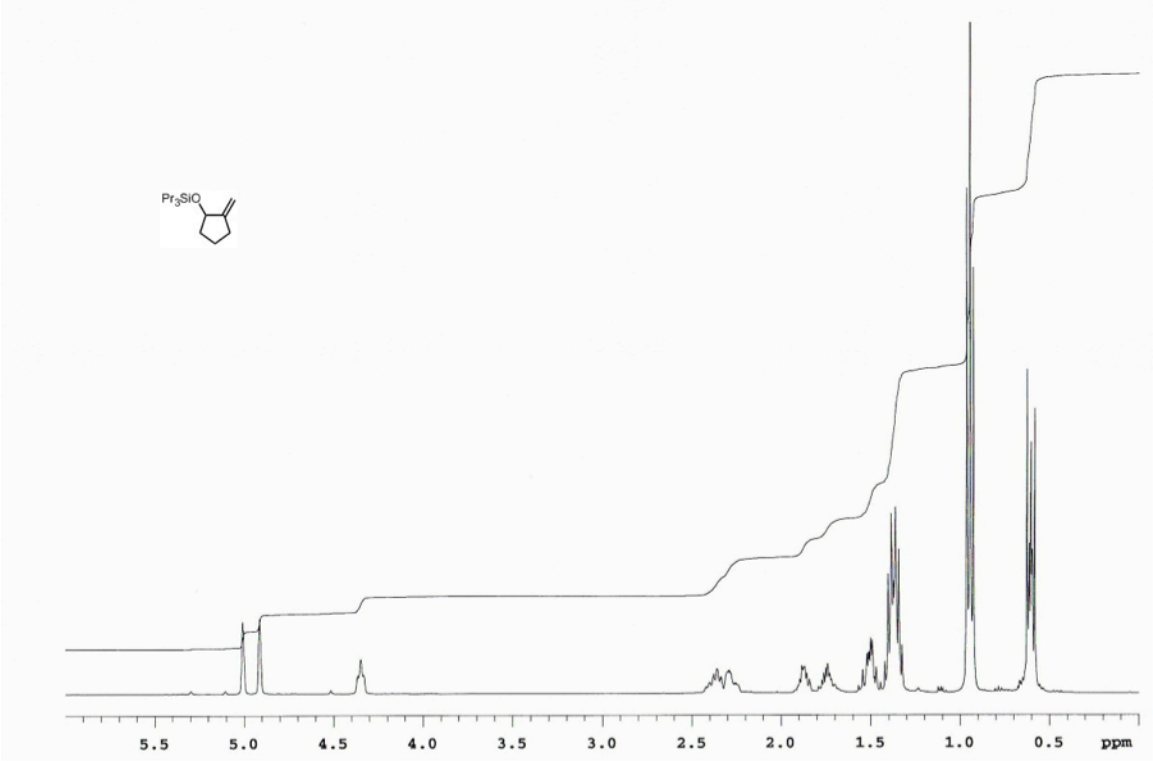
Pr3SiO
5.5
5.0
4.5
4.0
3.5
3.0
2.5
2.0
1.5
1.0
0.5
ppm

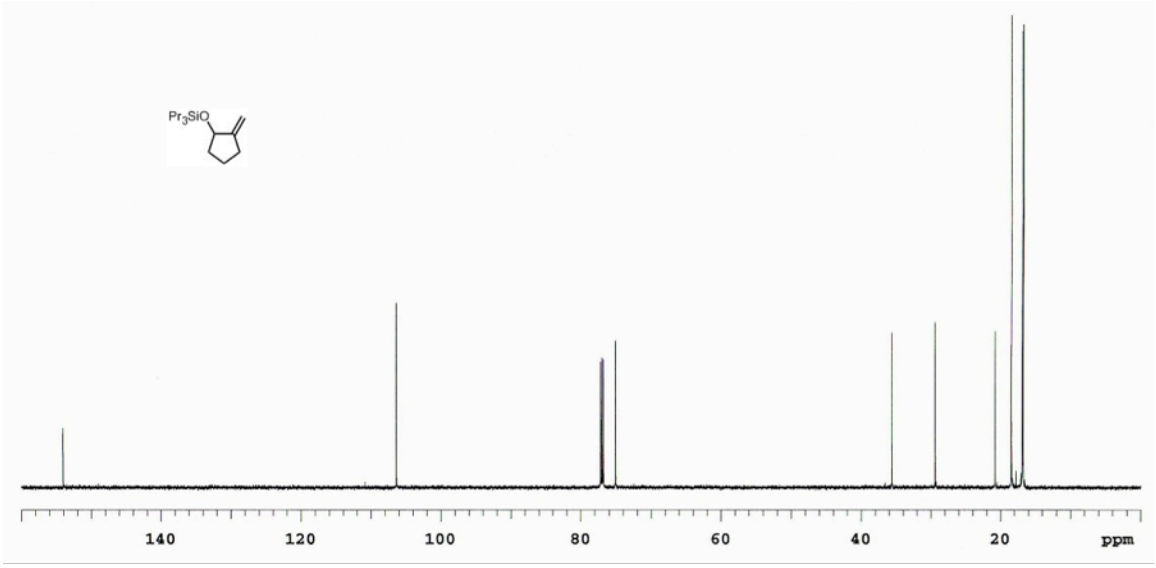
Pr3SiO
140
120
100
80
60
40
20
ppm

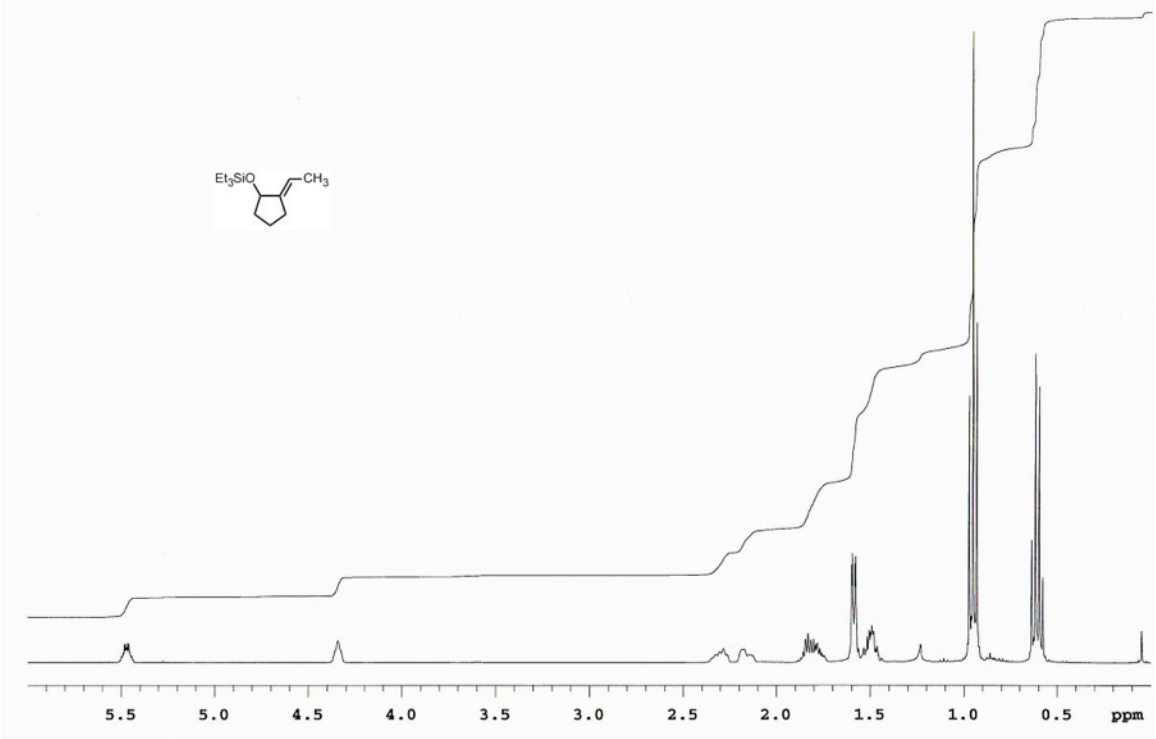
Et3SiO
CH3
5.5
5.0
4.5
4.0
3.5
3.0
2.5
2.0
1.5
1.0
0.5
ppm

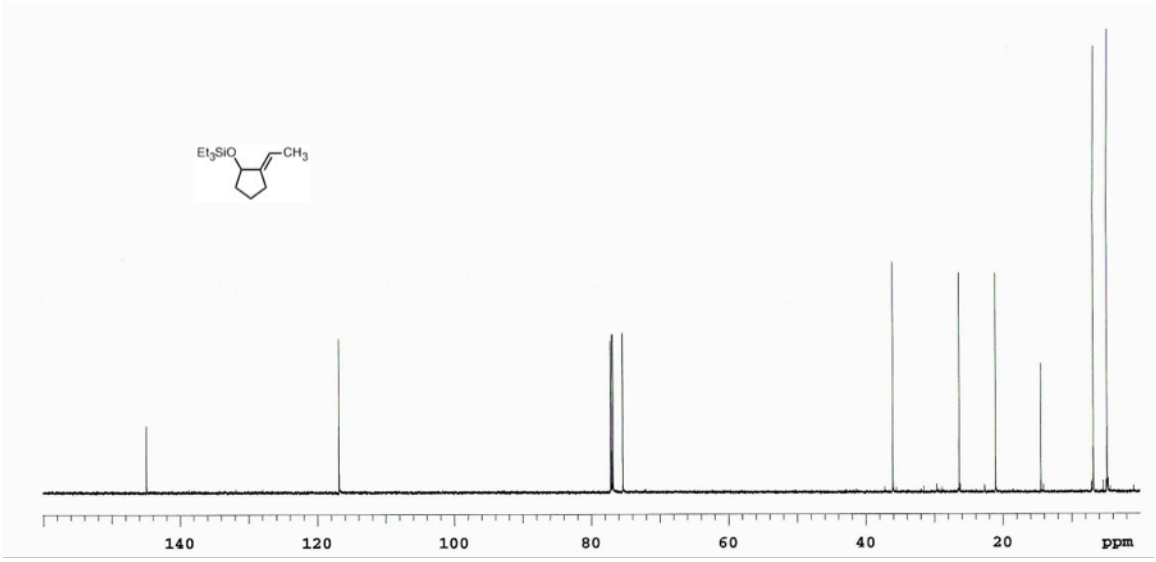
Et3SiO
CH3
140
120
100
80
60
40
20
ppm

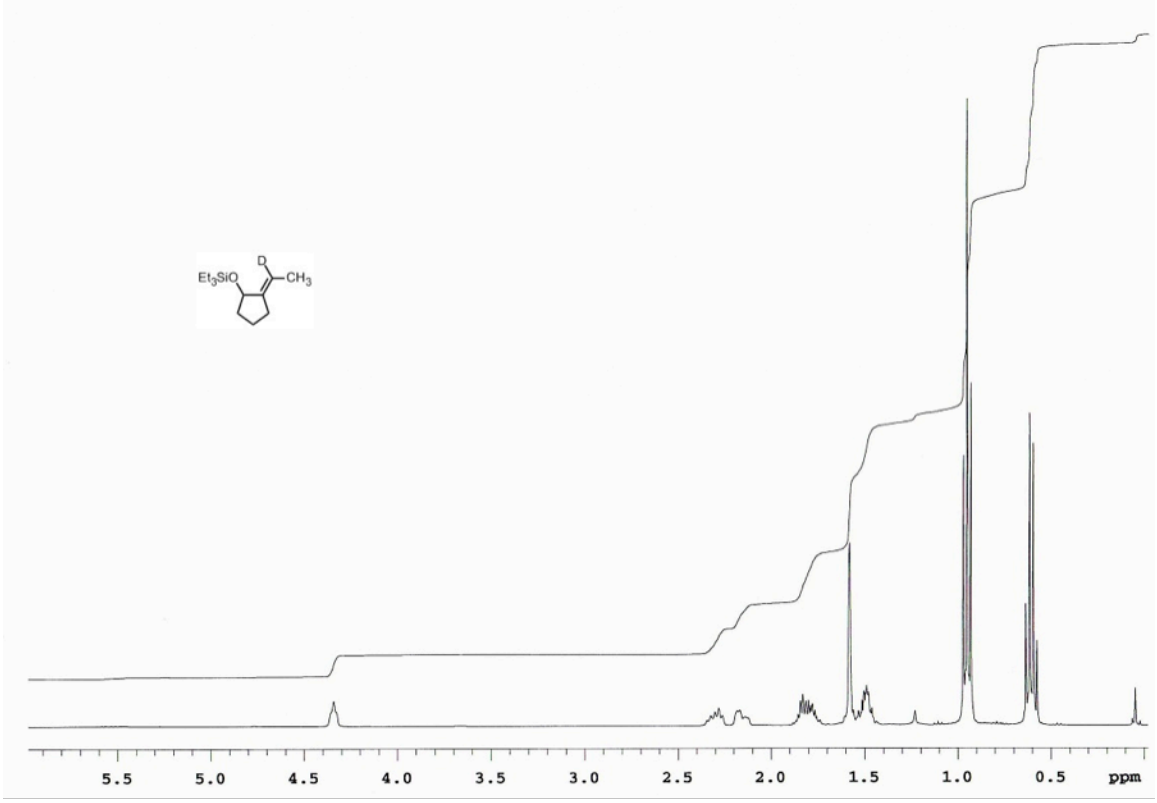
Et3SiO
D
CH3
5.5
5.0
4.5
4.0
3.5
3.0
2.5
2.0
1.5
1.0
0.5
ppm

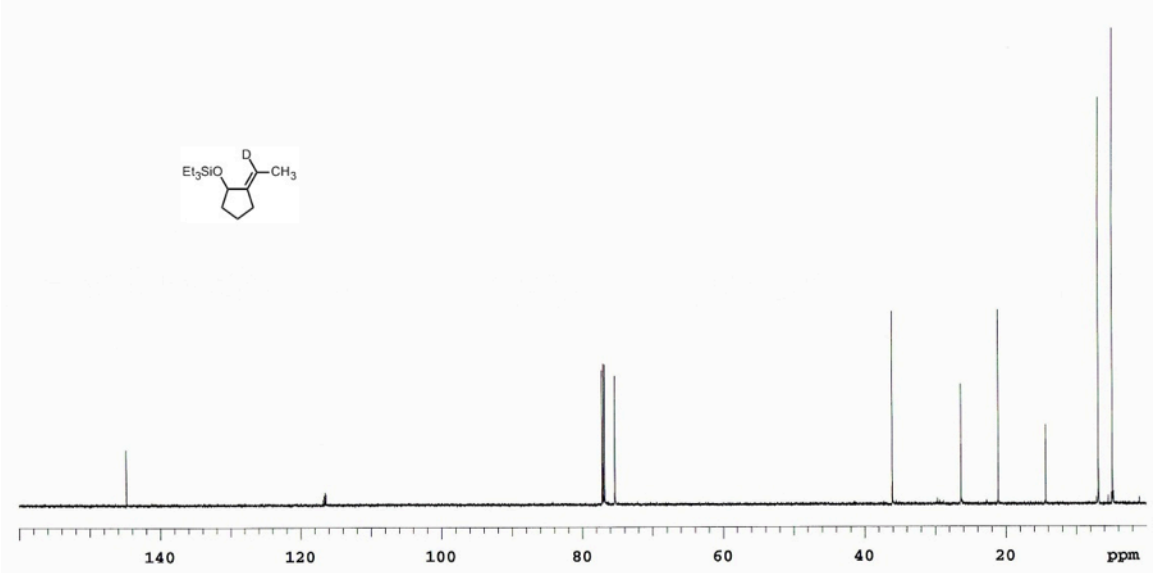
Et3SiO
D
CH3
140
120
100
80
60
40
20
ppm

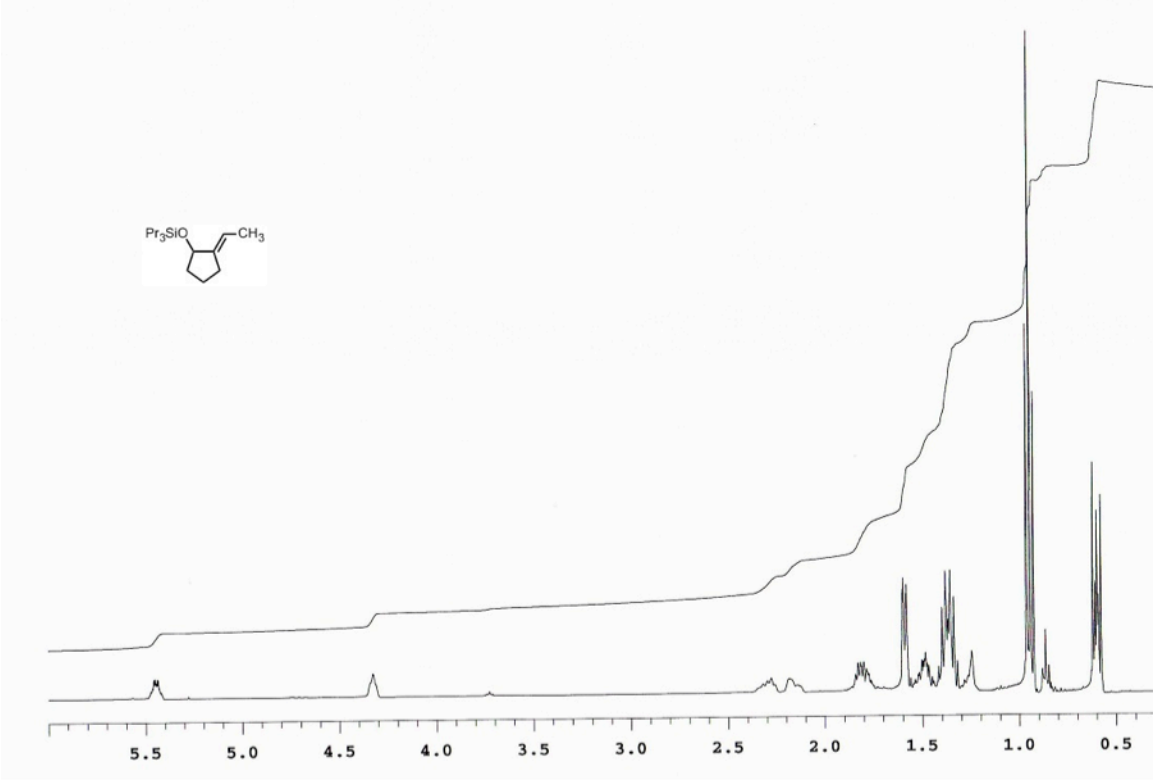
Pr3SiO
CH3
5.5
5.0
4.5
4.0
3.5
3.0
2.5
2.0
1.5
1.0
0.5

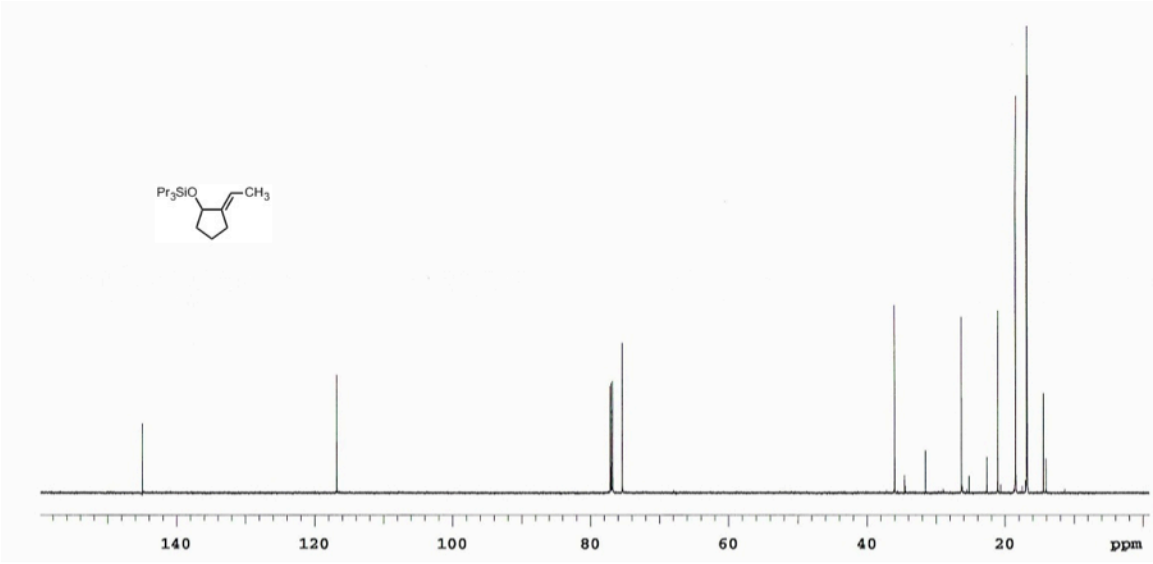
Pr3SiO
CH3
140
120
100
80
60
40
20
ppm

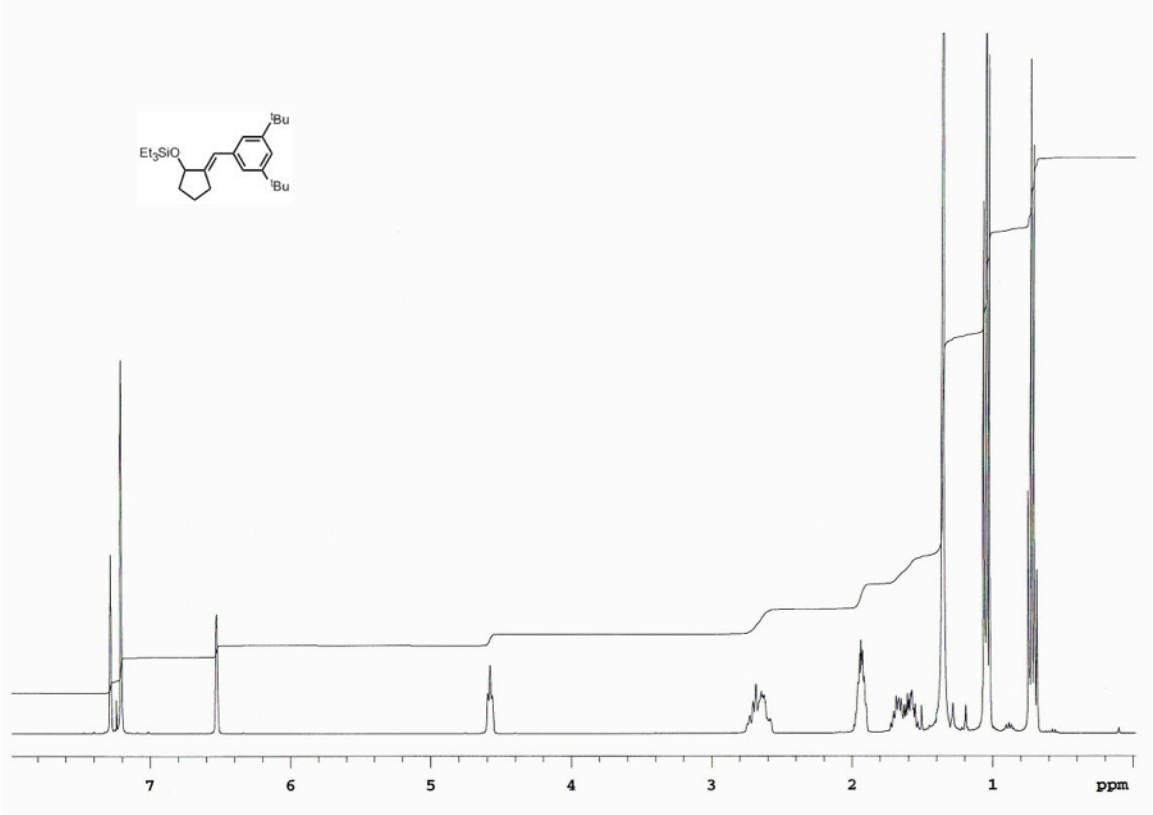
tBu
Et3SiO
tBu
7
6
5
4
3
2
1
ppm

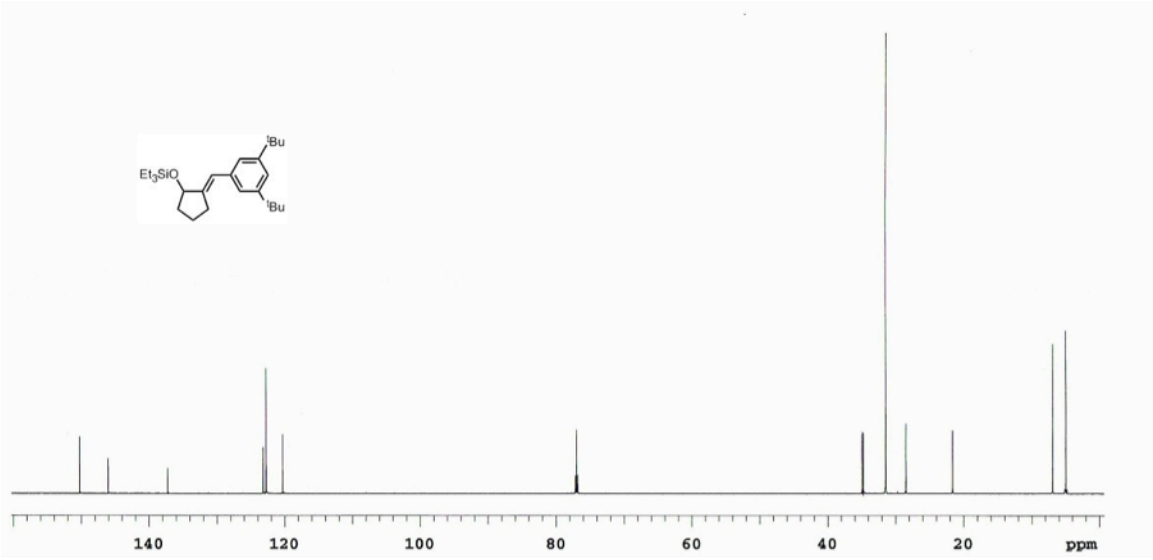
tBu
Et3SiO
tBu
140
120
100
80
60
40
20
ppm

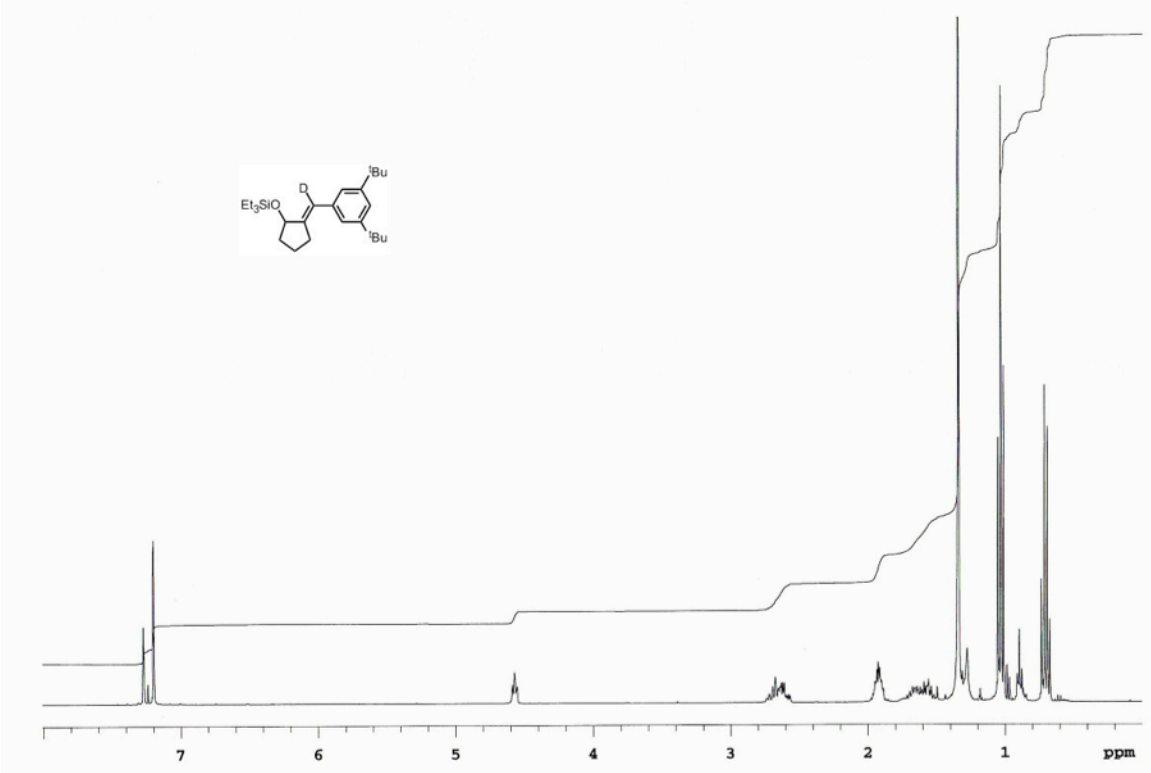
D
Et3SiO
tBu
tBu
7
6
5
4
3
2
1
ppm

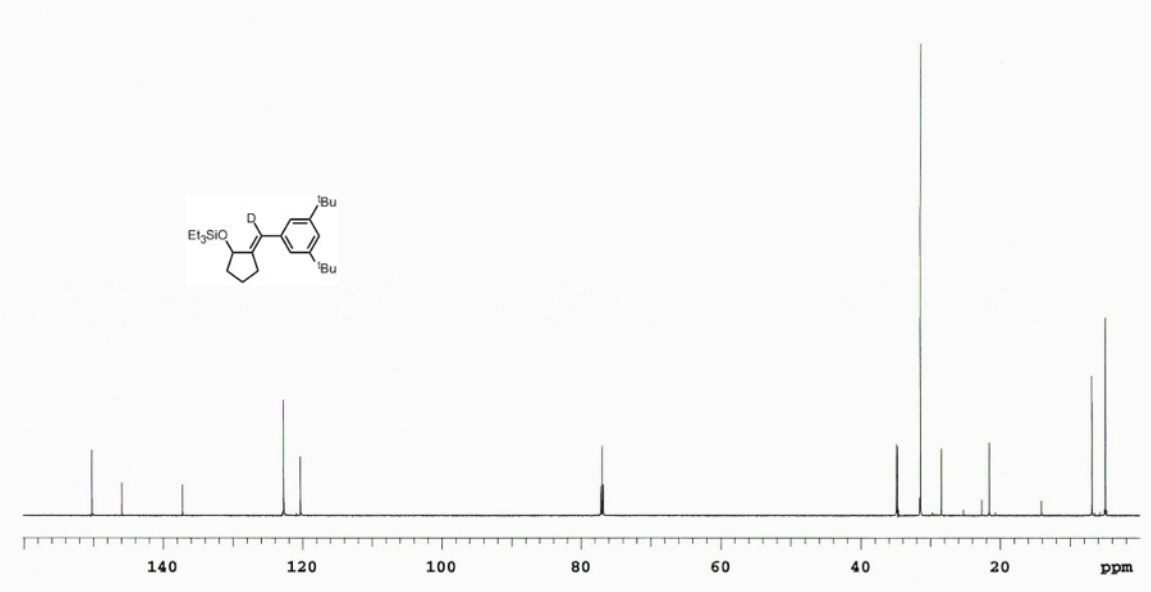
D
Et3SiO
tBu
tBu
140
120
100
80
60
40
20
ppm

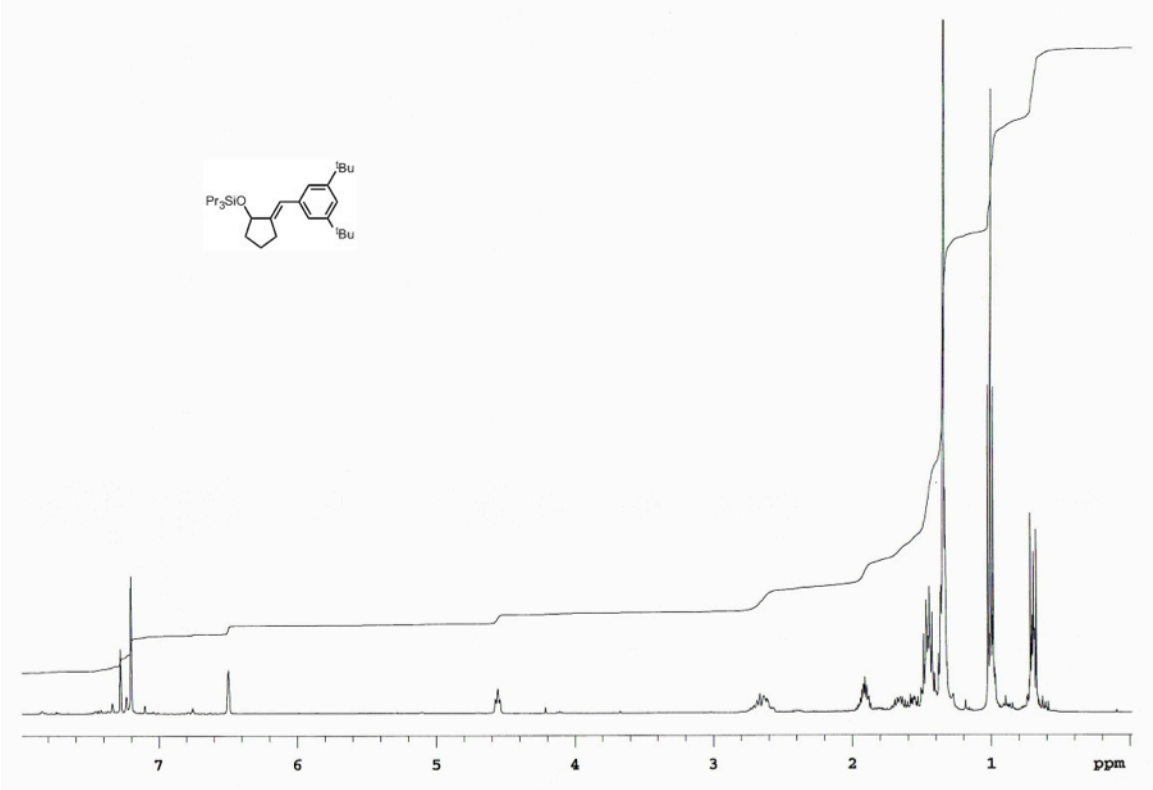
tBu
Pr3SiO
tBu
7
6
5
4
3
2
1
ppm

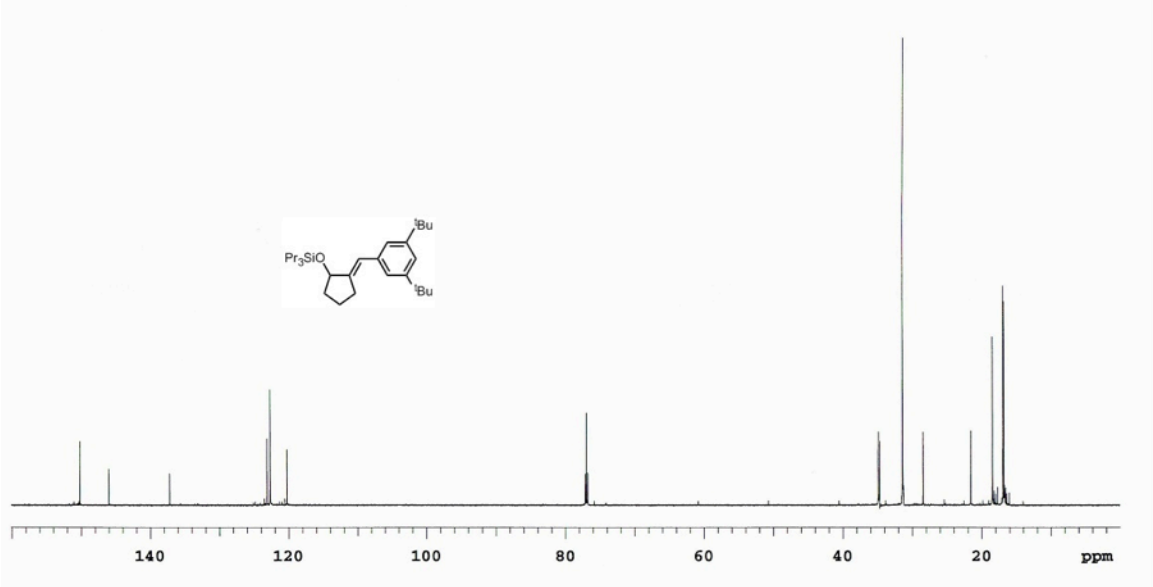
tBu
Pr3SiO
tBu
140
120
100
80
60
40
20
ppm

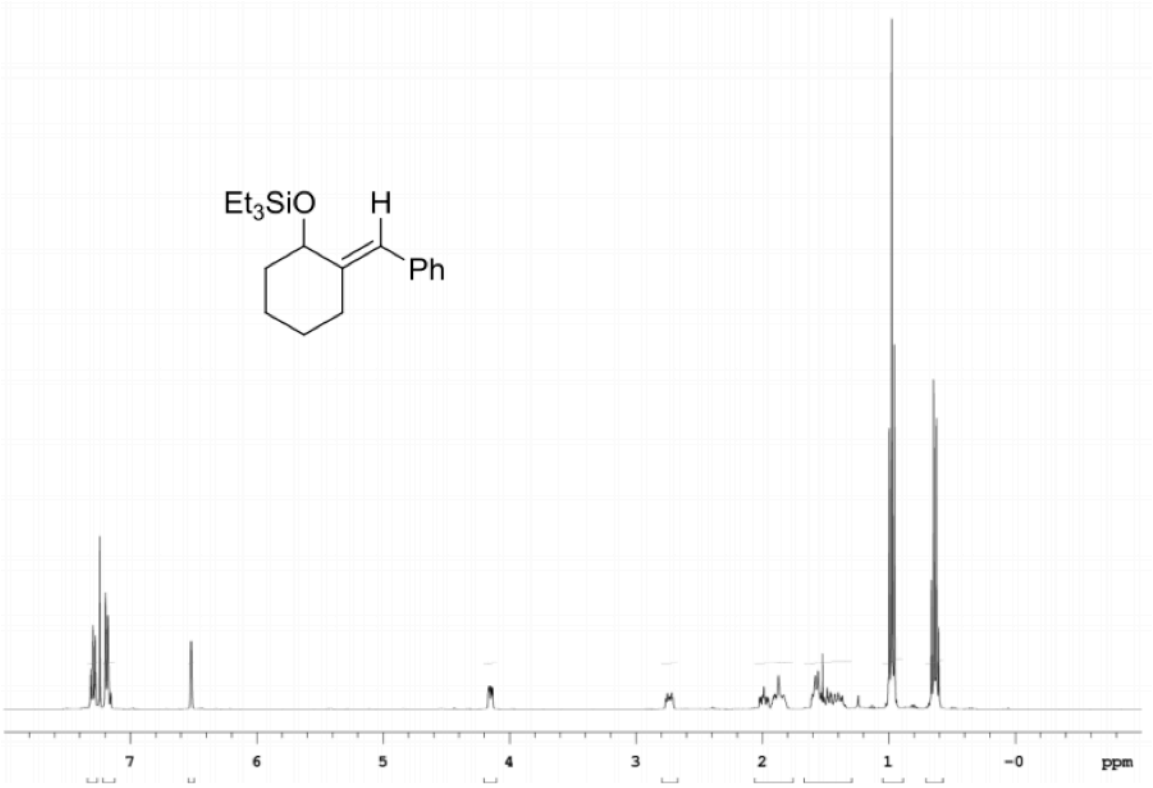
Et3SiO
H
Ph
7
6
5
4
3
2
1
-0
ppm

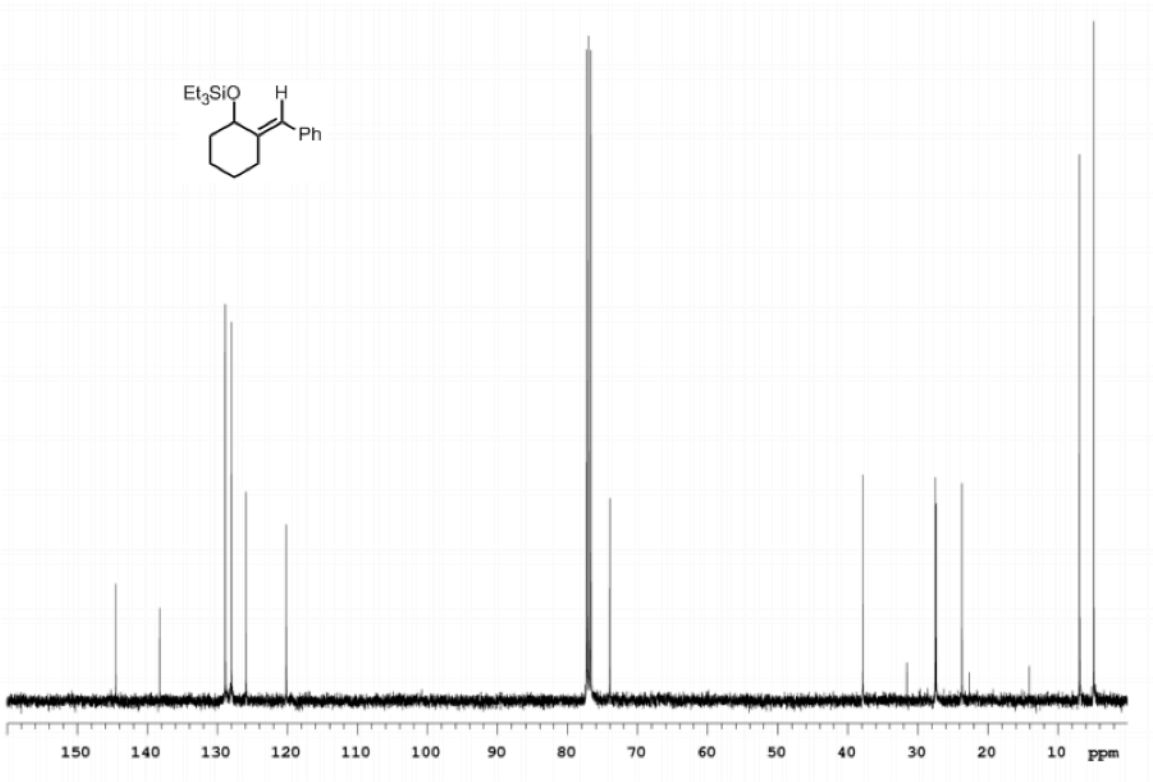
Et3SiO
H
Ph
150
140
130
120
110
100
90
80
70
60
50
40
30
20
10
ppm

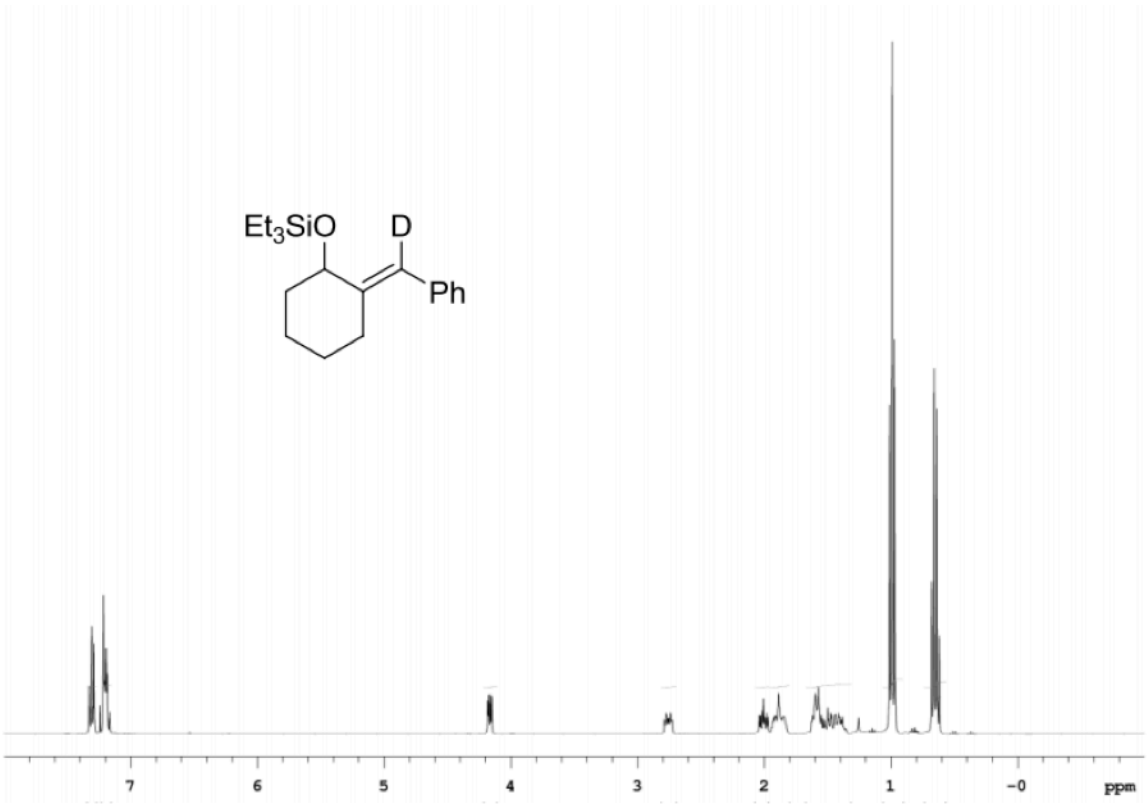
Et3SiO
D
Ph
7
6
5
4
3
2
1
−0
ppm

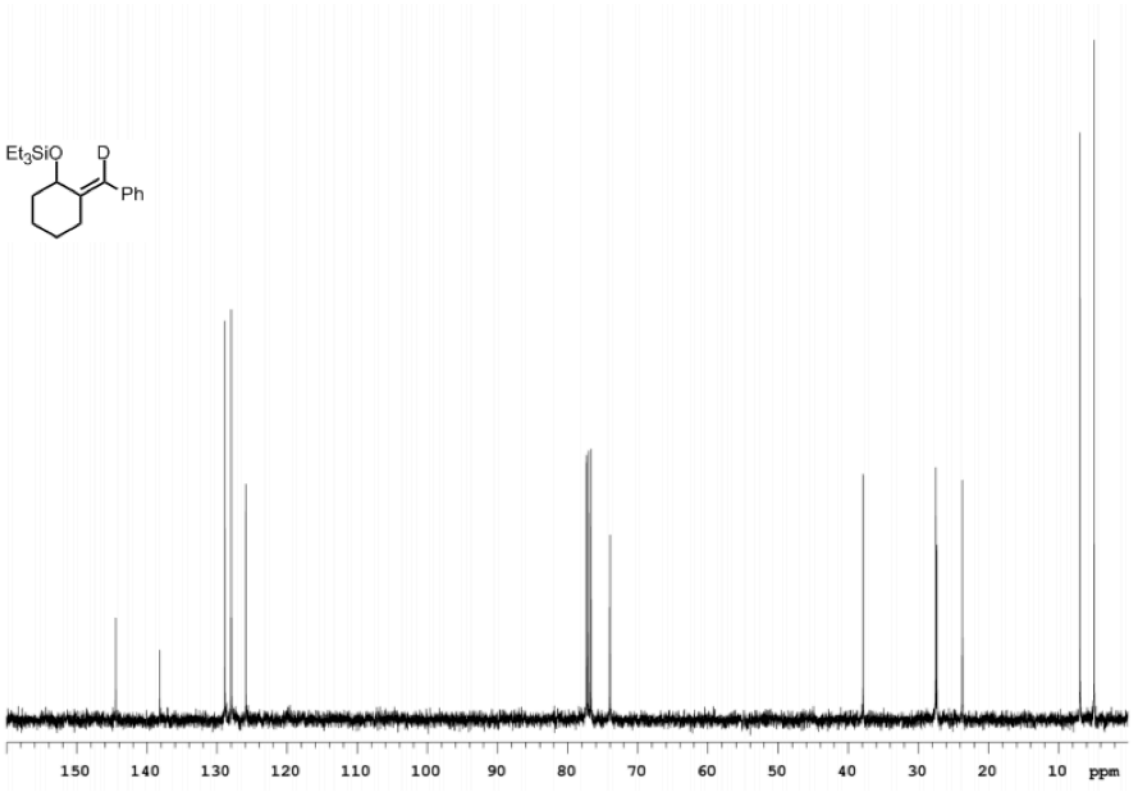
Et3SiO
D
Ph
150
140
130
120
110
100
90
80
70
60
50
40
30
20
10
ppm

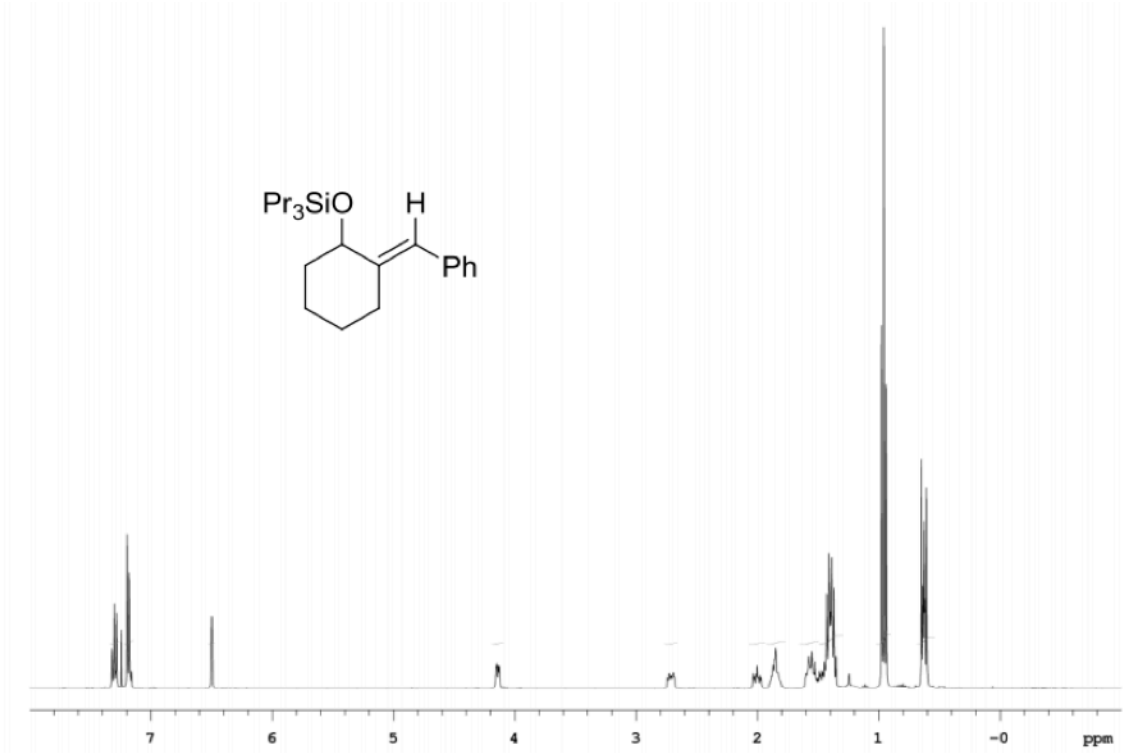
Pr3SiO
H
Ph
7
6
5
4
3
2
1
-0
ppm

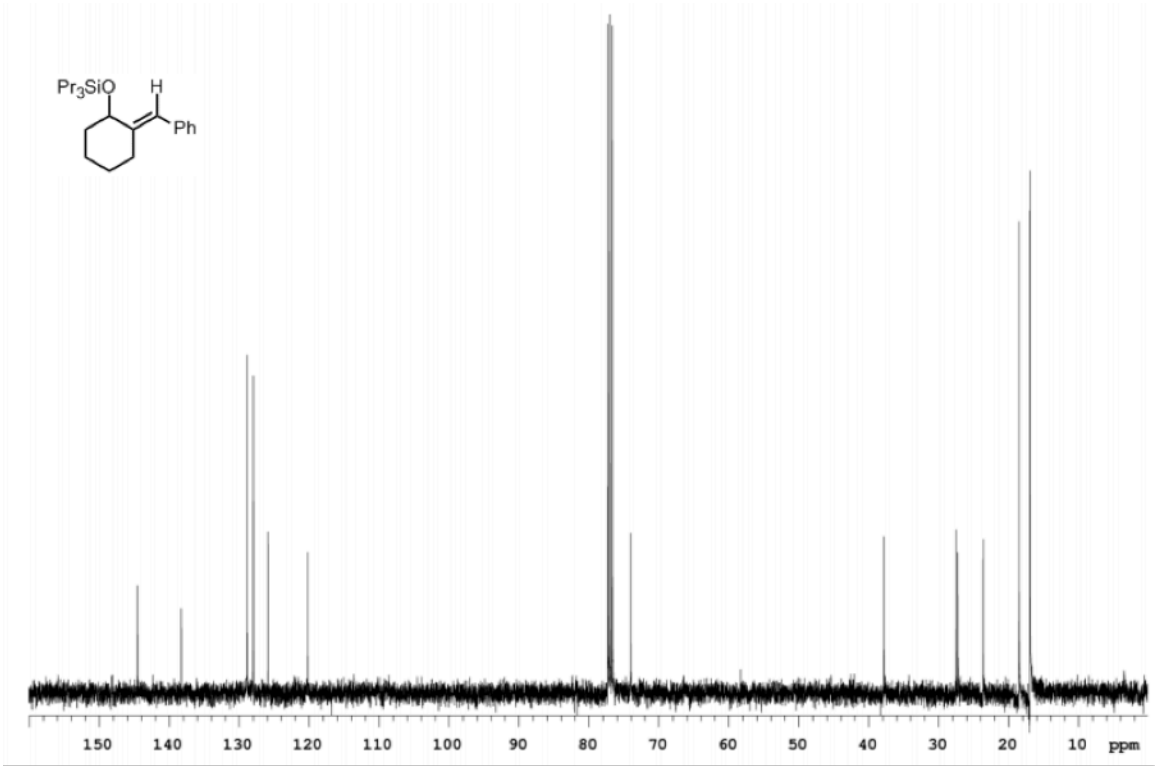
Pr3SiO
H
Ph
150
140
130
120
110
100
90
80
70
60
50
40
30
20
10
ppm

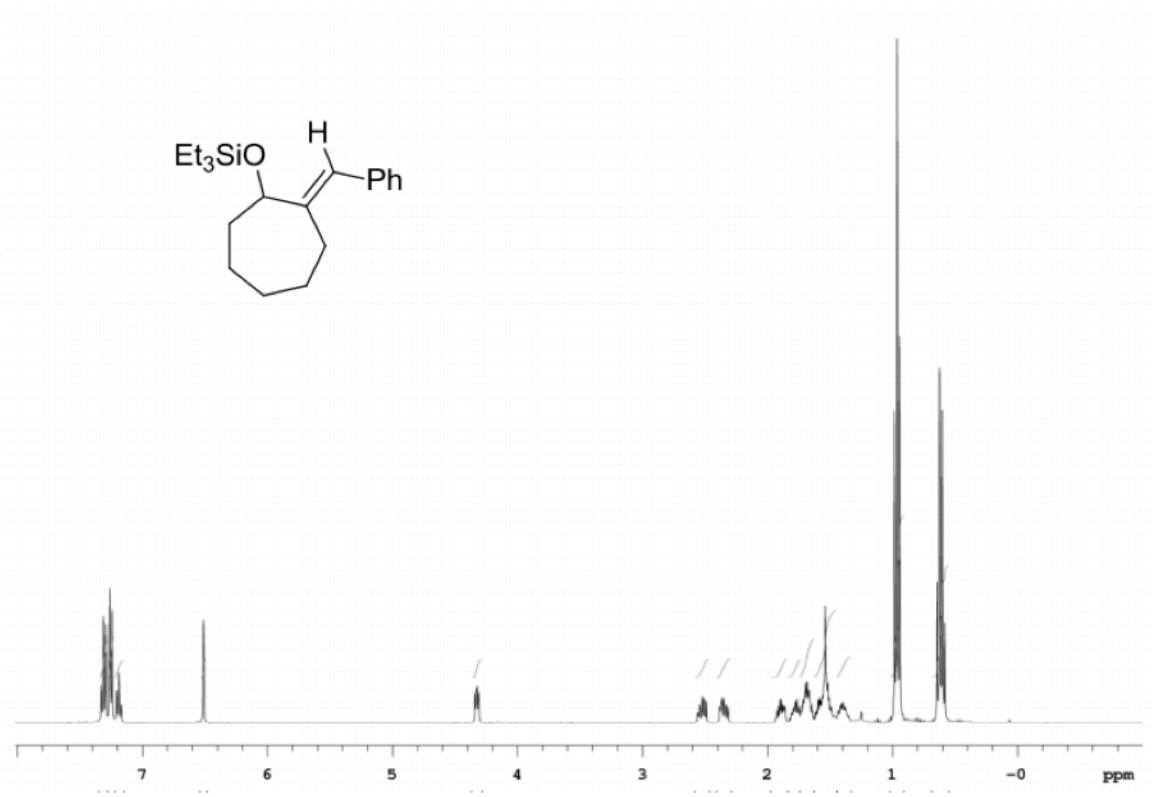
Et3SiO
H
Ph
7
6
5
4
3
2
1
−0
ppm

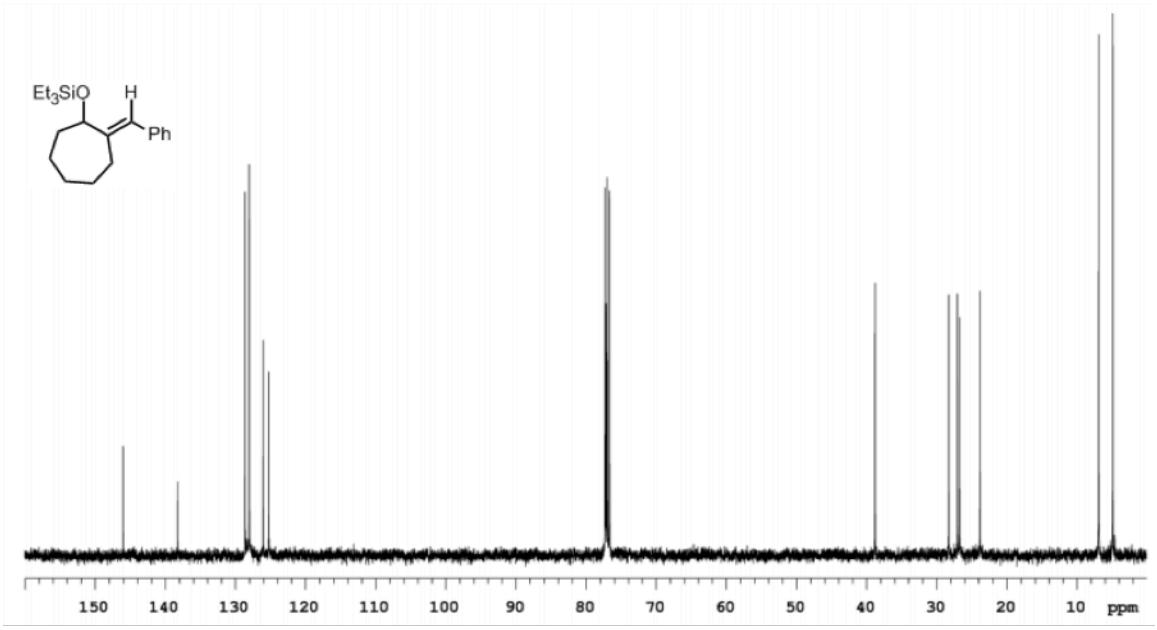
Et3SiO
H
Ph
150
140
130
120
110
100
90
80
70
60
50
40
30
20
10
ppm

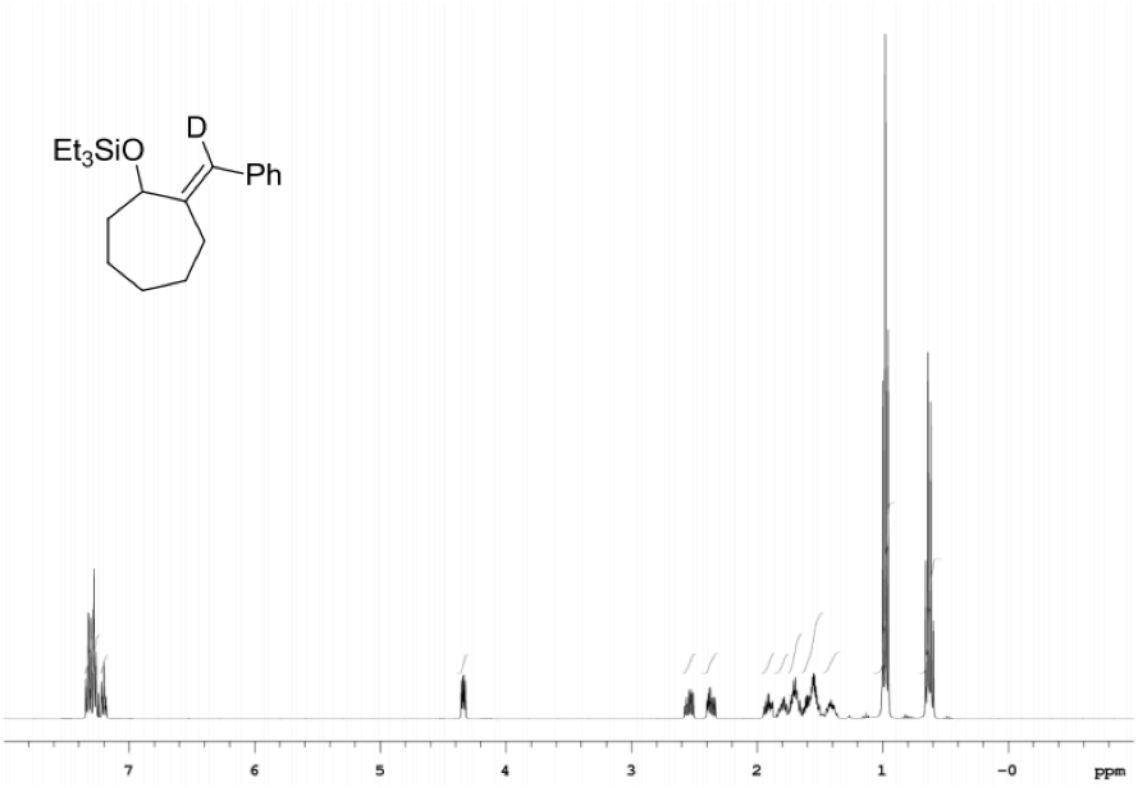
Et3SiO
D
Ph
7
6
5
4
3
2
1
−0
ppm

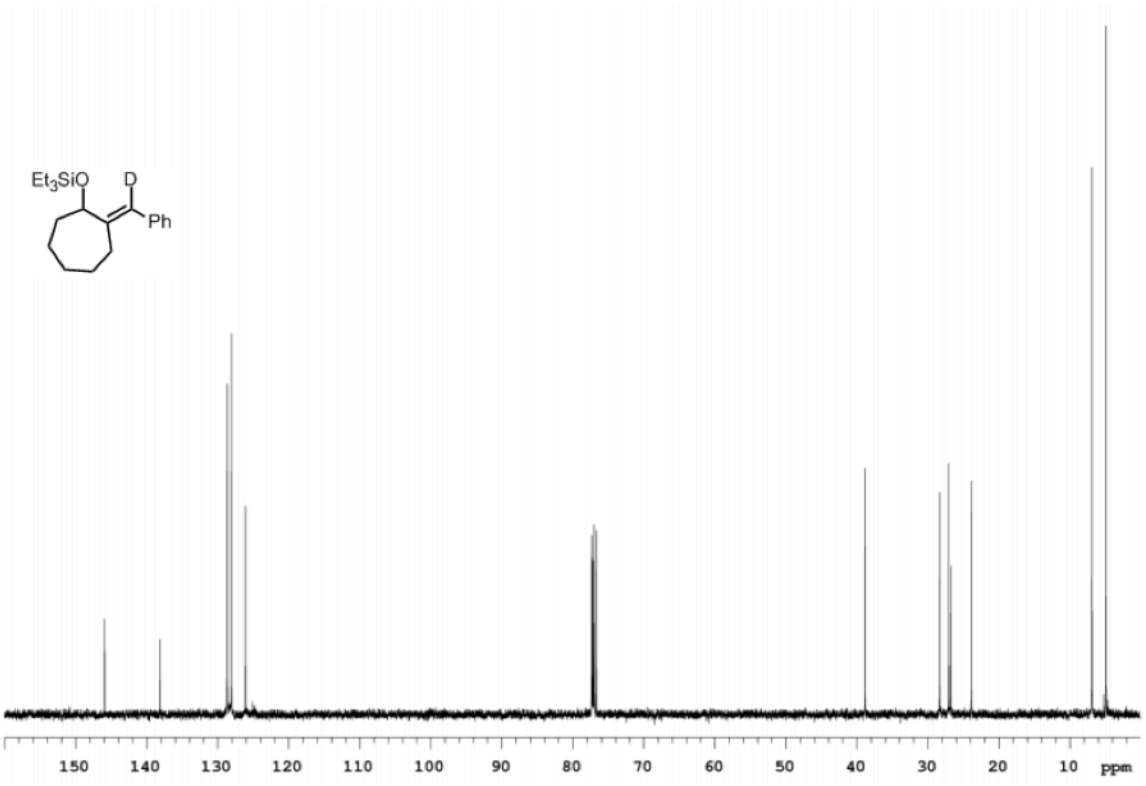
Et3SiO
D
Ph
150
140
130
120
110
100
90
80
70
60
50
40
30
20
10
ppm

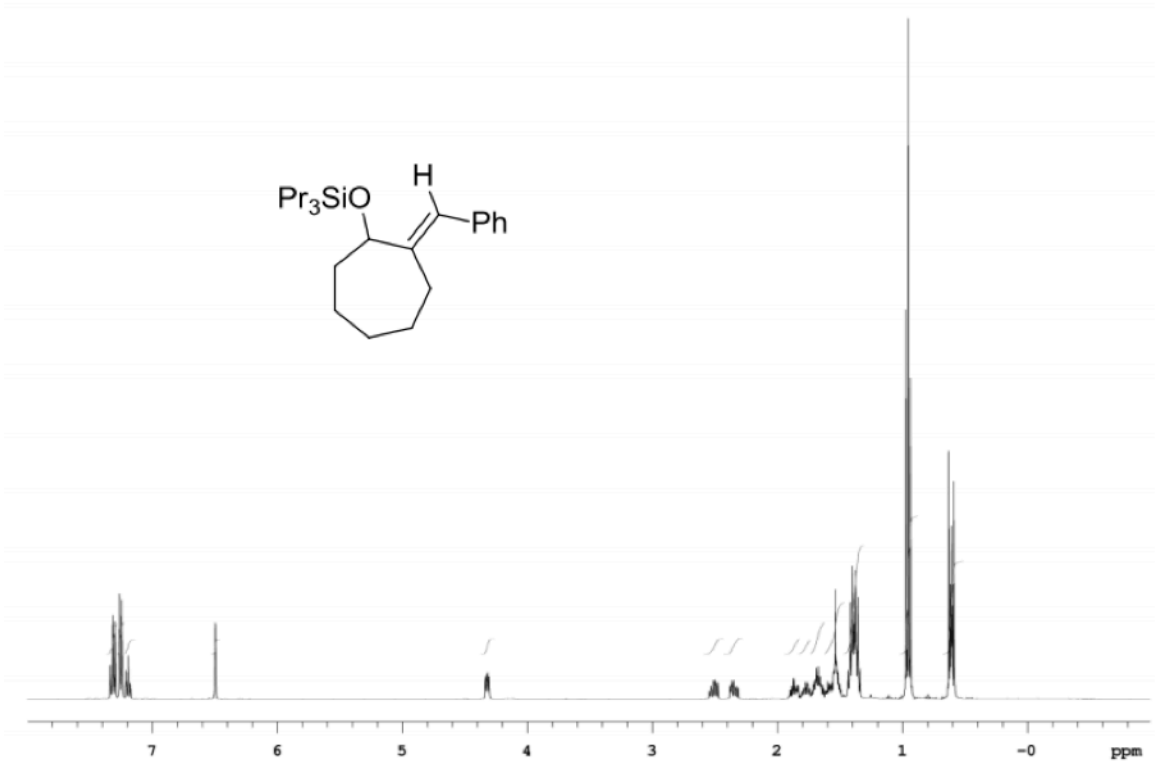
Pr3SiO
H
Ph
7
6
5
4
3
2
1
-0
ppm

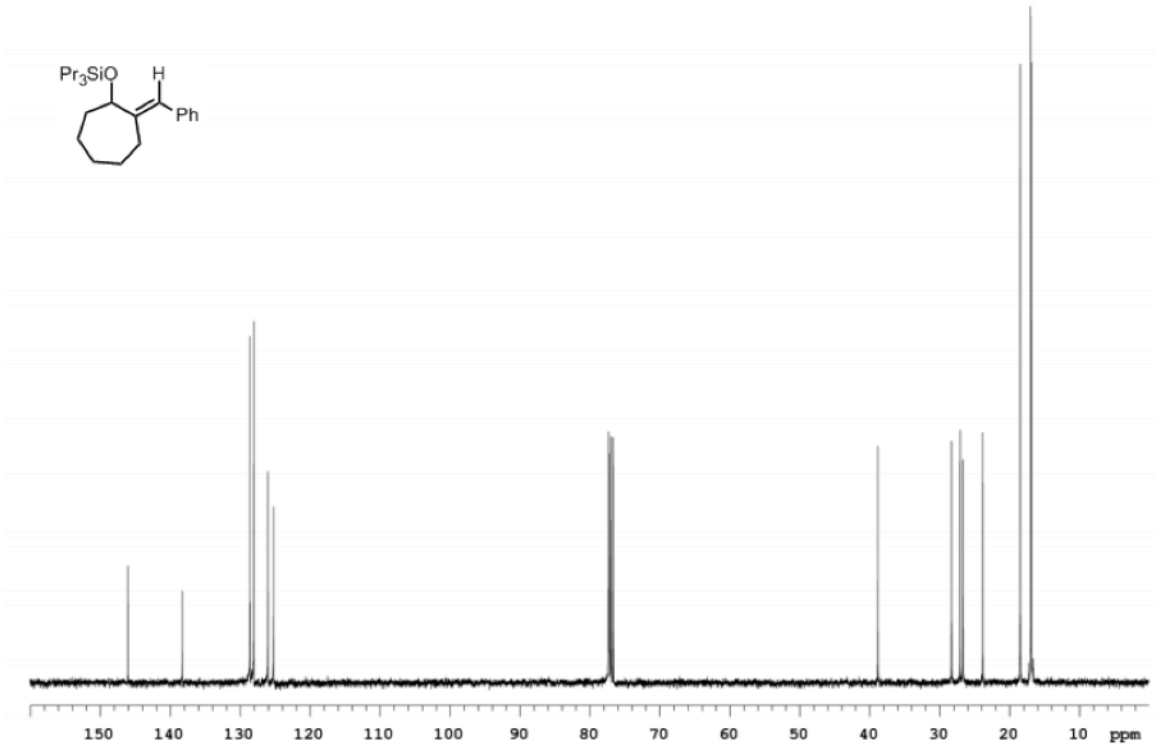
Pr3SiO
H
Ph
150
140
130
120
110
100
90
80
70
60
50
40
30
20
10
ppm

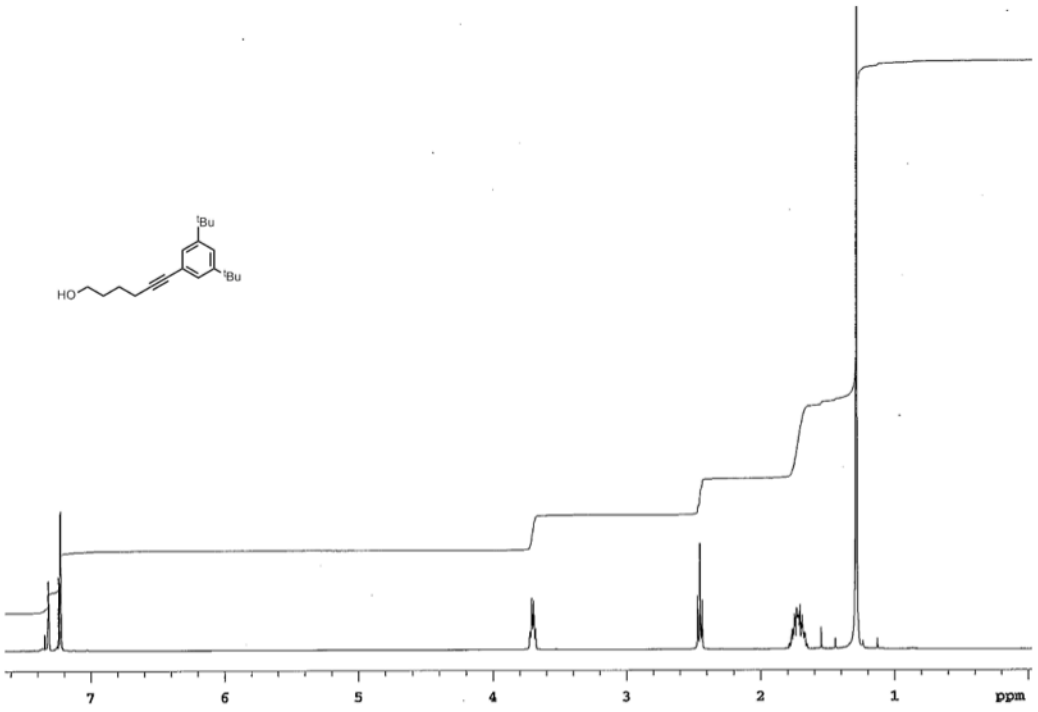
tBu
tBu
HO
7
6
5
4
3
2
1
ppm

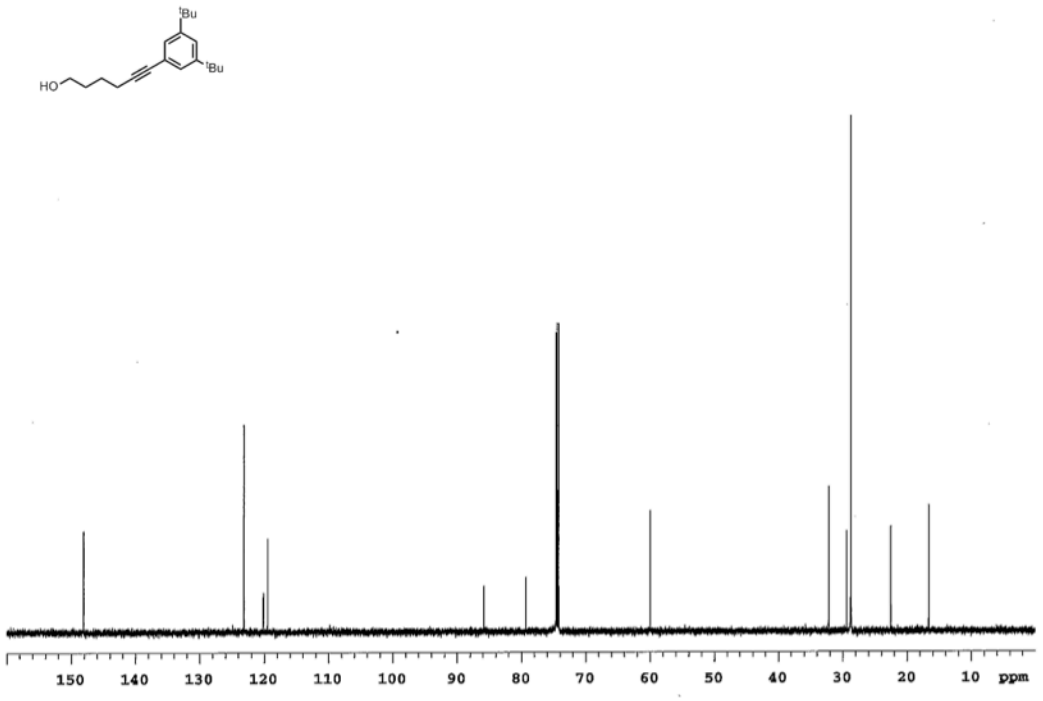
tBu
tBu
HO
150
140
130
120
110
100
90
80
70
60
50
40
30
20
10
ppm

5.4.2 Chapter 3 NMR Spectra

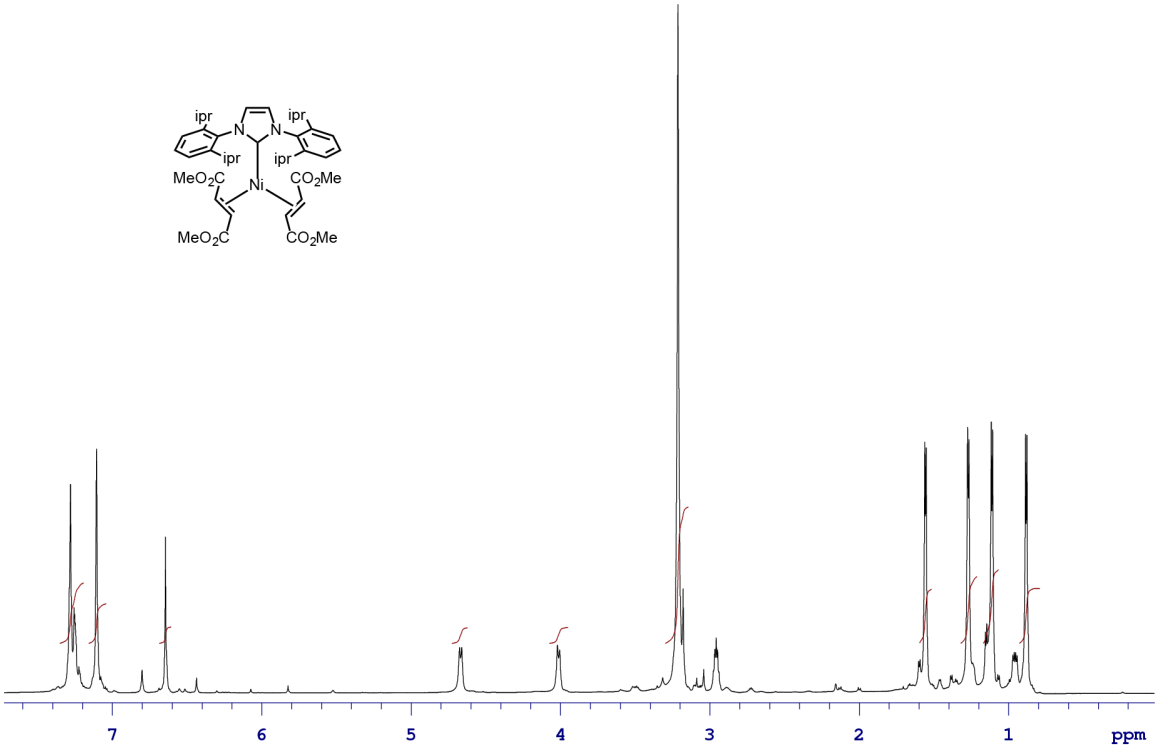

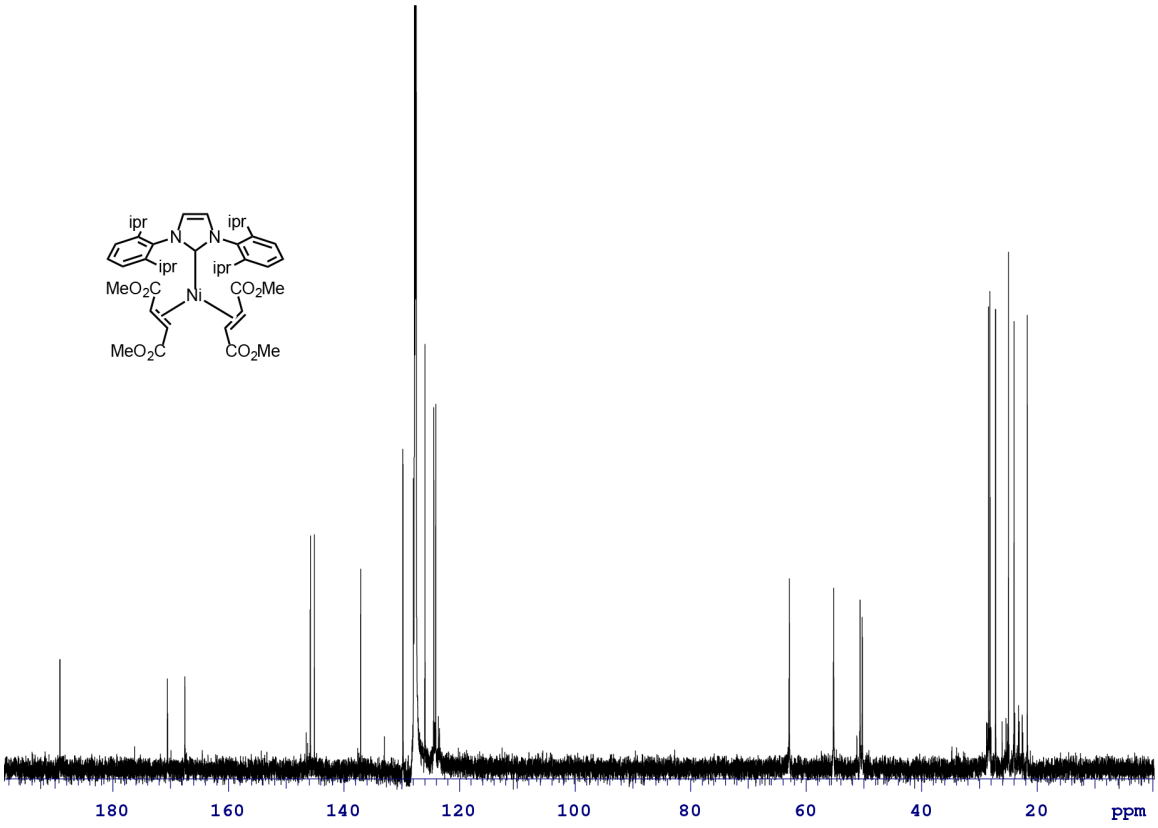

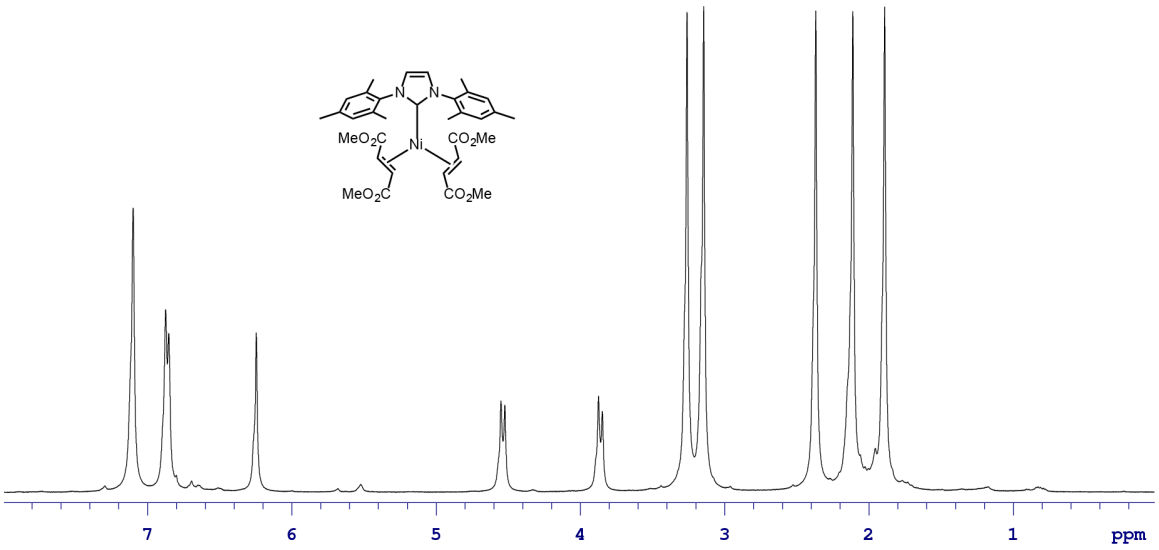
MeO2C
CO2Me
Ni
MeO2C
CO2Me
7
6
5
4
3
2
1
ppm

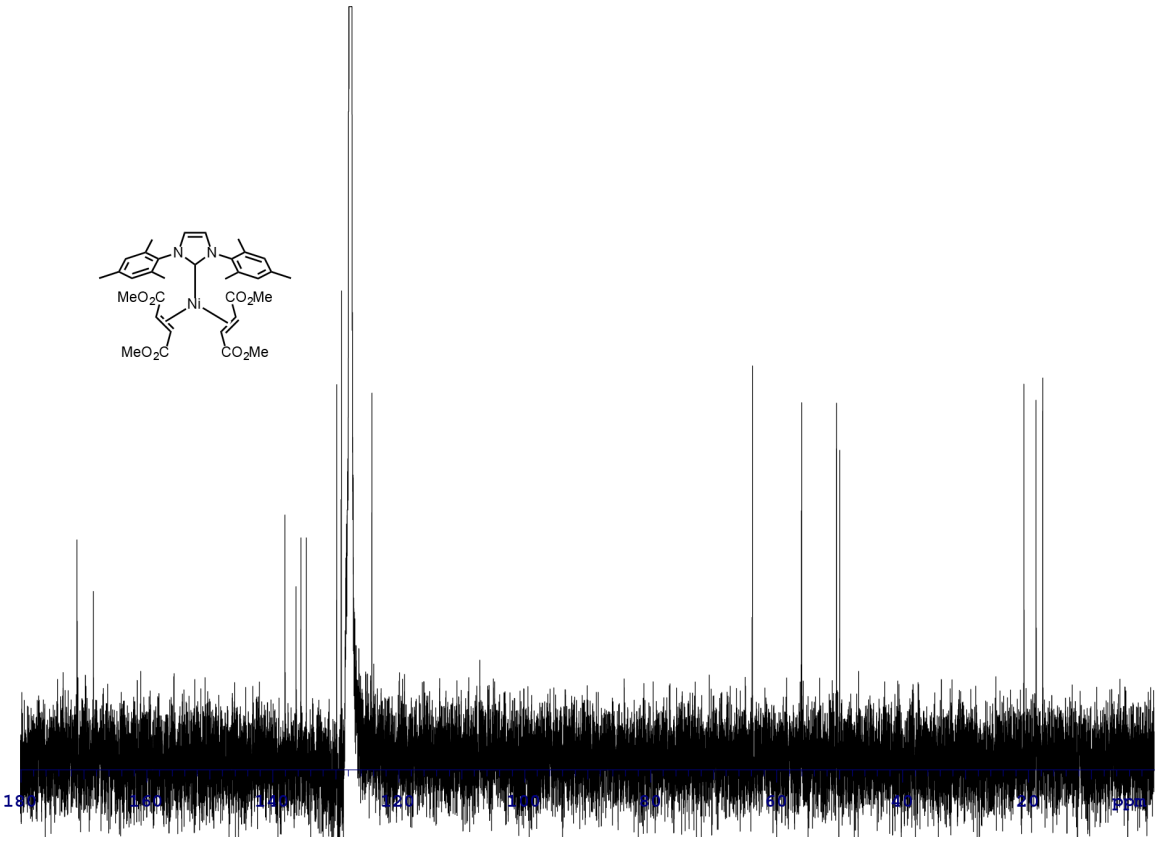
MeO2C
CO2Me
Ni
MeO2C
CO2Me
160
140
120
100
80
60
40
20
ppm

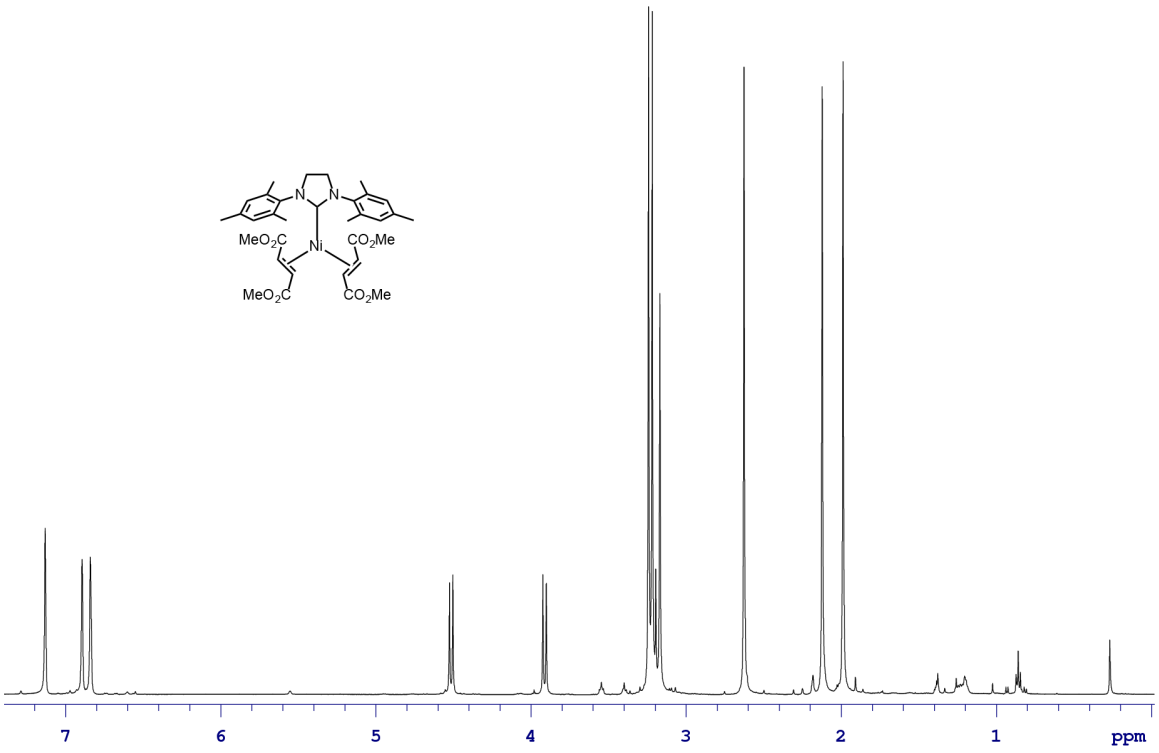
MeO2C
CO2Me
Ni
MeO2C
CO2Me
7
6
5
4
3
2
1
ppm

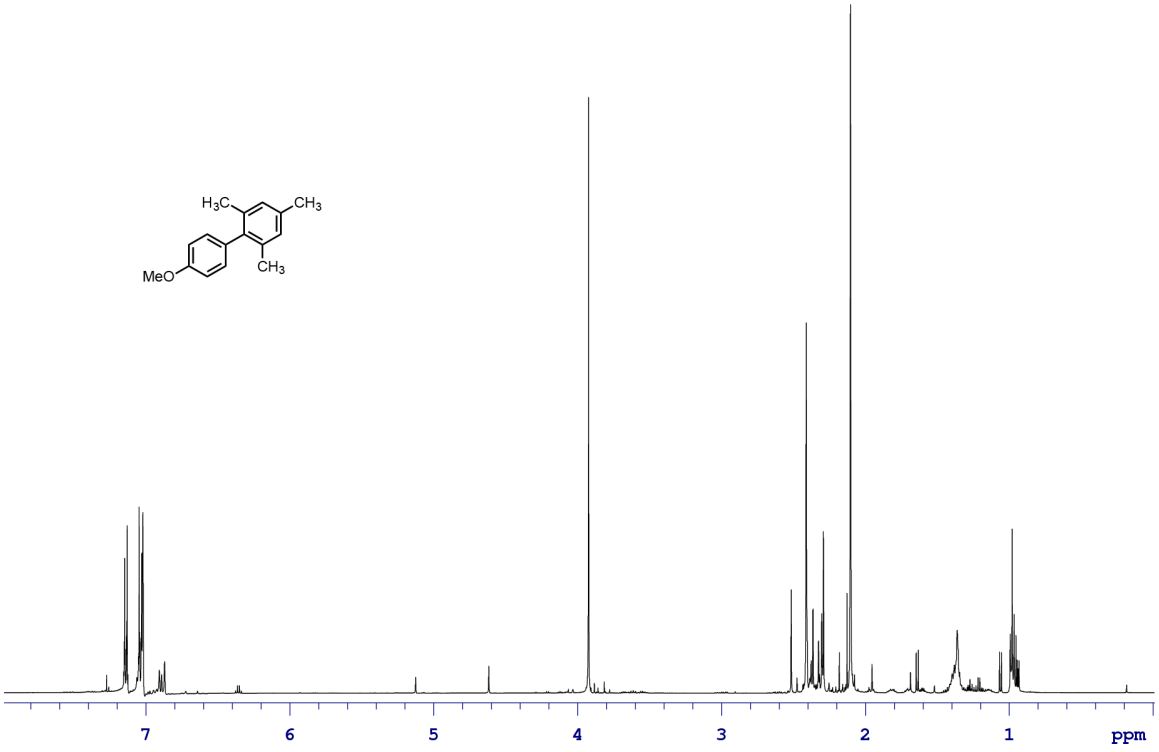
H3C
CH3
MeO
CH3
7
6
5
4
3
2
1
ppm

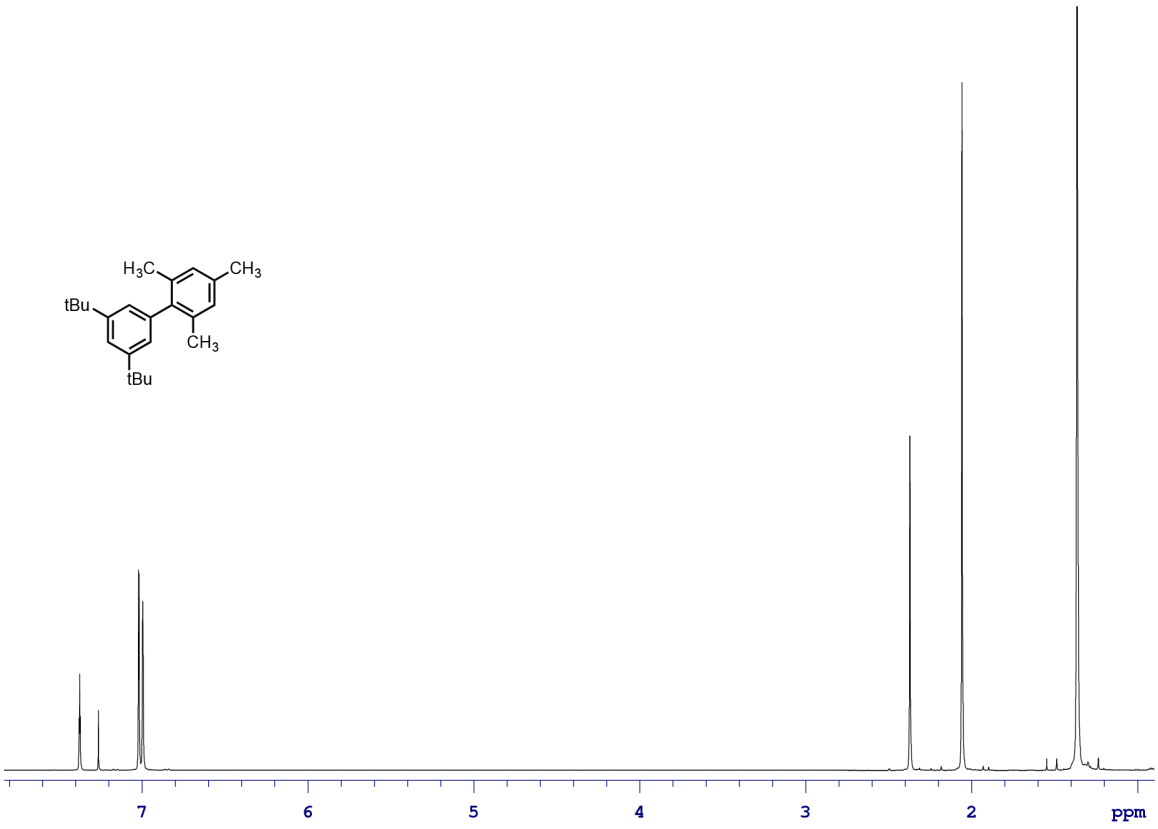
H3C
CH3
tBu
CH3
tBu
7
6
5
4
3
2
ppm

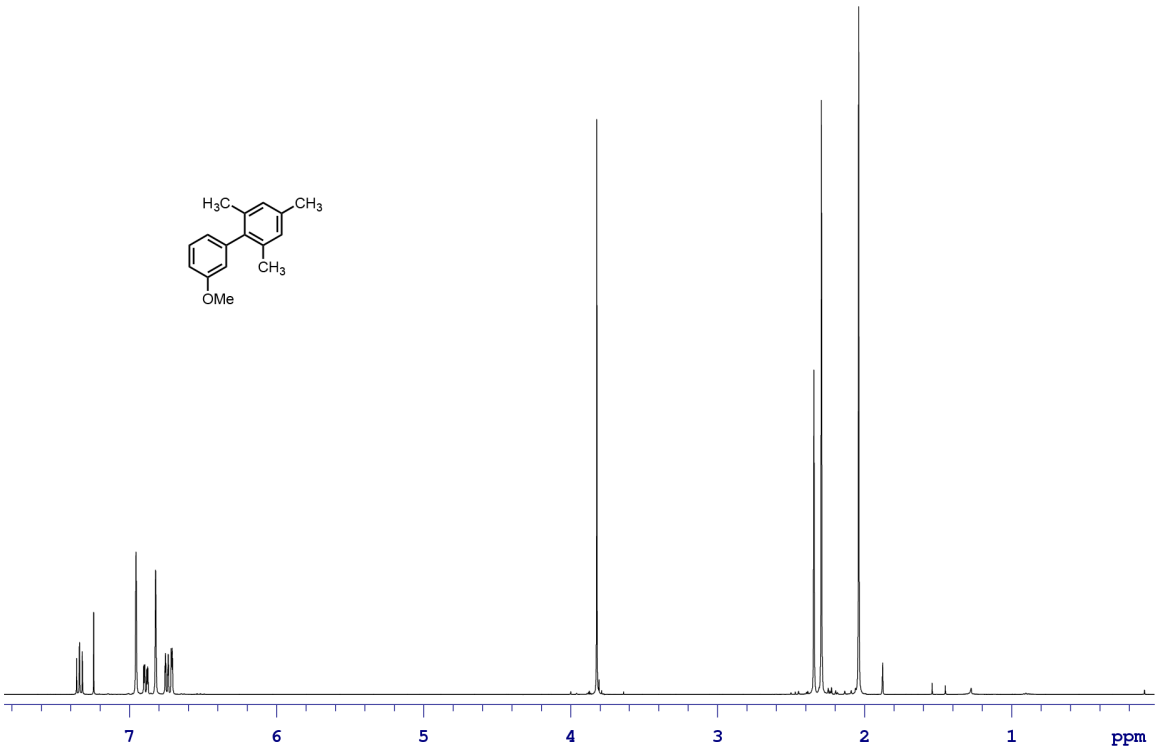
H3C
CH3
CH3
OMe
7
6
5
4
3
2
1
ppm

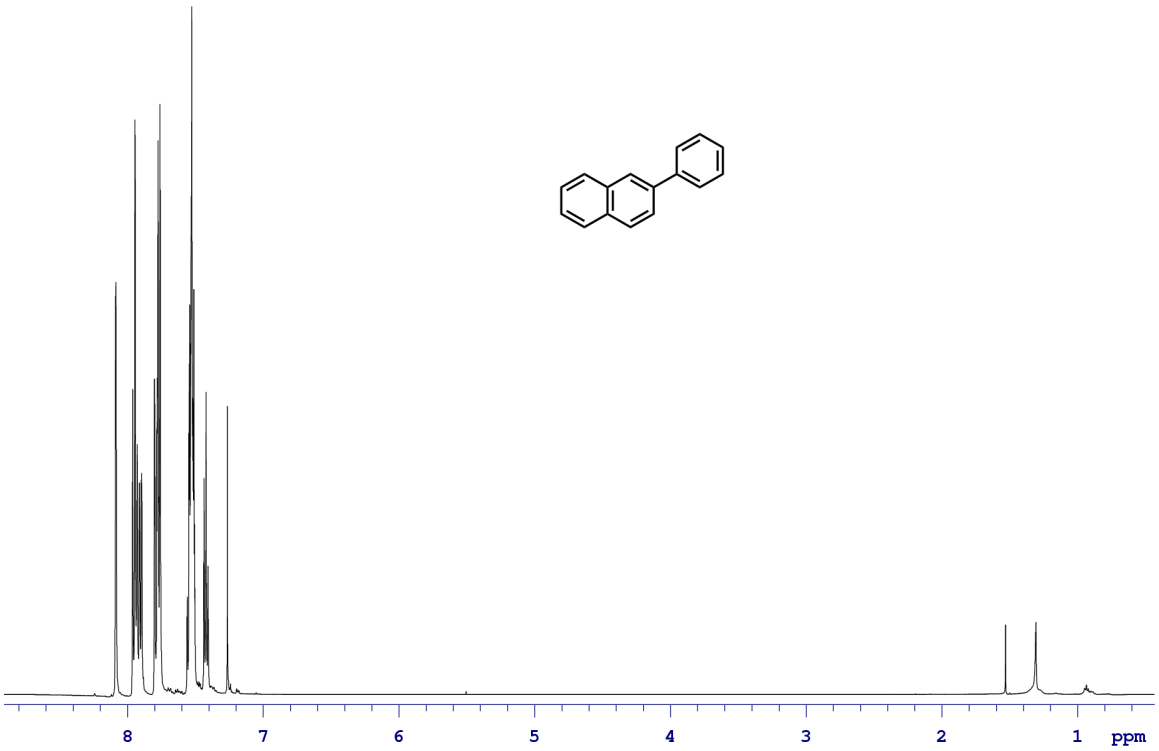
8
7
6
5
4
3
2
1
ppm

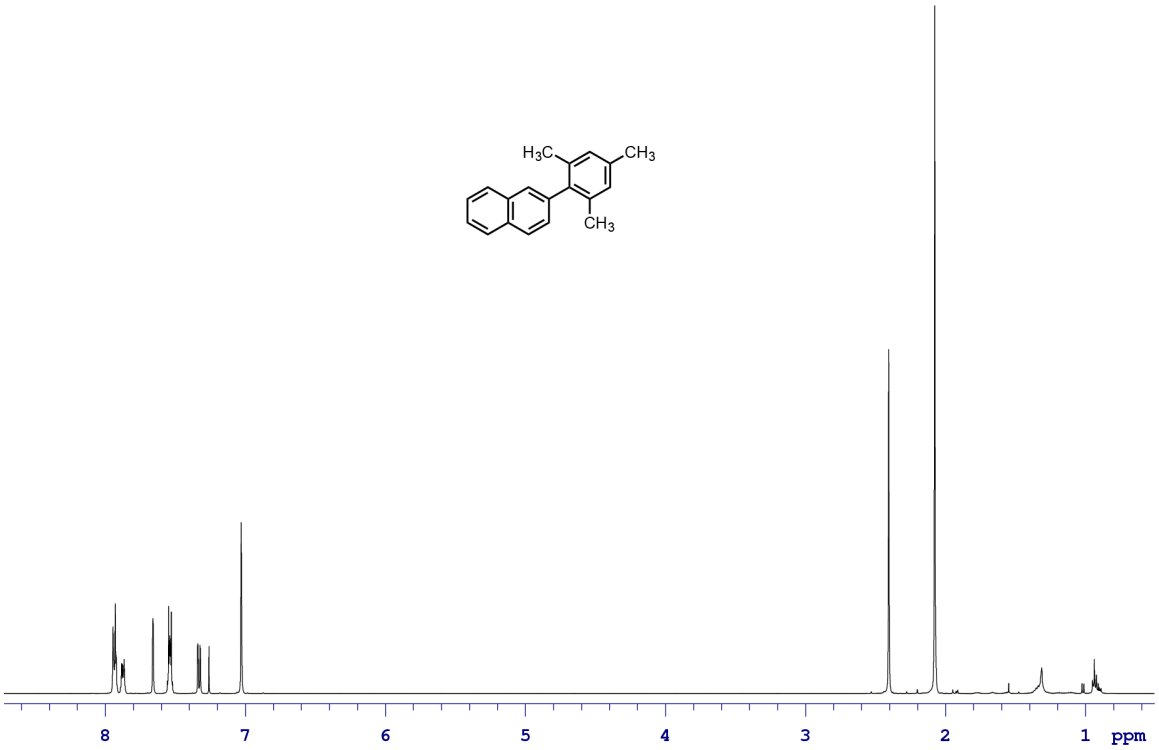
H3C
CH3
CH3
8
7
6
5
4
3
2
1
ppm

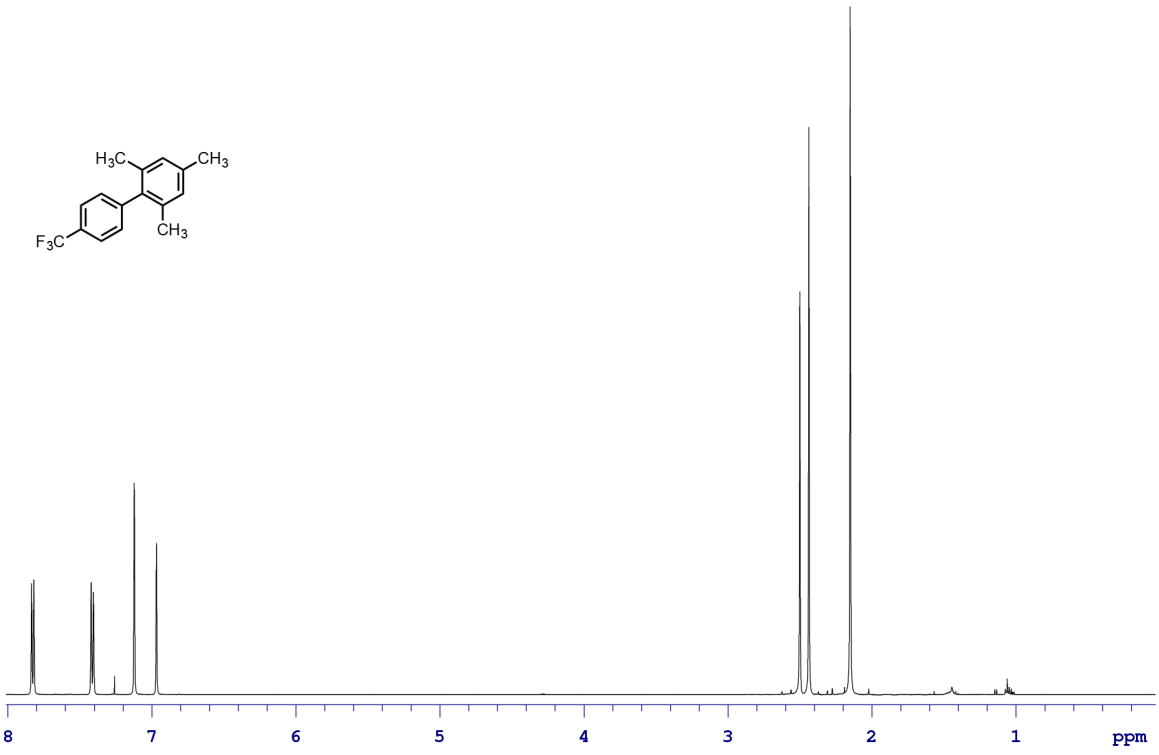
H3C
CH3
F3C
CH3
8
7
6
5
4
3
2
1
ppm

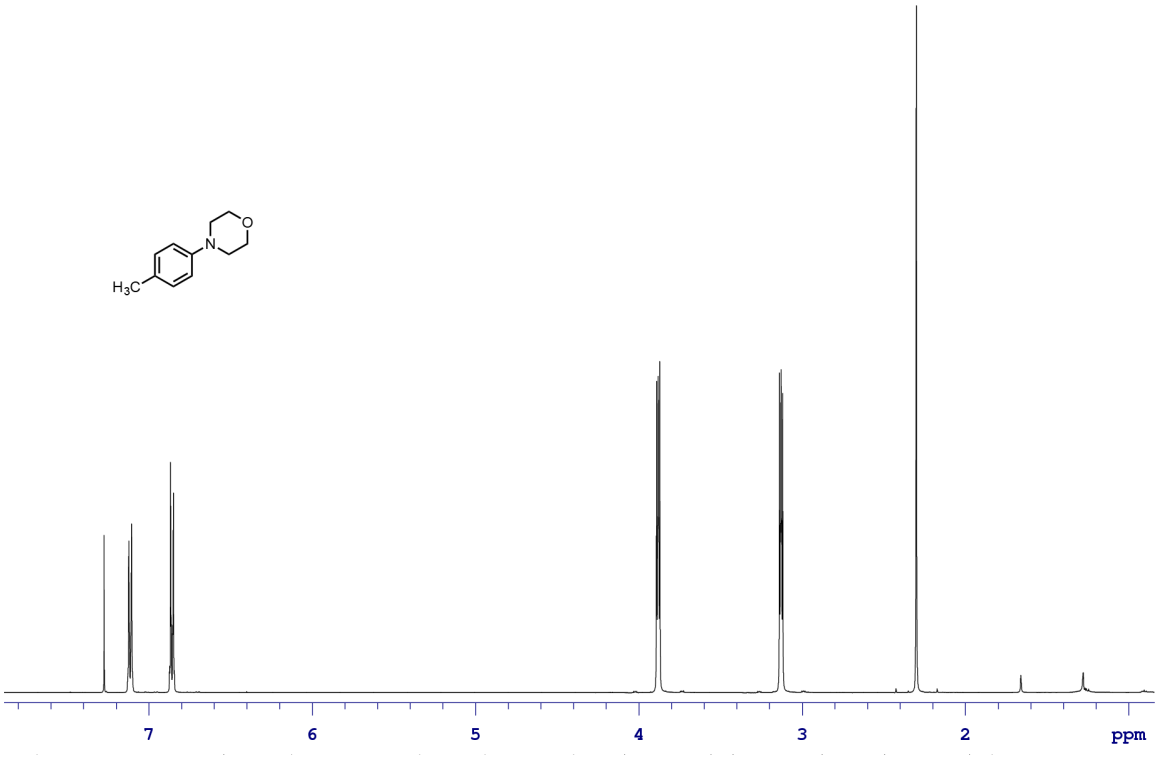
O
N
H3C
7
6
5
4
3
2
ppm

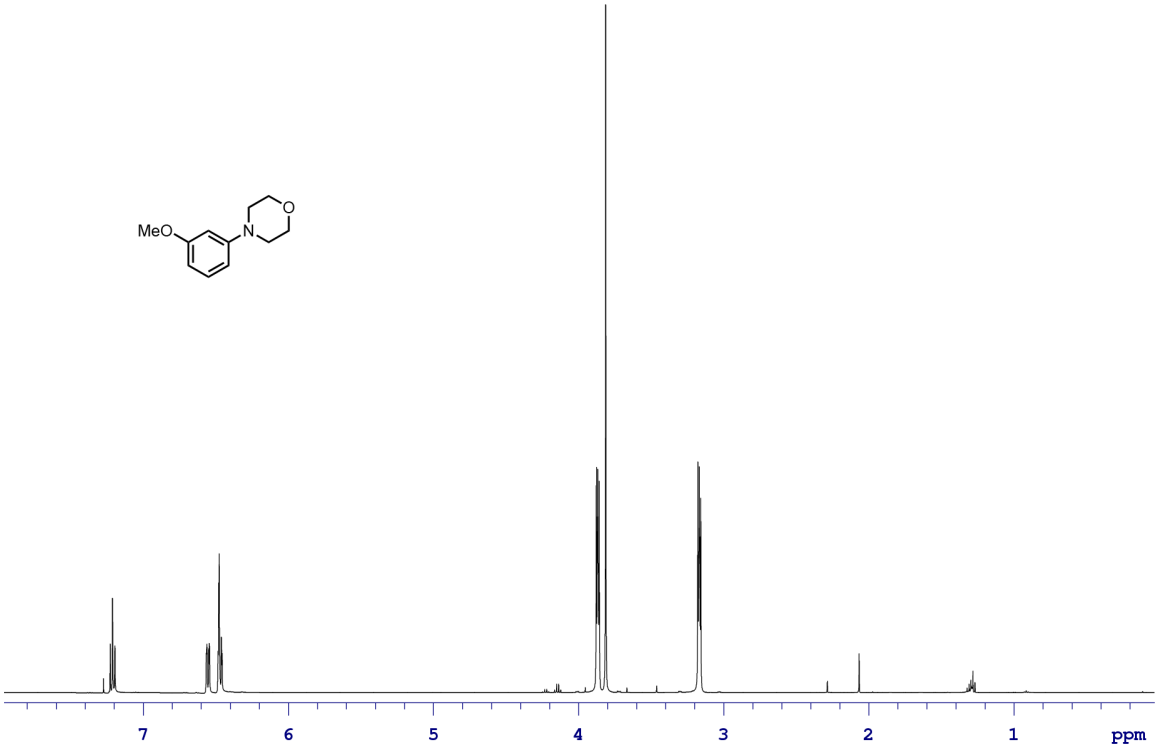
MeO
N
O
7
6
5
4
3
2
1
ppm

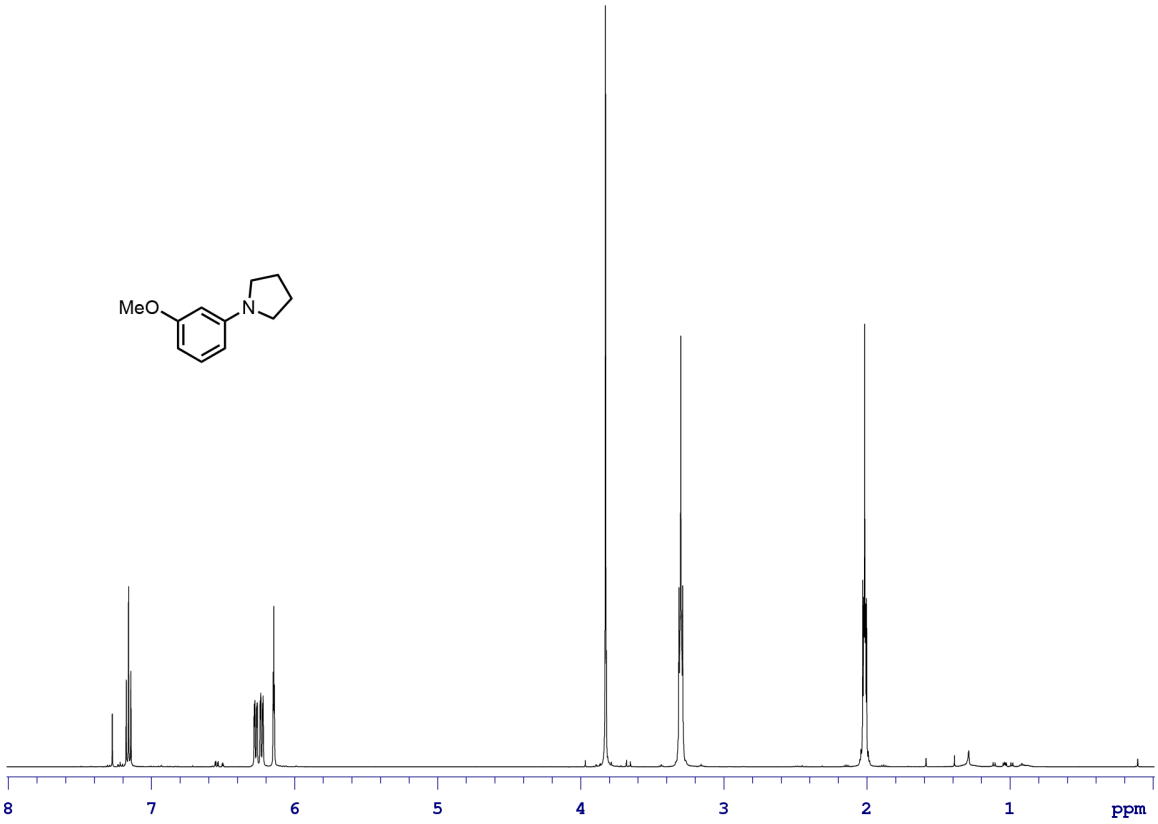
MeO
N
8
7
6
5
4
3
2
1
ppm

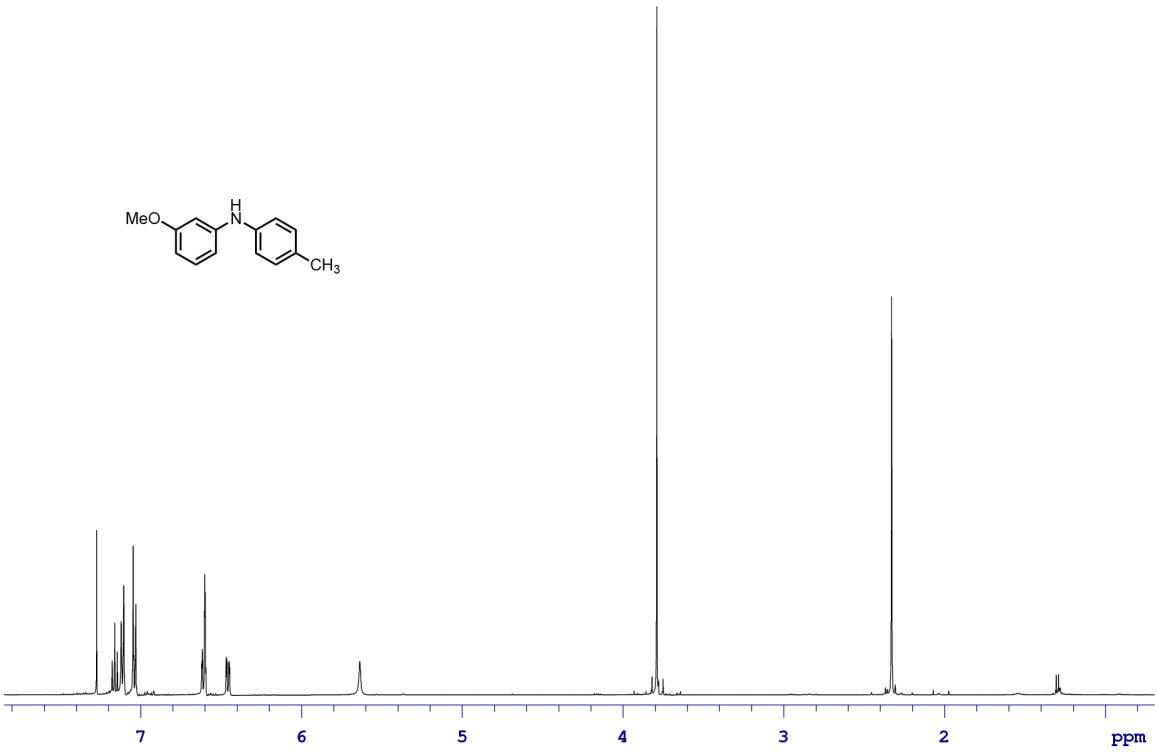
MeO
H
N
CH3
7
6
5
4
3
2
ppm

References

(1) "The Nobel Prize in Chemistry 2010". Nobelprize.org. Retrieved 2009-10-06.

(2) Wilke, G. *Angew. Chem. Int. Ed.* **1988**, *27*, 185–206.

(3) *Industrial Organic Chemistry,* Klaus Weissermel, Hans-Jurgen Arpe John Wiley & Sons; 3rd 1997, ISBN: 3-527-28838-4

(4) For reviews on carbenes in general, see: de Fremont, P.; Marion, N.; Nolan, S. P. *Coord. Chem. Re*v. **2009**, *253*, 862–892.

(5) Ofele, K. *J. Organomet. Chem.* **1968**, *12*, 42– 43.

(6) Wanzlick, H.-W.; Scho¨nherr, H.-J. *Angew. Chem., Int. Ed. Engl.* **1968**, *7*, 141–142.

(7) Arduengo, A. J., III; Harlow, R. L.; Kline, M. *J. Am. Chem. Soc.* **1991**, *113*, 361–363.

(8) Lappert, M. F.; Pye, P. L. *J. Chem. Soc., Dalton Trans.* **1977**, 2172– 2180.

(9) Braband, H.; Abram, U. *Organometallics* **2005**, *24*, 3362-3364.

(10) Katsuki, T.; Sharpless, K.B. *J. Am. Chem. Soc.* **1980**, *102*, 5974.

(11)Johnson, W.S.; Werthemann, L.; Bartlett, W.R.; Brocksom, T.J.; Li, T.L.; Faulkner, D.J.; Petersen, M.R. *J. Am. Chem. Soc.* **1970**, *92*, 741-743.

(12)Wharton, P.; Bohlen, D. "Communications- Hydrazine Reduction of α,β- Epoxy Ketones to Allylic Alcohols" *J. Org. Chem*. **1961**, *26*, 3615-3616.

(13) Kishner, N.J. *Russ. Phys. Chem. Soc.* **1911**, *43*, 582.

(14) Arundale, E.; Mikeska, L.A. *Chem. Rev.* **1952**, *51*, 505–555.

(15) Yadav, J.S.; Subba Reddy, B.V.; Gupta, M.K.; Biswas, S.K. *Synthesis*, **2004**, 2711-2715.

(16) Waitkins, G. R.; Clark, C. W. *Chem. Rev.* **1945**, *36*, 235-289.

(17) Laurence, I.W.; Corey, E.J. *J. Am. Chem. Soc.,* **1993**, 115, 9327

(18) Gastner, T.; Furstner, A. *Org. Lett.,* **2000**, *2*, 2467

(19) Evans, D. A.; Andrews, G. C. *Acc. Chem. Res.* **1974**, *7*, 147-155.

(20) Molander, G. A. *Chem. Rev.* **1992**, *92*, 29-68.

(21) Basavaiah, D.; Rao, A.J.; Satyanarayana, T. *Chem. Rev.* **2003**, *103*, 811-892.

(22) Oppolzer, W.; Radinov, R. N. J. *Am. Chem. Soc*. **1993**, *115*, 1593-1594.

(23) Wipf, P.; Xu, W. J. *Tet. Lett*. **1994**, *35*, 5197-5200.

(24) Kataoka, Y.; Miyai, J.; Oshima, K.; Takai, K.; Utimoto, K. *J. Org. Chem*. **1992**, *57*, 1973-1981.

(25) Jang, H. Y.; Krische, M. J. *Acc. Chem. Res*. **2004**, *37*, 653-661.

(26) Ngai, M. Y.; Kong, J. R.; Krische, M. J. *J. Org. Chem.* **2007**, *72*, 1063-1072.

(27) Patman, R. L.; Chaulagain, M. R.; Williams, V. M.; Krische, M. J. *J. Am. Chem. Soc*. **2009**, *131*, 2066-2067.

(28) Crowe, W.E.; Rachita, M. J. *J. Am. Chem. Soc.* **1995**, *117*, 6787-6788.

(29) Okude, Y.; Hirano, S.; Hiyama, T.; Nozaki, H. *J. Am. Chem. Soc.* **1977**, *99*, 3179-3181.

(30) Furstner, A. *Chem. Rev.* **1999**, *99*, 991-1046.

(31) Inoue, M.; Suzuki, T.; Nakada, M. *J. Am. Chem. Soc.*, **2003**, *125*, 1140-1141.

(32) Savchenko, A. V.; Zhao, Y.; Montgomery, J. *J. Org. Chem.***1995**, 60, 5699.

(33) Oblinger, E.; Montgomery, J. J. Am. Chem. Soc. **1997**, 119, 9065.

(34) Tang, X. Q.; Montgomery, J. *J. Am. Chem. Soc.* **1999**, *121*, 6098.

(35) Tang, X. Q.; Montgomery, J. *J. Am. Chem. Soc.* **2000**, *122*, 6950.

(36) Baxter, R.; Montgomery, J. *J. Am. Chem. Soc.* **2008**,*130*, 9662.

(37) Mahandru, G.M.; Liu, G.; Montgomery, J. J. Am. Chem. Soc. **2004**, *126*, 3698.

(38) Malik, H. A.; Sormunen, G. J.;Montgomery, J. J. Am. Chem. Soc. **2010**, *132*, 5966-5967.

(39) Liu, P.; Montgomery, J.; Houk, K.N. J. Am. Chem. Soc, **2011**, *133*, 6956-6959.

(40) Shareef, A.R.; Sherman, D.H.; Montgomery, J. Chem. Sci., **2012**, *3*, 892-895.

(41) Böhm, V. P. W.; Weskamp, T.; Gstöttmayr, C. W. K.; Herrmann, W. A. *Angew. Chem. Int. Ed.* **2000**, *39*, 1602–1604.
(42) Böhm, V. P. W.; Gstöttmayr, C. W. K.; Weskamp, T.; Herrmann, W. A. *Angew. Chem. Int. Ed.* **2001**, *40*, 3387–3389.
(43) Kremzow, D.; Seidel, G.; Lehmann, C. W.; Fürstner, A. *Chem. Eur. J.* **2005**, *11*, 1833–1853.
(44) Macklin, T. K.; Snieckus, V. *Org. Lett.* **2005**, *7*, 2519–2522.
(45) Matsubara, K.; Ueno, K.; Shibata, Y. *Organometallics* **2006**, *25*, 3422–3427.
(46) Inamoto, K.; Kuroda, J.; Sakamoto, T.; Hiroya, K. *Synthesis* **2007**, *2007*, 2853–2861.
(47) Xi, Z.; Liu, B.; Chen, W. *J. Org. Chem.* **2008**, *73*, 3954–3957.
(48) Gu, S.; Chen, W. *Organometallics* **2009**, *28*, 909–914.
(49) Liu, A.; Zhang, X.; Chen, W. *Organometallics* **2009**, *28*, 4868–4871.
(50) Miyazaki, S.; Koga, Y.; Matsumoto, T.; Matsubara, K. *Chem. Commun.* **2010**, *46*, 1932–1934.
(51) Zhang, C.; Wang, Z.-X. *Organometallics* **2009**, *28*, 6507–6514.
(52) Brenner, E.; Fort, Y.; Poincare, H. *Tetrahedron Lett.* **2001**, *42*, 5689–5692.
(53) Desmarets, C.; Schneider, R.; Fort, Y. *J. Org. Chem.* **2002**, *67*, 3029–3036.
(54) Omar-Amrani, R.; Thomas, A.; Brenner, E.; Schneider, R.; Fort, Y. *Org. Lett.* **2003**, *5*, 2311–2314.
(55) Kuhl, S.; Fort, Y.; Schneider, R. *J. Organomet. Chem.* **2005**, *690*, 6169–6177.
(56) Mesganaw, T.; Silberstein, A. L.; Ramgren, S. D.; Nathel, N. F. F.; Hong, X.; Liu, P.; Garg, N. K. *Chem. Sci.* **2011**, *2*, 1766.
(57) Hie, L.; Ramgren, S. D.; Mesganaw, T.; Garg, N. K. *Org. Lett.* **2012**, *14*, 4182–4185.
(58) Ramgren, S. D.; Silberstein, A. L.; Yang, Y.; Garg, N. K. *Angew. Chem. Int. Ed.* **2011**, *50*, 2171–2173.
(59) Iglesias, M. J.; Blandez, J. F.; Fructos, M. R.; Prieto, A.; Álvarez, E.; Belderrain, T. R.; Nicasio, M. C. *Organometallics* **2012**, *31*, 6312–6316.
(60) Zhang, Y.; Ngeow, K. C.; Ying, J. Y. *Org. Lett.* **2007**, *9*, 3495–3498.

(61) Yoon, H.-J.; Choi, J.-W.; Kang, H.; Kang, T.; Lee, S.-M.; Jun, B.-H.; Lee, Y.-S. *Synlett* **2010**, *16*, 2518–2522.
(62) Iglesias, M. J.; Prieto, A.; Nicasio, M. C. *Adv. Synth. Catal.* **2010**, *352*, 1949–1954.
(63) Guan, P.; Cao, C.; Liu, Y.; Li, Y.; He, P.; Chen, Q.; Liu, G.; Shi, Y. *Tet. Lett.* **2012**, *53*, 5987–5992.
(64) Berini, C.; Brayton, D. F.; Mocka, C.; Navarro, O. *Org. Lett.* **2009**, *11*, 4244–4247.
(65) Berini, C.; Winkelmann, O. H.; Otten, J.; Vicic, D. A.; Navarro, O. *Chem. Eur. J.* **2010**, *16*, 6857–6860.
(66) Maekawa, T.; Sekizawa, H.; Itami, K. *Angew. Chem. Int. Ed.* **2011**, *50*, 7022–7026.
(67) Chaulagain, M. R.; Mahandru, G. M.; Montgomery, J. *Tetrahedron* **2006**, *62*, 7560–7566.
(68) Miller, Z.D.; Li, W.; Belderrain, T.R.; Montgomery, J. *J. Am. Chem. Soc.*, **2013**, *135*, 15282-15285.
(69) Buchan, Z. A.; Bader, S. J.; Montgomery, J. *Angew. Chem. Int. Ed.* **2009**, *48*, 4840–4844.
(70) Louie, J.; Gibby, J. E.; Farnworth, M. V; Tekavec, T. N. *J. Am. Chem. Soc.* **2002**, *124*, 15188–15189.
(71) Tekavec, T. N.; Arif, A. M.; Louie, J. *Tetrahedron* **2004**, *60*, 7431–7437.
(72) Tekevac, T. N.; Louie, J. *Org. Lett.* **2005**, *7*, 4037–4039.
(73) Tekavec, T. N.; Louie, J. *J. Org. Chem.* **2008**, *73*, 2641–2648.
(74) Duong, H. A.; Cross, M. J.; Louie, J. *J. Am. Chem. Soc.* **2004**, *126*, 11438–11439.
(75) Duong, H. A.; Louie, J. *Tetrahedron* **2006**, *62*, 7552–7559.
(76) McCormick, M. M.; Duong, H. A.; Zuo, G.; Louie, J. *J. Am. Chem. Soc.* **2005**, *127*, 5030–5031.
(77) Stolley, R. M.; Maczka, M. T.; Louie, J. *Eur. J. Org. Chem.* **2011**, *2011*, 3815–3824.
(78) Anslyn, E.V.; Dougherty, D.A. *Modern Physical Organic Chemistry*: University Science Books, 2006, pg 746-747.
(79) Harris, J. R.; Haynes, M. T.; Thomas, A. M.; Woerpel, K. A. *J. Org. Chem.* **2010**, *75*, 5083–5091.
(80) Ogoshi, S.; Arai, T.; Ohashi, M.; Kurosawa, H. *Chem. Commun.* **2008**, 1347–1349.

(81) Baxter, R.D.; Montgomery, J. J. Am. Chem. Soc., **2011**, *133*, 5728-5731.
(82) Potential energy surfaces of the monomeric and dimeric pathways calculated with M06/SDD-6-311+G(d,p)//B3LYP/LANL2DZ-6-31G(d)
(83) Hoshimoto, Y.; Ohashi, M.; Ogoshi, S. *J. Am. Chem. Soc.* **2011**, *133*, 4668–4671.
(84) Caddick, S.; Cloke, F. G. N.; Hitchcock, P. B.; de K. Lewis, A. K. *Angew. Chem. Int. Ed.* **2004**, *43*, 5824–5827.
(85) Lee, C. H.; Laitar, D. S.; Mueller, P.; Sadighi, J. P. *J. Am. Chem. Soc.* **2007**, *129*, 13802–13803.
(86) Iglesias, M. J.; Blandez, J. F.; Fructos, M. R.; Prieto, A.; Álvarez, E.; Belderrain, T. R.; Nicasio, M. C. *Organometallics* **2012**, *31*, 6312–6316.
(87) Clement, N. D.; Cavell, K. J.; Ooi, L. *Organometallics* **2006**, *25*, 4155–4165.
(88) Findlay, N. J.; Park, S. R.; Schoenebeck, F.; Cahard, E.; Zhou, S.-Z.; Berlouis, L. E. A.; Spicer, M. D.; Tuttle, T.; Murphy, J. *J. Am. Chem. Soc.* **2010**, *132*, 15462–15464.
(89) Arduengo, A. J.; Rasika Dias, H. V.; Harlow, R. L.; Kline, M. *J. Am. Chem. Soc.* **1992**, *23*, 5530–5534.
(90) Herrmann, W. A..; Gerstberger, G.; Spiegler, M. *Organometallics* **1997**, *16*, 2209–2212.
(91) Enders, D.; Breuer, K.; Raabe, G.; Runsink, J.; Teles, J. H.; Melder, J.; Ebel, K.; Brode, S. *Angew. Chem. Int. Ed.* **1995**, *34*, 1021–1023.
(92) Nyce, G. W.; Csihony, S.; Waymouth, R. M.; Hedrick, J. L. *Chem. Eur. J.* **2004**, *10*, 4073–4079.
(93) Bittermann, A.; Baskakov, D.; Herrmann, W. a. *Organometallics* **2009**, *28*, 5107–5111.
(94) Arduengo, A. J.; Davidson, F.; Dias, H. V. R.; Goerlich, J. R.; Khasnis, D.; Marshall, W. J.; Prakasha, T. K. *J. Am. Chem. Soc.* **1997**, *119*, 12742–12749.
(95) Wang, H. M. J.; Lin, I. J. B. *Organometallics* **1998**, *17*, 972–975.
(96) Chen, C.; Qiu, H.; Chen, W.; Wang, D. *J. Organomet. Chem.* **2008**, *693*, 3273–3280.
(97) Paulose, T. A. P.; Wu, S.-C.; Olson, J. A.; Chau, T.; Theaker, N.; Hassler, M.; Quail, J. W.; Foley, S. R. *Dalton Trans.* **2012**, *41*, 251–260.
(98) Clement, N. D.; Cavell, K. J.; Ooi, L. *Organometallics* **2006**, *25*, 4155–4165.

(99) Berini, C.; Brayton, D. F.; Mocka, C.; Navarro, O. *Org. Lett.* **2009**, *11*, 4244–4247.
(100) Berini, C.; Winkelmann, O. H.; Otten, J.; Vicic, D. A.; Navarro, O. *Chem. Eur. J.* **2010**, *16*, 6857–6860.
(101) Matsubara, K.; Miyazaki, S.; Koga, Y.; Nibu, Y.; Hashimura, T.; Matsumoto, T. *Organometallics* **2008**, *27*, 6020–6024.
(102) Wu, J.; Faller, J.; Hazari, N *Organometallics* **2012**, *31*, 806-809.
(103) Work performed by Evan Jackson of the Montgomery Laboratory
(104) Work performed with Jeanne Kochkodan in the Montgomery Laboratory
(105) Jackson, E.P.; Malik, H.A.; Sormunen, G.J.; Montgomery J. *Angew. Chem. Int. Ed.* **2014**, *Manuscript in Preparation*
(106) Baxter, R.D., "Method Development and Mechanistic Investigation of Nickel-Catalyzed Reductive Coupling Processes" Ph.D. Dissertation, University of Michigan, Ann Arbor, MI, 2010.
(107) Sun, Chang-Liang; *Nature Chemistry* **2010**, *2*, 1044-1049.
(108) Raviola, C.; Canevari, V.; Protti, S.; Albini, A.; Fagnoni, M. *Green Chemistry* **2013**, *15*, 2704-2708.
(109) Guan, B.T. et al. *Organic Letters* **2010**, *12,* 396-399.
(110) Lee, H.W. et al. *Angew. Chem. Int. Ed.* **2009**, *48*, 7436-7439.